INSTITUTE
FOR
AEROSPACE STUDIES

UNIVERSITY OF TORONTO

A THEORY OF GAS-SURFACE INTERACTIONS

AT SATELLITE VELOCITIES

by

D. P. Jackson

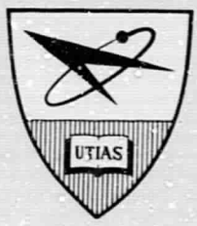

November, 1968.

UTIAS Report No.134

A THEORY OF GAS-SURFACE INTERACTIONS AT SATELLITE VELOCITIES

by

D. P. Jackson

Manuscript received August, 1968

November, 1968

UTIAS REPORT No. 134

ACKNOWLEDGEMENTS

My sincere thanks to Professor J. B. French for his valuable advice, assistance and encouragement throughout the course of this work. I am also grateful to Professor A. J. Howsmon for many helpful comments and suggestions.

Dr. R. A. Oman of the Grumman Aircraft Engineering Corporation and Dr. F. O. Goodman of the Department of Aerospace Engineering, University of Virginia provided many helpful suggestions in correspondence and discussed the present research with me on several occasions. Their kindness to me is greatly appreciated.

The calculations were done on the IBM 7094 computer at the Institute of Computer Science, University of Toronto, to which the author is indebted for the use of these facilities. I would also like to thank Mrs. B.Waddell and Miss S. Miller for the typing and production of this report.

This work was supported by NASA under grant number (NsG-367; NGR-52-026-001) this support is gratefully acknowledged. The author would also like to thank the Faculty of Applied Science and Engineering for a fellowship awarded during this work.

Finally, I wish to thank my fellow students who did much to make my stay at the Institute the pleasant experience that it was.

SUMMARY

A classical three-dimensional model of the interaction of rare gas atoms with clean metal surfaces at satellite velocities is presented. The surface is assumed to be an ideal crystal plane with no thermal motion. The surface atoms are decoupled in collision and resume their original positions after a collision. The surface field is modeled by repulsive hard sphere collisions at an appropriate radius of interaction and a smooth normal attractive field due to the entire semi-infinite solid. The latter's magnitude is characterized by the ratio of the incoming beam energy to the attractive field strength. Aside from the parameters which are fixed in an experiment, the model has two disposable parameters: the interaction radius and the attractive field energy. A series of numerical experiments were performed and trapping, accommodation and flux and velocity distributions were found for a wide variety of situations.

A systematic study of the influence of the parameters on the functions of interest is given. It is shown that even for the simple assumptions of the model the interaction is very complex. In particular, recognizing the difference between semi-trapped and absolutely trapped particles is essential for accurate calculation of trapping and accommodation. Structure was found in some of the distributions and was explained by the differences in the behaviour of trajectories of singly and multiplely colliding particles. The absolute flux levels obtained, when reasonable values of the two disposable parameters were used, compared well with an intermediate energy scattering experiment. Preliminary approximate satellite drag calculations based on this comparison show that drag for clean surfaces can be quite low.

TABLE OF CONTENTS

NOTATION

The following table contains most of the notation used in the present work. Some symbols have several meanings that are clear from the context in which they are used; the sections where a certain definition is used will be noted in cases of doubt.

A	Co-ordinates (a_1,a_2,a_3). The centre of the surface sphere impacted. Sections 4.2 and 4.3
A	Absolute trapping probability
A_{ij}	Matrix of absolute trapping probabilities or an element thereof
A_f	Full or corrected absolute trapping probability
a	Slope factor in the Morse potential (section 3.3.1) Appendices
a_i	Co-ordinate of A, the centre of the surface sphere impacted
B	Factor used in range calculation. Defined in Eq. (4.5.12)
b	Impact parameter
b^*	Non-dimensional impact parameter. b/σ
C	Centre of gas sphere on impact
C	General parameter in Eq. 3.3.1 (section 3.3.1)
C'	General parameter in Eq. 3.3.2 (section 3.3.1)
c_i	Co-ordinates of a gas atom at impact
c	Non-dimensional slope factor in the Morse potential (section 3.3.1 and Appendices)
D	Well depth energy in the Morse potential
D	Determinant defined by Eq. 4.2.6 (section 4.2)
d	Spacing between atoms in a (100) surface array
d_ℓ	Bulk lattice spacing. Identical with d for body-centered-cubic lattices
E	General symbol for energy
E_o	Incoming gas atom's energy (or the incoming energy of a beam) at infinity, before interaction with the surface
E^*	Non-dimensional energy E/E_t

E^*_o	Non-dimensional incoming gas energy E_o/E_t
E_s	Energy of an incoming gas atom at the surface after the attractive field has been applied to it
E'_s	Energy of a reflected gas atom at the surface before the surface field is applied and after the hard sphere interaction
E_t	Energy of the attractive field, i.e. the energy acquired by a gas atom on going from infinity to the surface
F	The normalized primary flux
F_i	Special function used only in section 4.4, defined by equation 4.4.7
F_f	The normalized primary flux of the single colliders only
F_m	The normalized primary flux of the multiple colliders only
G	Escape probability
G_{ij}	Matrix of escape probabilities or an element thereof
g	Relative speed of approach
g^*	Reduced relative speed of approach $g^{*2} = \mu^* g^2 / 2\epsilon$
I	Factors used to correct the AC's. Defined in Eq. 4.6.6
j	Indexing symbol used in section 4.8 with reference to the computer program
K	Range used in section 4.5.3
Kn	Knudsen number. The mean free path of a gas divided by a characteristic dimension of a body in it
k	Boltzmann's constant
k'	General parameter in Eq. 3.3.2
$\tilde{k}$	Parameter which determines energy ranges for the STD
ℓ	Symbol for x-axis direction cosine
ℓ'	X-direction cosine of a reflected trajectory
ℓ'_∞	X-direction cosine of a reflected trajectory at infinity i.e. after the attractive field corrections
ℓ_o	X-direction cosine of an incident trajectory

$\tilde{\ell}$	X-direction cosine of the line of centres of a gas atom and a surface atom on impact
M	General symbol for momentum (section 2.1.2)
M	Fraction of particles having multiple collisions
M_e	Fraction of escaped atoms (primary) having multiple collisions
m	Symbol for Y-axis direction cosine, other symbols containing "m" are defined similarily to the ℓ's
m_1	Mass of a gas atom, used in section 4.3
m_2	Mass of a surface atom, usedin section 4.3
N	Number of trajectories or particles
n	Symbol for Z-axis direction cosine, other symbols containing 'h"are defined similarily to the ℓ's
n	Number of atoms per unit cell (Appendix B)
P	A point in the target area. Aiming point of an incoming trajectory
P'	The point of intersection in the XY plane of a reflected trajectory or its extension
p_i	Co-ordinate of P
p_i'	Co-ordinate of P'
$\tilde{p}_i$	Defined by Eq. (4.5.14)
p_i^*	Aiming point of a re-colliding semi-trapped particle, section 4.5.3
R	Interaction radius. The distance between the centre of a gas atom and the centre of a surface atom at impact
R*	Normalized interaction radius. R/d
r	Centre to centre distance between two atoms
r_o	Well depth distance of interatomic potential functions
r_m	Minimum separation of two atoms during a collision
r*	Non-dimensional interatomic distance r/σ
S	Semi-trapping probability
S_{ij}	Semi-trapped probability matrix or an element thereof

S_1	Function used in sections 4.3 and 4.4
$T_{surface}$	Surface temperature (section 2.1)
$t(k,\ell)$	Semi-trapped distribution for a case with initial energy and altitude angle corresponding to the central values of "box" k,ℓ
$t^{(a)}$	Absolutely trapped component of STD after splitting, see Eq. 4.5.20
$t^{(g)}$	See Eq. 4.5.20
$t^{(s)}$	See Eq. 4.5.20
U	Initial velocity of a surface atom (section 4.3)
U	Normalizing factor for the calculation of STD's. Defined by Eq. 4.5.22
U'	Final velocity of a surface atom (section 4.3)
v	Velocity of incoming gas atom (section 4.3)
v'	Velocity of a reflected gas atom (section 4.3)
$\bar{v}$	Average (mean) velocity
v_o	Initial velocity of a gas atom (or beam) at infinity
$\bar{v}_f$	Average velocity of single colliders only
$\bar{v}_m$	Average velocity of multiple colliders only
$W^{(a)}(k,\ell)$	Weighting matrix accumulated during the STD iteration process for the case (k,ℓ). It gives the fraction of the initial particles absolutely trapped at the energy and altitude angle corresponding to the element considered
$W^{(g)}(k,\ell)$	Weighting matrix accumulated during the STD iteration process for the case (k, ℓ). It gives the fraction of the initial particles escaped at the energy and altitude angle corresponding to the element considered
z_m	Maximum height above the surface (section 4.5.3)

Greek Symbols

α_e	Energy accommodation coefficient
α_n	Normal momentum accommodation coefficient
α_t	Tangential momentum accommodation coefficient

α_A	Electronic polarizability of an adatom (Appendix B)
α_M	Electronic polarizability of a solid (surface) (Appendix B)
β	Complement of accommodation coefficient: $\alpha = 1 - \beta$. Subscripted a,n, and t to correspond to accommodation coefficients
$\tilde{\beta}$	Total (or corrected) complement of the full accommodation coefficient
γ	Angle through which an atom is turned in a hard sphere collision $\gamma = \lvert\psi' - \psi\rvert$ (section 4.4)
δ_i	$\delta_i = p_i - a_i$ see Eq. 4.2.4
ϵ	Lennard-Jones well depth
θ_o	Initial altitude angle of an incoming atom (or beam) measured from the surface normal
θ_m	Polar angle of the point of nearest approach to the scattering centre of an atom in a collision (section 3.3.2)
θ_r	Altitude angle at which a distribution measurement is made
θ_s	Altitude angle of an incoming atom at the surface after correction for attractive field effects
θ'_s	Altitude angle of a reflected atom at the surface before correction for attractive field effects
λ	Parameter used for writing the parametric equations for a trajectory
μ	Mass ratio = mass of gas atom/mass of surface atom
μ^*	Reduced mass in a centre of mass collision
ρ	Resolution of the simulated detector. Defined in section 4.7
ρ	Atomic density of a crystal lattice (Appendix B)
r	Value of "r" when the potential is zero for interatomic potential functions. Cf. Fig.3.1
τ	Characteristic interaction time (section 2.2)
τ	Distance below the surface used in the integrations in Appendix B
φ_o (Φ_o)	Initial azimuth angle of incoming atom (or beam)
φ_d	Offset azimuth angle of detector

φ_r (Φ_r)	Azimuth angle at which a distribution measurement is made
φ_{KM}	Kirkwood-Muller interaction potential
φ_{LJ}	Lennard-Jones interatomic potential
φ_M	Morse interatomic potential
χ	Turning angle in an interatomic collision. (section 3.3.2)
χ_A	Diamagnetic susceptibility of an adatom
χ_M	Diamagnetic susceptibility of a material (surface)
ψ	Angle between an incoming trajectory at impact and the line of centres of the gas atom and surface atom
ψ'	Angle between a reflected trajectory after impact and the line of centres of the gas atom and surface atom
ω_n	Natural lattice frequency (section 2.2)

Special Symbols and Abbreviations

AC	Accommodation Coefficient
COL	Coupled Oscillator Lattice
IOL	Independent Oscillator Lattice
LJ	Lennard-Jones
LOC	Line Of Centres
STD	Semi-Trapped Distribution
1-D	One-Dimensional Similarly 2-D and 3-D
"$\|\|$"	Subscript Parallel
"$\perp$"	Subscript Perpendicular
$\otimes$	Schur Product. Defined in Eq. 4.5.19

INTRODUCTION

A satellite passing through a highly rarefied atmosphere may be considered as a body in free molecule flow (Ref. 1). In this regime the Knudsen number is very large (i.e. the mean free path of a molecule is large compared with a characteristic dimension of the body). Hence the probability of gas-gas collisions is negligibly small and the aerodynamic behaviour of the body is determined by the collisions of molecules with its surfaces. For this reason a knowledge of gas-surface interactions is essential for the understanding of satellite flight and the flight of vehicles in rarefied planetary atmospheres.

In the past decade there have been extensive experimental efforts to investigate this problem using molecular beam techniques ; a recent review of this work has been given by French (Ref. 2). However, as yet there are few results for monoenergetic beams of satellite velocities on well-defined surfaces - a notable exception is the work of O'Keefe (Ref.3); for the most part the available data is generally confined to thermal velocity beams often on poorly defined surfaces. There has been a corresponding theoretical effort in this field which has followed the experimental work in the sense that much of it has concerned effects likely to be most important in the thermal range. At present there are few theories which are directly applicable to the satellite case ; the present work is intended as a contribution to this case.

The precise problem considered here is that of a monoenergetic beam of rare gas atoms impinging on a well-defined clean crystalline metal surface. The main reason for choosing this situation , aside from its simplicity, is that it is the one that many current experiments try to produce (see for instance Ref.3). In addition it is a necessary first step to an understanding of the more complex phenomena likely to be involved in the most general situations. In such circumstances polycrystalline surfaces, adsorbed gas layers, mixed atmospheres, gross surface roughness and other complications are introduced which may obscure the more basic processes taking place at the surface. However, it seems plausible to speculate that these more complex situations might be treated as a superposition of a number of the above elementary cases. In any case it is clear that physical insight into these general cases presupposes a knowledge of the elementary ones.

The plan of this work is as follows: Various general considerations and previous theories are covered in the next section. In section III the assumptions and limitations are discussed and then the details of the model are presented in section IV. The results obtained are presented in sections V to IX, under the headings; General Results, Trapping and Accommodation, Flux Distributions, Velocity Distributions and Comparison with Experiment respectively. The Conclusions are given in section X. The casual reader, not interested in details is advised to read this section after reading parts 3.1 and 3.5 which summarize the model.

II. GAS-SURFACE INTERACTIONS

2.1 Basic Considerations

2.1.1. Orbital Parameters

To get an indication of the magnitudes of the quantities involved in

satellite-surface interactions one can refer to the paper of Johnson (Ref.4), there can be found some typical values for an orbital height of 200 km:

orbital velocity = 7.78×10^5 cm/sec

mean free path = 7×10^{-4} cm

partial flux of N = 2.5×10^{14} molecules/cm^2/sec

Knudsen no. (1m body) = 700

It is clear from these numbers that the regime is free molecule flow - Kn = 10 is usually regarded as the lower boundary of this regime, in fact Kn > 10 for all altitudes > 125 km (Ref.4). The orbital velocity corresponds to energies of (.34, 1.25, 4.40, 5.03, 6.35, 12.5 ev) for (H, He, N, O, Ne, A) respectively the principal species present at that altitude (200 km). On this basis one can see that the range of energies for satellite-surface interactions is about 1 to 15 ev , although this may be smaller or larger depending on the gas mass and the speed of the body. In the case of a super-orbital re-entering vehicle ,for instance, the energies may be much higher.

The present work will not consider ions although they are a major constituent of the upper atmosphere; there is however a possibility of including them in a "neutral model" (such as this one) when the neutralization process at the surface is well characterized, for a recent discussion of this problem see Prince (Ref.5). The diatomic gases present at somewhat lower altitudes are also excluded. The present investigation will be confined to the rare gases since they are most frequently used in molecular beam simulations and because they give rise to the simplest situations with no chemisorption.

Considering the magnitude of the typical partial flux given above, which is somewhat larger than those usually encountered in experiment (Ref.3), an important fact emerges. That is that the incoming flux bombards the surface rather sparsely per unit time. For tungsten one has about 10^{15} atoms per cm^2 assuming for example a flux of 10^{15} mols/cm^2/sec this means that each surface atom is struck on the average about once per second. This is a significant point which will be discussed further in section 3.2.3.

It is difficult to discuss in detail the surface temperature of a body in space. The temperature is defined by the radiation balance achieved by the body in relation to the sources in space. In particular for an earth satellite this would depend on its position relative to (mainly) the sun, this changes during the orbit of course. Hence the temperature would depend on the body's position, what parts of it were exposed, the thermal inertia of the material as it passed in and out of the radiation and many other factors such as whether the satellite spins or not. The temperature of different parts of the body might range from a few to a few hundred degrees Kelvin. In the laboratory the temperatures are generally of the order of room temperature.

2.1.2. Functions of Interest

The accommodation coefficients are used to calculate the lift and drag coefficients of convex bodies in free molecule flow - Patterson gives the

details of this calculation in Ref.1. Historically they were defined on the basis of a now obsolete theory (Ref 6) due to Maxwell and others (see Ref.7) which assumed that molecules reflected from a surface belonged to either of two components : a specularly reflected component which left the surface at the mirror angle of the original angle and a diffuse component effusing from the surface as a Maxwellian cosine distribution with temperature that of the surface. French has discussed this in more detail in Ref.2. For the present work the modern definitions of Oman (Ref.8), Goodman (Ref.9) and others will be used. The general form of the accommodation coefficient will be:

$$\frac{\text{total energy (or momentum) absorbed by the solid (surface)}}{\text{total energy (or momentum) incident on the surface}} \qquad (2.1.1.)$$

Using E to represent energy, the subscripts "i" and "r" to indicate incident and reflected quantities, and $M^{(n)}$ and $M^{(t)}$ to denote normal and tangential momenta respectively, the definitions of the energy, normal momentum and tangential momentum AC's (accommodation coefficients) are:

$$\alpha_e = 1 - \frac{E_r}{E_i} \qquad (2.1.2.)$$

$$\alpha_n = 1 - \frac{M_r(n)}{M_i(n)} \qquad (2.1.3.)$$

$$\alpha_t = 1 - \frac{M_r(t)}{M_i(t)} \qquad (2.1.4.)$$

It should be noted that there is no physical reason why these ratios must be positive. If α_e is negative the surface is heating the gas, this won't be found in the present work because $E_i \gg k\, T_{surface}$, however, the reader is referred to the comments of Goodman (Ref.6) on this. If either of the momentum AC's are negative it merely means that the momentum has been exchanged between the tangential and normal components by the surface interaction. It is also clear from the definitions that if no particles leave the surface, all the AC's are unity i.e. the gas is fully accommodated to the surface. It should also be noted that various authors use a variety of notations and definitions and care must be used in comparing the values of AC's between papers.

The energy accommodation coefficient is not directly involved in the calculation of aerodynamic forces on satellites, however, it is of fundamental importance for certain problems of heat transfer in vacuum systems etc (see Ref.10). Although the accommodation coefficients are usually sufficient for convex satellite calculations, the flux and velocity distributions are needed for problems with concave or enclosed geometries (see for example the work of Townsend (Ref.11)). In addition as one considers lower satellite altitudes the transition flow regime is encountered and in that case a full knowledge of the distributions is also required. Finally the distributions are needed for comparison with experimental results as a rigorous test of the validity of theoretical work.

2.1.3. Theoretical Difficulties

Before discussing the theories that have been proposed for gas-surface interactions it would be well to emphasize the difficulties involved in obtaining an adequate theory. Formulating the problem in its simplest terms

to a single gas particle approaching a surface; it is clear that one has immediately a many-body problem. Hence some simplifications must be introduced to make the problem solvable. In most cases the assumptions are designed to reduce the interaction to the sum of a few pairwise interactions with perhaps an overall integrated potential to account for the influence of the other solid atoms. Considering a pairwise interaction between a gas atom and a surface atom it is not clear how the results for two similar atoms in free space can be applied to the situation. In other words the question is: how does the fact that one of the atoms is in a surface affect the situation? The answer to this is not well known and unfortunately there have been few fundamental studies of problems of this nature, for more discussion of this see section 3.4.1. and 3.5.1. below.

Another essential difficulty lies in the concept of a surface as such. In the problems of solid state physics, surfaces are often considered as undesirable singularities and are avoided by the introduction of boundary conditions the details of which are not precisely described. This is reasonable for the purposes of the theories involved but it gives little information about the surface. In fact, at the surface the physical properties typical of the solid bulk will not be valid because of the asymmetrical bonding of the surface atoms; for instance, the lattice spacing may increase (Ref.12) and the Debye temperature will be smaller (Ref.13). The fact is that the surface is an interface and by its very nature difficult to treat. In addition the quantum-mechanical effects which are involved in any realistic discussion of solids may also play a part in the interaction. This ennumeration of problems could be extended almost indefinitely. However, the basic point here is that in most physical problems describing a complex situation the method is to reduce the problem to an explanation in terms of simple well-understood phenomena. At present, in surface physics even these "simpler" situations, into which the overall problem could be broken down are not well understood. A good solution therefore depends on a good selection of assumptions.

2.2. Outline of Previous Theories

It is necessary to discuss previous theories not only to indicate why a further one is needed but also because many of them give useful insights into problems specific to gas-surface interactions at satellite velocities. The results of some of them will be the basis of assumptions to be made in the next chapter. In order to make a full presentation of gas-surface interaction theories one should probably use the historical approach; there will be no attempt to do this here and one can refer to the review of Hurlbut (Ref.14) or Trilling (Ref.7) for example for such surveys. The object of this and the following sections is to review the main trends, or means of attack, that have been used and to place the present theory in relation to them.

The first natural division of theory is between classical and quantum mechanical types. The latter is of course the most general and strictly valid point of view for any problem and the question is merely whether it is necessary from a practical viewpoint to go to this level of complexity. This will be discussed in section 2.6 and for the remainder of this section the exposition will be confined to purely classical theories. They can be classified, on the basis of the major effect treated, into lattice, thermal and field theories. Referring to Fig.2.1, the main lines of development in classical theory, represented by selected papers, have been outlined by a schematic diagram. This

has been drawn to aid the explanation and is not intended to be a chart of publication priorities or an exhaustive classification. Putting a theory into one of these groups does not of course mean that they are mutually exclusive or that it depends exclusively on the phenomenon indicated but it does indicate the main content of the theory before modifications are made. The present theory has been included to indicate its position relative to the others. A brief discussion the main trends in the diagram is now presented.

Generally the lattice theories are concerned with the energy exchange between a gas atom and a harmonic nearest-neighbour restituitive lattice. Depending on the type of lattice employed they can be further broken down into those using one-dimensional (1-D) and those using three-dimensional lattices (3-D) lattices. Typical contributions to the former method have been made by Cabrera (Ref.15), Zwanzig (Ref.16) and McCarroll and Ehrlich (Ref.17) and to the latter by Goodman (Ref.18), Trilling(Ref.19) and Kinzer and Chambers (Ref.20). This kind of theory will be covered in more detail in section 2.3. Surface Temperature (or thermal) theories mainly concern the contribution to the energy exchange at the surface due to the thermal motions of the surface atoms. Representative work on this has been done by Goodman (Ref.6) and Logan et al(Ref.21) and it will be discussed in section 2.4. Surface field theories are concerned more with the overall form of the interaction potential due to the structured nature of the surface as distinct from other types which are essentially involved with one pairwise interaction with the gas atom. They can be subdivided into two groups: the integration theories which try to obtain approximations to the field and the simulation theories which basically perform numerical experiments on an assumed form of the potential. The work of Baule (Ref.22) and Erofeev (Ref.23) are typical of the former whereas the work of Oman et al (Ref.24) and Goodman (Ref.9) is of the latter type. As indicated in the diagram the present theory falls into this category. These theories are discussed in section 2.5.

The range of conditions under which these theories can be used is not well known at present. Where one type is sufficient or preferable to the others is not clear - there is a need for a gas-surface interaction number to separate these different "regimes". An obvious suggestion is the ratio of the gas energy to the surface energy, say E_g/E_s then:

$$E_g/E_s \gg 1 \quad \text{field theory}$$

$$E_g/E_s \gtrsim 1 \quad \text{thermal theory}$$

$$E_g/E_s \lesssim 1 \quad \text{lattice theory}$$

Clearly this is too crude and the boundaries are too indistinct, and of course, it does not consider the properties of the atoms taking part in the interaction. A more useful scheme has been proposed by Oman (Ref.39) in co-operation with Goodman, in which a hierarchy of applicability may be based on the powers of $\omega_n\tau$ (ω_n = characteristic frequency of the lattice and τ = a characteristic collision time for the interaction) that are significant for a particular case. This includes the energies and many other properties of the atoms in the interaction implicitly in the calculation of ω_n and τ. From this, in general, if the term in $(\omega\tau)^n$ is significant:

$(\omega_n\tau)^0$ field theory ($\omega_n\tau \to 0$)

$(\omega_n\tau)^2$ thermal theory

$(\omega_n\tau)^4$ lattice theory

This appears to be a very useful way of categorizing the regimes.

2.3 Harmonic Lattice Theories

In these theories the solid is represented by an array of atoms held together by nearest neighbour central forces i.e. "harmonic springs"; the array may be 1-D (in the direction of the surface normal) or 3-D. The gas atom interacts with the end of the line of atoms in the 1-D case or a selected surface atom in the 3-D case usually with a realistic potential function; this sets up what is in effect a wave train type of disturbance in the lattice which in part absorbs energy before the collision. The rest of the energy exchange is inertial in character and is concerned in the direct collision itself. It is of course an assumption of this type of theory that the former phenomenon is important and of significant magnitude for the cases considered.

The first theories were 1-D consisting of a semi-infinite chain of atoms joined together by harmonic "springs". This is the model that was considered by Cabrera (Ref.15), Zwanzig (Ref.16) and McCarroll and Ehrlich (Ref.17). Goodman has shown (Ref.18) that the restitutive properties of 1-D chains are fundamentally different from those of the 3-D lattice and therefore a 3-D model is necessary for physical reality. This view is now widely held and the 1-D model is used now only for situations including other effects which lead to problems too complex for the 3-D case (note the theory of desorption recently proposed by Goodman (Ref.26)). For this reason no further discussion of the 1-D case will be given here.

Goodman in an acclaimed series of papers (Ref's. 18, 27, 28, 6, 29, 30) has developed a 3-D lattice theory of great generality. A cubic lattice is used with harmonic spring forces in the direction normal to the surface and linear spring forces in the directions parallel to the surface. The method of solution is to calculate a response function which describes the motions of the lattice atom under a unit force (or impulse). There are in general three such functions for each atom corresponding to the three directions in the lattice - two of which are identical. It is then shown how to find the response function of an atom when the original force is applied to another atom in the lattice. A realistic potential function is used to model the interaction between the gas atom and the surface atom and the response functions of the atoms in the lattice are then summed over all the modes of the waves due to this interaction. The response functions are used in this connection in a manner analogous to Green's function. From this the energy of the interaction absorbed by the lattice results which gives the energy accommodation coefficient. It is found that when the α_e's so calculated are compared with experiment the agreement is very good for reasonable fitted values of the potential function parameters; this is done in Ref.28.

Extensions have been made to the original work; the effect of impur-

ities was investigated in Ref.27 and the effect of thermal motions in Ref.30. Other workers have made further modifications; for instance Trilling (Ref.19) has considered the case where the incoming gas atom is not normally incident on the surface, although the assumption of zero-impact parameter is retained as in the original work. Kinzer and Chambers (Ref's. 20, 31, 32) have treated a similar model with considerable mathematical ingenuity which gives essentially the same results as Goodman's. Recently work due to Karamcheti and Scott (Ref.33) gives weight to the speculation that the 3-D model may be more elaborate than necessary just for the calculation of α_e; they scaled experimental data on the basis of a 1-D elastic continuum model to fit a common curve for α_e - this is till under study. It may be that the α_e alone is not a sensitive enough function to require a 3-D model which of course is clearly the model of choice.

The lattice type theories do not attempt flux or velocity distribution calculations and are therefore not of great use in the solution of rarefied gas-dynamic problems. The momentum AC's are also not given by these theories and hence they cannot be applied to the satellite flight case. The reason for these omissions is that the theories are closely related to the thermal cell experiments done for example by Thomas and Schofield (Ref.34) and other workers. They find only the α_e of the system which is of interest in thermal conductivity work. Also since the interactions in these models are pairwise and there are no scattering mechanisms, in the spatial sense, such calculations are not possible.

2.4. Surface Temperature Theories

These theories are based on a paper due to Goodman (Ref.6). It concerns the calculation of 1-D distribution functions for the reflected gas atoms in terms of the surface temperature. In this model surface atoms are constrained to move in potential "boxes" with a 1-D Maxwellian velocity distribution normal to the surface appropriate to the surface temperature. The gas atoms make head-on hard sphere collisions with them in their line of motion. Since the surface atoms are constrained they may rebound after the initial collision and make further collisions with the gas atom before it leaves the "box". The authors of the work discussed in this section denote this occurrence as a multiple collision. Since this term means something different in the present work they will be called repeated collisions here. There appears in the analysis (Ref.6) various cases depending on the possibilities of the repeated and non-repeated collisions, each case being solved individually and contributing to the final calculation of the distribution function. Although this work cannot be applied directly to the problems under discussion it has many interesting aspects, one of which is that the Maxwell hypothesis about the accommodation coefficients (see section 2.1.2.) is not valid even for this comparatively simple case.

Logan and his co-workers (Ref.21, 35, 36) extended this method to a 2-D case. They assumed that the incident gas atom's velocity could be resolved into a normal and tangential component, the former interacts with the surface in the manner of the Goodman model above and the latter remains unchanged in the interaction. The variable velocity of the surface atom, which is in the general case a harmonic oscillator, gives rise to a 2-D flux distribution. The distributions so calculated show good agreement with experimental trends (see Ref.35); this is remarkable because there are no fitting

parameters involved in the simple model. It has been modified recently by Logan and Keck (Ref.37) to include a somewhat more realistic interaction potential (although the model remains essentially pairwise) which allows trapping and eliminates some difficulties concerning repeated collisions.

At present there appears to be inconsistences between this model and the field model of Oman (see the next section). Since the latter is more general and includes all the phenomena in the simpler model, it seems reasonable to assume that the temperature models should approach the general model in a certain range of energies. This does not seem to be the case at the moment with respect to the momentum exchange, the trapping fractions and other matters. The former difficulty may be explained by the fact that the above models, because of the assumption about the tangential energy, cannot produce satisfactory momentum AC's. This also precludes their contributing to the satellite aerodynamics problem. The surface structure question is avoided in these models and it may be that there is an averaging procedure of some type occurring in the range of the experiments which enables it to be neglected. In some recent comparisons with experiment however the flux distributions predicted by the theory are considerably narrower than those found experimentally (Ref.3) and there is some theoretical attempt to include surface roughness (Ref.37). The best test of these theories may be their ability to predict the correct values of the absolute intensities expected from experimental determinations of the flux; the velocity distributions will probably provide the ultimate test of these theories. These questions cannot be settled at the moment because of the lack of relevant experimental data.

2.5. Surface Field Theories

The first theoretical attempt to calculate the energy AC was due to Baule (Ref.22) in which he applied approximations to an array of hard spheres. A somewhat more general calculation in the same vein was done by Erofeev who in addition calculated flux distributions and momentum AC's (Ref.23). However, in these theories some rather drastic approximations are used; the only way of determining their validity is to do the full calculation. The results of the present model will show that in fact some of these approximations introduce large errors.

The most complete classical model of gas-surface interactions is that of Oman and his co-workers (Ref's. 24, 25, 8, 39, 40). The surface is assumed to consist of a small array of atoms embeded in a semi-infinite solid; the atoms have a realistic potential function in their interactions and the solid remaining is represented by an integrated potential function. This is the only model discussed up to now which has more than one surface atom interacting with the gas atom at the same time. The three dimensional mechanics of the trajectory problem results essentially in a series of implicit integral equations which must be solved stepwise by numerical methods. Oman has used a wide variety of conditions in this model such as trying solids consisting of harmonic oscillators both coupled and uncoupled, realistic surface temperatures, other types of potentials etc., to study the relative importance of these phenomena. Indeed this work has been quoted by many authors in connection with neglecting (or including) various effects in formulating other theories - the present writer is no exception to this. It can be said, in a real sense, that since this model is the most general, every model is in some way an approximation to it under certain conditions and hence should predict similar results in the range of validity of the approximation.

In fact, the essential difficulty with this model is that it is so complex. This is a disadvantage for two reasons. Firstly, one would prefer to have a simpler model in order to clarify the physical mechanisms in an easily understandable way and in order to facilitate the derivation of simple closed form expressions for the functions of interest. Secondly, the calculations described above require long computation times which limits the number of trajectories available for study especially with respect to the distributions of interest. Recently Oman (Ref.40) has introduced some statistical methods for approximating these functions but it still seems desirable to have as many trajectories as possible for these calculations.

An attempt to overcome these problems was made by Goodman (Ref.9) who used an array of hard spheres in a manner similar to the present work. In fact Goodman's work can be regarded as a special case of the present theory when the surface attractive field is zero. Goodman's paper appeared during the course of the present work and provides corroboration in that, in the limit of zero attractive field, the present work reduces to this case.

2.6. Quantum Mechanical Theories

No attempt will be made here to discuss in detail the various quantum-mechanical models proposed for the problem at hand, for this, the reader is referred to the recent review of Beder (Ref.41). However, one can make the point that up to now there is no definitive answer to the question; where can the classical mechanics approximation be used in the gas-surface interaction problem? It seems that the approach of Howsmon (Ref.42,43) is the most general and likely to provide the answer to the question. However, as yet the numerical results needed for the precise definition of the limits in question have not been obtained from the analytic solution given by Howsmon(Ref.43) because of the formidable complexities of the calculation.

One can point out some facts which tend to suggest that classical mechanics may be used with safety in the satellite energy range. The first such argument is that the classical models have had some significant successes in experimental comparisons for energies generally an order of magnitude below the satellite energy range; it is apparent that quantum mechanical effects are not grossly in evidence in these experiments. It may be that there are effects present which might be detected by more sensitive experiments,but this remains to be seen.

The magnitude of the deBroglie wavelength for satellite energies (e.g. for 1 ev Ar on a tungsten surface the de B. wavelength is about 1/72 of the lattice spacing) suggests that diffraction effects may not play an important part in the reflection process at the surface for these energies. In a typical case the energy exchanged at the surface will be of the order of many lattice phonons for satellite energy gas atoms which suggests that the quantum mechanical nature of the solid may not make itself felt in such an interaction.

The above are however merely plausibility arguments and although suggestive they are not sufficient to answer the question under discussion which must be considered still open.

III. ASSUMPTIONS OF THE MODEL

3.1. Introduction

The purposes of the model proposed here are fourfold:

(i) to incorporate approximations which are appropriate in the satellite energy range and which have adequate physical realism

(ii) to provide a formulation in terms of which experimental data can be easily interpreted

(iii) to produce enough information for the accurate computation of the quantities of interest and in particular for the calculation of the distributions

(iv) to provide a suitable basis from which analytic (closed -form) expressions can be developed for use in rarefied gasdynamics and particularly in satellite aerodynamics

It is clear that none of the previous theories meet all these criteria, some are clearly superior in one aspect or more but none fulfill them all. Of course the paucity of experimental data leaves many questions open. Before trying to achieve (iv) one has to show that (ii) has been done satisfactorily and hence presumably (i) and (iii) have been accomplished. This cannot be established for any theory (in the satellite range) at the present time and therefore one must concentrate on (i) and (iii) and attempt to find agreement with the experimental data available; this is what will be done in the present work.

Before starting a detailed discussion of the model it is convenient to outline the assumptions for orientation. The main thesis of the model is that the major mechanisms governing the interaction at satellite velocities are firstly,the topological variation of the surface field and secondly, the presence of the attractive field of the solid. The surface is taken to be a perfect array of spheres, in the case considered here a square array corresponding to the (100) face of a body-centered crystal. The thermal motions of the surface are neglected as are the effects of the forces between the surface atoms themselves, that is, before a collision they are motionless and free-floating (i.e. unaffected by the other surface atoms). The repulsive inertial part of the interaction is simulated by a hard sphere collision at a radius of interaction which in general may be determined from the high energy limit of a realistic interatomic potential function. This part of the problem reduces to calculating the variation of the impact parameter for the hard sphere collision over a representative area of the surface; it turns out that in the general case this must be done numerically. This three-dimensional variation is basic to the calculation of realistic scattering intensities. The attractive field of the solid is assumed to be smooth (i.e. acting in the direction of the surface normal only with no variation along the surface) in the context of the relative magnitude of the incoming gas atoms' energies. Other than this the attractive field of the solid is not further described; the parameter which characterizes it is the ratio of the incoming gas energy to it. This taken together with the interaction radius mentioned above, comprise the two basic variable parameters of the model. (Aside from the mass ratio and the usual angles which in practice are fixed by experimental conditions and hence cannot be varied). This attractive field accelerates the incoming gas atoms and decelerates the reflected ones. It may also happen that

the gas atom cannot overcome this field to escape and this leads to trapping and other associated phenomena. The trajectories which result from the above calculations may then be averaged and sorted to produce the functions of interest.

The remainder of this chapter will be devoted to covering these assumptions in detail. To organize the discussion they are broken down into the following statements (after each appears the section in which it is treated):

1. The validity of the classical mechanics approximation is assumed for the satellite energy range.(This is an open question and it cannot be proven or disproven at present. Some arguments for this point of view have been indicated in section 2.6).

2. The surface is assumed to be an ideal crystal plane with no imperfections. The surface atoms have no initial velocities or displacements before collision. (section 3.2.1.).

3. The surface atoms interact with the gas atoms as completely decoupled particles. Forces between the surface atoms are negligible in the collision problems. (section 3.2.2.).

4. After undergoing a collision and before the next collision a surface atom assumes its original state as described by 2. above. (section 3.2.3.).

5. The repulsive part of the interaction is represented by a hard sphere collision at an appropriate radius of interaction and with an impact parameter determined from the geometry of the collision. (section 3.3.2.).

6. A smooth solid attractive field acts on the gas atoms. It's strength is characterized by the ratio of the incoming gas energy to it. (section 3.4.2.).

3.2.1. The Surface before the Interaction

Assumption 2 consists of two statements: the first of which is that the surface is assumed to be an ideal crystal plane with no imperfections. This is almost the state of current work in the preparation of crystal surfaces; nearly perfect surfaces are now available to experimenters, for instance, the crystals used by O'Keefe (Ref.3) are of this type. Hence this statement is reasonable in the context of recent work, however, there are methods of incorporating gross surface irregularities if this becomes necessary (such as in the case of so-called "technical" surfaces which are produced by standard machining methods). One such scheme has been proposed by Healy (Ref.44). There are no conceptual difficulties presented by this problem although, care must be taken to get an adequate representation of the surface roughness.

The second part of assumption 2. states that the surface atoms have no initial displacements or velocities before collision. There are two possible sources of surface disturbance: the first is clearly due to a previous collision with a gas atom and the second is due to the thermal vibrations of

the solid. Discussion of the first point is deferred to section 3.2.3. and in fact, the content of assumption 4. (therein covered) is that there will be negligible disturbance from previous collisions. The main point at issue here therefore is the thermal behaviour of the surface.

Several authors have pointed out that the motions of surface atoms due to thermal effects are different from those of bulk atoms (Ref's. 45, 46, 30) due to the asymmetric bonding at the surface. Wallis (Ref.45) has shown that the mean-square displacement of a surface atom is generally greater than that of a bulk atom using a 1-D chain lattice model of the solid. This was confirmed experimentally by MacRae (Ref.46). However, this model is not sufficient for good estimation of these effects, for this one must refer to Goodman (Ref.30) where the problem is considered in terms of a 3-D lattice theory (see section 2.3.). This is a quite sophisticated analysis involving a fairly realistic lattice: the effect of thermal motions are evaluated in terms of the correlations between the modes set up in the lattice. In order to calculate the velocities at low temperatures a quantum-mechanical model is used to take into account zero-point phenomena. Fortunately for the present considerations Goodman has given numerical examples for tungsten lattices (because of course this is the metal most often used as the scatterer in gas-surface interaction experiments); it was found that at $0^{\circ}K$ the root mean square displacement and velocity of a surface atom in the normal direction were about 0.028 A and 65 m/sec respectively. The values at room temperature (about $300^{\circ}K$) were approximately twice the above. The corresponding quantities for directions parallel to the surface are somewhat smaller than those quoted for the normal direction. Thus in the range of temperatures likely to occur in satellite-surface interactions (see section 2.1.1.) it follows that the RMS displacement of a tungsten atom is at most about 2% of the lattice spacing, hence it is reasonable to neglect initial thermal disturbances in this problem. In fact, Logan et al (Ref.35) have shown that they can be neglected even in a thermal theory! An RMS velocity of 130 m/sec corresponds to an energy of approximately 1.6×10^{-2} ev; this is significant in the context of the thermal theories where the incoming gas energies are of the order of a few tenths of an ev. However, for the satellite case considered here at worst (high surface temperature and low end of the energy range (1 ev)) the incoming gas energy is about 60 times the surface energy. Oman (Ref.39) has also found that the effects of the surface thermal vibrations are only significant when the surface temperature is comparable to the incoming beam temperature. Therefore, it is reasonable to neglect the surface velocities in the light of this for the present model.

3.2.2. The Surface During Collision

Referring to assumption 3. it states that the surface atoms interact with the gas atoms as completely decoupled particles or stating it another way that forces between surface atoms are negligible in the collision problem. In terms of the lattice models of section 2.3 the opposite view from them is taken here namely that the inertial effects are far more important than the lattice effects for the present energy range. Roughly speaking this happens when the speed of the gas atoms is so great that the springs in the lattice do not have time to react significantly before the collision is complete. A crude calculation illustrates this point: Suppose the gas atom has satellite velocity (for the purposes of argument say, 7×10^{13} A/sec (section 2.1.1.)) and the characteristic frequency of the lattice is about 10^{12} /sec (Ref.47).

The gas atom travels about 70 A in one period but most of the energy exchange will take place in the last few angstroms hence the response of the lattice atoms is confined to a fraction of a period at most.

A more refined study of this problem has been given by Oman (Ref.39). He was looking into the differences between his independent oscillator lattice model and his coupled oscillator lattice model (for short IOL and COL) the first of which is an Einstein lattice of the type considered by the thermal theories (see section 2.4) and the second a 3-D lattice of the kind discussed in section 2.3. Fortunately Oman has given not only an approximate analysis of the differences between these and the hard sphere model but he has also included a table from which one can deduce these values for various gas-surface types. For tungsten with satellite velocity gas atoms one gets errors of 5% by not using the IOL model and of about .2% by not using the COL model. As he says " (the energy exchange) is always less than the hard sphere limit " (for the IOL model) and hence errors will be introduced by using the hard sphere limit. The justification for accepting these errors is that they are relatively small in the satellite case and the gains in flexibility and simplicity of the resulting model are relatively great.

3.2.3. The Surface After the Interaction

Assumption 4. states that after a collision and before the next collision the surface atom struck resumes its original position. This is based on the flux levels usually found in satellite flights and their simulation by molecular beams; it was shown in section 2.1.1. that a flux of 10^{15} molecules /cm^2/sec implies that each surface atom (or target area), on for instance, a tungsten surface, is hit about once per second. This means in effect that the surface atoms have ample time to dissipate their energy obtained from a collision into the lattice and hence collision events on the surface are decoupled. This result can be shown in a more quantitative way by considering the three dimensional lattice model of Goodman discussed in section 2.3. As was explained there he has calculated response functions which reflect the motion of lattice atoms under the influence of a unit pulse of energy. It was found as one would expect that the main part of the motion occurred in a few periods of the lattice and died out in a rapid way as the time after the event increased. Assuming that the natural frequency of the lattice is of the order of about 10^{12} per sec and making the conservative assumption that all the nearest neighbours of a struck atom are excited with it for one hundred lattice periods after the collision then the probability of an incoming atom striking a disturbed atom is about one in 10^7.

The threshold for the penetration of rare gas ions into tungsten has been found by Kornelson (Ref.48) to vary from about 10 ev for helium to 120 ev for xenon, these are the smallest energies at which any penetration can be found. Hence at satellite energies there is very little possibility of the lattice being disrupted by the interpenetration of beam atoms. The other source of disruption of the lattice is sputtering, however, this is again unlikely because the binding energy of a tungsten to a tungsten solid is of the order of 8 ev (Ref.47). Such an energy would have to be applied in the direction of the outward normal to detach the atom which is improbable at satellite energies. Therefore it can be seen that lattice destruction is not a problem at the present energies.

It should be noted in connection with assumptions 2,3, and 4

that they refer to the absence of spring effects in the collision problem only and do not mean . there are no springs at all. If this latter statement were the case, then obviously assumption 4 would not be possible,for then no mechanism would exist to carry away energy from the surface. Although this may seem a semantic point it has a valid physical significance.

3.3. The Interaction-Repulsive Part

3.3.1. Interatomic Potentials in Free Space

This problem has been studied for some time not only for its basic importance but also in particular for its connection with the properties of real gases. Such properties of gases and liquids as viscosity, thermal conductivity and the equation of state depend on the nature of the potential acting between the constituent atoms of these systems. What is often done is to assume a form of the potential and then to calculate macroscopic properties of the gas in terms of the parameters of the function, thereby a method of finding values for these parameters results. This type of work is discussed in detail by Hirschfelder, Curtiss and Bird (Ref.10).

The best established functional form for the potential is a difference of attractive and repulsive parts which is what is indicated by physical intuition. The London dispersion theory (Ref.10) is often used to derive the attractive portion of the potential. This explains the attraction between neutral atoms by means of the mutually induced instantaneous dipoles which arise from the motion of their electron distributions. This motion may be time averaged to show that there is no permanent dipole moment; however, the dipole-dipole forces averaged over time give rise to an attraction of the form:

$$Cr^{-6} \qquad (3.3.1.)$$

where C is a constant and r is the distance between the atoms' centres. One can extend this calculation to higher induced moments such as dipole-quadrapole, quadrapole-quadrapole, etc, however, these are often neglected in practice (for more detail see Ref.10).

The repulsive part of the interaction arises in a more fundamental way from the forces resisting the interpenetration of electron clouds. The exponential or Born-Mayer form (Ref.10) is considered to be appropriate in this case:

$$C'e^{-k'r} \qquad (3.3.2.)$$

where C' is a constant as is k' and the r is the distance between atom centres. The "best" form of interaction potential hence appears to be a difference of terms of the type (3.3.1.) and (3.3.2.), this is basically the Buckingham or Exp-6 potential. Recent work due to Abrahamson indicates that this form is probably the most appropriate (Ref's. 49,50). However, there are problems with this potential involving a singularity and a relative scarcity of data for cases of interest. In practice one uses either the Lennard-Jones formula:

$$\Phi_{LJ}(r) = 4\epsilon\left(\left(\frac{\sigma}{r}\right)^{12} - \left(\frac{\sigma}{r}\right)^{6}\right) \qquad (3.3.3.)$$

or the Morse formula:

$$\varphi_M(r) = D\left\{e^{-2c(r-r_o)/\sigma} - 2e^{-c(r-r_o)/\sigma}\right\} \qquad (3.3.4.)$$

These equations are plotted for Ar/Ar self interaction in Fig.3.2. In the equation (3.3.3.): ϵ is the depth of the potential minimum (in ev) & σ is the distance for zero potential. In Eq..(3.3.4.) D is the well depth σ is the distance for zero potential and r_o is the location of the minimum potential and . where $c = \sigma a$. and a is a slope factor. These equations are constructed for purposes of mathematical convenience and although each contains some suggestion of physical reality they must be regarded as essentially curve-fitting formulae in the sense discussed above. Both of them have been useful, the Lennard-Jones in the properties of real gases (see Ref.10) and the Morse in the theory of metals particularly (e.g. Ref.51). They have been compared in the work of Konowalo and Hirschfelder (Ref. 52) to the effect that the difference between the Morse and Buckingham is small enough to justify the use of the former for most problems and there is little doubt that the Morse is the potential of choice except for the fact that when integrated it does not give the well-established inverse cubic form of the surface attractive field. This form has been indicated by several workers (see section 3.4.2.) and for this reason the Lennard-Jones function will be used in the present work for the making of attractive field strength estimates. It should be emphasized at this point that the present model does not really depend on the choice of a particular potential function in the calculations; however, for the purposes of some of the approximations, and calculations related to them, it is convenient to assume a particular potential function. This point will emerge with more clarity in later sections of this chapter.

The calculation of the parameters used in the above potentials is a matter for detailed discussion this is given in Appendix A.

3.3.2. The Hard Sphere Approximation

Assumption five indicates that a hard sphere potential is used to represent the repulsive part of the collisions at the surface. This is an assumption that is often used in atomic collision problems especially in kinetic theory (see for instance Chapman and Cowling (Ref.53)) and is sufficiently well-known to preclude an extensive justification here. However, it is worthwhile to obtain quantitative estimates as to its validity in the particular cases considered in this work.

Hirschfelder et al (Ref.10) have examined the approach of a Lennard-Jones potential to its hard sphere limit as the relative energy of the colliding particles increases. They showed that the deflection angle χ in a central potential can be represented as:

$$\chi(b^*,g^*) = \pi - 2b^* \int_{r_m^*}^{\infty} \frac{dr^*/r^{*2}}{\sqrt{1-\varphi^*(r^*)/g^{*2}-(b^*/r^*)^2}} \qquad (3.3.5.)$$

where the "*" indicates a normalized parameter; most of these parameters are illustrated in the insert in Fig.3.2. They are:

$r^* = r/\sigma$ = normalized interatomic distance

$b^* = b/\sigma$ = normalized impact parameter

$\varphi^* = \varphi/\epsilon$ = normalized potential energy

$g^{*2} = \mu^* g^2/2\epsilon$ = normalized relative kinetic energy

g = initial relative speed of the colliders

μ^* = reduced mass

To put g^{*2} in a form more compatible with the work following:

$$g^{*2} = E_o/\epsilon\ (1 + \mu) \qquad (3.3.6.)$$

where μ = mass of gas atom/mass of surface atom and E_o is the kinetic energy of the gas atom at infinity. Equation (3.3.5.) has been calculated in Ref.10 and the curve for $g^{*2} = 10$ is plotted in Fig.3.2. It can be seen that at this value the interaction is already well-approximated by a hard sphere limit with an interaction radius slightly smaller than the Lennard-Jones σ. Using the values of the Lennard-Jones parameters given in Appendix A one finds for the rare gas - tungsten systems:

System	E_o for $g^{*2} = 10$	Orbital Energy (200 km)
He/W	.409 ev	1.25 ev
Ne/W	.677 ev	6.35 ev
Ar/W	1.35 ev	12.5 ev
Kr/W	1.86 ev	--------
Xe/W	2.64 ev	--------

Hence this seems to be a reasonable approximation for satellite energies keeping in mind the cautions given in section 2.1.3. In fact the approximation may be valid at somewhat lower energies because the ϵ's used above maybe somewhat larger than is in fact the case, this is mentioned in Appendices A and B. Another instructive aspect of the figure is that the influence of the gas atom is effectively confined to one gas atom at a time and therefore a collision between a gas atom and a surface atom doesn't involve other surface atoms to an appreciable extent. This is useful for the considerations involved in assumption 3 because it illustrates that the initial collision has little effect on neighbouring atoms; in other words the collision of a gas atom with one surface atom has a negligible direct effect on its neighbours and hence they are not coupled by the collision itself. All of these results are not really surprising from an intuitive point of view and they are suggested by the form of the potential functions as can be seen in Fig.3.1.

One other phenomenon which has a bearing on this problem is the focussing effect which some authors have suggested (see Ref. 43 for instance) to account for certain of their results. By this they mean that the surface field may affect the incoming trajectories in such a way as to favour certain types of collisions, usually it is inferred that low impact parameter collisions (approximated by the zero impact parameter case) are preferred. This has been invoked to explain the success of certain of the lattice theories in spite

of their assumption of head-on collisions, however, this is not yet established and other explanations are possible (see section 2.3.). If in fact focussing is present there is at yet no description adequate to allow its incorporation into the present theory and therefore the question must remain in abeyance at this time.

Before leaving this question, it is worthwhile noting that the latest results of Oman (Ref.40) point to the validity of hard sphere collisions for high incident energies. He states (Ref.40) "it is encouraging to theoreticians to note that the cases tested at high E_i show scattering strongly suggestive of hard sphere mechanics". This is very likely the result of the approximation discussed above applied to the Lennard-Jones potentials used in his more general model.

3.4. The Interaction-Attractive Part

3.4.1. Remarks Concerning Physical Adsorption

Before discussing the model of the attractive field to be proposed in the next section, some relevant comments should be made about physical adsorption. For a full review of this extensive subject one can refer to the text of Young and Crowell (Ref.54) and for a state-of-the-art report the recent paper of Halsey (Ref.55). The present discussion is based on these references. Traditional physisorption work is involved with gases in equilibrium with surfaces in a well defined closed thermodynamic system. The usual experiment is to change one of the system parameters and after the new equilibrium is established to measure the effect on the adsorption. Most often the measurements are made for pressure changes and the well-known adsorption isotherm is produced; this is not only useful for practical purposes but is probably the most convenient experimental measurement hence much of the literature on the subject revolves around this function. Similarly the theoretical work concerns its prediction by thermodynamic methods. The best known of these theories are the Langmuir theory for coverages of a monolayer of adsorbate (or less) and the BET theory for multilayers. Although there are difficulties in these theories, especially the former, concerning the physical realism of their assumptions it has been found that the functional forms given for the isotherms can be used to successfully fit experimental data for many gas-solid systems. It must be emphasized however that these theories make no particular assumptions about the nature or magnitude of the surface field and therefore are not of much use in studying this question; although they do predict heats of adsorption there is no clear way in which they can be related to the surface field magnitude as has been pointed out by Young and Crowell (Ref. 54). There is also the more fundamental difficulty from the point of view of molecular beam experiments of determining how the thermodynamic system of traditional physisorption work can be related to them. On examination it is very difficult to see how the results of the latter can be applied to the former (except of course for background gases in equilibrium with the target) for the beam gas is not in equilibrium with the target as such and the definition of the thermodynamic system is difficult. The point of this, then, is that traditional physisorption work is not very helpful in obtaining information on the surface field from the point of view of the work considered here.

Turning the question, posed above, around one can ask what can molecular beam experiments tell one about physisorption? There are good reasons

for believing that a definitive theory of physisorption will contain a good description of the surface field. For instance, the so-called potential theories of physisorption such as the one due to Polanyi (see Ref.54) have been very successful. This theory assumes only that a surface field exists which varies in strength with distance from the surface. Even with this very limited hypothesis he was able to show that the isotherms of different gases on the same surface could be found from the knowledge of one of them. The theory of Frenkel, Hill and Halsey (Ref.54) also makes a similar assumption. However, the field is specified as being inverse cubic with distance from the surface; the results were good for cases in which there were several adlayers. Hence it is reasonable to assume that a full description of the surface field will lead to a more satisfying theory of physisorption than the traditional macroscopic theories. There are hopeful signs that a molecular beam experiment in conjunction with an adequate theory can provide the missing data since these beams will be affected by the field in their scattering. Using theory one can then propose and test models of the field and hopefully by comparison with experiment determine an adequate one on which a good microscopic theory of physisorption could be based.

There is another class of experiments which give important qualitative information on physisorption; field emission and field ion microscopy are typical of this type. These are familiar techniques which provide very good opportunities to study the physisorption process in detail as it takes place. Representative work of this type is that of Ehrlich and Hudda (Ref. 56) in which they studied rare gases on tungsten. Aside from the well-known information that adatoms have preferred sites and that different crystallographic planes adsorb at different rates there were several specific results which have a bearing on the present problem. The first was that the (100) crystal plane adsorbed the most of all the common plane types. Even for this plane however no adsorbed gases were observed at room temperature ($300^{o}K$) for example xenon was removed at $114^{o}K$ and argon at $64^{o}K$ so that it appears improbable that the trapping fractions of the rare gases will be high in molecular beam experiments, (note these values held up to the relatively high pressure of 10^{-5} torr). They were also able to make estimates of the heat of desorption (which will be discussed in Appendix B) and also the activation energy of diffusion of the gas over the surface which will be covered in the next section. In spite of giving this very useful data it is not clear how precise quantitative information on the field can be found using these methods; the same seems to be true for other methods such as LEED and soft X-ray techniques.

3.4.2. The Smoothed Attractive Field

Assumption 6 can be restated in more detail in the following terms: an attractive field composed of the effects of all the atoms in the semi-infinite solid acts on the gas atoms in a direction normal to the surface only; it is smooth in that variations parallel to the surface are assumed to have negligible effect on the interaction. No particular form is assumed for the field. It's magnitude is expressed by the ratio of the gas atoms' energy at infinity (i.e. before the potential is felt) to the energy of the field which is the energy added to an incoming gas atom in the direction normal to the surface on going from infinity to the surface. (It may also be defined in the outward direction by a reciprocal definition). This ratio of course will be different for various gas-surface pairs. This assumption is more general than

necessary since the functional form of the surface potential is probably inverse cubic with distance; this is the form given by all theories except for one (see Appendix B) and it has been verified by experiments of which the work of Bowden (Ref.57) is a good example. However, for the work below a precise form of the field is not needed and one would still be faced with the problem of getting good values of the field magnitude; the latter problem is discussed with numerical examples in Appendix B. This form of the potential is used to guide the selection and calculation of the estimates and it is also used to illustrate a point in section 4.5.3. below, but these are side issues and neither plays an integral part in the model.

The one point that is important from the point of view of physical realism is the assumed smoothness of the field; this will require some detailed discussion. It should be noted at the outset that the smoothness of the attractive part of the field only is at issue; the repulsive part may be quite structured as expressed by assumption 5. This question has been investigated for some time because of experimental evidence that adsorption varied according to the crystallographic plane considered and from point to point on a given plane. Theoretical work to explain these results has been undertaken by summing the pairwise potentials between a gas atom located at various sites and all the atoms of the solid. This leads to three dimensional sums which cannot be evaluated directly; before the availability of large digital computers approximations were used by Crowell (Ref.58), Hove and Crumhansl (Ref.59) and Drechsler (Ref.60). Later computations were done to evaluate the sums directly; this was done by Bacigalupi and Neustadter (Ref.61) for pairwise Lennard-Jones potentials. More recently Goodman (Ref.62) has done the same with modifications. These theories were partially successful in explaining the experimental data; they found that the potential map of the surface region showed significant variations with distance along and above the surface. It should be noted that the repulsive part of the potential was included and hence this variation was much greater than it would be for the attractive part alone. Furthermore, this variation rapidly decreased as the interaction radius became larger than the lattice spacing; this will be the case in most of the systems studied in the present work. Before leaving this method it might be pertinent to note that there is a school of thought that considers this type of calculation is missing the point (see Young and Crowell (Ref.54)) and what should be considered is the effect due to the population of free electrons in a metal. Some theories of this nature are discussed in Appendix B - notable among them is the work of Margenau and Pollard (Ref.63) who using a free-electron method found that the effect of the ionic cores on the attractive potential was of the order of five percent and hence their periodicity had only a small effect. However, there are problems with this theory and it is uncertain how much confidence can be placed in this particular result.

For the special case of rare gases on tungsten there is good experimental evidence for the smoothness approximation from the results of Ehrlich and Hudda (Ref.56). As will be recalled they found that the gas atoms were highly mobile at relatively low surface temperatures or that at a low level of thermal motion of the surface atoms the barrier to surface diffusion is overcome. This means that the adatoms are unable to distinguish between sites on the basis of energy and hence the variation of the surface field is apparently damped out at the distance of nearest approach of an adatom to the surface. It is plausible then to infer that the differences in the attractive potential over the surface are of the order of the energy of thermal motion or, from the conside ations of section 3.2.1., of the magnitude of less than

.01 ev and therefore it is reasonable to neglect their effect for satellite energy particles.

Hence it can be said in summary that it appears from present knowledge that the smoothness assumption is at least a reasonable first order approximation to the actual situation. Indeed it is difficult to justify the use of any particular form of the potential more complicated than this at the moment, as Halsey (Ref.55) says, "there is still no unambiguous information about the exact form of the potential function".

3.5. Extensions and Limitations

In this section each of the assumptions will be discussed from the point of view of its general validity and in particular to suggest how it might be relaxed or extended if necessary. These extensions are ones which are feasible without destroying the essential simplicity of the model but of course there are definite limitations on how far it might be stretched, they will also be indicated. These possible extensions have been gathered together in this section rather than including them in the previous sections so as not to confuse what actually was done with what could be done.

Considering each assumption in turn:

1. It seems reasonable to assume that any quantum mechanical model for this energy range will produce a significant inelastic scattering component. If this turns out to be the case then the present model may prove useful in the interpretation of the major effects involving this type of scattering in a simple way. However, the degree of validity of this approach will be determined when full quantum-mechanical solutions to the problem are available for comparison. Since such models are now in progress (see section 2.6.) it does not seem feasible or practical to attempt modifications to the present model to incorporate pseudo-quantum-mechanical effects in order to obtain a so-called semi-classical solution.

2. Although thermal effects do not appear to be important for the present energy range there are possible stratergies for incorporating them in the present model if one wished to extend its validity to lower energies, Goodman (Ref.9) has suggested methods of modifying the accommodation coefficients found in his hard sphere model which could be carried over to the present model with some modification. However, one would probably be more interested on the effects displayed in the distributions which from order of magnitude considerations would be greater than those felt by the AC's. That is as one approaches the range of significant thermal motions the distributions will likely be more sensitive to temperature than the changes in energy and momentum exchange might indicate. A line which could be taken in this problem is to perturb the zero surface velocity trajectories now used (i.e. from collisions with surface atoms with no initial motion) in accordance with an assumed distribution of surface velocities. The same sort of thing that is done by the thermal theories could be applied to the model but without the necessity of the simplications used in these theories. Since the present model is solved numerically this modification could be easily incorporated. These microscropic (or atomic) thermal effects discussed here should of course be distinguished from gross or bulk heating which may also occur in satellite flight and re-entry vehicles. This might arise from meteorite impacts or leading edge vaporization, for instance, in which case, the surface would experience very large fluxes and corresponding

heating. This is a formidable problem and it is not probable that the present model would contribute to its solution.

3. There will be small errors introduced into the model by neglecting spring forces in the collisions; these are accepted to keep the model simple. If it were desirable to extend the model to lower energies this effect could be introduced by some perturbation method such as was suggested for 2. above or there might be some mathematical way to simulate it perhaps based on the analysis of Oman (Ref.39). The utility of this type of modification would probably be in illustrating how much of an effect was felt from the springs rather than as a permanent feature of the model for satellite velocities; the same applies to the perturbation methods.

4. The assumption that the gas atoms are restored to their original positions before a subsequent collision would seem to valid for all systems of interest in satellite flight and molecular beam simulations. If it failed then it is difficult to see how any present model of gas surface interactions could hold true including this one. The only method which might be possible is to try to describe an equilibrium state of motion for the surface atoms and then perhaps proceed as for thermal motions. In this case the surface would have been "heated" by the gas collisions to some temperature. How to discover what this temperature would be theoretically appears to be a formidable problem. The comments about bulk heating and large fluxes made at the end of paragraph 2 above are also very relevant to this assumption.

5. The hard sphere assumption is flexible enough to account for changes in the potential function choice since no particular form is specified. This will hold for some range of energies and the values at which it is valid for the rare-gas-tungsten system considered here are likely somewhat conservative (see Appendix A). This should be a property of any physical attractive-repulsive potential function. The lack of information about the free-space-solid assumption allows room for speculation about possible unusual and hitherto unknown effects the existence of which might prejudice the validity of the model; what would happen then remains to be seen.

6. In regard to the attractive field assumption again, lack of information precludes an accurate assessment of the model's validity. The assumption that has been made is very general and it should at least be a first order approximation to the real case. From what is known at present, it is not an unreasonable one.

If the model does prove a good approximation to the real situation, then there are a variety of problems to which it might be applied. The most obvious of these is to other gas-surface systems and to other surface geometries which could be done with no modification to the assumptions and only minor changes in the calculations. Having done this, it is a short step to producing functions of interest for surfaces composed of different crystal planes in different orientations by averaging and weighting according to metallographic data. Similar methods for dealing with gross surface irregularities are possible and Healy (Ref.44) for instance, has indicated one approach. The more general problem of ion scattering could also be done since after neutralization which occurs above the surface one has the basic problem of the model again; of course, some corrections for image forces etc., may be necessary to the incoming trajectories. Collisions of a beam with gas adatoms already on the surface

might also be possible but careful consideration would have to be given to the model proposed; the same applies to the treatment of polyatomic molecules impinging on the surface.

Before leaving this section, the general limitations of the model having been discussed here and elsewhere, it is appropriate to note that there may be particular cases where the model breaks down. In a situation where one of the parameters is very small or very large in an otherwise valid case one or more of the assumptions might break down. Therefore this should always be kept in mind in the discussion of the results.

IV DETAILS OF THE MODEL AND COMPUTATION

4.1. Introduction

This chapter will discuss how the model is constructed in detail from the assumptions given in the previous chapter. Some of the parameters that will be used have been introduced previously we shall now list them and define others:

μ = massof gas atom / mass of surface atom

(Note that this is the definition used by Goodman (Ref.9) but the inverse of that Oman (Ref.8)).

E_o^* = incoming gas energy / attractive field energy of the surface = E_o/E_t

R^* = interaction radius / lattice spacing = R/d
where "R" is the distance between the centres of a gas atom and a surface atom when they are touching, "d" is the lattice spacing.

θ_o = incident altitude angle measured from the surface outward normal (the range of the reflected altitude angles is from - 90°. to + 90°. as a matter of convention - the incident angle on the range of the graphs is - θ_o)

φ_o = the incident azimuthal angle measured from the X axis of the Cartesian co-ordinate system defined by Fig's. 4.1. and 4.2.

This is then the basic parameter set and obviously the object of the calculations is to determine how the final conditions of accommodation, flux etc., vary with them. Of course for a comparison with experiment θ_o, φ_o, μ, d and E_o are fixed and there are only two disposable parameters namely R and E_t. So that essentially this is a two parameter model. It is convenient to think of the surface as an array of spheres of radius R* which helps to visualize the problem although this is not necessary mathematically. The pattern of this array depends on the crystallographic plane selected for study; the only case considered in the present work is the square array (Fig.4.2.) although any other array desired could be looked at with small modifications to the theory. The square array is typical of the (100) plane of a body - centered

cubic crystal such as tungsten; the notation of crystal types and planes can be found in standard texts such as (Ref.47) for example. Now turning to Fig.4.2, the surface is the XY plane, the origin is at the centre of an arbitrarily chosen sphere and the X and Y axis are taken along the principle directions as shown (these same definitions apply to Fig.4.1. too). The XY plane bisects all the spheres shown and the Z axis is the outward surface normal coming out the page in Fig.4.2. The interatomic spacing is d. This is the actual crystal spacing (d_ℓ) for a b.c.c. lattice (e.g. $d = d_\ell = 3.16$ for tungsten in angstrom units from Ref.47 but $d = d_\ell / \sqrt{2}$ for a f.c.c. lattice (e.g. d = 2.72 A for nickel from Ref.47). In terms of d the nearest neighbours of the centre sphere at (0,0,0) are, in the XY plane, centered at:

$$(0,d)\quad (d,d)\quad (d,0)\quad (d,-d)\quad (0,-d)\quad (-d,-d)\quad (-d,0)\quad (-d,d) \qquad (4.1.1.)$$

A target areas is defined by the dashed lines in Fig.4.2. it's vertices in the XY plane are:

$$(-d/2,-d/2)\quad (-d/2,d/2)\quad (d/2,-d/2)\quad (d/2,d/2) \qquad (4.1.2.)$$

Such an area can be drawn about each surface sphere so that the union of the set of all such areas is the XY plane and the intersection is null. Therefore all the possible geometrical situations that could be encountered in a collision of a gas sphere with the array are present in the analysis of one such area. Points in the target area, i.e. aiming points, are denoted as $P_i = (p_{1_i}, p_{2_i}, 0)$. The incoming trajectories will have a common set of direction cosines ℓ_o, m_o, n_o and will pass through P_i's uniformly distributed over the entire target area. (Note that ℓ_o m_o n_o are direction cosines and not direction numbers as is the usual notation).

The initial direction cosines will now be derived from θ_o and φ_o. Since only angles are involved we may without loss of generality take the origin as the aiming point. Referring to Fig.4.1. one selects an arbitrary point on the incoming trajectory R, this "R" is not related to the interaction radius. The projections of this line on the X, Y and Z Axis are OM, MN and NR respectively. Hence:

$$\ell_o = OM/RO \quad m_o = MN/RO \quad n_o = NR/RO$$

and

$$-\cos\theta_o = NR/OR = n_o; \quad \cos\varphi_o = OM/ON; \quad ON = OR \sin\theta_o$$

therefore

$$\ell_o = OM/RO = (OM/ON)\ (ON/RO) = -\cos\varphi_o \sin\theta_o$$

and since we are dealing with direction cosines:

$$\ell^2 + m^2 + n^2 = 1 \qquad (4.1.3.)$$

and so:

$$\ell_o = -\cos\varphi_o \sin\theta_o$$

$$m_o = -\sin\theta_o \sin\varphi_o \qquad (4.1.4.)$$

$$n_o = -\cos\theta_o \qquad (4.1.4.)$$

They are all negative because of the definition of RO. The general equation of a trajectory is given parametrically by:

$$(x - p_{1_i})/\ell_o = (y - p_{2_i})/m_o = z/n_o = \lambda \qquad (4.1.5.)$$

where $-\infty \leq \lambda \leq \infty$: the values of λ have a one-to-one correspondence with the points on the trajectory line. This can be rewritten:

$$x = \lambda\ell_o + p_{1_i} \quad y = \lambda m_o + p_{2_i} \quad z = \lambda n_o \qquad (4.1.6.)$$

4.2. The Incidence Problem

The problem here is to determine which sphere of the surface array an incoming gas sphere hits first on encountering the surface given its trajectory. This is called the "incidence problem" for brevity. Define:

$A = (a_1, a_2, a_3)$ = the centre of the surface sphere struck

$C = (c_1, c_2, c_3)$ = the centre of the gas sphere at collision

The criterion for impact is that CA = R. Let the trajectory be represented parametrically by Eq. (4.1.6.) in other words C which is a point on the trajectory corresponding to the centre of the case sphere on impact is denoted by a particular value of λ:

$$c_1 = \lambda\ell_o + p_1 \quad c_2 = \lambda m_o + p_2 \quad c_3 = \lambda n_o \qquad (4.2.1.)$$

The question is now, is there a value of λ such that

$$(c_1-a_1)^2 + (c_2-a_2)^2 + (c_3-a_3)^2 = R^2 \qquad (4.2.2.)$$

It is easily shown that this statement completely defines the problem. To find λ one substitutes Eq. (4.2.1.) into Eq. (4.2.2.) and using Eq.(4.1.3.)·

$$\lambda^2 + 2\lambda(\ell_o\delta_1 + m_o\delta_2 + n_o\delta_3) + (\delta_1^2 + \delta_2^2 + \delta_3^2) - R^2 = 0 \qquad (4.2.3.)$$

where

$$\delta_1 = p_1 - a_1 \quad \delta_2 = p_2 - a_2 \quad \delta_3 = p_3 - a_3 \qquad (4.2.4.)$$

The solutions of (4.2.3.) are:

$$\lambda = -(\ell_o\delta_1 + m_o\delta_2 + n_o\delta_3) \pm \sqrt{D} \qquad (4.2.5.)$$

where:

$$D = (\ell_o\delta_1 + m_o\delta_2 + n_o\delta_3)^2 - (\delta_1^2+\delta_2^2+\delta_3^2) + R^2 \qquad (4.2.6.)$$

(Note that in the planar surface array case a_3 and p_3 are always zero and are carried here for symmetry).

There are three possibilities depending on the sign of D:

(i) $D = 0$ two identical real roots - the trajectory is parallel to the tangent plane of the sphere through the point of impact

(ii) $D > 0$ two distinct real roots the conditions for impact are fulfilled for two values of λ

(iii) $D < 0$ conjugate complex roots-spheres do not collide

The above can be simply related to the impact parameter b which is defined as the closest distance of approach of the incoming particles trajectory extended from infinity to the scattering centre. The distance from A to the trajectory is:

$$b^2 = (\delta_1^2 + \delta_2^2 + \delta_3^2) - (\delta_1 \ell_o + \delta_2 m_o + \delta_3 n_o)^2 \qquad (4.2.7.)$$

so effectively:

$$D = R^2 - b^2 \qquad (4.2.8.)$$

and the interpretation of the cases is obvious.

The incidence problem for a given trajectory can therefore be solved by constructing a D for each possible A and testing its sign. There is however the question of the two λ's for case (ii). It is clear from the geometry that there will be two possible impact cases generally since the mathematical formulation does not contain the physical restraint that the spheres cannot pass through each other. The criterion is then to select the value of λ which gives the maximum positive value of c_3. This is of course where the concept of "first" arises that was mentioned in the incidence problem statement. It is also part of the reason that the model cannot be solved analytically in closed form for the value of A. Not only is the solution set discreet but there is this maximum problem.

A somewhat similar situation arises when one considers that for the same trajectory line there may be many geometrical intersections with various surface spheres above and below the XY plane. The solution is to select again the solution with the maximum positive value of c_3. It can be seen from this that several values of A must be tested to insure the correct solution. When θ_o is large, or equivalently the trajectory line makes a small angle with the XY plane, the gas spheres may hit surface spheres far from the target area. Hence, to estimate the location of the spheres involved in the impacts one can use Eq. (4.2.1.) in the form:

$$c_{1_i} = (\ell_o/n_o)\, c_{3_i} + p_{1_i} \leq (\ell_o/n_o)\, R + p_{1_i} \qquad (4.2.9.)$$

$$c_{2_i} = (m_o/n_o)\, c_{3_i} + p_{2_i} \leq (m_o/n_o)\, R + p_{2_i}$$

since R is the maximum value of c_3. Varying Eq's (4.2.9.) over the range of the P_i's one obtains an area on the XY plane in which the appropriate A's will lie and use them for the tests. One other possibility on initial impact is that identical λ's are found for two adjacent A's. This means that the gas sphere has struck two surface spheres simultaneously. This can only occur at the boundaries and the practical probability of it occurring is negligible; it is

avoided by choosing aiming points not on the boundaries.

After the initial impact, the details of which are discussed later, a gas sphere may or may not impact with another surface sphere. If it does such an event is called a multiple collision (note that this is not the same as the definition used by Goodman (Ref.6) and Logan and Stickney (Ref.21) - see section 2.4.). This is a more complicated case than the initial impact since the reflected trajectory may be inward or outward with respect to the solid. If it is outward, $n > o$, one chooses the minimum positive c_3 and if inward, $n < o$, the maximum positive c_3. It must be remembered that the first sphere struck must be eliminated from the solution set and that the new c_3 must be greater or smaller than the previous one (i.e. at the last impact) depending on whether $n > o$ or $n < o$ respectively. This process is repeated until the gas atom has completed all its collisions with the surface atoms.

4.3. The Analysis of a Collision

The collision of a gas sphere with a surface sphere is analyzed in this section. It is the usual and standard hard sphere situation and it is given here for purposes of clarity and notation.

Define:

m_1 = mass of the surface atom

m_2 = mass of the gas atom

$\underline{v}$ = initial velocity of the gas atom

$\underline{v}'$ = final velocity of gas atom

$\underline{U}$ = initial velocity of surface atom

$\underline{U}'$ = final velocity of surface atom

ψ = angle between the LOC (line of centres i.e. CA) and v

ψ' = angle between the LOC and $\underline{v}'$

Since the collision is assumed perfectly elastic and frictionless the only changes in momentum will occur through the LOC. The subscripts "$\parallel$" and "$\perp$" will denote components of velocity parallel and perpendicular to the LOC respectively. The geometry is shown in Fig. 4.3. Assuming the surface atom to be initially at rest (see section 3.2.):

$$U_{\parallel} = 0 \qquad U_{\perp} = 0$$

The conservation of momentum equations are:

$$m_1 U_{\parallel} + m_2 v\cos\psi = m_1 U'_{\parallel} + m_2 v'\cos\psi' \qquad (4.3.1.)$$

$$m_2 v \sin\psi = m_2 v' \sin\psi' \qquad (4.3.2.)$$

and for the conservation of energy:

$$m_1 U_{\parallel}'^2 = m_2 v^2 - m_2 v'^2 \qquad (4.3.3.)$$

To eliminate $U_{\parallel}'$: from Eq's. (4.3.1.) and (4.3.3.) are obtained:

$$U_{\parallel}'^2 = \mu (v^2 - v'^2) \qquad (4.3.4.)$$

$$U_{\parallel}' = \mu (v \cos\psi - v' \cos\psi') \qquad (4.3.5.)$$

Rewriting Eq. (4.3.4.):

$$\begin{aligned} U_{\parallel}'^2 &= \mu \left\{ v^2 (\cos^2\psi + \sin^2\psi) - v'^2 (\cos^2\psi' + \sin^2\psi') \right\} \\ &= \mu \left\{ (v \cos\psi - v' \cos\psi')(v \cos\psi + v' \cos\psi') \right. \\ &\quad \left. + (v \sin\psi - v' \sin\psi')(v \sin\psi + v' \sin\psi') \right\} \end{aligned} \qquad (4.3.6.)$$

the last term is zero from Eq. (4.3.2.) hence, comparing Eq. (4.3.6.) with Eq. (4.3.5.) gives:

$$U_{\parallel} = v \cos\psi + v' \cos\psi' \qquad (4.3.7.)$$

This form is general for elastic collisions. Substituting in Eq. (4.3.1.):

$$v' \cos\psi' = \left(\frac{\mu - 1}{\mu + 1} \right) v \cos\psi \qquad (4.3.8.)$$

and from this and Eq. (4.3.2.) is obtained:

$$\cos^2\psi' = \frac{\cos^2\psi (\mu-1)^2}{(\mu-1)^2 \cos^2\psi + (\mu+1)^2 \sin^2\psi} \qquad (4.3.9.)$$

To define the angles ψ and ψ' the λ of the previous section is used.

Define:

$$\lambda^2 = \sum_{i=1}^{3} (c_i - p_i)^2 \qquad (4.3.10)$$

$$R^2 = \sum_{i=1}^{3} (c_i - a_i)^2 \qquad (4.3.11)$$

$$S_1 = \sum_{i=1}^{3} (c_i - a_i)(c_i - p_i) \qquad (4.3.12)$$

Hence

$$\cos^2\psi = S_1^2 / \lambda^2 R^2 \qquad (4.3.13)$$

and from Eq. (4.3.9.):

$$\cos^2 \psi' = \frac{S_1^2(\mu-1)^2}{(-4\mu S_1^2 + (\mu+1)^2 \lambda^2 R^2)} \qquad (4.3.14)$$

The expression for the reflected speed can be found from Eq. (4.3.8.):

$$v' = v\left(\frac{\mu-1}{\mu+1}\right)\left(\frac{\cos\psi}{\cos\psi'}\right) \qquad (4.3.15)$$

4.4. The Direction Cosines After A Collision

The new direction numbers must be found now from the collision equations and the previous d.c.'s. The following additional notation is used:

ℓ, m, n = d.c.'s of the gas sphere before collision

ℓ', m', n' = d.c.'s of the gas sphere after collision

$\tilde{\ell}$, $\tilde{m}$, $\tilde{n}$ = d.c.'s of the LOC

(Note that ℓ,m,n may be ℓ_o, m_o, n_o if this is the initial impact or otherwise if it is the multiple collision case).

The first condition on ℓ',m',n' is that the angle between the outgoing trajectory and the LOC is ψ' hence:

$$\ell' \tilde{\ell} + m' \tilde{m} + n' \tilde{n} = \cos \psi' \qquad (4.4.1.)$$

Since no changes in momentum can occur except in the plane defined by the LOC and $\underline{v}$ there can be no component of $\underline{v}'$ out of this plane. Hence $\underline{v}$, $\underline{v}'$ and the LOC are coplanar:

$$\ell' (\tilde{m}n - m\tilde{n}) + m'(\ell\tilde{n} - \tilde{\ell}n) + n' (\tilde{\ell}m - \ell\tilde{m}) = 0 \qquad (4.4.2.)$$

The final condition is dervied from Eq. (4.3.2.) and Eq. (4.3.8.):

$$\tan \psi' = \left(\frac{\mu+1}{\mu-1}\right) \tan \psi \qquad (4.4.3.)$$

Define: $\gamma = |\psi' - \psi|$ hence

$$\tan \gamma = \frac{2 \tan \psi}{(\mu+1)\tan^2\psi+(\mu-1)} \qquad (4.4.5.)$$

So we have:

$$\ell' \ell + m' m + n' n = \cos \gamma \qquad (4.4.5)$$

There are now three linear equations for ℓ',m',n' i.e. Eq's. (4.4.1.), (4.4.2.) and (4.4.5.). Solving by Cramer's rule:

$$\ell' = -[\ell F_1 - \tilde{\ell} F_2] / \sin^2 \psi$$

$$m' = -[m F_1 - \tilde{m} F_2] / \sin^2 \psi$$

$$n' = -[n F_1 - \tilde{n} F_2] / \sin^2 \psi \qquad (4.4.6.)$$

where

$$F_1 = \cos \psi' \cos \psi - \cos \gamma$$

$$F_2 = \cos \psi' - \cos \quad \cos \psi \qquad (4.4.7.)$$

This solution can be verified by substitution and Eq's. (4.4.6.) lead to a relation of the form of Eq. (4.1.3.) in ℓ', m', n'.

The method of solution is thus to find ψ and ψ' from Eq. (4.3.13) and (4.3.14) and to use these with Eq. (4.4.4.) to find γ. Of course care must be taken to insure that the correct signs are used in connection with ψ. However, the rules for this are obvious. In addition to knowing the d.c.'s of the outgoing trajectory one must also know a point on it for determining the multiple collision question. It is convenient for computational purposes to find the intersection of the trajectory with the XY plane, this point is called P_i' although of course, it may not necessarily be in the original target area. It is clear from Eq. (4.1.6.)

$$p'_1 = - \ell'/n' \cdot c_1 + c_3 \qquad (4.4.8.)$$

$$p'_2 = - m'/n' \cdot c_2 + c_3$$

It should also be noted that Eq. (4.4.3.) is a transcendental equation which is another reason that the calculations have to be done numerically.

4.5. The Attractive Field and Trapping

In this section the effects of the attractive field will be considered. The first of these is the effect on the incoming particles.

4.5.1. Incoming Particles

Denoting the attractive field energy as E_t the definition of E_o^* is

$$E_o^* = E_o / E_t \qquad (4.5.1.)$$

where E_o is the energy of the incident particles at infinity (i.e. before they are influenced by the field), hence, the energy of a particle after passing through the field is

$$E_s = E_o + E_t \qquad (4.5.2.)$$

The subscript "s" denotes conditions at the surface. Now the attractive field is applied only in the direction of the surface normal, hence, this increase is all in the normal component of the velocity. So using "$\parallel$" and "$\perp$" to denote components parallel and perpendicular to the surface and since the velocity is associated with the energy in the obvious way:

$$E_{s_{\parallel}} = E_{o_{\parallel}} \qquad (4.5.3.)$$

$$E_{s_{\perp}} = E_{o_{\perp}} + E_{t_{\perp}} \qquad (4.5.4.)$$

If the original incidence angle of the trajectory was θ_o (with corresponding n_o d.c.) then the new incidence angle at the surface is θ_s (n_s d.c.) from Eq. (4.5.3.) and Eq. (4.5.4.):

$$n_s^2 = \frac{n_o^2 + (E_o^*)^{-1}}{1+(E_o^*)^{-1}} 1 \;, \quad \ell_s = \frac{\sqrt{1-n_s^2}}{\sqrt{1-n_o^2}} \ell_o \;, \quad m_s = \frac{\sqrt{1-n_s^2}}{\sqrt{1-n_o^2}} m_o \qquad (4.5.5.)$$

It is clear from this that the new angle θ_s will be larger than θ_o and as $E_c^* \to \infty$ the effect of the field is negligible as one would expect. All the incoming particles will undergo the same deflection so that this offers no problem in selecting the target area; one merely chooses the trajectories at infinity which, after the correction, will cover the target area.

Note that in this section and in the following work that for convenience the velocity associated with E_o is unity i.e. $v_o = 1$.

4.5.2. Reflected Particles

The same sort of correction applies to the outgoing trajectories except that the field is subtracted. The prime superscript denotes reflected particles whose properties at infinity are denoted by the subscript "∞".

$$E'_{\infty_{\perp}} = E'_{s_{\perp}} - E_{t_{\perp}} \qquad (4.5.6.)$$

$$n'^2_{\infty} = \frac{n'^2_s - E_t/E_s'}{1 - E_t/E_s'} \;, \quad \ell'_{\infty} = \frac{\sqrt{1-n'^2_{\infty}}}{\sqrt{1-n'^2_s}} \ell'_s \;, \quad m'_{\infty} = \frac{\sqrt{1-n'^2_{\infty}}}{\sqrt{1-n'^2_s}} m'_s \qquad (4.5.7.)$$

However, it is immediately clear that some particles may not escape the field. Define an absolutely trapped particle as one for which:

$$E'_s < E_t \qquad (4.5.8.)$$

and to avoid possible complex roots in Eq. (4.5.7.) define a semi-trapped particle as one for which:

$$E'_{s_{\perp}} < E_t \qquad (4.5.9.)$$

$$E'_s > E_t$$

And of course, an escaped particle is one for which:

$$E'_{s_{\perp}} > E_t \qquad (4.5.10.)$$

$$(E'_s > E_t)$$

For these one merely applies Eq's. (4.5.6.) and (4.5.7.) to find the energy

and angle after reflection. The semi-trapped particles form an intermediate category; eventually such a particle must either escape or be absolutely trapped. Absolutely trapped particles can never escape the surface in this model, but ways of accounting for them will be discussed later on. Particle paths representative of these categories have been sketched in Fig.4.3.

4.5.3. The Semi-Trapped Particles - Direct Method

In this section a direct method of calculating the eventual disposition of the semi-trapped particles will be presented. Considering the physical aspects of the attractive field it can be seen that a semi-trapped particle will leave the surface and then come to a point where its normal velocity is zero at which it will curve back to the surface along a path symmetric about this point because the field only acts normal to the surface. Therefore, the angle to the surface, the energy and the direction along the surface are not changed. What is changed is the impact point and to find this one must know the particle range K.

It is clear that the velocity component parallel to the surface is unchanged; along the trajectory and measured above the plane $z = R = R^*d$, where the attractive field is assumed cutoff, the range K is:

$$K = 2\, v_{\parallel}' \sqrt{B} \int_{R}^{z_m} \frac{dz}{\sqrt{z^{-3} - z_m^{-3}}} \qquad (4.5.11.)$$

where

$$B = E_t / E_s' \cdot R^3 \qquad (4.5.12.)$$

and z_m is the maximum height of the loop (at z_m, $v_{\perp}' = 0$) which can be found from the equation:

$$v_{\perp}^2 (R) - B/R^3 = - B/z_m^3 \qquad (4.5.13.)$$

Having found these expressions one can find the new aiming points (p_1^*, p_2^*) which are in the XY plane from:

$$(p_1^* - \tilde{p}_1)^2 = \frac{\ell'^2 K^2}{(\ell'^2 + m'^2)}$$

$$(p_2^* - \tilde{p}_2)^2 = \frac{m'^2 K^2}{(\ell'^2 + m'^2)} \qquad (4.5.14.)$$

and where:

$$\tilde{p}_1 = R\,(\ell'/n') + p_1'$$

$$\tilde{p}_2 = R\,(m'/n') + p_2' \qquad (4.5.15.)$$

In all of the above formulae the primed variables refer to conditions in effect just as the particle passes through the z = R plane on starting the loop. It turns out that the integral Eq. (4.5.11.), is elliptic and reduces to incomplete elliptic integrals of all three kinds. This of course makes the numerical calculation of the range lengthy and complex. There is however, a more funda-

mental reason for rejecting this approach and that is that any small deviation in the horizontal smoothness of the surface attractive field would throw out the calculation. In other words the method is too closely linked to an exact knowledge of the surface field which is too uncertain (see the discussion of section 3.4.2.). Hence it will be necessary to use a less direct method of following the semi-trapped particles; this is presented in the next section.

4.5.4. The Semi-Trapped Distribution

This section outlines an indirect method of calculating the outcome of the semi-trapped particles. The first assumption is that the aiming points on re-impacting with the surface are randomly distributed meaning that any aiming point in the typical target area is equally likely. This is an approximation and it may be that in actuality certain portions of the target area are favoured (see the discussion on focussing in section 3.4.2.). The second assumption is that the azimuth angle has little effect on the values of the accommodation coefficients and the trapping probabilities. This is what is found from the computations. However, one could approach these quantities as being azimuth-averaged, that is, averaged over the range of azimuthal angles. Hence, if necessary all the quantities in this section may be considered as azimuth-averaged which is sufficient unless there are gross variations with azimuth angle. This might happen in the case of a "rough" non-coplanar surface array.

Having eliminated the azimuth angle one need only sort the semi-trapped particles by altitude angle θ and energy E. To construct the semi-trapped distribution (STD) one sorts the particles into the boxes:

$$E_i - \Delta E \leq E \leq E_i + \Delta E$$
$$\theta_j - \Delta\theta \leq \theta \leq \theta_j + \Delta\theta \qquad (4.5.16.)$$

A particle in this range will contribute to the ij-th component of the semi-trapped distribution (STD), in what follows the first subscript always refers to energy and the second to the altitude angle. In practice $E_i = i\tilde{k}E_t$ where $\tilde{k}$ is a factor depending on the magnitude of the energy range considered because it is best computationally to consider a fixed number of "boxes", usually $\theta_j = (j-1).10^o$, $\Delta\theta = 5^o$. Define the ij-th component of the STD:

$$t_{ij} = \frac{\text{no. of semi-trapped particles in ij-th range}}{\text{total no. of semi-trapped particles}}$$

The matrix of all such components is the STD .

Consider a typical case with incident energy and altitude k and ℓ then the calculations for this case will give:

$t(k,\ell)$ = STD for the case

$A_{k\ell}$ = the fraction of the incoming particles absolutely trapped

$S_{k\ell}$ = the fraction of the incoming particles semi-trapped

$G_{k\ell}$ = " " " " " escaped (gone)

It is clear from these definitions that:

$$A_{k\ell} + S_{k\ell} + G_{k\ell} = 1 \qquad (4.5.17.)$$

Now to discover which of the semi-trapped particles are ultimately absolutely trapped and which escape it is necessary to know the values of the above four functions for all the possible cases. The analysis proceeds as follows. The first process is to split the elements of the STD into components in order to simulate the conditions after re-impact with the surface, for a typical term t_{nm} in $t(k,\ell)$:

$$t_{nm} = A_{nm}\, t_{mn} + G_{nm}\, t_{nm} + S_{nm}\, t_{nm} \qquad (4.5.18.)$$

The first term is the fraction of the particles represented by this component that are absolutely trapped on re-impact, in the same way the second is the fraction escaped. The third term refers to the portion that are again semi-trapped, it indicates the relative weight that the nm-th STD distribution contributes to the "new" STD. In order to generalize this method define the Schur matrix product denoted by $\otimes$ for two matrices $A = \{a_{ij}\}$ and $B = \{b_{ij}\}$:

$$A \otimes B = \begin{Bmatrix} a_{11}b_{11} & a_{12}b_{12} & a_{1n}b_{1n} \\ a_{21}b_{21} \cdots\cdots\cdots\cdots & & \\ a_{n1}b_{n1} \cdots\cdots\cdots a_{nn}b_{nn} & & \end{Bmatrix} \qquad (4.5.19.)$$

This of course is not the usual matrix product. So the process (4.5.18.) for the whole STD:

$$\begin{aligned} t^{(a)}(k,\ell) &= t\,(k,\ell) \otimes A \\ t^{(g)}(k,\ell) &= t\,(k,\ell) \otimes G \\ t^{(s)}(k,\ell) &= t\,(k,\ell) \otimes S \end{aligned} \qquad (4.5.20.)$$

where G is the matrix of all G_{ij}'s etc, and $t^{(a)}, t^{(g)}$ and $t^{(s)}$ are defined. As is clear from the preceeding discussion one uses $t^{(s)}$ to construct the new STD $(t'(k,\ell))$ in the following way:

$$t'(k,\ell) = \frac{1}{U} \sum_{i,j}{}' t_{ij}\,(k,\ell)\, S_{ij} \quad [t\,(i,j)] \qquad (4.5.21.)$$

In order that $t'(k,\ell)$ be a true STD in the sense that it is normalized, one must divide each component by:

$$U = \sum_{i,j} t_{ij}\,(k,\ell)\, S_{ij} \qquad (4.5.22.)$$

For example, the actual number of particles represented by the nm-th component of t' (k,ℓ) referred to N as the total number of original particles is:

$$N\, S_{k\ell}\, t'_{nm}$$

$S_{k\ell}$ is carried throughout the calculation to get the correct proportions. In the same way the remaining matrices in Eq. (4.5.20.) are accummulated in the matrices:

$$W^{(a)}\ (k,\ell)$$
$$W^{(g)}\ (k,\ell) \qquad (4.5.23.)$$

which will be used to find the accommodation coefficients in the next section because in order to get the correct values of the final AC's one must know the details of the escaped particles as to energy and altitude angle which they had on leaving.

This process is then repeated Eq's (4.5.20) to (4.5.23) basically) until all the semi-trapped particles escape or are absolutely trapped. This method converges because:

a) the energy decreases after each collision and hence, the probability of absolute trapping increases for any given semi-trapped particle

b) in view of (a) a finite number of particles are reduced after each iteration and no others are added

4.6. The Accommodation Coefficients

4.6.1. Definitions in Terms of the Present Model

For the calculations it has been convenient to assume that the velocity associated with the incoming energy (E_o) is unity, i.e. $v_o = 1$. This does not change the values found for the AC's but it is reflected in the definitions which follow. Following Eq's (2.1.2), (2.1.3) and (2.1.4):

$$\alpha_e = 1 - \frac{\sum_i v_i^2}{N} = 1 - \beta_e \qquad (4.6.1)$$

$$\alpha_n = 1 - \frac{\sum_i v'_i \cos\theta'_i}{N \cos\theta_o} = 1 - \beta_n \qquad (4.6.2)$$

$$\alpha_t = 1 - \frac{\sum_i v_i' \cos(\varphi_i' - \varphi_o) \sin\theta_i'}{N \sin\theta_o} = 1 - \beta_t \qquad (4.6.3.)$$

The sums are taken over all particles at infinity, i.e. after the interaction is over. All the subscripts refer to conditions at this point except for the "o" which refers to initial conditions at infinity before any interaction with the surface. The β's are defined in the indicated way for convenience in the manipulations to follow. Using Eq. (4.1.4.) and its related expressions for reflected particles, Eq. (4.6.2.) and Eq. (4.6.3.) may be rewritten in terms of the d.c.'s:

$$\alpha_n = 1 - \frac{\sum_i v_i' n_i'}{N n_o} \qquad (4.6.4.)$$

$$\alpha_t = 1 - \frac{\sum_i v_i' (\ell_i' \cos\varphi_o + m_i' \sin\varphi_o)}{N \sqrt{1 - n_o^2}} \qquad (4.6.5.)$$

4.6.2. The Accommodation Coefficients from the Semi-Trapped Distributions

Consider the case k,ℓ discussed in section 4.5.4. as a typical example. The problem is to calculate the full AC's, that is, those in which the semi-trapped particles are taken into account (as distinct from the un-corrected AC's where this is not done, these terms will be used when presenting results since the latter values are of interest in charting trends). As indicated in the last section, the fact that the initial velocity for all cases is taken to be unity requires a correction to put the different energies of the cases on the same basis, this also applies to the altitude angles since they are involved in Eq. (4.6.2.) and Eq. (4.6.3.). Define:

$$I_{(e)}(i,j) = (E_i/E_k)$$
$$I_{(n)}(i,j) = (E_i/E_k)^{\frac{1}{2}} \frac{\cos\theta_j}{\cos\theta_k}$$
$$I_{(t)}(i,j) = (E_i/E_k)^{\frac{1}{2}} \frac{\sin\theta_j}{\sin\theta_k} \qquad (4.6.6.)$$

In view of Eq's (4.5.23) the total outgoing energy is when normalized (i.e. the corrected $\tilde{\beta}_e$,:

$$\beta_e(k,\ell) + \sum_{ij} \left\{ W_{ij}^{(g)}(k,\ell)\, I_{(e)}(i,j) \delta_e(i,j) / G_{ij} \right\} \qquad (4.6.7.)$$

$$+ \left[\sum_{ij} W_{ij}^{(a)}(k,\ell) \right] \times 0 = \tilde{\beta}_e$$

The zero in the last term refers to the assumption that the absolutely trapped particles do not contribute to the reflected energy. It is of course possible to assign, in practice, a temperature distribution to them on the basis of the surface temperature and to assume that the same number leave as are trapped per unit time. However, this is not within the scope of the present assumptions and is, in fact, not consistent with the work of section 3.2.1. A similar situation arises in the next section and the discussion continues there. Because of the energies involved however, and the number of particles absolutely trapped in this range the contribution of these particles turns out to be negligible in practice. The definition of Eq. (4.6.7) will therefore be used.

For the momenta one has:

$$\beta_n(k,\ell) + \sum_{ij} \left\{ W_{ij}^{(g)}(k,\ell) - I_n(i,j)\beta_n(i,j) / G_{ij} \right\} = \tilde{\beta}_n \qquad (4.6.8)$$

$$\beta_t(k,\ell) + \sum_{ij} \left\{ W_{ij}^{(g)}(k,\ell) - I_t(i,j)\beta_t(i,j) / G_{ij} \right\} = \tilde{\beta}_t \qquad (4.6.9)$$

/ in the calculation of the final accommodation coefficients is now obvious. Similarly the final trapping probability is:

$$A_T(k,\ell) = A(k,\ell) + \sum_{ij} W_{ij}^{(a)}(k,\ell) \qquad (4.6.10)$$

4.7 Distributions

In this section the construction of the distributions from the reflected trajectories will be discussed. Four such distributions are considered in the present work; the flux distribution which is the spatial distribution of the outgoing particles, the velocity mean distribution which is the distribution of the velocity means in space, the spatial momentum distribution and the velocity distributions which are the distributions of velocities at a fixed point in space. To clarify these definitions by example consider the spatial interval defined by the angular limits:

$$\theta_n - \Delta\theta \leq \theta' \leq \theta_n + \Delta\theta$$
$$\varphi_m - \Delta\varphi \leq \varphi' < \varphi + \Delta\varphi \qquad (4.7.1)$$

where the prime refers to a typical reflected trajectory. For brevity any particle which satisfies (4.7.1) will be said to lie in the nm-th "box". Now the nm-th component of the flux is merely the number of particles which lie in the box, usually this is divided by the total number of incoming particles for convenience and the result is called the normalized flux. The flux distribution is just the totality of all such components - the boxes covering all of the hemisphere in which reflection can occur. The nm-th component of the velocity mean distribution is formed by summing the velocities of the particles in the nm-th box and dividing by the number of such particles (i.e. the flux). Because of the definition v_o=1 in this work, each component is a number less than unity. The nm-th component of the momentum distribution is formed by summing the velocities in the box and then by dividing by the total number of outgoing particles. This may seem inconsistent with the flux definition given above, but the purpose of the calculation is merely to study how the momentum is carried away from the surface and the momentum distribution is hence expressed as percentages (of the momentum outgoing). The velocity distribution for box'nm' is formed by sorting the velocities of the particles there by magnitude so that one can make a statement such as: there are N_j particles with velocity v_j in box 'nm'. In this work the velocity distributions are given in terms of the fraction of the total particles in the box which have velocities in the interval indicated.

There are two methods used to define the intervals used for the sorting process. One has already been given in Eq's (4.7.1) , this is essentially by spherical co-ordinates and will be known as the angular mode. This is found to be very useful for getting an understanding of the three dimensional structure of the distributions, for example. The effect of the basic parameters on the width and spread of them can be investigated. The method is done for $\Delta\theta$ and $\Delta\varphi$ both 5 degrees and the boxes cover the whole hemisphere. The other method is the detector mode to indicate its similarity to the experimental situation. In this method the action of a particle detector is simulated, that is, the boxes into which the sort is made are of equal area, the ones in the angular mode

of course depend on angle and hence, are unequal. To characterize the size of the detector we use the following special definition of resolution which will always mean in the present work, the angular width of the detector azimuth limits when its centre lies in the XY plane. It could be defined as the angular width of the altitude angle since the boxes are in effect "square". Now since we work in direction cosines some manipulation is necessary to use the detector mode. For a reflected particle with direction cosines ℓ',m',n' to lie in the box centered on θ_i and within an angular width or resolution ρ:

$$\cos(\theta_i - \rho) > n' \geq \cos(\theta_i + \rho)$$
$$\left| m'/\ell' \right| < \rho \sqrt{1-n'^2} \qquad (4.7.2.)$$

In order to accommodate a situation in which the detector is inclined to the principal axis of the XY plane define φ_d as the angle the detector plane makes with the X axis in this plane (note the detector plane contains the incoming beam and the Z axis). Using the transformation:

$$\ell'' = \ell' \cos\varphi_d + m' \sin\varphi_d$$
$$m'' = -\ell' \sin\varphi_d + m' \cos\varphi_d \qquad (4.7.3.)$$
$$n'' = n'$$

and then use these new variables in the process (4.7.2.). In practice the resolutions used are 2,5 and 10 degrees.

The distributions may also be classified according to the particles which comprise them. The terms multiple and single distributions will be used to denote distributions consisting of only multiple particles (i.e. those which have undergone multiple collisions) and those which have had only one collision with the surface atoms respectively. The expression total distribution used in a context involving the above will merely mean the distribution of both taken together or the usual situation. The term primary distribution will mean the distributions containing only particles which escape without having been semi-trapped or absolutely trapped. Again, the problem arises of how to incorporate trapped particles into a full distribution arises in the sense that one would like to account for all the particles leaving the surface. Now although the assumptions used to calculate the semi-trapped distributions appear to be good for accommodation calculations, it is not clear how they would apply to the fluxes and other distributions. For this reason and the lengthy computation involved in producing a full distribution, in the order of hours on the computer, in addition to violating the no-temperature assumption it was decided not to attempt this at present. All the distributions in the present work are primary distributions. However, it is feasible when enough comparison with experiments indicate whether or not this theory as a whole is worth pursuing into additional levels of complexity. This does not prevent qualitative speculations on the effects likely to be seen when one does put the semi-trapped but later escaped particles in a distribution. This will be done in the later chapters.

4.8. Computation

4.8.1. Introduction

The incidence problem and the related problem of multiple collisions do not appear to have convenient analytical solutions as was explained in section 4.2, hence, it is necessary to attack the problem numerically. A series of computer programs have been written for this purpose to run on the IBM 7094 computer at the Institute for Computer Science at the University of Toronto. The problems encountered in the calculation are similar in many respects to those usually found in Monte Carlo solutions. It should be emphasized however, that the present work is not based on a probabilistic principle and hence, cannot be classed as Monte Carlo. Nevertheless, one has the same difficulties of keeping track of large numbers of particles and following them through a series of events (albeit deterministic in the present case). This is in contrast to the more usual situation in scientific computation when does a comparatively large amount of calculation on a relatively small amount of data such as, for instance, in the numerical solution of differential equations. For this reason one must be concerned with obtaining enough trajectories to reflect the result in the minimum of computer time, the major object of the programming is to achieve this.

In selecting appropriate stratergies to obtain distribution in the shortest computation time one must keep in mind the practical requirement of flexibility in the program which means in effect that the modular or subroutine method must be used. However, it takes a small but significant time to "call" subroutines and so a compromise must be made here. This is done by utilizing the maximum amount of core storage available in the machine, in the present program batches of 1,000 trajectories are done at once, requiring 10,000 words of storage, this means that each subroutine in the program is called once per 1,000 instead of once per trajectory giving a significant saving in computation time. Many other methods can be used to cut down the time if one has this consideration in mind when programming. For instance, in the sorting of the reflected trajectories the calculations give n' (i.e. cos θ') and instead of sorting these on the angle θ' (in degrees or radians) the cosine values are used to delineate the "boxes" (see the previous section). This in effect saves an arcosine step for every trajectory again giving a saving in time. There are several other places where time can be conserved by careful program design. The time to run the full program is generally less than one second per 100 trajectories (e.g. a run of 40,000 takes 6 minutes on the average) depending on the percentage multiple and other factors. This is a thousand-fold improvement in information, for the computer time used, as compared with the more general method of Oman (Ref.40) which produces about one trajectory in ten seconds.

The numerical accuracy of the program was not a problem because there was a relatively small amount of computation involved in each trajectory, certainly not extensive enough to introduce serious error. Hence, there was no need to use extended precision arithmetic or other devices to ensure accuracy as often happens in other types of scientific computations. In any case it would be absurd physically to quote five figure accommodation coefficients, for instance, in view of the assumptions made in the previous chapter. The precision used then is sufficient for confidence in the graphs shown in the following chapters. A related but different problem is whether enough trajectories have been used to give the maximum information, obtainable at reasonable cost, about the distributions. This will be discussed with illustrations in section 5.1.

The program was carefully debugged employing the usual methods of checking each subroutine with test values individually to ensure that the correct answers were given by each one. The overall results of the program were examined for consistency, symmetry and plausibility. The same was done for series of runs to ensure the trends which resulted were intuitively feasible and that no untoward circumstances arose. During the execution of the calculations internal checking devices were always in operation to look for unusual or special circumstances which possibly had not been allowed for in the programming. In addition to these conventional methods the fortunate circumstance mentioned in section 2.5 - namely that the no-attractive-field case of the model was done independently by Goodman (Ref.9) allowed a direct comparison with an independent calculation. The results of the present model agreed exactly with Goodman's in the no-field case. (The author is indebted to Dr. F. O. Goodman for providing him with a manuscript of this work which contains many more data curves than were published in the references cited and before the publication of his full repot (Ref.9)).

4.8.2. Outline of the Program

The purpose of this section is to show how the program is constructed in general terms. It consists of about 2500 FORTRAN IV statements in its full form and there seems to be little benefit to the reader in going over the program statement by statement. Not only is it unlikely to interest him but the author has found (at least from his own experience) that the time needed to understand the intricacies of a large program is comparable to the time one would need to write it. However, since the program (actually several programs) was a major portion of the work its central core in the most general version will be discussed to illustrate the methods used.

Figure 4.4. is a block diagram of the subroutine calling program. During the time of execution for a particular trajectory the following information is necessary to keep track of it:

$$(p_1, p_2, a_1, a_2, \lambda, \ell, m,n,v,j,(R^*))$$

where j is a particle status indicator which shows whether it is trapped and what collision the particle is undergoing (e.g. j = 996 means absolutely trapped after one collision, etc). R^* may or may not be carried for each particle although the former method was not used for the results presented in this work. This means that the storage required for trajectory information (1000 at a time) was 10-11 k (k=1000) words. An additional 3k was needed to other variables and distribution results. Taken together with the program and the system routines (arithmetic, IOCS and monitor) almost the entire 32k capacity of the computer was used. Each subroutine in the block diagram will now be briefly described so that it can be understood.

"MAIN" (main calling program)

This reads in the data from cards for the case or cases (the program can handle a sequence of cases varying on one parameter) to be solved. It then calls the subroutines in order and controls the loops X and Y in the block diagram. There are also a group of initialization instructions which prepare the accumulator areas. This subroutine has a number of instructions which call in the debuging utility ("BUGOUT") on request or automatically in case

There is also another option in this subroutine which will produce a similar printout (see Fig.5.2.2.) to show the final disposition of the trajectories (e.g. multiple and semi-trapped etc,). This is based on the final values of "j" and is called by "OUT" (see below). To avoid complications this routine can only be called for 30 by 30 grids.

"COLL" (collision)

This solves the collision problem based on the equations of sections 4.3 and 4.4. It contributes new values of ℓ',m',n',v',p'_1,p'_2. Hence these parameters are ready to be used for another collision should it be necessary.

"FINC" (following incidence)

This does the incidence problem for trajectories which are the result of "COLL" to look for multiple collisions. It tests the nearest neighbours of the surface atom involved in the previous collision for the trajectory under consideration by the methods indicated at the end of section 4.2. The status of the particle is set, according to the result, in "j". If a multiple collision is indicated new values of a_1,a_2 and λ are entered for the next pass through "COLL". In loop X the processing is done by type of collision , i.e. all first collisions on the first pass, all seconds on the second, etc. The parameter "j" is used to supervise this and avoid repeated calling of "FINC" when the particle has already been classed as finished colliding.

"DIS" (dispersion)

This program is concerned with the effects of the attractive field; it has two parts:

1) The effect of the field on the incoming as atoms. Corrects the initial direction cosines and velocity for field effects, as shown in Eq. (4.5.5.).

2) The effect of the field on outgoing atoms. Tests for trapping, accumulation of trapping numbers, production of the STD and corrections to the escaped trajectories are done according to the equations given in section 4.5.

"CONCL" (conclusion)

This program is concerned with the production of various percentages, averages and the accommodation coefficients. It is written in three parts:

1) This does the intermediate processing for each Y loop so that the information for each batch of trajectories is preserved. This part is called before the attractive field effects are applied by "DIS 2".

2) Similar to 1 except that the values after the attractive field is applied are found. This technique is useful for studying the effects of the field.

There is also another option in this subroutine which will produce a similar printout (see Fig.5.2.2.) to show the final disposition of the trajectories (e.g. multiple and semi-trapped etc,). This is based on the final values of "j" and is called by "OUT" (see below). To avoid complications this routine can only be called for 30 by 30 grids.

"COLL" (collision)

This solves the collision problem based on the equations of sections 4.3 and 4.4. It contributes new values of ℓ',m',n',v',p'_1,p'_2. Hence these parameters are ready to be used for another collision should it be necessary.

"FINC" (following incidence)

This does the incidence problem for trajectories which are the result of "COLL" to look for multiple collisions. It tests the nearest neighbours of the surface atom involved in the previous collision for the trajectory under consideration by the methods indicated at the end of section 4.2. The status of the particle is set, according to the result, in "j". If a multiple collision is indicated new values of a_1,a_2 and λ are entered for the next pass through "COLL". In loop X the processing is done by type of collision , i.e. all first collisions on the first pass, all seconds on the second, etc. The parameter "j" is used to supervise this and avoid repeated calling of "FINC" when the particle has already been classed as finished colliding.

"DIS" (dispersion)

This program is concerned with the effects of the attractive field; it has two parts:

1) The effect of the field on the incoming gas atoms. Corrects the initial direction cosines and velocity for field effects, as shown in Eq. (4.5.5.).

2) The effect of the field on outgoing atoms. Tests for trapping, accumulation of trapping numbers, production of the STD and corrections to the escaped trajectories are done according to the equations given in section 4.5.

"CONCL" (conclusion)

This program is concerned with the production of various percentages, averages and the accommodation coefficients. It is written in three parts:

1) This does the intermediate processing for each Y loop so that the information for each batch of trajectories is preserved. This part is called before the attractive field effects are applied by "DIS 2".

2) Similar to 1 except that the values after the attractive field is applied are found. This technique is useful for studying the effects of the field.

3) This is the final processing step for the values to be given in the final results. This is done after all the trajectories have been processed and consists of division to get averages, etc.

"FLUX" (flux and other distributions)

This subroutine constructs all the distributions. At the end of each Y cycle the trajectories in the batch are sorted according to methods given in section 4.7. There are a variety of options possible; the two major ones are: (i) detector mode 2,5 and 10 degree resolutions and (ii) the angular mode with 10 degree boxes which is capable of producing distributions consisting of non-multiples, multiples alone and both together, this is very helpful in distribution structure studies. The velocity distributions are found by method (i) for 10 degrees resolution in order to obtain enough trajectories per box.

"OUT" (output)

This does the preparation of the distribution for printing. It has several versions depending on the type of "FLUX" used. It also prints out all the results of the calculations as illustrated by the typical output sheet reproduced in Fig 4.5.

"RADS" (radius options)

This provides for the variation of the interaction radius by a variety of rules. It was used for some early studies in the work and although the present work has been done for one radius, which is constant throughout a case, the capability for variation has been retained.

In summary, the basic program works by means of the three important loops X, Y and Z. The last is used to reset the program to handle successive cases, the Y loop is used to process trajectories in groups to save time and allow for any number desired and the X loop is used to follow the particles in their various collisions with the surface.

4.8.3. The Iteration of the Semi-Trapped Particles

The basic method of computing a case as explained above is also used for the programs which calculate the corrected accommodation coefficients and the correct trapping fractions. However, several modifications are required in view of the large amounts of information needed for these calculations. It is clear from section 4.5. that one requires firstly all the G's, A's, S's AC's and STD's for a hundred cases which must be calculated and secondly, that they be available for calculations in the iteration process. Hence, some special techniques are required here.

The program is essentially one which repeats loop Z of Fig.4.4 without "FLUX", "IMAP" and a new version of "OUT" in addition to the iteration routines which follow. Now in order to make the calculation feasible from the computer time aspect, the number of trajectories needed for each case has been reduced to 400 per case making only one pass through the Y loop and the storage for trajectory information is thereby reduced to 4 k. In spite of this, one still must provide for the storage of about 12 k of the accumulated

results from the 100 cases solved: it is not reasonable to use auxiliary storage devices such as tape or disc because of the time needed for the large number of occasions on which they would have to be accessed during the iterations. Although overlap programming is a possibility it was found that the information could all be kept in core by noting that the STD's were sparsely occupied by non-zero values. In view of this, only those values needed to be stored with labels indicating their location in the STD they belonged to. To do this, routines were written which compressed each STD after calculation and which could produce the STD in its full form when required in the calculations. This stratergy was very effective and the whole process of doing a hundred calculations and the iterations took on the average about 7 to 8 minutes.

There is one further feature of this program which should be discussed. That is the concept of <u>equivalent incoming energies and angles</u>. It is clear for obvious reasons that one would like to deal with incoming angles and energies which correspond to the central values of the boxes used in the construction of the semi-trapped distributions. This means that these values must hold after the effect of the field is considered, i.e. after passing through the field region of Fig.4.3on the way in, since this is where the STD's are constructed i.e. just at the upper boundary of the collision zone. So the problem is: what values of energy and incidence angle at infinity give the required central value after correction for the field? These values are called the equivalent incoming energy and angle and may be found by solving Eq's. (4.5.2.) and (4.5.5.) in the other direction. It is clear from these equations that the angles will vary depending on the value of E_o^* so that a plot of a function of interest against must be adjusted for this effect. This can be done by cross plotting the function by angle on lines of equal E_o^*. Although this may appear to be a complicated way of doing things, it turns out to be much more convenient than the elaborate programming needed to account for the effect directly. It is also clear that the Eq's. (4.6.7,8,9) must be normalized in terms of the equivalent angles and energies. This was done in the program and was not shown in these equations since this process is an artifice for easy calculation and has no physical significance.

V. GENERAL RESULTS

5.1. Information and Resolution

It is very important to ensure that the results obtained in the following chapters are not spurious in the sense that they arise because of numerical effects, in other words one must use enough trajectory information to produce adequate and accurate representations of the functions of interest. The summed functions such as accommodation coefficients, trapping probabilities, etc., are not a problem and quite precise values are found which vary negligibly with increasing numbers of trajectories once more than a few hundred trajectories are included. For this reason most of these functions have been calculated on the basis of 400 trajectories although some are based on 40 k trajectories since they came from runs whose major purpose was to determine distributions.

This, of course, is not the situation with the distributions since many more particles must be employed to fix them adequately. Since there appears to be no a priori statistical scheme to indicate the number of trajectories needed for a distribution, one has to use trial and error methods. The most obvious of these is to find the distribution for increasing numbers of trajectories and to note how it changes if at all. This was the method employed here. A more or less typical case was chosen (Ar/W mass ratio*, $R^* = 1.2$, $E^* = 20$, $\theta_0 = 45^\circ$, and $\varphi_0 = 0^\circ$) and a range of trajectory numbers was calculated (10k, 23k, 40, and 81k) to see how the distribution changed. Of course there is no guarantee on the basis of one case that one can always use the same number of trajectories and get uniformly valid distributions for all cases but it was the practice during the present work to pursue any unusual or unlikely development in a distribution to higher trajectory numbers to verify its validity or eliminate it as spurious.

---

* The expression Ar/W mass ratio means that the value of μ (=.217 in this case) corresponding to argon on tungsten is used. While the result may or may not be correct for argon on tungsten (depending on whether or not the other parameter are chosen correctly), the policy of choosing mass ratios representative of reality has been followed so that experiment may more easily be related to these results.

Returning to the case mentioned above: in Fig. 5.1.1. the results found for the flux distributions are plotted for the four values of the trajectory number indicated. Deferring structure considerations until chapter 7 below and considering the distribution as the result of a series of numerical experiments one sees that there are only small variations in the data as the number of trajectories is increased. Surprisingly the 10 k case appears to be better (in the sense that it is closer to the 81 k case considered as best) than the 23 k case; there does not appear to be any specific reason for this and it may be fortuitous. The 40 k results appear to be a very good approximation to the 81 k values and hence to avoid numerical problems this was used as the standard number of trajectories (i.e. 40 k) for all the distributions calculated in the present work in view of computer time limitations. This was found to be sufficient in the calculations to insure a good degree of confidence in the results.

In Fig. 5.1.2. the same calculation has been done for the velocity

mean distribution; here we see that there is even less variation as the trajectory number is increased. This is due to the fact that if the mean velocities vary, in the geometrical sense, with a reasonable degree of continuity relatively fewer trajectories are needed to determine the average velocity more accurately than the flux level. It appears that for these distributions one could use considerably fewer trajectories than for the flux, however, since the velocity mean distributions were calculated in conjunction with the flux distributions they too are all based on 40 k trajectories. This is more than sufficient for accuracy.

Up to now the results that have been discussed have been for a simulated detector resolution of 10 degrees(see section 4.7 for a definition of this convention) it is interesting to note how changing the resolution changes the distribution. Fig. 5.1.3. shows the results for 2,5 and 10 degrees resolution for the above typical case based on 81 k trajectories. The 5 and 10 degree cases have been scaled by .16 and .04 respectively on an equivalent area basis for comparison on a convenient graph. As far as one can see on the basis of these results the gross shape of the curve is similar for all three resolutions but the 2 degree case shows some interesting peculiarities. Particularly with respect to the points from about 5 to 25 degrees in reflected angle one sees that there seem to be two flux levels that the distribution varies between. One is immediately tempted to invoke the numerical noise induced by having few trajectories per interval to explain this result.

In Fig. 5.1.4. the same process is repeated for the velocity mean distribution. Again it is found that it is much less sensitive than the flux distribution to changes in resolution for much the same reasons discussed above for Fig. 5.1.2.

The policy adopted in the chapters following was to determine the distributions for the 10 degree resolution case to avoid the numerical difficulties which would be introduced if one attempted to use a finer resolution. This is sufficient to indicate any gross structure and is a convenient reference standard for comparison with other work. Only if the distribution varies very strongly as one leaves the detector plane would one expect to find serious discrepancies between the 2 and 10 degree resolutions.

One other form of distribution remains to be discussed and that is of course the velocity distribution. To give an accurate determination of a velocity distribution requires many more particles in a geometric "box" than are available conveniently in this model. However, for the numbers available one can still see some of the salient features of these distributions and a discussion of these is all that is attempted in the present work. An indication of the number of trajectories typically represented in a velocity distribution is given by the bracketed numbers in Fig. 8.4.5 and there appear to be enough trajectories to justify the limited conclusions made in chapter 8. For this reason these distributions are, of course, plotted as bar graphs.

5.2 Impact Maps and Final Disposition Maps

Impact maps and final disposition maps were discussed in section 4.8. Basically, an impact map shows which surface atom an incoming gas atom initially impacts with, that is, it illustrates the solution of the "incidence problem" of section 4.2. The computer output of a typical map is shown in Fig.

5.2.1; this is for the same case as the computer output shown in Fig. 4.5. A final disposition map illustrates the outcome or eventual fate of the incoming trajectories mapped against their aiming points. The final disposition map corresponding to the impact map of Fig. 5.2.1. is shown in Fig. 5.2.2. (in the computer output the term "first" is used to denote single colliders). Before considering some maps in detail, the point should be made that maps were used as one method of checking the results for symmetry and consistency for a wide variety of initial parameters. One example of symmetry can be seen by glancing at Figs. 5.2.3. and 5.2.4; this is X-axis symmetry since $\varphi_o = 0^o$ for both figures. This was a very useful method which helped to verify the basic validity of the mathematical and numerical procedures used in the calculations.

Fig.5.2.3. shows the maps for three values of R*; these cases have Ar/W mass ratios and $E_o^* = 20$, $\theta_o = 45^o$, $\varphi_o = 0^o$. Two general points are immediately apparent: firstly, the impact maps show that the impacted surface atom is more frequently the origin atom as R* decreases, and secondly, the final disposition maps show that the interaction becomes more complex as R* decreases. Considering the R* = 2.0 maps in detail, it is observed that the semi-trapped trajectories (labeled "4") occur at aiming points just preceding the transition of the impacts from surface atom 2 to surface atom 1. It is clear for geometrical reasons that these particles make relatively glancing (high impact parameter) collisions with surface atom 2, hence, their reflected trajectories lie nearer to the surface compared to the other trajectories included in the zones labeled "0". Their normal components of velocity are therefore lower and they are semi-trapped. There are no multiples for this case since the interaction radius is quite large. Referring to the R* = 1.3 maps, the same sort of glancing collisions occur before the transition from surface atom 2 to surface atom 1. However, in this case, these glancing collisions belong to two classes: nearer the transition zone multiples appear and further from the boundary of the zone there are semi-trapped trajectories. The explanation for this is that the trajectories nearest the boundary are the lowest lying and because the interaction radius is smaller than the previous case they can make a further glancing collision with surface atom 2 and hence, be turned upward and escape. The semi-trapped particles preceeding do not lie low enough for a further collision but are low enough to be semi-trapped. It is a general observation that the semi-trapped regions and the multiple regions are related in this way. These same phenomena are present at the left-hand side of the final disposition map except that the next surface atom is involved. For the R* = 0.9 case the interaction is even more complex although again the same effects are present for the same reasons. Looking at these three sets of maps, it can be seen that the trends in them evolve in a consistent way as R* changes. However, since the analysis needed to produce the maps is so complex, it is unlikely that a closed form function could be found to describe the transformation of one map into another.

Fig 5.2.4. shows the maps for three values of mass ratio; the other parameters are R* = 1.3, $E_o^* = 20$, $\theta_o = 45^o$ and $\varphi_o = 0^o$. These cases all have the same impact map since it is not a function of the mass ratio. Comparing the three final disposition maps it is clear that the interaction becomes more complex as the mass ratio increases. In order to see how this develops, it is convenient to compare the Xe/W and He/W cases to the Ar/W case, using it as a reference. For the He case the semi-trapped regions are smaller because of the lower energy losses in the hard sphere collisions. However, the number of multiples is also smaller because the lower energy losses mean that the tra-

jectories do not lie so near the surface. This is illustrated by the regions near the right-hand side of the two final disposition maps. For the Ar/W mass ratio case, this region consists of a band of multiples which escape preceded by a band of semi-trapped particles. At the He/W mass ratio this multiple region has shrunk to a few points since the trajectories are higher because of the lower normal energy losses; they have been replaced by semi-trapped particles. Furthermore, some of the original semi-trapped particles are able to escape also because of the lower energy losses and hence the single-escaped region shown. Similar changes can be seen for the other parts of the He/W map. Turning to the Xe/W final disposition map, this region (corresponding to atom 2 impacts) now consists of all multiples because all the trajectories now lie low enough for a further collision because of the greater normal energy losses. The semi-trapped particles now dominate the interaction in this case because of these higher energy losses and indeed this is shown by the appearance of significant numbers of multiple colliders which are semi-trapped. It is interesting to note that no absolutely trapped atoms occur even for this high mass ratio; however, the reason for this will be discussed in section 6.1.

The above observations are quite useful for discussing many of the results noted in the following sections.

5.3. Multiple Collisions

Multiple collisions (of one gas atom with more than one surface atom) were found to play an important role in many of the results discussed below. This section will outline some of the trends characteristic of these particles.

Fig. 5.3.1. is a plot of the fraction of the incident particles having multiple collisions (M) as a function of μ for curves of equal R*: the other parameters are $\theta_o = 0^o$ and $\varphi_o = 0^o$ (E_o^* is not relevant here since $\theta_o = 0^o$). It was found that M increased with μ for a fixed R* and M increased with decreasing R* for a fixed μ. The former effect results from the larger number of trajectories which lie near the surface due to the greater losses in normal energy as μ increases. The latter effect is geometrical and results from the greater penetration of the incoming atoms into the spaces between the surface atoms as R* decreases. The curves in the figure indicate that at $\mu = 1$ M = 1 for all R*; this of course, is a physical consequence of the fact that all gas atoms (except perhaps for the exact head-on impact one) must have multiple collisions at $\mu = 1$.

Fig. 5.3.2. is a plot of M versus θ_o for two values of R*; the other parameters are Ar/W mass ration, $\varphi_o = 0^o$, $E_o^* = 0^o$. In connection with E_o^* one can extrapolate these results for any E_o^* value by calculating a value of θ_s using Eq. 4.5.5. and then reading M for θ_s on the figure; these results concern the hard sphere interactions at the surface and are not involved with the attractive field except in this way. Naturally the figure shows higher values of M for R* = 0.9 than for R* = 1.4 in accordance with the results of Fig. 5.3.1. The variation with θ_o is geometrical and depends on the areas on the surface spheres which are available for multiple collisions; in other words depending on the values of R* and θ_o (and also φ_o) certain of the surface spheres will be shadowed by other surface spheres. It is clear that for large θ_o an incoming atom will see only the tops of the surface atoms and hence will have few if any multiple collisions. For small θ_o the number of multiple

collisions depends on the size of the target area compared to the effective size of the spheres (determined by R*). Consider a beam of $\theta_o = 0^o$ particles impinging on a target area. If the projection of target area onto the sphere at the origin (i.e. the area on the sphere in which impacts occur) covers only a small area of the top of the sphere, multiple collisions would be rare; this is the case for large R*. If this projection, however, covered parts of the sides of the sphere then multiple collisions become likely; this is the case for small R*. The peaks in the curves can be explained as follows: for small θ_o the impact area is on the top of the sphere. As θ_o increases this projection moves down the side of the sphere and M increases, at some point in this process the projection starts to appear on the neighbouring sphere and glancing multiple collisions of the kind discussed in section 5.2. start to take place. This process reaches a maximum for some value of θ_o but then M decreases as θ_o increases since the impacts occur more frequently with the upper portions of the next sphere until at very high θ_o the incoming gas atoms only "see" the tops of the surface atoms and there are no multiple collisions. Hence the behaviour of the curves is as shown.

A measure of the complexity of the interaction process is the number of different types of collisions which are possible. Fig. 5.3.3. shows this complexity as a function of R* by graphing the proportion of the incoming particles which have a certain integral number of collisions with the surface atoms (these cases have parameters corresponding to Xe/W mass ratio, $\theta_o = 0^o$, $\varphi_o = 0^o$). It is clear from the figure that the interaction becomes more complex as R* decreases; for R* = 0.9 there is even a small but measurable number of particles which make 4 collisions with the surface atoms. Similarly Fig. 5.3.4. shows that the complexity increases with increasing μ. These trends are what one would expect from the foregoing work. However, they do illustrate two important points in conjunction with the results of section 5.2. Firstly, a single collision interaction model is not likely to give good results for distributions unless R* is very large and μ is quite small, and secondly, it will be very difficult to obtain approximate expressions for the distributions, except in simple cases, by other than empirical curve-fitting means. Furthermore, it seems that there is no substitute for a three-dimensional model either by a two-dimensional model or a one-dimensional model; it is quite clear from the maps of the previous section that the type of collision a particle experiences is determined by the position in the XY plane and not only by the point on the X-axis that it is aimed at. Hence, there is no doubt from these observations that a three-dimensional model is essential for the quantitative prediction of scattered distributions (this is not to say, however, that accommodation coefficients and the other averaged functions are not amendable to calculations using simple approximations).

VI. TRAPPING AND ACCOMMODATION

6.1. Semi-Trapping

The purpose of this section is to discuss the conditions which are in effect after the initial collision of each gas particle with the surface, that is before the iteration scheme of sections 4.5.4. and 4.6.2. is undertaken. The key process here is semi-trapping; as the reader will recall a semi-trapped particle is defined by equations 4.5.9. It is a particle whose total energy is greater than that of the attractive field but whose normal energy is less than that of the attractive field. In order to examine some of the features of this

process the results for the cases: Kr/W mass ratio, $E_o^* = 4.5$, $R^* = 1.3$, $\varphi_o = 0^o$ have been plotted as a function of initial incidence angle θ_o in Fig.6.1.1. Examining first the dashed curve which shows the probability of absolute trapping on the initial encounter with the surface it is seen that it has maximum at the normal and decreases rapidly as θ_o increases. This can be readily explained by noting that at near normal incidence the impact parameters are quite small and hence energy losses are quite large; as the incidence angle increases the impacts become steadily more glancing and the energy losses become smaller. Also comparing this curve to the total semi-trapped curve one notes that semi-trapping is much more prevalent than absolute trapping; this general conclusion is brought out more clearly in the subsequent results. Turning now to the curve of the total semi-trapped probabilities: it is composed of two components which have been plotted, these are particles that have had a single collision with the surface and those which have had multiple collisions. The fraction of multiple collisions has been plotted along with its complement, the fraction of single collisions, for illustrative purposes - it has the form expected from the discussions of section 5.3. With regard to the multiple component it is seen that a considerable fraction of the multiples are semi-trapped but more importantly a significant portion of them are <u>not</u> semi-trapped. This has been found to be an even more prominent effect for lower mass ratios and in fact it was observed for some cases that the probability of a particle being semi-trapped was greater for the single colliders than the multiples. This is because the overall average velocity of the multiples is often larger than that of the singles which is in turn due to the glancing nature of their collisions; this is discussed in more detail in chapter 8 below. This is an important remark in terms of the model of Erofeev (see section 2.5) who assumes that the multiples behave in a manner similar to absolutely trapped particles because in his model they are assumed to be re-emitted as a cosine distribution with the temperature of the surface; this is in spite of the fact that he assumes no attractive field. Whatever the general validity of the present model might be, it is in the limit $E^* = \infty$ the numerical solution of the situation that Erofeev approximates (this is also true of Goodman's model - see section 2.5). Hence even for a case where there is a substantial field, shown here, large numbers of multiples escape with obviously significant velocities so that Erofeev's approximation is quite poor, this will become very apparent in the next chapter. Another point is that there are no multiples absolutely trapped which again confirms the substantial velocities of the multiples. With regard to the curve of the singles semi-trapped it is observed to have an interesting structure with a definite peak at about 35 degrees. It is postulated that this was caused by three effects: (i) energy losses are greatest near the normal and decrease toward the surface tangent, the reasons for this have already been discussed above (ii) as θ_o increases the reflected trajectories lie nearer the surface and hence, have smaller energy components in the normal direction and (iii) particles which would ordinarily be semi-trapped are in the present case absolutely trapped due to the relatively high mass ratio and low incident energy used here. This leads to the peak shown. The form of the curve can then be explained in terms of these effects as follows: assuming the absolutely trapped particles to be a subcase of the semi-trapped, and therefore taking into account effect (iii) above, the curve decreases as θ_o increases due to effect (i) but at the angles near 60 degrees this is being counterbalanced by effect (ii) which starts to predominate from then on leading to an increase in the fraction semi-trapped as the surface tangent is approached. This then is the general situation occuring at the first encounter of the beam with the surface.

In order to show how S the fraction semi-trapped varies with the basic

parameters, curves of its variation with θ_o, R* and μ in conjunction with E_o^* will now be discussed (consideration of the φ_o variation is deferred to the end of this section). Fig. 6.1.2 shows the variation of S with θ_o for lines of equal E_o^* for the case Ar/W mass ratio, R* = 1.3, φ_o = 0°. (The half-integral values of E_o^* are a result of the process used for the treatment of the semi-trapped particles, see section 4.5.4). Here one sees the same form of curve discussed above in connection with Fig. 6.1.1 for the lower values of E_o^* but there is a gradual transition to another shape typified by the E_o^* = 20 curve. The explanation of this type of curve is thought to be that the effect (i) is not important here because the energy losses although still greatest near the normal are not sufficient to cause semi-trapping alone, the mass ratio is about half of what it was in the case above but more important the energy of incidence is now much larger compared to the trapping energy. Another effect that increases S for low E_o^* values is that the incoming trajectories are steeper, i.e. nearer the surface normal, and hence, the energy losses are greater. The increase in the curves as they approach the surface tangent are due to effect (ii) as before.

The effect of R* is shown in Fig. 6.1.3 as a function of E_o^* for the case Ar/W mass ratio, θ_o=45°,φ_o=0°. It is clear that S is a relatively weak function of R*. The difference noted, i.e. that S increases as R* decreases, is due to the fact that the energy losses and hence, S is greater because of the higher degree of particle deflection experienced at lower R*'s. This leads to overall average velocities (i.e. the average velocity of all particles reflected from the surface) which are lower and hence, explains the observed trend. (Note that this refers to overall velocity average and is not in conflict with the situation in the detector plane discussed below in sections 8.1 and 8.2). The dashed lines indicate that absolute trapping is taking place at the same time as the semi-trapping for the range of E_o^* shown; this causes the sharp peak and this of course is explained by the discussion of effect (iii) above.

The effect of μ is shown in Fig. 6.1.4 for mass ratios characteristic of the rare gases on tungsten for the cases R* =1.3, θ_o=45°, φ_o= 0° plotted for values of E_o^*. (Recall that the convention in the present report is to use mass ratios corresponding to rare gases on tungsten however, as explained in section 5.1 an expression such as "Ar/W" only means that the mass ratio is .217 and not that the curve presented is intended to apply in a direct way to argon on tungsten - since for instance in Fig. 6.1.4 the five systems may in general have different R*'s). It is clear that semi-trapping has a strong dependence on the mass ratio, this is of course because the fraction of energy lost in a hard sphere collision is a strong function of the mass ratio. This function is non-linear in μ and increases rapidly with increasing μ and hence, S increases with μ. Another very significant aspect of this figure (and indeed of the previous figures in this section) is that even for comparatively large E_o^* there are substantial fractions of particles semi-trapped, for instance, one can see that even for He in the area of E_o^* =20 there are about 10% semi-trapped. This means that semi-trapping will have a significant effect on accommodation calculations even for high E_o^* and the assumption of no attractive field effects for high E_o^* is a somewhat dubious tactic in the light of this result, more will be said about this later. Again the dashed lines have the same nature as discussed above.

Fig. 6.1.5 shows the absolute trapping expected in an initial encounter of the atom with the surface for the cases R* = 1.3, θ_o = 45° and φ_o=0°

with varying μ and E^*_o. The outstanding feature of this graph is how relatively difficult it is to absolutely trap an incoming gas atom compared to semi-trapping it. In fact, there is no He trapped even for $E^*_o = .5$ at $\theta_o = 45$ degrees, however, as θ_o decreases some absolute trapping appears. The curves show, as one would expect, that absolute trapping increases with increasing mass ratio and decreases very sharply as E^* increases. This dependence is much more intuitively satisfying than the much slower decrease with E^*_o seen in the previous figure as a model for final or overall trapping. That is to say, making the assumption that the semi-trapped particles are absolutely trapped would lead to a variation as shown in Fig. 6.1.4 which is unsatisfactory.

Fig. 6.1.6 graphically illustrates this last point, here the values of the uncorrected accommodation coefficients are plotted together with the semi-trapped probability for the comparatively "mild" case Ar/W mass ratio, $R^* = 1.3$, $\theta_o = 45^\circ$, $\varphi_o = 0^\circ$. For comparison the $E^*_o = \infty$ or no field values are shown for the same case. It is clear that the approach of the uncorrected AC's to their infinity values is very slow even at high E^*_o this is contrary to what one expects intuitively. This can be accounted by the erroneous assumption made in the uncorrected AC's namely, that all semi-trapped particles are absolutely trapped. It is of particular interest with respect to the tangential momentum AC which appears to be about twice too large, this is of course, a key function in satellite drag calculations. Hence, the semi-trapped particles' treatment is of profound interest for the satellite situation. It is also obvious from this figure where S is shown that if all the semi-trapped are assumed absolutely trapped the variation of S dominates and masks the true behaviour of the AC's.

Before leaving the discussion of the initial conditions and before the iteration of the semi-trapped particles, there remains to be considered the variation of the functions under examination with azimuth angle - φ_o. The cases plotted are for Ar/W mass ratio, $R^* = 1.3$, $\theta_o = 45^\circ$, $E^*_o = 20$ and $E^* = \infty$. It is apparent that all the functions plotted have a very weak dependence on azimuth angle particularly for the square surface array treated in the present case. This is in agreement with the results of Goodman (Ref. 9) and Oman (Ref. 39). The latter found as one would expect that the azimuth angle's effect was only apparent for very rough surface arrays. For the remainder of this chapter, the effect of the azimuth angle will be considered negligible for the summed functions of interest, however, it will re-appear when distributions are discussed in later chapters.

6.2 The Semi-Trapped Distributions

Having established the important role that semi-trapped particles play in energy and momentum exchange at the surface, the purpose of this section is to explore the nature of these particles. The method of doing this will be to construct semi-trapped distributions (abbreviated STD from here on) as explained in section 4.5.4. Since the STD's are of theoretical interest only, because they are the result of a particular way of attacking the semi-trapped particles problem, no great level of detail will be attempted here; it will be enough just to point out the salient features of the STD's. Fig. 6.2.1 is a typical STD plot, here are shown the STD's for Ar/W mass ratio, $\theta_o = 45^\circ$, $E^*_o = 20$, $\varphi_o = 0^\circ$ and $R^* = 9, 1.3$, and 2.0. Passing over the R^* variation for the moment these will be discussed as representative of STD's. First a few comments on the interpretation of the figure; an STD is difficult to plot since it is a two

dimensional matrix of values, the method used here is to plot the components of it as a fraction of unity where unity represents the total number of semi-trapped particles. The horizontal divisions represent the central values of the energy range in which the element lies, along these lines the reflected altitude angle for the element is indicated. A bar graph method is used since the anglular interval is 10 degrees; this was found to be sufficient for good numerical results a point which will be covered in section 6.4. Now returning tothe characteristics of the STD's shown in the figure, three outstanding features are apparent; (i) there are few non-zero elements in the STD; two of the STD's shown have three elements and the other five (ii) the elements are concentrated at angles near the surface tangent and (iii) the energy values are quite high compared to the initial energies; that is the semi-trapped particles still have a considerable fraction of their initial energies. A note about the energy levels shown: the fact that the level $E^* = 20$ is shown in later graphs is due to the fact explained in section 4.5.4 that the STD's are constructed within the field region and hence, the outgoing effect of the field has not been accounted for in the energy levels but the incoming energy addition has. This makes the highest E^* level in the figures $E_o^* + 1$ but the calculations have been set up to account for this and it does not detract from the validity of the point made in (iii) above.

The trends in the STD's with the basic parameters will now be discussed. The R^* variation is shown in figure 6.2.1 as was mentioned above. The trend is to lower energy levels and somewhat higher values of θ being present as R^* decreases; this is because of the lower velocities overall at lower R^*'s due to the increased degree of deflection of the trajectories. The lower values of θ being represented (i.e. nearer surface normal) is basically due to the same effect and the fact that the velocities are related to the outgoing angles, namely the trajectories nearer the normal are slower than those near the surface tangent, this will be extensively discussed in chapter 8.

The variation with incident angle θ_o is plotted in Fig. 6.2.2. for the case Ar/W mass ratio, $R^* = 1.3$, $E_o^* = 20$ and $\varphi_o = 0^o$. Here the trend is to higher energy levels as the surface tangent is approached, i.e. as θ_o increases; this is a result of the lower energy losses as θ_o increases which in turn is a result of the generally larger impact parameters appearing in this direction. However, it should be noted the features of the STD's noted above (i) to (iii) still hold.

The variation with initial incident energy E_o^* is shown in Fig. 6.2.3 for cases with Ar/W mass ratio, $R^* = 1.3$, $\theta_o = 45^o$, $\varphi_o = 0^o$. Again, the trend is predictable: lower levels are represented as E_o^* decreases and lower angles are also represented.

The correlation between the angle and energy is even more apparent here because for instance, in the $E_o^* = 9.5$ case, the level centered at 80 degrees is well represented at energy level $E^* = 7.5$ and does not appear at all in the level $E^* = 6.5$. The reason for this is that the particles having angles of this order have energies exclusively in the upper level and hence, they do not appear in the lower level.

Fig. 6.2.4 shows the effect of the mass ratio on the STD's. The cases shown are for the cases Xe/W mass ratio and He/W with $E_o^*=20$, $R^* =1.3$,

$\theta_o = 45^o$, $\varphi_o = 0^o$. The trend is to a more diffuse STD with lower energy levels as μ increases. This is due of course to the increased energy exchanges as μ increases and hence, the more extensive range of velocities and angles where semi-trapping occurs.

The picture of the semi-trapped particles is then a group of particles with trajectories lying near the surface and with considerable energies which are semi-trapped only because their normal energy component is smaller than the attractive field energy due to their position.

6.3 Final Trapping

The iteration scheme described in section 4.5.4 was found to converge very rapidly and in fact after one pass usually about 90% of the semi-trapped particles were accounted for and thereafter usually only one more or at most two passes accounted for 99.99% of them. This was the point at which the iteration was terminated. The outstanding result of the calculation was that the largest fraction of the semi-trapped particles ultimately escaped by recollision with the surface. Since they had considerable energy and momentum to begin with, they were able to convert enough of their tangential energy into normal energy by a grazing collision to escape. How this later process is possible is graphically illustrated by the normal momentum accommodation coefficient curves shown in Fig.6.4.2. A glance at these curves shows that this function assumes negative values from about 70 degrees on, for these particular curves. This means that normal momentum is being created from the tangential momentum of the incoming particles and hence this phenomenon allows the escape of the semi-trapped particles.

Consider now the final trapping values for the cases Ar/W mass ratio, $R^* = 1.3$, $\varphi_o = 0^o$ for variable incidence angle θ_o and lines of equal E^*_o given in Fig. 6.3.1. Here it is seen that trapping is greatest near the normal decreasing as θ_o increases and then levelling off to increase slightly as the surface tangent is approached because of the equivalent angle method used for the calculations this latter effect could not be pursued any closer to the surface than 80 degrees. This is due of course to the higher energy losses near the normal as explained in previous sections. The most dramatic effect is however the escape of the semi-trapped particles, this can be seen by comparing the present figure to Fig. 6.1.2 which gives the semi-trapped fractions for equivalent cases.

In Fig. 6.3.2. the effect of μ is plotted for the rare gas tungsten mass ratios and the parameters $R^* = 1.3$, $\theta_o = 45^o$, $\varphi_o = 0^o$ for values of E^*_o. Here we see that the trends are a combination of those seen in Fig's. 6.1.4. and 6.1.5. The effect of mass ratio is very pronounced for high μ. This is due to the fact that the mass ratio's effect is double in the sense that it applies strongly in the second and subsequent bounces of the semi-trapped particles in addition to producing semi-trapped particles with lower energies in the first instance. This also means that the slope of the curves will be increasingly less steep as the mass ratio increases. This is what can be seen in the figure by comparing the curves for Ne and Xe for example. For the lowest three mass ratios the curves show a rapid falling off which is similar to that seen in Fig. 6.1.5 and which is expected from experimental considerations to be discussed below. There is no absolute trapping for He at this angle although it is present to some degree at lower values of θ_o.

It is interesting to compare these results with the experimental data available; the most important of the scattering experiments for this purpose was the work of Saltsburg and Smith who have measured the scattering of rare gases from epitaxially grown films of silver (ref.64 - references to other reports are given there). They have deduced by qualitative arguments from their data that trapping is not a major effect in the experimental systems investigated; these are done for energies much lower than satellite energies. Also in this vein and more directly related to the point at issue is the work of Ehrlich and Hudda (Ref.56) and Gomer (Ref.65) and the discussions of Appendix B wherein it is shown that the value of the attractive field energy as estimated from the Lennard-Jones potential is much too high in all likelihood. As explained this is probably the result of the use of too high ϵ's due to the dubious combination rule, i.e. equation A.5. This problem is probably one of the reasons for the high trapping found by Oman (Ref.40) in addition to the semi-trapped problem. This last point is the major disagreement found between the present work and Oman's work. He has found that the trapping falls off much more gradually with increasing incident energy than the present theory; this is due to the fact that most of the particles that are similar to semi-trapped particles in the present model are absolutely trapped in his model. He says that except for cases with substantial surface temperatures compared with the LJ ϵ "most such particles (i.e. semi-trapped) will be eventually trapped" (Ref. 40). It is not clear how this result comes about in Oman's model, that is why the semi-trapped particles do not convert enough tangential momentum into normal momentum to eventually escape. It is suggested that perhaps the introduction of this effect might solve some of these difficulties due to excessive trapping.

6.4. Full Accommodation Coefficients

The final stage of the semi-trapped treatment is to calculate the full (or corrected) accommodation coefficients. In order to do this it was necessary to know not only the eventual outcome of the semi-trapped particles but also the energies and altitude angles of those which escaped. This was done as explained in sections 4.5 and 4.6 and the results will be presented in this section.

Fig's. 6.4.1 to 6.4.3 show the corrected energy, normal momentum and tangential momentum accommodation coefficients, respectively, as functions of θ_o for curves of equal E_o^*. The other parameters are Ar/W mass ratio, $R^* = 1.3$ and $\varphi_o = 0^o$. An important general trend is illustrated in these figures. For the curves of lower E_o^* the trapping shown in Fig. 6.3.1 dominates the AC's; this is especially apparent for the $E_o^* = 1.5$ and 2.5 cases. As E_o^* increases the curves start to approximate the no-field curves and at high E_o^* the curves are almost parallel to them. The no-field curves are similar to those found by Goodman (Ref.9). Hence it is clear that the curves evolve from a trapping regime to approach the no-field values. Examining Fig. 6.4.1 α_e decreases with θ_o because of the lower energy losses as θ_o increases. However, α_n, plotted in Fig. 6.4.2, is more sensitive to θ_o; this is because the greatest losses are in normal momentum for relatively high θ_o. As θ_o increases incoming normal momentum is converted to reflected tangential momentum and hence, the curves assume negative values. Since α_e is not sensitive to transfer between normal and tangential velocity its variation with θ_o is not as pronounced. Fig. 6.4.3 shows that α_t is not very sensitive to θ_o; this is what one would expect since α_t would seem to depend more on the surface "roughness" than any other of the geometrical parameters. In fact, some of the curves seem to show a

slight maximum between $\theta_o = 60^o$ and 70^o (an effect also observed by Goodman for a similar set of parameters). This is possibly due to geometrical effects, namely that the surface appears "roughest" at these angles. For certain cases negative values of α_t were observed for very low θ_o; this is intuitively feasible because it is the analogue of the effect seen in the normal momentum at high θ_o values. However, due to the numerical uncertainties introduced by the very small values of $\sin\theta_o$ near the normal, confident values of α_t could not be produced there and hence, the effect could not be verified with certainty. This is a topic for further study.

Fig's. 6.4.4 to 6.4.6 show how the AC's approach their no-field values; for the rare-gas-tungsten mass ratios as a function of $E_o^* - R^* = 1.3$, $\theta_o=45^o$, $\varphi_o=0^o$. At the lower mass ratios the AC's are near their no-field values at $E_o^* = 10$ but at the higher mass ratios the AC's are dominated by the trapping shown in Fig. 6.3.2. For the Kr/W and Xe/W mass ratios this effect is obvious even for high E_o^*, however it is clear that the typical behaviour of all the curves is similar. It is clear also that α_e and α_n are steadily increasing functions of μ, however, this is not pronounced to such a great for α_t. The relative differences in the α_t as μ increases are small in the no-field limit; the substantially larger α_t's for the Kr/W and Xe/W cases are of course due to trapping effects. Hence μ is not an important influence on α_t for high E_o^*.

In Fig. 6.4.7 the corrected values of the AC's have been plotted as a function of R* for cases with Ar/W mass ratio, $E_o^* = 9.5$, $\theta_o = 45^o$, $\varphi_o = 0^o$. It is clear that while α_e and α_n show only small changes with R*, α_t is strongly dependent on R*. Hence α_t depends more on the relative roughness of the surface, as represented by R*, than on any other factor.

Finally, in Fig. 6.4.8 the corrected (or full), uncorrected and no-field values of the energy accommodation coefficient have been plotted as a function of θ_o for Ar/W mass ratio, R* = 1.3, $E_o^* = 20$ (except of course the no-field case) and $\varphi_o = 0^o$. The differences between the three methods are now obvious: the uncorrected method is unsatisfactory and the corrected method gives results which behave in an intuitively reasonable way when compared to the no-field results. However, the latter are too low even for $E_o^* = 20$, this is, of course, because the attractive field increases the AC's both through the semi-trapped particles and through its unequal influence on the lower energy reflected particles as compared to the incoming beam. Hence, even for relatively weak attractive fields these effects are present and must be accounted for to obtain accurate AC's, and therefore completely neglecting attractive field effects as a high energy approximation is not justified unless E_o^* is very high indeed, in fact, much higher than that for satellite energies and typical E_t's.

Before leaving this section, one point remains to be discussed in connection with the trapping effects and their influence on accommodation. This concerns the situation which might arise if there is a large absolute trapping component in the interaction and the incoming gas atoms might then collide with the adsorbed gas atoms. Whether or not this would happen for a given case depends on the "dwell-time" of the adatoms (i.e. how long, on the average, an adatom remains before desorption). If the adatoms spend a time on the surface comparable with the relatively long time between collisions at a lattice site (target area) then it is clear that gas-gas collisions will occur at the surface. Conversely if the dwell time were short then it is unlikely that gas-gas collisions would occur. However, this really should be treated as a reaction-rate

type of problem, since there is likely a spectrum of dwell-times which would depend on the temperature of the surface, etc. No current data on dwell-times is available and therefore this kind of question cannot be answered at present. There is one further consideration about this, namely that for satellite velocity beams, all the evidence points to no significant portion of adsorbed atoms. Hence, although the semi-trapped situation would still have to be taken into account to get the correct AC's even for high E_o^*'s, gas-adsorbed gas collisions would probably not be important to the results at satellite velocities. This discussion does not apply to chemisorbed atmospheric gases, with the further transition from trapped to bonded states; this is certainly a topic for further work.

VII FLUX DISTRIBUTIONS

7.1 The Structure of the Primary Flux Distributions

An interesting feature of some of the primary flux distributions calculated was the presence of definite structure. This structure will be discussed here before proceeding to the variation of the primary flux distributions with the basic parameters. When first encountering structure one might suspect that it was caused by statistical or numerical difficulties in the calculations; in other words that too few trajectories were used to construct the distributions. In the present case this possibility is disposed of immediately by the considerations of section 5.1 and in particuler by the results shown in Fig. 5.1.1 which illustrates the persistence of structure for a very large number of trajectories. Similarly Fig. 5.1.3 shows that the same structure is present for both large and small detector resolutions and hence it is not a peculiarity of the method used in sorting the trajectories to construct distributions. It is concluded then that the structure seen was real in the sense that it was a consequence of the assumptions of the model.

The angular method was used to study this structure since the past histories of the reflected particles were easier to reconstruct in this mode for purely computational reasons. To simulate the detector mode the results for the angular mode were divided by $\sin\theta$ (from solid angle considerations). This procedure will be called the angular-detector approximation. In Fig. 7.1.1 this approximation is compared with the actual results calculated using the detector method and the original angular results on which the approximation was based for the case: Ar/W mass ratio, $R^* = 1.3$, $E_o^* = 20$, $\theta_o = 45^o$, $\varphi_o = 0^o$. The approximation gives the correct shape when compared with the actual detector result and hence, it is reasonable to use it to study structure. (However, the flux levels given by the approximation are somewhat higher than the detector results for the same case and it is not desirable to use it when the absolute flux levels are important).

It is apparent in Fig. 7.1.1 that there is structure even in the angular mode. The same curve is shown in Fig. 7.1.2 as the sum of two subdistributions: the distribution of the single colliders and the distribution of the multiple colliders. It is clear now that the reason for the structure is that the single colliders have a relatively broad lobe and the multiples colliders a relatively sharp peak for their reflected distributions. This difference in the subdistributions is due to the fact that the initial aiming points that produce single colliders are well distributed over the target area in contrast to those producing multiple collisions which are localized in a relatively narrow band. This can be seen in Fig. 5.2.3; the $R^* = 1.3$ case in that figure corres-

ponds to the case considered here. In effect the range of reflected trajectory possibilities for the multiples is limited for this case and hence, their distribution appears as a peak. This division between single and multiple colliders in the reflected flux distribution is analogous to the situation in quantum-mechanical scattering theory where in general both elastic (no energy loss) and inelastic (finite energy loss) collisions may occur in a given case. In the present case the elastic component would be represented by the multiple colliders' peak and the inelastic component by the single colliders' lobe. However, although the multiples are generally more energetic than the singles, it is not claimed that this correspondence holds strictly in the present model since the multiples do have finite energy losses and hence, are not truly elastic. It would be interesting to see how the quantum-mechanical solution for this case would compare with the classical result and if so, whether there is validity in the above correspondence. This is not possible at the moment because quantitive results are not available for current quantum-mechanical theories. (see section 2.6).

This structure observed in the angular mode is accentuated in the detector mode (or strictly speaking in the angular-detector approximation). The structure for the same case (as Fig's 7.1.1 and 7.1.2) is shown in Fig. 7.1.3 for the angular-detector approximation). The structure is much more pronounced than in the angular mode but it arises for exactly the same reasons. Up to now structure has been discussed for just one case and in fact structure varies with the basic parameters. Looking ahead for a moment to Fig. 7.2.1 which gives the variation of the flux distributions with R* (the other parameters are the same as in the above cases) it is seen that structure is found only for the R* = 1.4 case. (This of course is similar to the case that has been discussed up to now). The R* = 2.0 case shows no structure because there are no multiples present. The R* = 0.9 (and also the R* = 1.0) case has no apparent structure and this is surprising at first glance since there are more multiple trajectories available at this R* value. The R* = 0.9 case is shown in Fig. 7.1.4 and it is clear that the reason for the absence of structure is that the multiple subdistribution is not sharply peaked but is quite broad. Referring to Fig. 5.2.3 for this R* value it is seen that the multiple collision possibilities are more extensive and hence, yield increased broadness of the subdistribution. The presence or absence of structure depends on the number and distribution of the multiples, these in turn depend on the basic parameters as indicated in sections 5.2 and 5.3. Arguments similar to the above can then be used to explain the variation of structure that will be seen in the following sections. (In fact, it happens that the case considered in Fig's 7.1.1 to 7.1.3 is one in which structure is quite prominent). One further feature of the structure phenomenon is illustrated in Fig. 7.1.5 in which the average value of the reflected incidence angle ($\bar{\theta}$) for all the particles is plotted as a function of μ (to the Xe/W mass ratio) for cases with R* = 1.3, $E_o^* = 20$, $\theta_o = 45^o, \varphi_o = 0^o$. The important point here is that the multiples on the average lie lower than the single colliders. The curves of the total and single averages approach the multiple curve because of the increasing proportion of multiples experienced as μ increases. Note that $\bar{\theta}$ may be less than the specular angle, this effect is due to the fact that for very low mass ratios the reflected distributions are quite broad spatially and the large numbers of particles that are highly deflected determine the average since the counter balancing trajectories near the surface have been cut off by the field. In other words, the overall average at $E_o^* = \infty$ would be just below the specular but the lower lying trajectories do not appear in the primary distri-

bution due to the semi-trapping and hence, the average value of $\bar{\theta}$ may be above the specular.

Structure of the kind found here has also been observed in the calculations of Oman (Ref.40) but it was not possible in that work to separate the gas particles which interacted mainly with one surface atom from those which interacted with more than one-classes analogous to the present single and multiple types. However, it appears highly likely that the structure seen by Oman is due to effects similar to those observed here; it is of course an advantage of the present model that these mechanisms can be studied with relative ease. There have also been experimental observations of flux distributions consisting of a sharp peak superimposed on a broad lobe notably for expitaxially deposited clean surfaces. This was reported for certain cases by Saltsburg and Smith (Ref.64) and Smith (Ref. 66) involving light polyatomic molecules. This last circumstance precludes any quantitive comparison with the present model. However, if as Smith (Ref.66) suggests "the rotational spacings" (of energy levels)" are large enough to preclude single phonon processes the molecules behave as a monatomic species," it might be possible to propose an explanation for the observed structure on the above lines. The presence or absence of structure for various species might then depend on the value of their effective R*. This is a possibility but certainly more experimental data at higher beam energies should be available before any definite proposals along these lines can be made.

It should be emphasized that none of the foregoing discussion has taken into account semi-trapped particles; all the distributions considered were primary. From an intuitive point of view it would seem that the semi-trapped particles are likely to be reflected in a more diffuse manner spatially than the primary distributions; this is especially so if one considers the complexity of a semi-trapped particle's trajectory for a realistic case. It has been argued in the preceding sections that there are reasonable approximations to account for the trapping and accommodation of these particles but whether the same kind of approximations can be used to calculate adequate distributions is another matter. It is by no means obvious whether this could be done; in any case as explained in section 4.7 it is not feasible at present to produce full distributions because of the extensive computation times required. Hence, the question of yet another type of structure due to the semi-trapped particles must be left open.

7.2. Primary Flux Distributions

The variation of the primary flux distributions with the basic parameters will be discussed in this section. All the results are in the detector mode and only primary distributions will be considered. On this last point the primary distributions should show the general trends of the full distributions except perhaps for cases where there are large numbers of semi-trapped particles. Even then it is unlikely that dramatic differences would be seen between the primary and full distributions. This statement is based on the observation that in most cases with large numbers of semi-trapped particles, they are spread over the STD for reasons which are inherent in the physical processes causing these large semi-trapping fractions (see section 6.2). Therefore one can infer that the escaped semi-trapped particles would in these cases give rise to relatively broad lobes. There may be some additional structure involved in the full distributions but barring some unforseen circumstance it is not apparent how the full distributions could show trends very different from the primary distributions.

Fig. 7.2.1 shows the variation of the flux distributions with R*; the parameters are Ar/W mass ratio, $E_o^* = 2.0$, $\theta_o = 45^\circ$ and $\varphi_o = 0^\circ$. The reasons for the variation shown have been explained, in part, in the previous section. Generally for R*=2.0 the distributions are lobular and have no back scattering; in fact, in this case flux is not detected for angles less than about 30°. There is no structure since there are no multiples present. This behaviour is due of course to the relative smoothness of the surface. For R*=1.4, the structure discussed previously is exhibited. For R*=1.0 and R*=.09, the distributions are broader and back scattering is seen due to the increased roughness of the surface. The reason for the lack of structure in these cases was explained in the preceding section. The location of the peaks (i.e. maximum flux levels) of these distributions are all below the specular and it is clear that the peaks move toward the surface tangent as R* increases. This trend, however, is due to several effects aside from the decreasing distribution spread as R* increases; for instance, it is clear that for the R*=1.4 case, the multiples play an important role in determining the peak location.

Fig. 7.2.2 shows the variation of the primary flux with θ_o; the parameters are Ar/W mass ratio, R*=1.3, $E_o^* = 20$ and $\varphi_o = 0^\circ$. For normal incidence the distribution is broad and symmetric about the surface normal as one would expect. As θ_o increases through 15° and 30°, the evolution of the distributions is to the forward scattering direction and the back scattering correspondingly decreases. At 45° structure appears and back scattering is not apparent. This structure is still suggested in the 60° case but then the distributions become somewhat broader, for 75° a lobular pattern appears because now the incoming atoms "see" only the top regions of the surface atoms. This trend is carried on in the 85° case to a greater extent and the distribution is sharper. The transition from 60° to 75°, in which the distribution becomes broader is because the sharpness of the 60° peak is due to multiples and the 75° peak is in the no-multiple regime. Another characteristic of the two higher θ_o peaks is the increasing steepness of the part of these curves from the peak to the surface because the particles represented by these distributions are faster as θ_o increases due to the smaller energy losses. Hence, there is less semi-trapping and the steeper slopes; a similar trend is present in the lower θ_o distribution although it is more easily seen in the higher ones. The peak locations (if such can be defined for the low θ_o cases) are generally nearer the surface tangent as θ_o increases. However, the presence of multiples again affects this observation and there may be a slight reversal of it between $\theta_o = 60^\circ$ and 75°. Conversely with regard to the considerations of section 7.1, this figure shows how dependent the presence of structure is on the geometrical parameters (in this case θ_o).

Fig. 7.2.3 shows the variation of the flux distributions with E_o^* for Ar/W mass ratio, R*=1.3, $\theta_o = 45^\circ$ and $\varphi_o = 0^\circ$. This variation has an obvious interpretation in terms of the attractive field effects. As E_o^* decreases from infinity, the peak moves toward the surface tangent, for $E_o^* = 20$ this displacement is slight but accelerates for the lower E_o^* values. This, of course, is explained by the non-linear (i.e. increasing for decreasing E_o^*) effects of the field on the outgoing trajectories. The decreasing overall flux levels are of course because of the increasing semi-trapped probability for decreasing E_o^*. However, there are some other points about this figure which reward further consideration. The subsidiary peak in the $E_o^* = \infty$ curve, which occurs at about $\theta_r = 80^\circ$, is not seen in the $E_o^* = 20$ curve; the reason for this is that the trajectories represented by this peak are semi-trapped in the latter case and hence, do not appear

there. This is an example of the same structure seen in section 7.1 being a function of E_o^*, since in the E_o^* =20 the single distributions highest point lies much nearer the multiple peak than in the $E_o^* = \infty$ case. In other words, the single distributions in the cases shown in section 7.1 have more pronounced peaks for the no-field cases but these lie near the surface tangent and hence, are removed by semi-trapping giving rise to the somewhat shapeless broad lobes for the singles in the E_o^*=20 case. Another interesting feature is the back-scatter seen in the E_o^*=2 case because the effect of the field makes the incoming beam steeper (nearer the surface normal) and more back-scatter appears due to the considerations of Fig. 7.2.2 above.

Fig. 7.2.4. shows the variation of the primary flux with the rare-gas-tungsten mass ratios for the parameters R* =1.3, E_o^*=20, θ_o=45° and φ_o=0°. Clearly the peaks tend toward the surface tangent as μ increases due to the increased normal energy losses. Surprisingly the peak heights increase as μ increases and the Xe/W peak is quite sharp. The reason for this can be seen from Fig. 5.2.4; that is from the Xe final disposition map. The trajectories comprising the Xe peak (labelled "0" in the map) come from a relatively small region of the total target area and hence, the limited number of reflected possibilities. The rest of the trajectories are semi-trapped; the number escaped is only about 41% for this case. But looking at the semi-trapped distribution for this case, Fig.6.2.4, there is every reason to infer that the contribution of the semi-trapped particles to the full distribution will be relatively broad since there are many non-zero elements in this STD. Hence, the behaviour shown in the figure should be present to a large extent in the full distributions. Another feature which is due to the multiples is the low values of the multiple peaks for low mass ratios; in fact, for He it is quite small. This occurs because of the decreasing number of multiples as μ decreases (section 5.3). A further feature of this curve is the effect of the field seen in the decreasing slope of the distribution as θ_r increases below the specular. Also the peak for this distribution lies nearer the specular, almost on it, than the other distribution because of the very small energy losses for this very low mass ratio. Hence, again the observed variation is due to a combination of factors.

Fig. 7.2.5 shows the variation of the distributions with φ_o the initial azimuth angle; the other parameters are Ar/W, R*=1.3, E_o^*=20, θ_o=45°. This variation can be explained partially in analogy with an increased effective lattice spacing and hence, a decreased R*. This would account for the increased back scattering and broadness as φ increases. However, this analogy is not strictly applicable because the geometrical situation is different. For example, the same structural features are still apparent although the multiple peak is much broader for the 45° case. It appears from this that the same general trends in the other parameters should hold for all azimuth angles.

7.3 Spatial Primary Flux Distributions

The angular mode was used to find the spatial variation of the primary flux distributions and hence, to study out of plane scattering. The distributions given in this section are all plotted as functions of θ_r and φ_r, to show the symmetries found, over the entire reflection half-space. Since the form of the distributions and their broadness in space are the points of interest, the fluxes are plotted as a percentage of the total particles which are represented in the figure.

Figs. 7.3.1 and 7.3.2 and 7.3.3 show the single, multiple and total components in space for the case Ar/W mass ratio, R*=1.3, E_o^*=20, θ_o=45° and φ_o=0°. Fig. 7.3.1 shows that the spread in space of the singles is quite extensive and the variation with θ_r and φ_r is smooth. As one would expect the largest overall fluxes are in the θ_r=50 degrees - 70 degrees range. Fig. 7.3.2 is another matter, however, and the distribution of the multiples is very complex which is not surprising considering the trajectory possibilities which the multiples have. The multiple distribution is more compact and has large components near the normal in this case. When these two distributions are added, the result is Fig. 7.3.3. There it can be seen how the multiples affect the total distribution and cause a spatial structure. Again these figures, especially Fig. 7.3.2 show the difficulty of producing analytic expressions for the distributions. The outstanding result is how much of the flux, even for R*=1.3, is out-of-plane.

The spatial trends of the distributions can be easily inferred from the effects discussed in section 7.2; therefore, no parametric examination will be done. There are, however, two points which are useful to examine. The first is the lack of structure in the R*=0.9 distribution; the spatial results are shown for this case in Fig.7.3.4 (only the positive φ_r component is plotted, the negative φ_r being its mirror image). Spatial structure can be seen for some θ_r values, however, this structure is again less pronounced than for the R*=1.3 case, due to the multiples broadness. Clearly, as one would expect from the results of the previous section, the distribution is much broader in space than the R*=1,3 case. Another point of interest is the sharpness of the Xe lobe of Fig. 7.2.4, the spatial distribution for this case is given in Fig. 7.3.5. This shows that the lobe is very compact in space and hence, the peak in the sector mode is confirmed by this figure. There is some structure in the θ_o=80° curve which is not found in the detector mode, this is probably again due to multiples.

A subsidiary result of the distributions shown in this section is their symmetry which is necessary evidence for the correctness of the calculations.

VII VELOCITY DISTRIBUTIONS

8.1 The Structure of the Primary Velocity Mean Distributions

In the same manner as chapter 7, the structure observed in the velocity mean distributions will be discussed here under a separate heading. Statistical effects due to insufficient trajectories may be eliminated as before by referring to the work of section 5.1 for the velocity mean distributions particularly Fig's. 5.1.2 and 5.1.4. (The angular-detector approximation is also used in this section for the same reasons mentioned in section 7.1). The basic reason for the structure is the same-namely that there are two subdistributions which form the total distribution. However, in this case the important difference between the two subdistributions is that the multiple particles are generally faster than the single particles. This is because the multiples usually have two or more glancing (high impact parameter) collisions and the singles usually have one near head-on (low impact parameter) collision. The former situation then leads to lower energy losses because of the strong dependence of reflected velocity on impact parameter.

In Fig. 8.1.1 the structure of the velocity mean distribution for the case: Ar/W mass ratio, R*=1.3, E_o^*=20, θ_o=45°, φ_o=0°, is shown. Here the multiple subdistribution contains higher velocities than the single subdistribution and is confined to a narrow range of angles. This causes the perturbation seen in the total distribution. The R*=0.9 case (the other parameters are unchanged) is shown in Fig.8.1.2, here the multiples are more spread out spatially and hence, the structure is not so pronounced.

There is no structure for the R*=2.0 case since there are no multiples. As with the flux distributions the characteristics of the structure, if any, depend on the values of the basic parameters.

Similar remarks to those made at the end of section 7.1, about the possible influence of the semi-trapped but escaped particles, also apply to the velocity mean distributions.

8.2 The Primary Velocity Mean Distributions

In this section the primary velocity mean distributions in the detector mode, corresponding to the flux distributions of section 7.2, will be considered. The comments about the use of primary distributions for inferring the trends of the full distributions are also applicable here.

Fig. 8.2.1 shows the variation of the velocity mean distributions with R* corresponding to Fig. 7.2.1 (this correspondence is not precise because R*=1.3 instead R*=1.4 is considered; however, both these cases have the same type of result). The reasons for the structure seen here have been explained in the previous section. The solid line represents the single component of each distribution, up to the limit shown. The reason that these parts of the distributions are coincident is because the same impact parameters are repeated for a portion of the incoming trajectories. For low R* there are more of these impact parameters available to the incoming trajectories, as R* decreases there are fewer impact parameters but these are a subset of the low R* impact parameters. This is obvious from the simple two dimensional geometry of a trajectory and a line of atoms. The reflected velocities increase toward the surface; this is in agreement with the experimental results for thermal beams (Ref.67).

Fig. 8.2.2 shows the variation of the mean velocities with θ_o, corresponding to Fig. 7.2.2. This shows clearly that the higher the incidence angle, the faster the reflected particles; this is caused by the increasingly lower energy losses as θ_o increases. Also, the velocities increase as the surface tangent is approached in the reflected distributions. The θ_o case shows symmetry and the reason for the lowest velocity at the normal is of course due to the head-on collisions there. Structure, is seen in the 45° case and to a slight extent in the 60° case.

Fig. 8.2.3 shows the variation of the mean velocities with E_o^*, corresponding to Fig. 7.2.3. The structure can be seen to move toward the normal with increasing E_o^* corresponding to flux results. The overall velocities are lower for lower E_o^* for obvious reasons, however, the slope of the curves near the surface tangent is increasing for increasing E_o^* (this is particularly true for the $E_o^* = \infty$ case) due to the decreasing attractive field strength. This region of increasing velocity corresponds to the extra peak on the flux

curves for the $E_o^* = \infty$ case.

Fig. 8.2.4 shows the variation with mass ratio. The variation of the overall velocities with mass ratio are clearly what one would predict. The structure mentioned above is not as clear for He and Ne as it is for Ar since there are fewer multiples for these cases. However, what structure there is becomes more pronounced as μ increases. In general, the higher the mass ratio, the greater the difference between the highest and lowest velocities in the distribution. The slight downturn in the Xe case is hypothesized to come from a combination of high energy losses, high trapping probability and low trajectories.

Fig. 8.2.5 shows the variation of mean velocity with φ_o. The structure seen here can be explained as before; however, the situation is more complex geometrically. The most interesting feature of the figure is how little variation on the whole there is in the distribution with φ_o. This confirms the same almost negligible variation in the accommodation coefficients with azimuth angle.

8.3. Spatial Primary Velocity Mean Distributions

The spatial velocity mean distributions corresponding to those of section 7.3 will be considered in this section. These results are for the angular mode and are plotted for the entire reflection half-space.

Fig's 8.3.1, 8.3.2 and 8.3.3 show the velocity mean distributions of the single, multiple and total distributions; these correspond to Fig's. 7.3.1 7.3.3. Fig. 8.3.1 shows clearly the trend to higher velocities at higher reflected angles. The greatest mean velocity for a given θ_r is in the "detector plane" at $\varphi_r = 0^o$; the velocities then are lower for out of plane scattering in this sense. The mean velocity curves shown here are very smooth which confirms the general observation, seen several times throughout this chapter, that the velocities are less sensitive than the flux distributions to the various interaction effects discussed here and in chapter 7. Fig 8.3.2 plots the multiple velocity mean sub-distribution. The multiples were found to be generally faster than the singles and this trend holds spatially as shown here. Again the complexity of the multiple sub-distribution, Fig. 7.3.2, is indicated in these results. Fig. 8.3.3 gives the total distribution; here it can be seen that the multiples distort the single distribution to produce the structure shown. However, the trend shown in Fig. 8.3.1 still hold here, namely, that the velocities decrease with distance from the "detector plane" ($\varphi_r=0^o$).

Following the remarks of section 7.3, there will be no parametric study of out-of-plane velocities since the trends can be deduced from section 8.2. and the above observations. Considering the two special cases of section 7.3: Figs 8.3.4 and 8.3.5 correspond to Fig's 7.3.4 and 7.3.5. Fig. 8.3.4 shows that the velocities are somewhat lower for the lower value of R* compared to those of Fig. 8.3.3. However, structure in the velocity mean distribution is almost nonexistent compared to that seen in the flux distributions which further illustrates the comparative insensitivity of these distributions. Fig. 8.3.5 for Xe/W mass ratio, shows the very small velocity range in the reflected trajectories which arises from the limited trajectory possibilities represented in the reflected distribution. The velocities are naturally lower and they fall off more rapidly from $\varphi_r = 0^o$ than in the Ar/W cases considered previously.

8.4. Primary Velocity Distributions

The purpose of this section is to point out the relevant features of the primary velocity distributions that can be observed on the basis of the present theory. In section 5.1 the point was made that there are not enough trajectories available in a detector "box" to allow any comment on the detailed form of the distributions, a glance at the bracketed numbers in Fig. 8.4.5 shows the order of trajectory numbers used in the present case. The bars in the figures represent the proportion of the total particles in the box that have speeds between the v values shown. Therefore, only the gross features will be discussed here and no attempt will be made to infer functional forms, etc., from these results. To simulate the measurement of a velocity distribution, the detector is fixed at a certain angle and the particles arriving in the detector are sorted by velocity; in the present work the detector is usually fixed at $\theta_r = 60^\circ$ since the results of the above chapters show that, at least for Ar/W, many interesting effects occur there.

To begin with, the effect of leaving the incidence angle fixed and varying the detector will be considered. Fig. 8.4.1 shows the results of doing this for the case Ar/W mass ratio, $R^* = 1.3$, $E_o^* = 20$, $\theta_o = 45^\circ$ and $\varphi_o = 0^\circ$. This figure illustrates many of the outstanding features of the velocity distribution results. Firstly, the velocity distribution are quite narrow compared to the total velocity range; this can be explained in terms of the hard sphere interactions at the surface. That is, for a given θ_r and φ_r there are only a very limited number of aiming points which give rise to trajectories in that box; hence, the range of possible impact parameters and correspondingly, reflected velocities is small. Secondly, a double peaked distribution appears in the 60° detector case; this comes from the single-multiple structure. The other trends in the figure follow from the previous sections. The movement of the peaks toward the surface tangent as θ_r increases has been observed in the velocity mean distributions. The appearance of the structure only at $\theta_r = 60^\circ$ is due to the narrowness of the multiple subdistribution as discussed in sections 7.1 and 8.1; there are no multiples present at the other detector angles.

Fig. 8.4.2 shows the variation of the velocity distributions with incidence angle for a detector fixed at 60°. The peaks become somewhat broader as θ_o increases since the lower incidence angles contribute relatively fewer particles to the 60° box, this number increases as θ_o increases. The broadening for the lower values of θ_o is again probably due to the increased proportion of the trajectories which lie in the 60° box. From 75° to 85° there is an increase in the heights of the higher velocity components and hence, the average velocity trend seen previously even though the distribution are located in the same range of v.

Fig. 8.4.3 gives the variation with R* for a detector fixed at 60°. For the $R^* = 2.0$ case the velocities are concentrated in one region, at $R^* = 1.3$ two bands appear, a faster one for the multiples and a slower one for the singles which is located in the same position as the band for the $R^* = 2.0$ case. This reinforces the interpretation given to Fig. 7.2.1 in section 7.2. For $R^* = 1.0$ the multiple band has diminished somewhat due to the fact that the multiples are not as concentrated as in the $R^* = 1.3$ case. This trend continues to the $R^* = 0.9$ case but here the single band starts to show a greater spread. This is probably due to the greater possibilities for the singles at lower R*.

Fig. 8.4.4 shows the variation with E_o^* again for a detector fixed at

60°. Here the two effects involved: firstly, the lowering of the overall speed of the reflected trajectories as E_o^* decreases due to the field and secondly, the movement of the multiple peak as seen in Fig. 7.2.3. The shift due to the field can be seen by comparing the $E_o^* = \infty$ and $E_o^* = 20$ cases. This comparison also shows how the multiple component for the latter increases over that of the former; this is due to the fact, mentioned in section 6.1, that more multiples escape than singles. Since the distributions are plotted by representing the proportion of the total particles in the box having a certain speed, the multiple band actually increases in the $E_o^* = 20$ case. The motion of the multiple peak in Fig. 7.2.3 brings it closer to $\theta_r = 60^{\circ}$ for $E_o^* = 10$ and hence, this case shows the largest multiple contribution; as this peak moves toward the surface tangent the multiple component decreases as seen in the $E_o^* = 5$ case but more clearly in the $E_o^* = 2$ case.

Fig. 8.4.5 shows the variation with the rare-gas-tungsten mass ratios for a detector fixed at 60°. The single distributions are broader as μ increases for the reasons discussed in connection with Fig. 8.2.4, namely, that high mass ratio magnifies small differences in impact parameter into large differences in velocity. For He there is very little velocity loss as one would expect and the single bands generally show the variation in their locations that one would expect as μ increases. The multiple component is greater for Kr than for Xe because the Kr peak (containing multiples) appears near $\theta_r = 60^{\circ}$ and the Xe peak below it. For the other three mass ratios the multiple component decreases since the multiple peaks begin to occur at $\theta r < 60^{\circ}$ as is shown in Fig. 7.2.4. Another interesting effect is that the difference in the spacing between the multiple and single peak increases because of the comparitively greater energy losses in head-on collisions compared to glancing collisions as μ increases.

A striking feature of these distributions is how localized they are on the v scale showing the interaction is very selective of preferred reflected velocities. This is the main reason for the widely held view that the velocity distributions will give the best means of verification for gas-surface intereaction theories. What perhaps has not been realized up to now and is shown by these results is how much information about the various mechanisms that occur at the surface can be obtained from velocity distributions. Apart from the two bands which result from the single-multiple structure discussed here, it is very likely that other bands will represent semi-trapped and re-emitted absolutely trapped particles in a full distribution. Hence, the prospect of the velocity distribution becoming almost a spectrum of bands, representing the contributions of several scattering mechanisms, is very real. If indeed the interaction can be as complex as the present work indicates, the importance of velocity distributions measurements for understanding it cannot be overestimated. Unfortunately there is no data of this kind available, although there is some velocity mean data for the thermal range. French and Locke (Ref.68) have suggested a time-of-flight experiment, for investigating velocity distributions but as yet, no surface interaction results have been obtained.

Before leaving this chapter, it was indicated in section 4.7 that momentum distributions were also calculated in the present work. However, on examining them no surprises were found and the information about them can be deduced from the work of this and the preceding chapter. Therefore, no momentum results have been presented since it did not appear to be worthwhile to include them.

IX COMPARISON WITH EXPERIMENT

9.1 Comparison with an Intermediate Energy Experiment

Few comparisons with experiment have been made in the preceding chapters; this was due to the scarcity of data, other than for the thermal energy range, on surface scattering. An exception to this is the work of O'Keefe (Ref.3) who investigated the scattering of argon atoms from well-characterized tungsten surfaces in the .25 to 1.35 ev energy range. This section is concerned with the comparison of this experiment and the present theory.

It is important to examine whether this comparison is a valid one, that is, whether one is justified in applying the theory to the experiment. There are two major obstacles to the comparison: firstly, the results at 300°K surfaces temperature refer to hydrogen saturated surfaces, but the clean surface results are for 2000°K surfaces, and secondly, the energy range of the experiments was an order of magnitude below satellite velocity. Each of these limitations will be discussed in turn. Concerning the first problem the important consideration is how the presence of hydrogen affects the scattering results. To study this O'Keefe measured selected flux levels before and after flash-desorption of the hydrogen and found no detectable difference. From this he inferred that there was no apparent difference between a clean surface at 2000°K and a hydrogen covered surface at 300°K in their scattering of argon atoms at these energies; at least there was no difference that the experiment could detect. In other words O'Keefe's clean surface results are for a surface temperature of 2000°K. The hydrogen - tungsten system is a complex problem in chemisorption, the mechanisms of which are imperfectly understood at present (Ref.69). Therefore, any explanation of this result (or theoretical attack upon it) is basically futile in the fact of this lack of information. Whatever physical processes occur between the incoming beam and the hydrogen layer, or alternately between the beam and a 2000°K surface the present theory cannot account for them and hence, the comparison must be regarded with caution. The second problem is that the energy range of the experiments was from .25 to 1.35 ev (clean surface results); thus the highest energy studied was about a tenth of satellite orbital energy for argon (about 12.5 ev). Therefore the energy range is lower than desirable for the theory which presumably appears to its best advantage for satellite velocities. For instance, the .25 ev case probably contains thermal vibration effects. There is one further point which should be noted: there is a third major difficulty which is implicit in the results of O'Keefe. That is the only clean surface results are confined to three energies at the same angles and for the same gas-surface pair. In other words the only data available for comparison (and it has the above two problems) consists of three curves, one of which suffers from severe experimental noise (Ref.3). Hence, no definitive judgement of the validity of the theory can be based on its success or failure for such a narrow range of parameters. All these points must be considered when making a critical evaluation of the results of the comparison.

In order to make the comparison some theoretical method must be used to account for the semi-trapped particles which ultimately escape; in other words, one would like to use the full distributions for the comparison. This is not possible at present and another approximation must be employed. The simplest possible assumption is that these particles are distributed equally over all space, this is in fact what was done. Although there are some grounds

for inferring that the re-emitted semi-trapped particles would be relatively spread out in space, this assumption is purely an approximation for convenient calculation which cannot be verified until full distributions are available. However, unless the semi-trapped particles show some sort of focussing in a preferred direction, the assumption is not likely to have a fundamental effect on the comparison. The other procedures used to make the comparison were straight forward. A detector of the same size as the experimental one was simulated and the Ar/W mass ratio was used. Although the incident altitude angle was verified in the experiment to be 45 degrees the azimuth angle was found to be 8 degrees which was used in the theoretical calculations. It was found in the calculations that this small shift in azimuth had a negligible effect on the theoretical results. A further experimental misalignment caused the detector to be out of the plane of the surface normal and incoming beam by about 6 degrees; this was taken into account by a co-ordinate rotation as indicated in Eq. 4.7.3. The problem then is to choose the values of R and E_t which best fit the experimental data; one set of these must be used to fit all three curves of course. Using these means then, a comparison of the absolute flux levels was made.

The results of the comparison are shown in Fig. 9.1. First the values of R and E_t are within reason. The former value of $R^* = 1.3$ for the argon-tungsten system was somewhat higher than expected from Appendix A although it is not unreasonably high. The value of $E_t = .0675$ ev is much lower than the integration method of Appendix B would indicate, but it is similar to the experimental value found by Gomer (Ref. 65) which was .082 ev. This result for E_t is suggestive of the possibility that too high values of the attractive field strength may have been estimated in the past. This procedure of finding the system parameters from comparison with scattering data is an example of how information about the surface field can be deduced from a molecular beam experiment. The comparison shows that the absolute flux levels predicted by the experiment are in good agreement with the experimental results and the peaks for the two higher energies also are in reasonable agreement. The peak for the lower energy curve is somewhat lower than the experimental value; this may be due to thermal effects at this low energy. The unexplained difference between the theory and the experiment as shown in the figure is the overly high values predicted for the region between 15 and 30 degrees. This is the structure effect and it was not apparent in the experiment. The reasons for this that could be suggested are various. A possibility is that the structure phenomenon perhaps appears only for very ideal surfaces and not in the experimental situation. Or perhaps it is a thermal effect in that the clean surface results are for a high surface temperature (2000°K). However, possible explanations must await the presentation of more experimental data which is necessary before any definite explanation can be given. In spite of this it is an encouraging result that the theory is able to give reasonable absolute flux levels when compared with experiment. Apparently it is the only theory which has been able to do this up to the present.

9.2 Some Comments on Satellite Drag

The experimental results of O'Keefe seem to indicate a relatively low degree of accommodation. This was indeed found to be the case when the full accommodation coefficients for the fitted cases were calculated. It is interesting to apply these accommodation coefficients to a very preliminary calculation of satellite drag keeping in mind the cautions expressed about the

comparison mentioned in the previous theory. The infinite speed ratio approximation for the drag on a flat plate in free molecule flow is:

$$C_D = 2 \sin(90^\circ - \theta_o) \left\{ \alpha_t + (2-\alpha_n-\alpha_t)\sin^2(90^\circ-\theta_o) \right\} \qquad (9.2.1)$$

This equation is given by Schaaf and Talbot (Ref.70) for instance; it has been rewritten in the notation of the present work. The accommodation coefficients and the corresponding drag coefficients are:

Energy	α_e	α_n	α_t	C_D
1.35 ev	.35	.37	.22	1.31
.56	.41	.43	.26	1.30
.25	.60	.62	.45	1.30

There are several notable points about this calculation. Firstly, if the diffuse ($\alpha_n=\alpha_t=1$) and specular ($\alpha_n=\alpha_t=0$) limits are used in Eq. 9.2.1 the same value of C_D results namely $\sqrt{2}$ ($=1.41$). This is because the momentum transferred to the plate is essentially the same for both cases in that it is basically the incoming stream momentum. Of course the 45 degree angle-of-attack means the reflected molecules in the specular case are perpendicular to the stream and hence, do not modify the drag. Therefore, the same value of C_D for both limits is not surprising when the basic physical meaning of the limits is examined. The situation is then that the calculated C_D's are less than both limits which is remarkable. The reason for this is that the distribution peaks lie below the specular angle and hence, momentum is reflected along the same direction as the stream and therefore the drag is lower. Another interesting feature of the drag coefficients is their relatively constant values as energy changes. It is not clear whether there is some fundamental reason for this or whether it is merely fortuitous. This is a topic for further study.

The conclusion of this very preliminary drag calculation is therefore that accommodation coefficients for clean surfaces can be quite low.

X. CONCLUSIONS

A three-dimensional classical model for satellite-surface interactions has been presented. Numerical experiments involving large numbers of trajectories were used to study the accommodation, trapping probabilities and flux and velocity distributions for a wide variety of physical parameters. The model was sufficiently simple so as to allow physical interpretation of the observed trends and sufficiently flexible for the study of the mechanisms in operation at the surface.

The accommodation coefficients were similar in trend to those found in other theories concerning the surface field. However, it is important to examine the fate of the semi-trapped particles because not only do sufficient number escape to give much lower values of the trapping fraction but also calling them absolutely trapped leads to significant errors in the accommodation coefficients. It was shown that these particles could be accounted for by the semi-trapped distribution method which gave physically reasonable values of the

trapping probabilities and accommodation coefficients. This effect in particular indicates that the attractive field of the surface must be an integral part of any gas-surface interaction model even at relatively high incident beam energies.

The distributions of flux and velocity showed that several processes contribute to their form and their variation with the basic parameters. A notable feature of these distributions was the presence of definite structure for certain values of the interaction parameters. This structure arises from the summation of two subdistributions to form the observed distribution: one consisting of the particles which had one collision with a surface atom and the other consisting of those which had collisions with more than one surface atom. This structure has been seen in other theoretical work but was hitherto unexplained; it has also been observed in some experimental results but in not enough detail to confirm this interpretation of it.

A comparison with an intermediate energy experiment was performed and the theory showed an encouraging ability to predict the experimental absolute flux levels. This comparison is contingent on the recognition of certain difficulties in the experiment and cannot provide conclusive information about the validity of the model. The fitting of the model to the experimental results illustrates that information about the surface field parameters can be obtained in this manner. Preliminary drag calculations based on this comparison showed that the drag coefficients for clean surfaces can be quite low.

The most remarkable result of this study is the very complex picture of the interaction which evolves from a relatively simple set of assumptions. It seems unreasonable to expect that more elaborate assumptions will lead to less complexity in the results and hence, it must be concluded that there are no easy solutions to this problem. For instance, it is clear that the distributions will in general be composed of a superposition of several subdistributions; the derivation of closed form expressions for the distributions is thus a formidable problem in itself. More success may be achieved in the representation of the accommodation coefficients. The model given in this work then has brought attention to and clarified some of the mechanisms which are present in gas-surface interactions and hopefully these insights will contribute to the further understanding of satellite aerodynamics.

REFERENCES

1. Patterson, G. N. — "A State-of-the-Art Survey of Some Aspects of the Mechanics of Rarefied Gases and Plasmas", University of Toronto, UTIAS Review No. 18 (1964)

2. French, J. B. — "Molecular Beams for Rarefied Gasdynamics Research" NATO AGARDograph No. 112 (1966)

3. O'Keefe, D. R. — "The Scattering of High Energy Argon Atoms from a Well Characterized (100) Tungsten Surface", University of Toronto, UTIAS Report No. 132 (1968)

4. Johnson, F. S. — "Atmospheric Structure", Astronautics, American Rocket Society, (1964)

5. Prince, R. H. — "The Interaction of Low-Energy Atmospheric Ions with Controlled Surfaces", University of Toronto, UTIAS Report No. 133 (1968)

6. Goodman, F.O. — "On the Theory of Accommodation Coefficients IV: Simple Distribution Function Theory of Gas Solid Interaction Systems", J. Phys. Chem. Solids 26, (1965)

7. Trilling, L. — "Theory of Gas-Surface Collisions" in FGSI* (1967)

8. Oman, R.A. — "Numerical Calculations of Gas-Surface Interactions" NASA Contractor Report CR-481 (1966)

9. Goodman, F.O. — "Three Dimensional Hard Spheres Theory of Scattering of Gas Atoms from a Solid Surface I. Limit of Large Incident Speeds". Surface Science 7 (1967)

10. Hirschfelder, J.O.
Curtiss, C. F.
Bird, R. B. — "Molecular Theory of Gases and Liquids", Wiley, New York. (1954)

11. Townsend, S. J. — "Free Molecule Flow Through Axi-Symmetric Tubes", University of Toronto, UTIAS Report No. 106 (1965)

12. Benson, G. C.
Yun, K. S. — "Surface Energy and Surface Tension of Crystalline Solids in "The Solid-Gas Interface", Vol I. (Flood ed) New York, (1967)

13. Lyon, M. B.
Somorjai, G. A. — "Surface Debye Temperatures of the (100), (111) and (110) Faces of Platinum", J. Chem. Phys. 44, (1966)

14. Hurlbut, F. C. — "Current Developments in The Study of Gas-Surface Interactions" RGDS V(Oxford), 1966 **

15. Cabrera, N. " The Structure of Crystal Surfaces" Disc. Faraday Soc. 28 (1959)

16. Zwanzig, R. W. "Collision of a Gas Atom with a Cold Surface" J. Chem. Phys. 32 (1960)

17. McCarroll, B. Ehrlich, G. "Trapping and Energy Transfer in Atomic Collisions with a Crystal Surface", J. Chem. Phys. 38 (1963)

18. Goodman, F. O. "The Dynamics of Simple Cubic Lattices. I. Applications to the Theory of Thermal Accommodation Coefficients", J. Phys. Chem. Solids 23 (1962)

19. Trilling, L. "A Theory of Energy Accommodation", J. de Mécanique. 3 (1964)

20. Kinzer, E. T. Chambers, C. M. "On the Collision of Atoms with Crystal Surfaces" Surface Science 3 (1965)

21. Logan, R. M. Stickney, R. E. "Simple Classical Model for the Scattering of Gas Atoms from a Solid Surface", J. Chem. Phys 44 (1966)

22. Baule, B. "Theoretische Behandlung der Ersheinungen in Verdunnten Gasen", Ann. Physik 44 (1914)

23. Erofeev, A. I. "On the Interaction of Atoms with the Surface of a Solid Body" Grumman Research Translation TR-38 (1966) from Inzhenernyi Zhurnal V. IV no. 1 (1964)

24. Oman, R. A. et al "Interactions of Gas Molecules with an Ideal Crystal Surface", J. AIAA 2 (1964)

25. Oman, R. A. "Research in Gas-Surface Interactions. 1964-65. Part I. Numerical Calculations of Gas-Surface Interactions", Grumman Research Report RE-222 (1965)

26. Goodman, F. O. "One Dimensional Theory of Desorption". Surface Science 5 (1966)

27. Goodman, F. O. "The Dynamics of Simple Cubic Lattices II. The Effects of Surface Impurities on the Lattice Motion". J. Phys. Chem. Solids 23 (1962)

28. Goodman, F. O. "On the Theory of Accommodation Coefficients. III Classical Perturbation Theory for the Thermal Accommodation of Light Gases". J. Phys. Chem. Solids 24, 1451 (1963)

29. Goodman, F. O. — "On the Theory of Thermal Accommodation V. Classical Theory of Thermal Accommodation and Trapping" RGDS IV (Toronto) 1964

30. Goodman, F. O. — "Response Functions and Thermal Motions of a Simple n-Dimensional Lattice Model". Surface Science 3 (1965)

31. Kinzer, E. T. — "The Collision of a Particle with a Crystal Surface" Ph.D. Dissertation, University of Virginia (1961)

32. Chambers, C. M.
Kinzer, E. T. — "Higher Dimensional Crystal Models: A Theory of Thermal Accommodation Coefficients" Surface Science 4, (1966)

33. Karamcheti, K.
Scott, L. B. — Discussion, Pg. 536 FGSI (1967)

34. Thomas, L. B.
Schofield, E. B. — "Thermal Accommodation Coefficients of Helium on a Bare Tungsten Surface", J. Chem. Phys. 23 (1955)

35. Logan, R. M.
Keck, J. C.
Stickney, R. E. — "Simple Classical Model for the Scattering of Gas Atoms from a Solid Surface II. Additional Analyses and Comparisons", RGDS V (Oxford) 1966

36. Stickney, R. E.
Logan, R. M.
et al — "Simple Classical Model for the Scattering of Gas Atoms from a Solid Surface III. Analyses for Monoenergetic Beamd and Lock-In Detector Signals", FGSI (1967)

37. Logan, R. M .
Keck, J. C. — "Classical Theory for the Interaction of Gas Atoms with Solid Surfaces", M.I.T. Fluid Mechanics Lab Pub. No. 67-8 (1967)

38. Oman, R. A.
Bogan, A.
Li, C. H. — "Theoretical Prediction of Momentum and Energy Accommodation for Hypervelocity Gas Particles on an Ideal Crystal Surface, RGDS IV (Toronto) 1964

39. Oman, R. A.
Calia, V. S.
Weiser, C. H. — "Research on Gas-Surface Interactions 1965-66", Grumman Research Report RE-272 (1966)

40. Oman, R. A. — "Research on Gas-Surface Interactions 1966-67 Part II - Numerical Experiments on Scattering of Noble Gases from Single Crystal Silver". Grumman Research RE-306 (1967)

41. Beder, E. C. — "Quantum Mechanics in Gas-Crystal-Surface Van der Waals Scattering" in "Advances in Atomic and Molecular Physics", Vol. III. Bates and Estermann ed. New York (1967)

42. Howsmon, A. J. — "Atomic Scattering from a Perfect Crystal I". RGDS IV (Toronto) 1964.

43. " — "Atomic Scattering from a Perfect Crystal II". RGDS V (Oxford) 1966

44. Healy, T. J. — "The Scattering of Particles from Rough Surfaces" FGSI (1967).

45. Wallis, R. F. — "Surface Effects on Lattice Vibrations". Surface Science 2 (1964)

46. Macrae, A. U. — "Surface Atom Vibrations". Surface Science 2, (1964)

47. Kittel, C. — "Introduction to Solid State Physics", 3rd edition, New York (1966)

48. Kornelson, E. V. — "The Ionic Entrapment and Thermal Desorption of Inert Gases in Tungsten for Kinetic Energies of 40 ev to 5 Kev". Can. J. Phys. 42, (1964)

49. Abrahamson, A. A. — "Repulsive Interaction Potentials Between Rare Gas Atoms. Homonuclear Two-Centre Systems", Phys. Rev. 130, (1963)

50. " — "Repulsive Interaction Potentials Between Rare Gas Atoms. Heteronuclear Two-Centre Systems", Phys. Rev. 133, (1964)

51. Girifalco, L. A. Weizer, V. G. — "Application of the Morse Potential to Cubic Metals", Phys. Rev. 114, (1959)

52. Kon owalow, D. D. Hirschfelder, J. O. — "Intermolecular Potential Functions for Non-Polar Molecules", Phys. Fluids 4, (1961)

53. Chapman, S. Cowling, T. G. — "The Mathematical Theory of Non-Uniform Gases", Cambridge (1960)

54. Young, D. M. Crowell, A. D. — "Physical Adsorption of Gases" London (1962)

55. Halsey, G. D. "A Survey of Physisorption" in FGSI, (1967)

56. Ehrlich, G.
Hudda, F. G. "Interaction of Rare Gases with Metal Surfaces I. Ar, Kr and Xe on Tungsten", J. Chem. Phys. 30 (1959)

57. Bowden, F. P. "The Nature and Topography of Solid Surfaces and the Study of Van der Waals Forces in Their Immediate Vicinity", in FGSI (1967)

58. Crowell, A. D. "Approximate Methods of Evaluating Lattice Sums", J. Chem. Phys. 22, (1954)

59. Hove, J.
Krumhansl, J. A. "The Evaluation of Lattice Sums for Crystals", Phys. Rev. 92 (1953)

60. Drechsler, M. "Berechnung Von Adsorption-energien und Platzwechsel-energien on Eirikristallflachen von Metallen", Z. Electrochem 58 (1954)

61. Bacigalupi, R. J.
Neustadter, H. E. "Dependence of Adsorption Properties on Surface Structure for Body-Centered Cubic Substrates", NASA TN D-3141 (1965)

62. Goodman, F. O. "Interaction Potentials of Gas Atoms with Cubic Lattices on the 6-12 Pairwise Model", Phys. Rev. 164, (1967)

63. Margenau, H.
Pollard, W. G. "The Forces Between Neutral Molecules and Metallic Surfaces", Phys. Rev. 60, (1941)

64. Saltsburg, H.
Smith, J. N. "Molecular Beam Scattering from Solid Surfaces", in FGSI (1967)

65. Gomer, R. "Adsorption and Diffusion of Inert Gases on Tungsten", J. Chem. Phys. 29, (1958)

66. Smith, J. N. "Interactions Between Hydrogen and Oxygen Atoms and Surfaces", Gulf General Atomic GA-8273 (1967)

67. Hinchen, J. J.
Malloy, E. S.
Carroll, J. B. "Scattering of Thermal Energy Gas Beams by Metallic Surfaces", United Aircraft Report F910439-7 (1967).

68. French, J. B.
Locke, J. W. "A Time-of-Flight Velocity Analyser Using Metastable Molecules", RGDS V (Oxford) 1966.

69. Gomer, R. "Chemisorption" in FGSI (1967)

70. Schaaf, S. A.
Talbot, L. "Handbook of Supersonic Aerodynamics" section 16. NAVORD Report 1488, Vol. 5 (1959)

71. Pauling, L. C. "The Nature of the Chemical Bond", New York (1960)

72. Pierotti, R. A.
Halsey, G. D. "The Interaction of Krypton with Metals. An Appraisal of Several Interaction Theories", J. Phys. Chem. 63 (1959)

73. Neastadler, H. E.
Luke, K. P. "Low Coverage Heat of Adsorption I", NASA TN D-2430 (1964)

---

* FGSI: "Fundamentals of Gas-Surface Interactions", Saltsburg, Smith and Rogers ed. New York, (1967)

** RGDS: "Rarefied Gas Dynamics Symposium Proceedings", published by Academic Press.

APPENDIX A: ESTIMATION OF THE LENNARD-JONES POTENTIAL PARAMETERS

In this appendix, methods of estimating the Lennard-Jones (abbreviated LJ) potential parameters will be discussed for rare gas-tungsten systems and numerical results shown for these calculations. There are two distinct problems to be considered; the first is to obtain LJ parameters for the gases and the metal in self-interaction and the second is to obtain from them parameters for the gas-metal interactions. Therefore, there are two stages of approximation. For gases interacting with themselves data has been given by Konowalow and Hirschfelder (Ref.52).

		MORSE		LENNARD-JONES		
Gas	α	D ev	r_o A	σ A	ϵ ev	r_o A
He*	-	-	-	2.56	.00088	-
Ne	5.1	.00379	3.152	2.81	.00313	3.16
Ar	5.0	.0125	3.855	3.45	.0103	3.87
Kr	4.5	.0158	4.038	3.60	.0137	4.04
Xe	4.9	.0236	4.420	3.97	.0197	4.46

* the values for He are taken from Ref. 10

TABLE A.I

In this table the value $\alpha = \sigma a$ is given along with the Morse potential (abbreviated MP) parameters for later use.

To find the LJ parameters for tungsten an approximation must be made since only the MP parameter values are given in the literature; Girifalco and Weizer (Ref.51) give:

$$a = 1.4116 \quad A^{-1}$$

$$r_o = 3.032 \quad A$$

$$D = .9906 \quad ev$$

TABLE A.II

Now to get the LJ values from these: it was observed in Ref. 52 that the maximum well-depth distances were approximately the same for both potentials; this can be seen in Table A.I. Hence

$$r_o(LJ) = 2^{1/6} \sigma = r_o(M) \qquad (A.1)$$

where the relationship between $r_o(LJ)$ and σ is found by solving equation (3.3.3) for r_o. From this one gets for tungsten $\sigma = 2.70A$. A further approximation is needed to get ϵ; a method due to Hirschfelder et al (Ref.10), which was employed by Goodman (Ref.18) in going from LJ to MP, will be used

here. It is to assume that both potentials give the same effective integrated well depth. Therefore, from Eq's 3.3.3 and 3.3.4 one gets:

$$\int_{\sigma}^{\infty} D\left\{e^{-2c(r-r_o)/\sigma} - 2e^{-c(r-r_o)/\sigma}\right\} dr \qquad (A.2)$$

$$\simeq \int_{\sigma}^{\infty} 4\epsilon \left\{\left(\frac{\sigma}{r}\right)^{12} - \left(\frac{\sigma}{r}\right)^{6}\right\} dr$$

$$\frac{2D}{a} \simeq \frac{24\epsilon\sigma}{55} \qquad K = \frac{55D}{12\epsilon a\sigma} \simeq 1 \qquad (A.3)$$

where K is a parameter to indicate the validity of the approximation. The values of K for gas-gas interactions can be seen from Table A.I to be 1.07, 1.09, 1.14 and 1.10 for Ne, Ar, Kr and Xe respectively showing that the approximation is reasonable. From the values given in Table A.II one finds ϵ = 1.20 ev for tungsten self-interaction; although this may appear too large at first sight it should be noted that the energy required to remove a tungsten atom from a tungsten surface is about 8 ev (Ref.47) which accounts for the high melting point of tungsten, etc.

The next problem is to calculate the LJ parameters for the gas-metal systems. The rules that are usually used for heterogeneous systems are (see Ref.10):

$$\sigma_{12} = \tfrac{1}{2}(\sigma_{11} + \sigma_{22}) \qquad (A.4)$$

$$\epsilon_{12} = \sqrt{\epsilon_{11}\,\epsilon_{22}} \qquad (A.5)$$

where the notation is obvious. The rule (A.4) appears to be reasonable from an intuitive point of view, although there is no real physical justification for it but (A.5) may not be so obvious. It can be shown that it is what should be expected from the London forces (Ref.10) but clearly from a numerical viewpoint the possibility for error is substantial particularly when the ϵ's are very different. In any case using these rules in combination with the values already found for the metal and the gases:

System	σ A	ϵ ev
He/W	2.63	.040
Ne/W	2.75	.061
Ar/W	3.07	.111
Kr/W	3.15	.128
Xe/W	3.33	.154

TABLE A.III

It is interesting to compare these values with those used by Goodman (Ref.9) for σ in his hard sphere theory and those used by Bacigalupi and Neustadter (Ref.61).

	Table A.III		Goodman (Ref.9)	Bacigalupi et al (Ref.61)	
System	σ A	ϵ ev	σ A	σ A	ϵ ev
He/W	2.63	.040	3.16	--	--
Ne/W	2.75	.061	--	2.76	.0281
Ar/W	3.07	.111	3.48	2.94	.0586
Kr/W	3.15	.128	--	3.02	.0760
Xe/W	3.33	.154	3.79	3.20	.0857

TABLE A.IV

The values used by Bacigalupi et al (Ref.61) were found by using the combination rule A.4 on atomic radii given by Pauling (Ref.71) and the ϵ's were obtained by comparing the integrated potential equation to the Kirkwood-Muller potential equation, this will be discussed in Appendix B. It is interesting to note that Goodman obtains values of σ that are somewhat larger than those found by the above approximations. The ϵ's used by Bacigalupi et al are about 50% lower than those found here and it will be indicated in the following appendix that the Table A.III ϵ's seem to be quite high from other evidence.

An important result of these remarks is that the estimation of the LJ parameters is by no means a routine procedure as the discrepancies shown above indicate. For this reason the present model has been formulated in more general terms so that it is not dependent on any particular assumed values of the LJ parameters.

APPENDIX B: ESTIMATION OF THE ATTRACTIVE FIELD ENERGY

The surface field energy E_t plays an important role in gas-surface interactions. Unfortunately determining a definitive value of E_t for a particular system is not an easy problem since there are several ways to do this. The purpose of this discussion is to illustrate this point and to indicate the possible magnitudes of the E_t's for the rare-gas-tungsten systems. Therefore, no attempt will be made to survey this topic in detail and of course, since the present model makes no assumptions about the value of E_t for any system it is not essential from this point of view to determine precise values.

The most obvious and earliest method of evaluating E_t is by integrating a free space potential over the semi-infinite solid. That is one assumes an interatomic potential to act between a gas atom and each element of the solid and the total potential acting on the gas atom is obtained by integrating over all elements in the solid. Since it is well established that an r^{-3} variation best describes the interaction (Ref.54) the attractive part of the Lennard-Jones potential seems the most likely possibility integrating Eq. 3.3.3:

$$4\epsilon\sigma^6 \rho \int_0^{\infty}\int_0^{\infty}\int_0^{2\pi} \frac{R\, dR d\theta d\tau}{((z+\tau)^2+R^2)^3} = -\frac{2\epsilon\sigma^6\rho\pi}{3\, z^3} \qquad (B.1)$$

This integration has been done in a cylindrical co-ordinate system (R, θ, $z + \tau$) where z is the height of the gas atom above the surface and τ is the depth of the potential element below the surface. The parameter ρ is used to correct for the fact that each unit volume of the semi-infinite solid does not contain exactly one atom. In terms of the interatomic spacing d of a body-centered-cubic lattice: $\rho = n/d^3$ where n is the number of atoms per unit cell of the lattice. This number is 2 for a body-centered-cubic solid such as tungsten. In order to obtain a value of E_t some value of z must be assumed to represent the distance from the surface where the field is cut off because Eq. B. 1 has an infinity at zero. There are a few likely possibilities for this cutoff: σ, d and r_o. However, there is no strong reason for using any one of these values, in effect a wide range of E_t values can be produced by various choices of the cutoff. Oman (Ref.25) has suggested using σ on the basis of his calculations; this value will be used here. Clearly the estimates given by Eq. B.1 also depend on the LJ potential parameters and hence, are subject to any errors in the estimation of these parameters. When the parameters of Table. A.III are used the field values obtained are those shown under "integration" in Table B.I.

System	E_t Integration	E_t Kirkwood-Muller	E_t Experimental
He/W	.082 ev	--	--
Ne/W	.170	.079 ev	--
Ar/W	.420	.199	.082 ev
Kr/W	.535	.279	--
Xe/W	.760	.373	.347

TABLE B.I

As indicated in section 3.4.1 there are other ways of calculating the field. Kirkwood and Muller (see Ref.61) have evaluated the potential between two dissimilar atoms directly and hence, avoided the combination rule Eq. A.5 for finding ϵ. Their expression for the potential was:

$$\varphi_{KM}(r) = -\frac{6\,mc^2}{r^6} \quad \frac{\alpha_A\,\alpha_M}{\frac{\alpha_A\,\alpha_M}{\chi_A\,\chi_M}} \qquad (B.2)$$

where:

χ = diamagnetic susceptibility

α = electronic polarizability

m = electron rest mass

c = velocity of light

and the subscripts "A" and "M" refer to the adatom and the metal respectively. Basically the method proceeds by integration using an ϵ determined by comparing the integrated forms of Eq's B.1 and B.2:

$$4\epsilon\sigma^6 = 6mc^2 \quad \frac{\alpha_A\,\alpha_M}{\frac{\alpha_A\,\alpha_M}{\chi_A\,\chi_M}} \qquad (B.3)$$

Following the technique of Bacigalupi and Neustadter (Ref.61), the values of σ are estimated using the averages of the atomic covalent radii given by Pauling (Ref.71). Then ϵ can be found from Eq. B.3. The parameters thus obtained were given in Table A.IV. The resulting E_t values are shown in Table B.1; they were found using exactly the same method used for the integration column except that these other values of the LJ parameters were employed. Comparison of this method and the integration method suggests that the high values of E_t given by the latter is likely due to the overestimation of ϵ using the combination rule Eq. A.5.

It was mentioned in section 3.4.2 that there is some doubt whether the pairwise summation and integration methods are physically correct; Young and Crowell (Ref. 54) have remarked on this. One type of theory considers the potential as arising from the London forces between the electron distribution in the solid and the gas atom. Typical of this approach is the work of Margenau and Pollard (Ref.63); several other theories of the same kind are reviewed in Ref. 54. However, in general numerical values of E_t are difficult to obtain from this type of theory and all of them seem to be beset by difficulties of one kind or another. Pierotti and Halsey (Ref.72) made a study of most of the proposed theories and compared the predictions with experimental results for the physisorption of krypton on tungsten which they had obtained. They concluded that the Kirkwood-Muller approach was the best. It should be noted that other such studies have concluded in favour of other theories, see for instance Ref.73. In general, the theory of the surface field is currently clouded with

uncertainties.

Some experimental measurements of the activation energy of desorption of the rare gases from tungsten are available. Assuming this quantity is similar to E_t one can regard these experiments as determinations of the surface field energy. Gomer (Ref.65) obtained a value of approximately .082 ev for the Ar/W case and Ehrlich and Hudda (Ref.56) found a value of .347 ev for Xe/W. These values have been entered in Table B.I under the heading "experimental". They suggest that the integration methods over estimate the field although the Kirkwood-Muller theory seems to give a good (i.e. near the experimental) value for Xe/W. Clearly this remark is provisional and there certainly is not enough data available on which to base sound conclusions.

It is clear even from this very brief survey that E_t cannot be determined with enough accuracy to justify its confident use in a gas-surface interaction theory. Hence, in the present model the non-dimensional ratio E^* has been used.

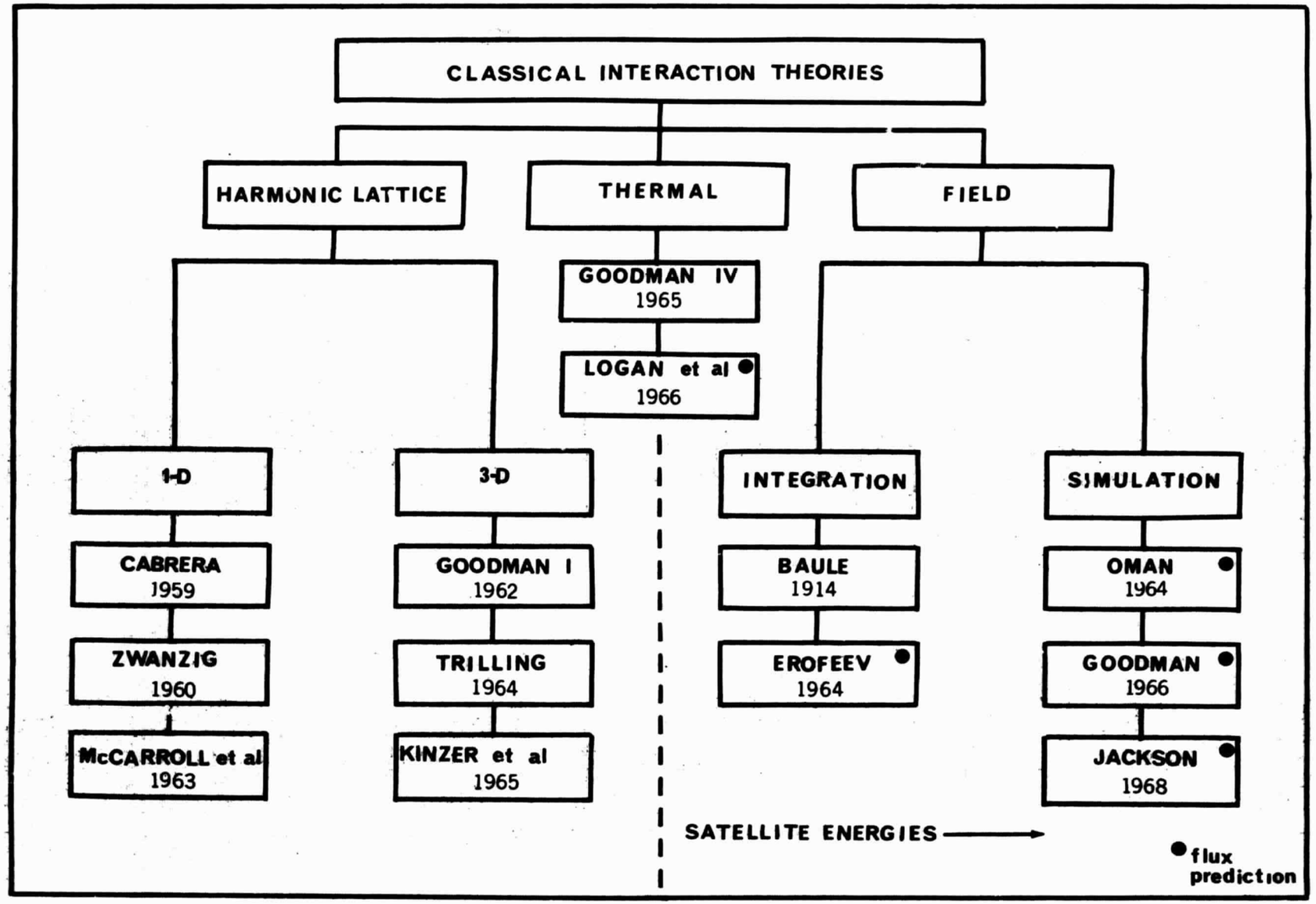

FIG. 2.1 CHART OF CLASSICAL GAS-SURFACE INTERACTION THEORIES

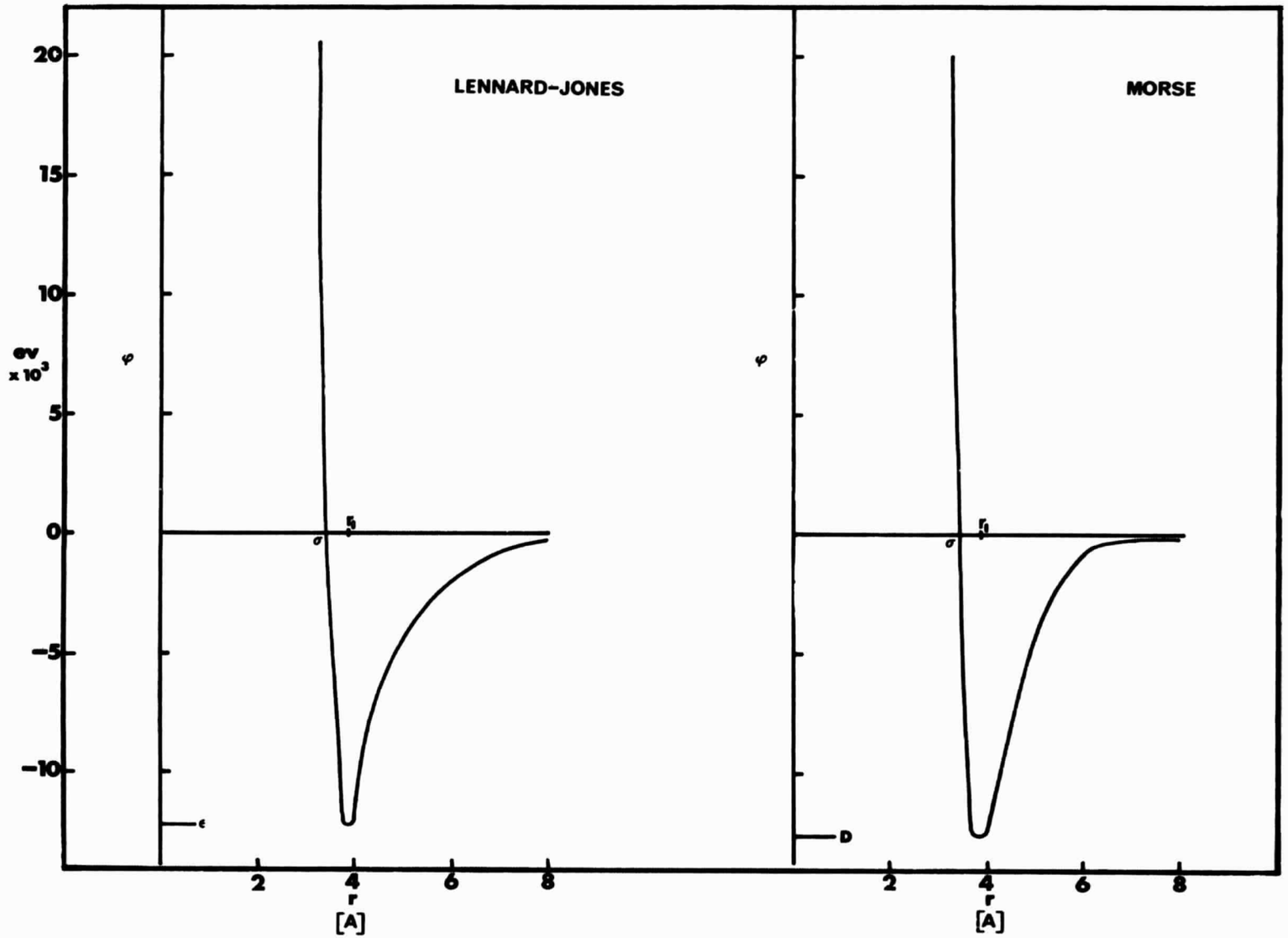

FIG. 3.1 THE LENNARD-JONES AND MORSE POTENTIALS.
Plotted to scale for the Argon self-interaction values given in Table A.I.

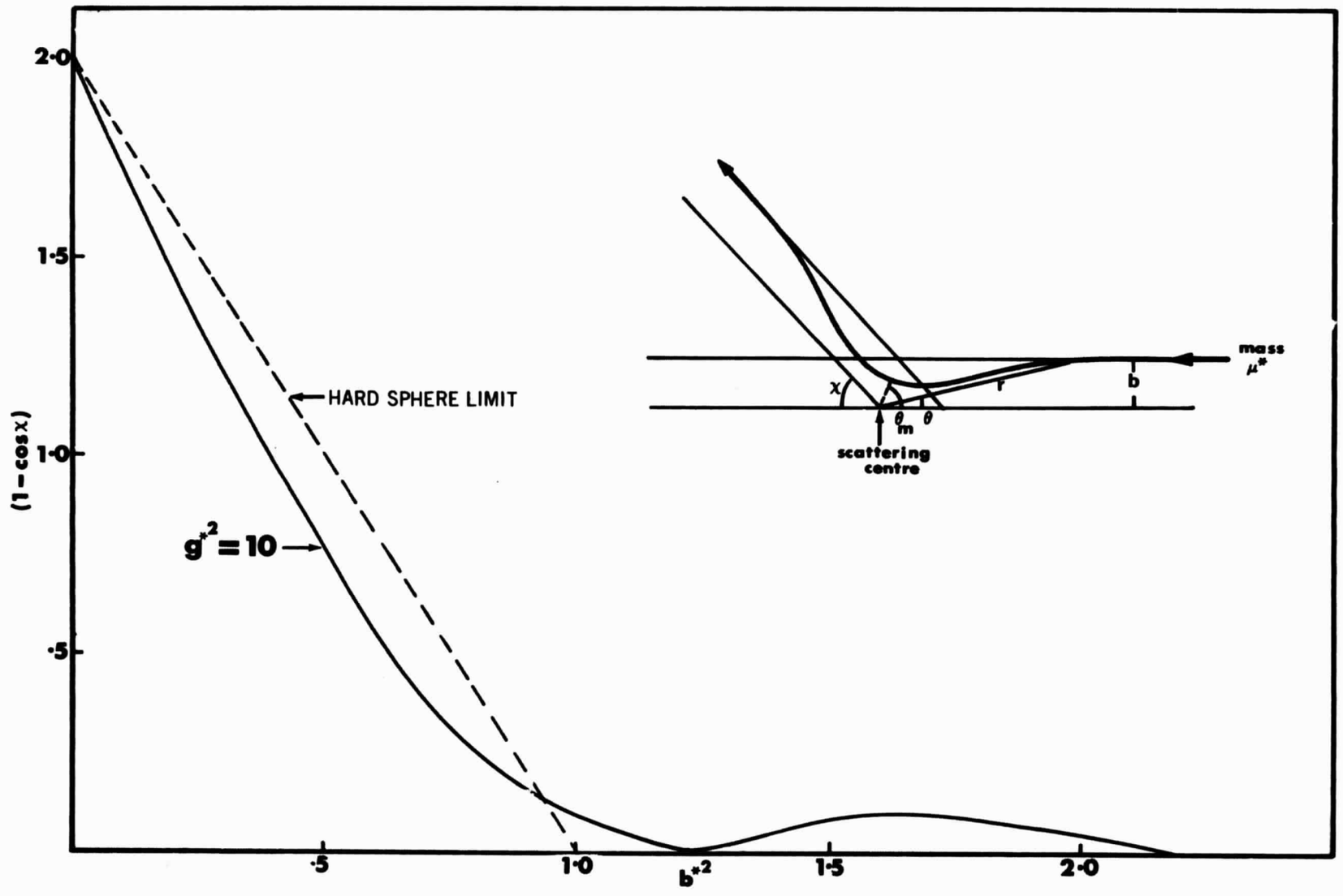

FIG. 3.2 THE HARD SPHERE APPROXIMATION TO THE LENNARD-JONES POTENTIAL.
Plotted from data given in Ref. 10.

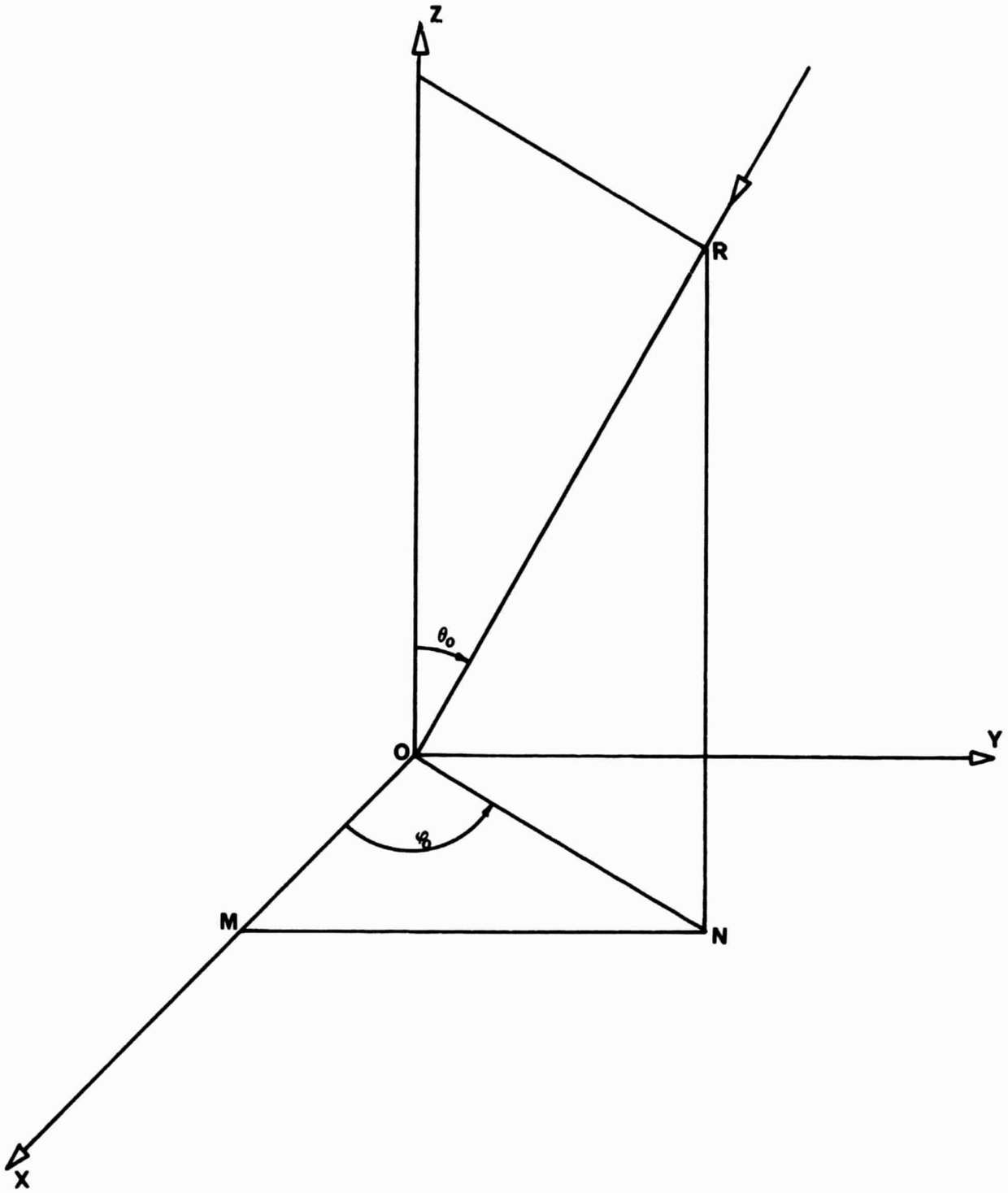

FIG. 4.1 DEFINITION OF THE INITIAL ANGLES.

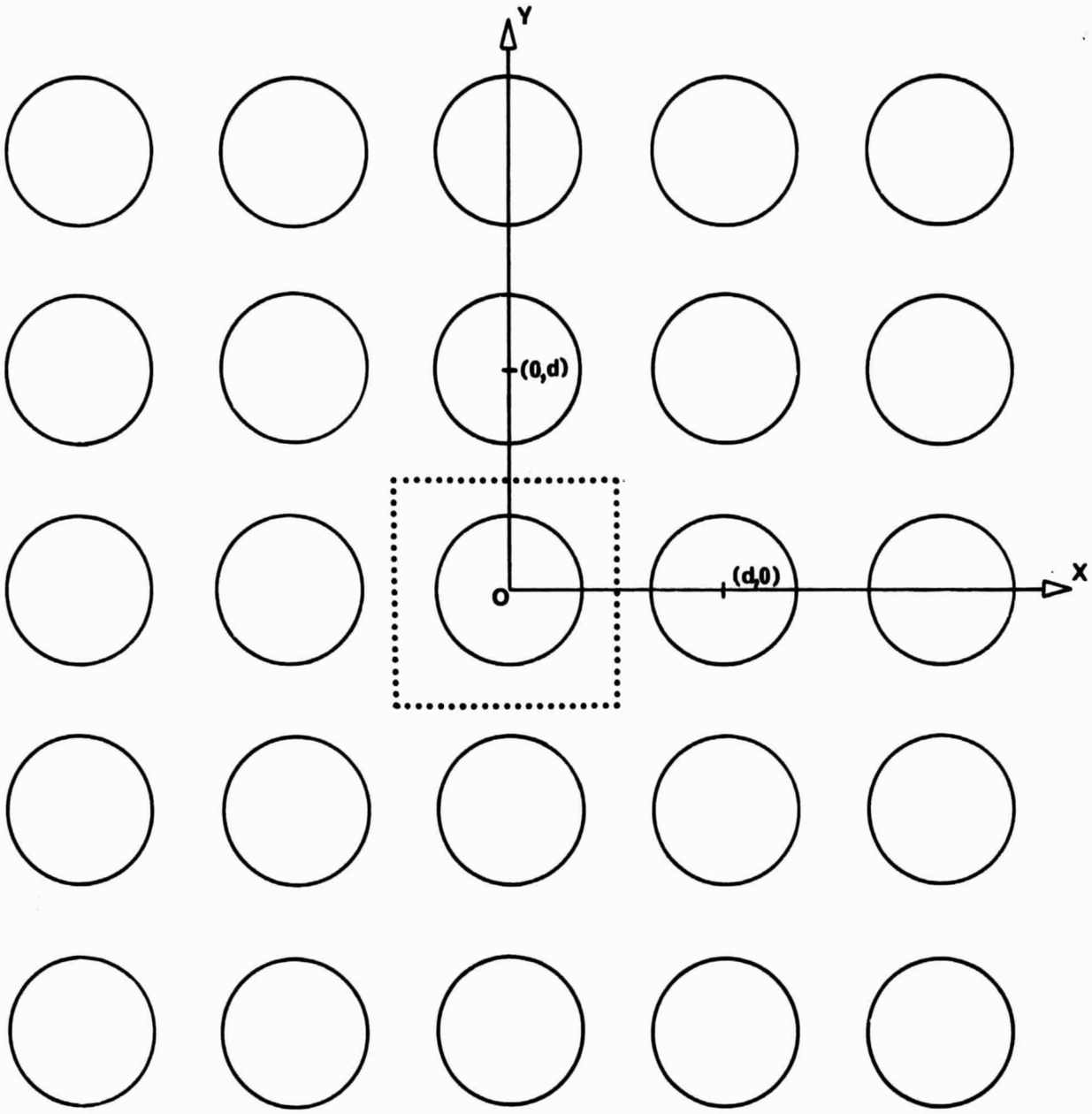

FIG. 4.2 THE SQUARE SURFACE ARRAY.
The dotted lines indicate the aiming (or target) area.

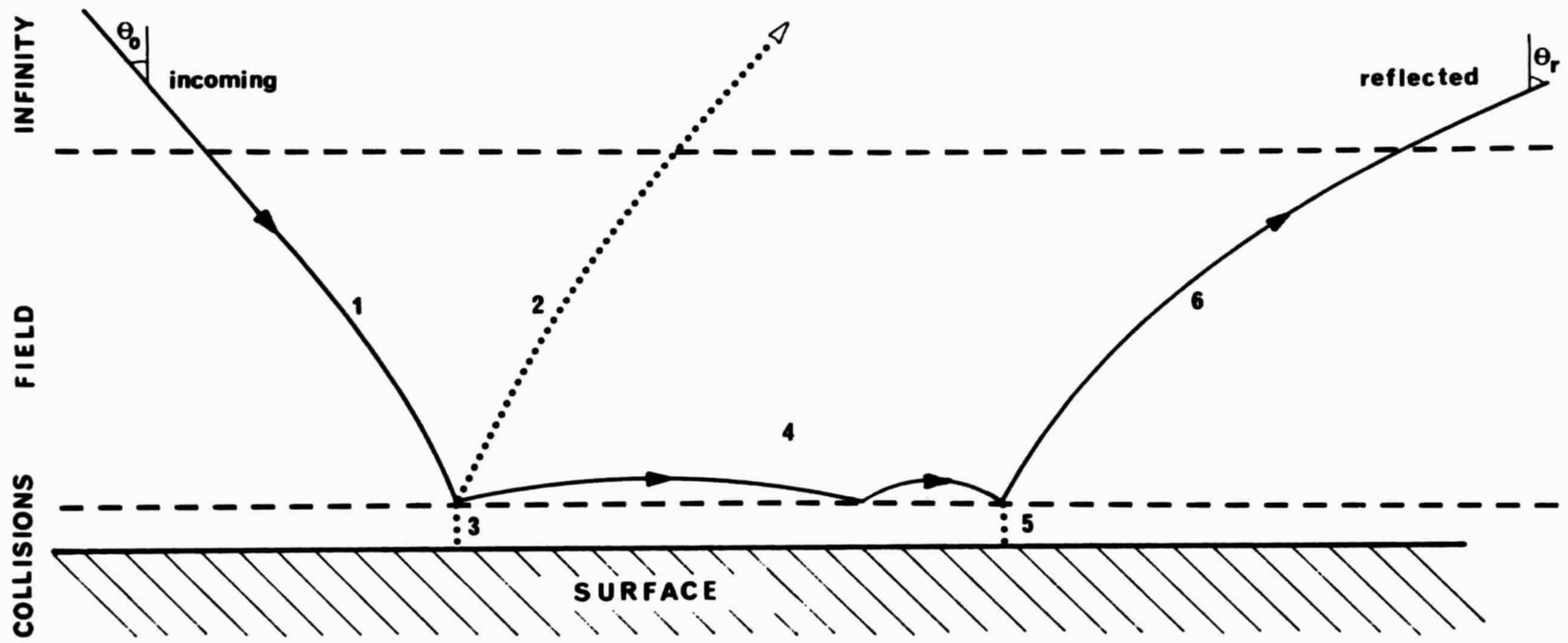

FIG. 4.3 SCHEMATIC ILLUSTRATION OF SOME OF THE TRAJECTORY POSSIBILITIES.
The surface and the regions above it are denoted as shown for illustrative purposes. The surface attractive field acts only in the region shown - collisions may be either single or multiple in the "collisions" region. The solid line shows the trajectory of a semi-trapped particle which eventually escapes; the dotted lines show some of the other possibilities.

1. An incoming trajectory which is curved inward by the field.
2. Escape after a single encounter with the surface.
3. Absolute trapping on the first encounter with the surface.
4. Semi-trapped with two subsequent encounters.
5. Semi-trapped - ultimately absolutely trapped.
6. Semi-trapped - ultimately escaped.

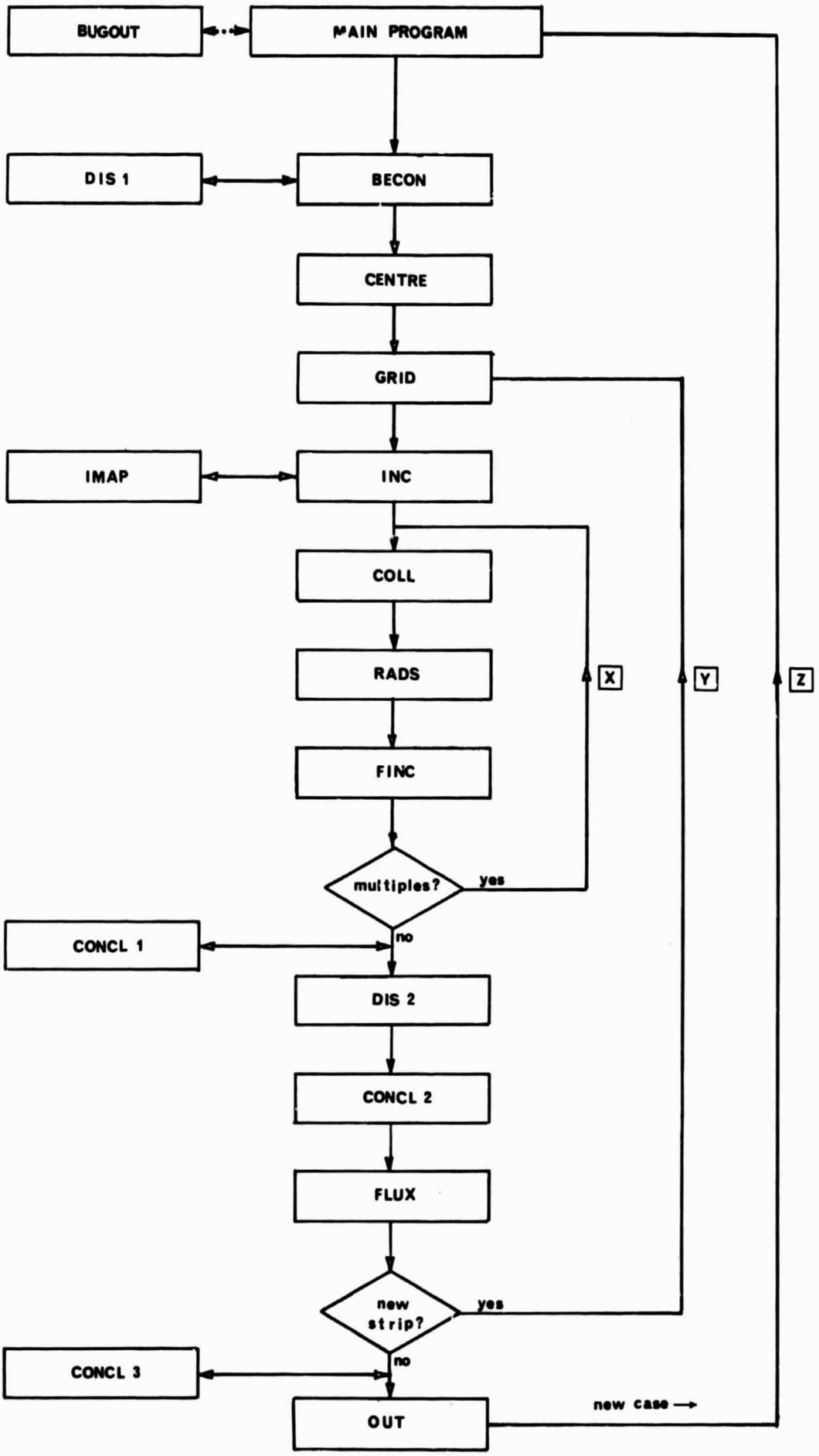

FIG. 4.4 BLOCK DIAGRAM OF THE BASIC COMPUTER PROGRAM

IMPACT MAP R=1.3 RUN 810

GAS.....ENERGY= 8.52 EV VEL= 6415.0 PS INC= 45.0 AZ= 0.0 MASS= 39.95 AMU DISP= 0.25 DISCN2= 0.0502

SURFACE.MASS= 183.90 AMU PL= 0.217 ELJ= 0.111 EV SLJ= 5.370 AU D= 3.160 AU TOTAL= 900 TIME= 8.3 SECS

COLLISIONS

	1	2	3	4	5	6	7	8	9	10
	830	70	0	0	0	0	0	0	0	0

R/D= 1.2566 AVENCOLL= 1.07778 MAX LOSS(PC)= 29.32 MIN FIRST EV= 6.022 BAULE(BASE)= 0.29323 BAULE(COLL)= 0.31206

AVERAGES-NC FIELD (INC= 43.63 EN= 8.95)

FIRST	INCR= 53.01	(COS)= 0.5671	DEV= -8.01	AZR= 360.00	DEV=-360.00	VELR= 0.8320	AVEN= 5.934	PC FLUX=	92.222
MULTIPLE	58.17	0.5231	-13.17	0.01	-0.01	0.9198	7.211		7.778
TOTAL	53.41	0.5637	-8.41	0.00	-0.00	0.8388	6.034		100.000

AVERAGES-FIELD

FIRST	INCR= 50.81	(COS)= 0.6012	DEV= -5.81	AZR= 360.00	DEV=-360.00	VELR= 0.7818	AVEN= 5.234	PC FLUX=	90.933
MULTIPLE	61.46	0.4728	-16.46	0.01	-0.01	0.8921	6.783		9.067
TOTAL	51.77	0.5856	-6.77	0.00	-0.00	0.7918	5.375		100.000

ACCOMMODATION COEFFICIENTS

	ENERGY	NORM MOM	TANG MOM
NO FIELD	0.29184	0.35416	0.18806
BASIC	0.54112	0.55075	0.58650
WITH SEMI	0.45888	0.44925	0.41350

TRAPPING

	FIRST	MULTIPLE	TOTAL
ABSOLUTE	0.00	0.00	0.00
SEMI	14.22	0.00	14.22
ESCAPED	78.00	7.78	85.78
TOTAL	92.22	7.78	100.00

SEMI-TRAPPED DISTRIBUTION

C	10	20	30	40	50	60	70	80	90
0.5	0.00000	0.00000	0.00000	0.00000	0.00000	0.00000	0.00000	0.00000	0.00000
1.7	0.00000	0.00000	0.00000	0.00000	0.00000	0.00000	0.00000	0.00000	0.00000
2.6	0.00000	0.00000	0.00000	0.00000	0.00000	0.00000	0.00000	0.00000	0.00000
3.4	0.00000	0.00000	0.00000	0.00000	0.00000	0.00000	0.00000	0.00000	0.00000
4.3	0.00000	0.00000	0.00000	0.00000	0.00000	0.00000	0.00000	0.00000	0.00000
5.1	0.00000	0.00000	0.00000	0.00000	0.00000	0.00000	0.00000	0.00000	0.00000
6.0	0.00000	0.00000	0.00000	0.00000	0.00000	0.00000	0.00000	0.00000	0.00000
6.8	0.00000	0.00000	0.00000	0.00000	0.00000	0.00000	0.00000	0.25000	0.00000
7.7	0.00000	0.00000	0.00000	0.00000	0.00000	0.00000	0.00000	0.42188	0.32813
8.6	0.00000	0.00000	0.00000	0.00000	0.00000	0.00000	0.00000	0.00000	0.00000

FIG. 4.5 TYPICAL COMPUTER OUTPUT.
Some of the entries are not significant for the present model.

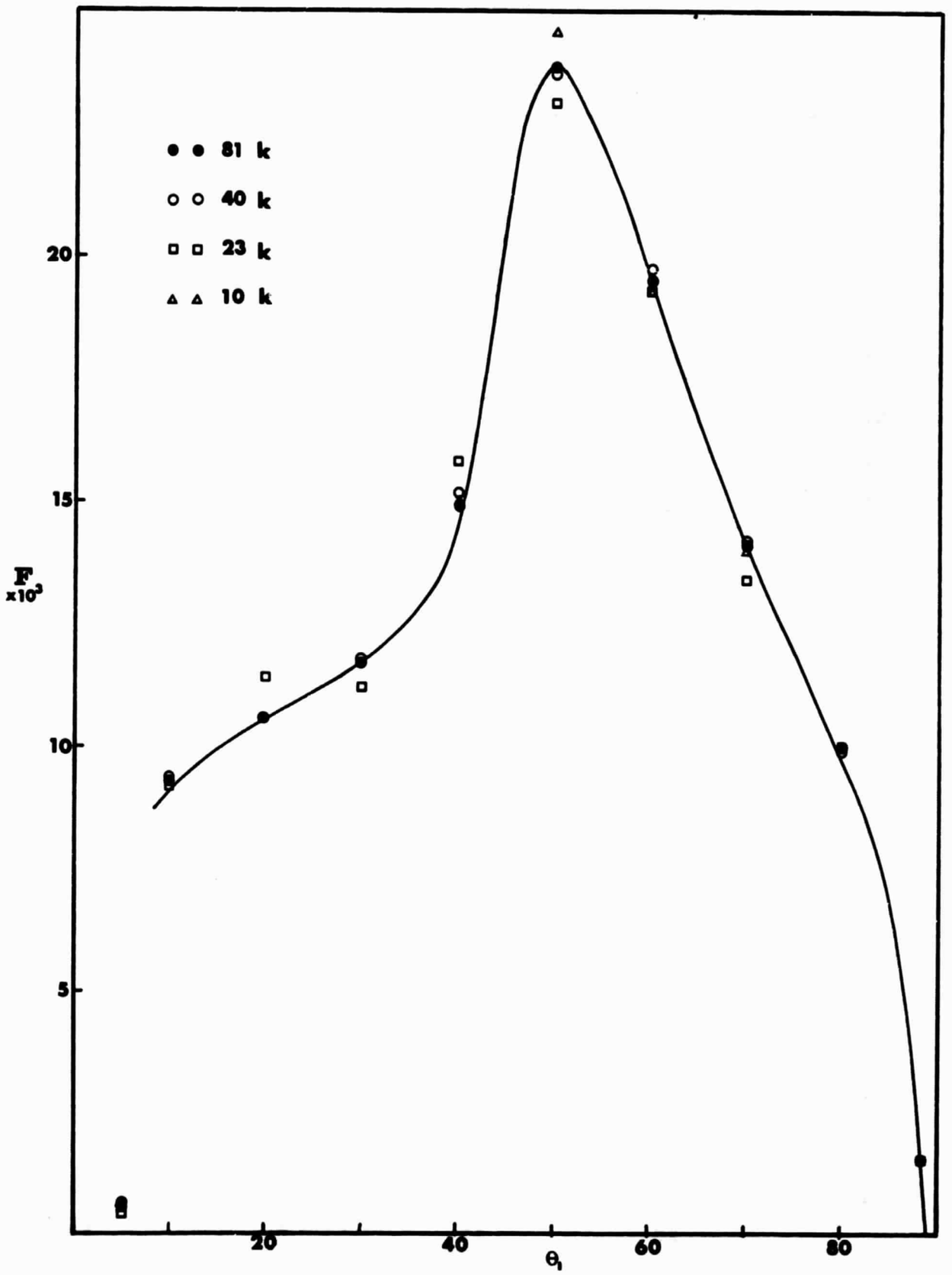

FIG. 5.1.1 VARIATION OF THE NORMALIZED PRIMARY FLUX (F) WITH THE NUMBER OF TRAJECTORIES.
Detector mode 10° resolution. Ar/W mass ratio, $R^* = 1.2$, $E_o^* = 20$, $\theta_o = 45°$, $\phi_o = 0°$.

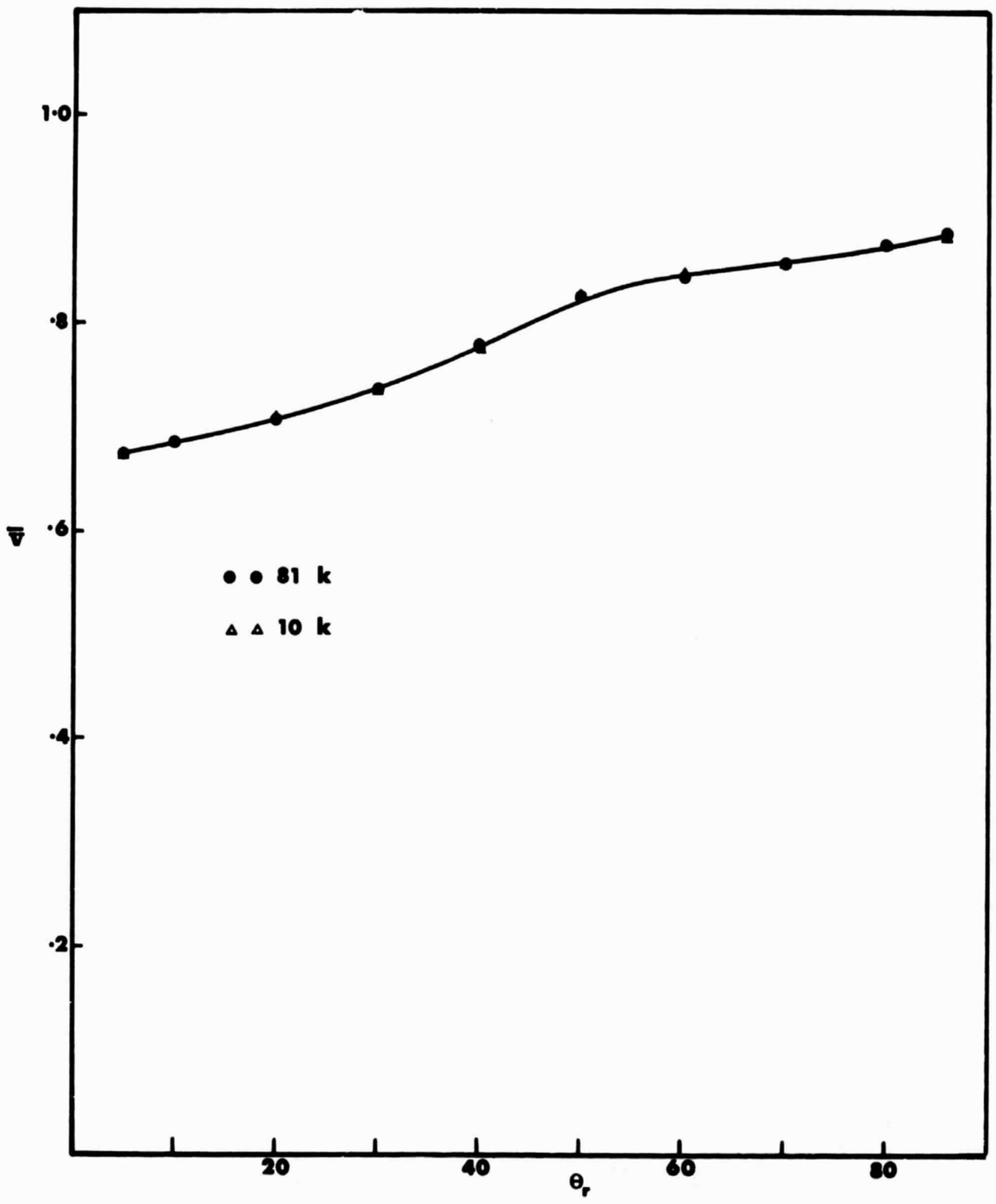

FIG. 5.1.2 VARIATION OF THE PRIMARY VELOCITY MEAN DISTRIBUTION WITH THE NUMBER OF TRAJECTORIES.
Detector mode 10^{o} resolution. Ar/W mass ratio, $R^{*} = 1.2$, $E_o^{*} = 20$, $\theta_o = 45^{o}$, $\phi_o = 0^{o}$.

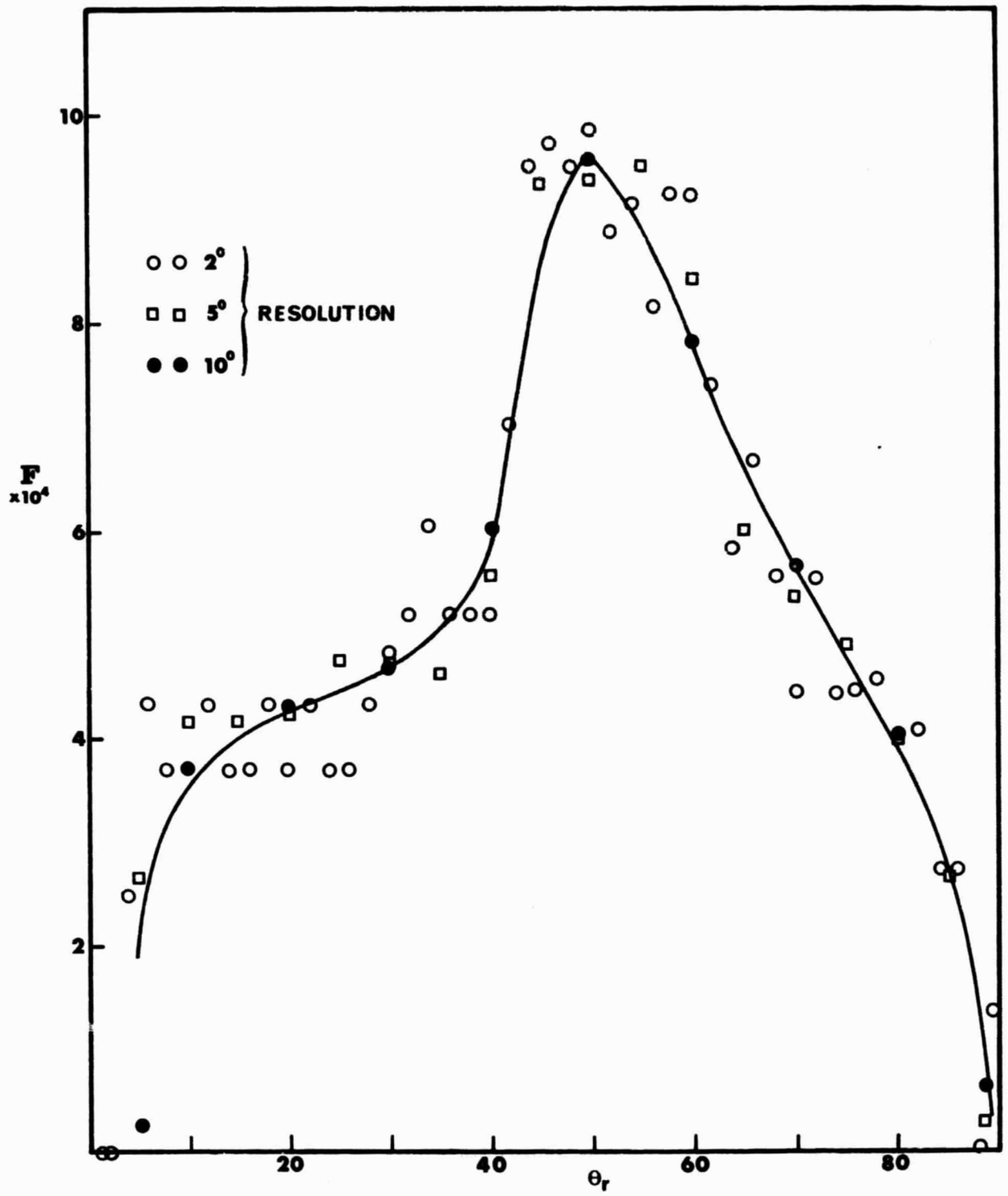

FIG.5.1.3 VARIATION OF THE NORMALIZED PRIMARY FLUX (F) WITH RESOLUTION. Detector mode. Ar/W mass ratio, $R^* = 1.2$, $E_o^* = 20$, $\theta_o = 45^o$, $\phi_o = 0^o$. The 5° and 10° resolution distributions have been scaled to their equivalent 2° resolution values by area ratio multipliers.

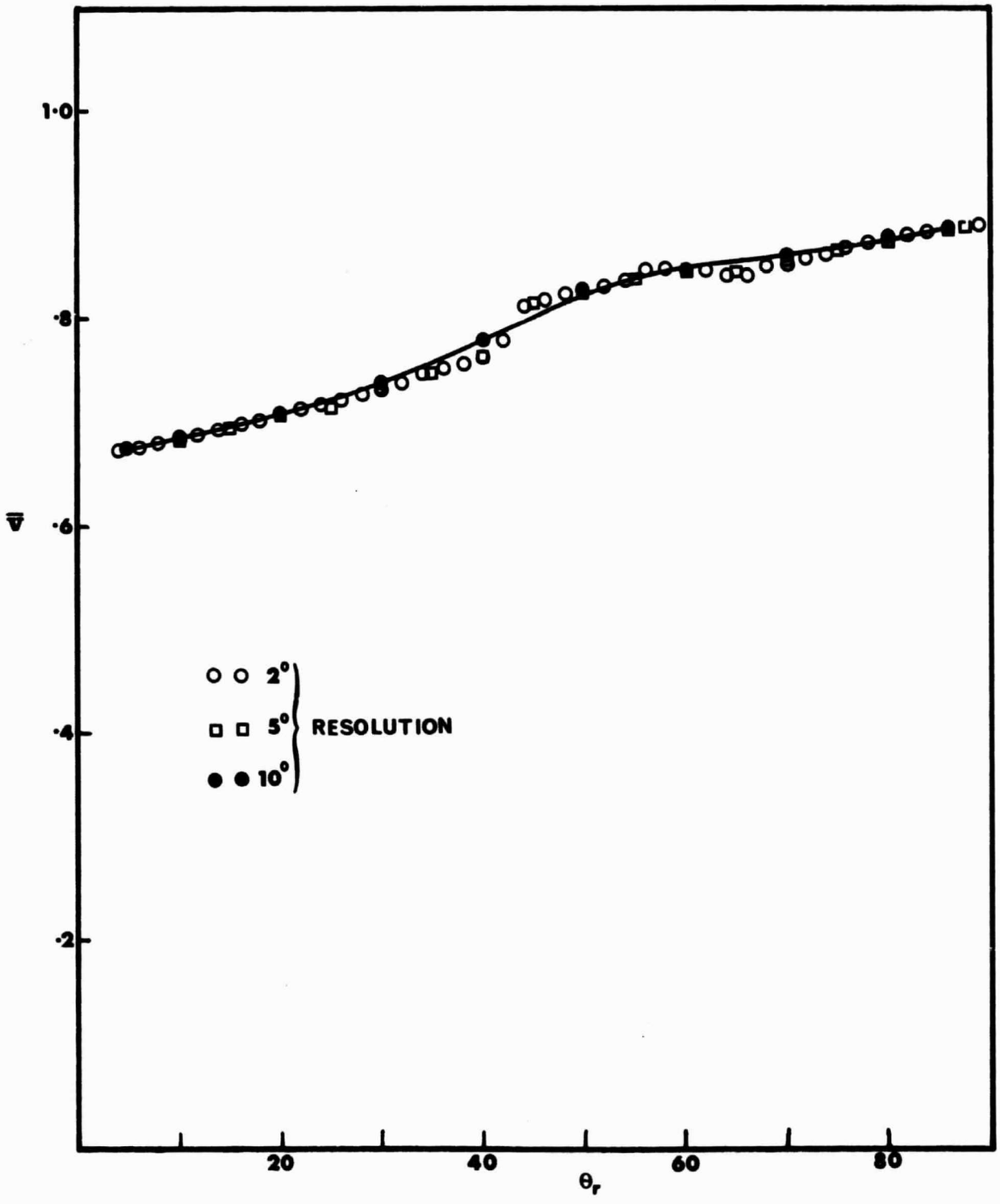

FIG. 5.1.4 VARIATION OF THE PRIMARY VELOCITY MEAN DISTRIBUTION WITH RESOLUTION.
Detector mode. Ar/W mass ratio, $R^* = 1.2$, $E_o^* = 20$, $\theta_o = 45^o$, $\phi_o = 0^o$.

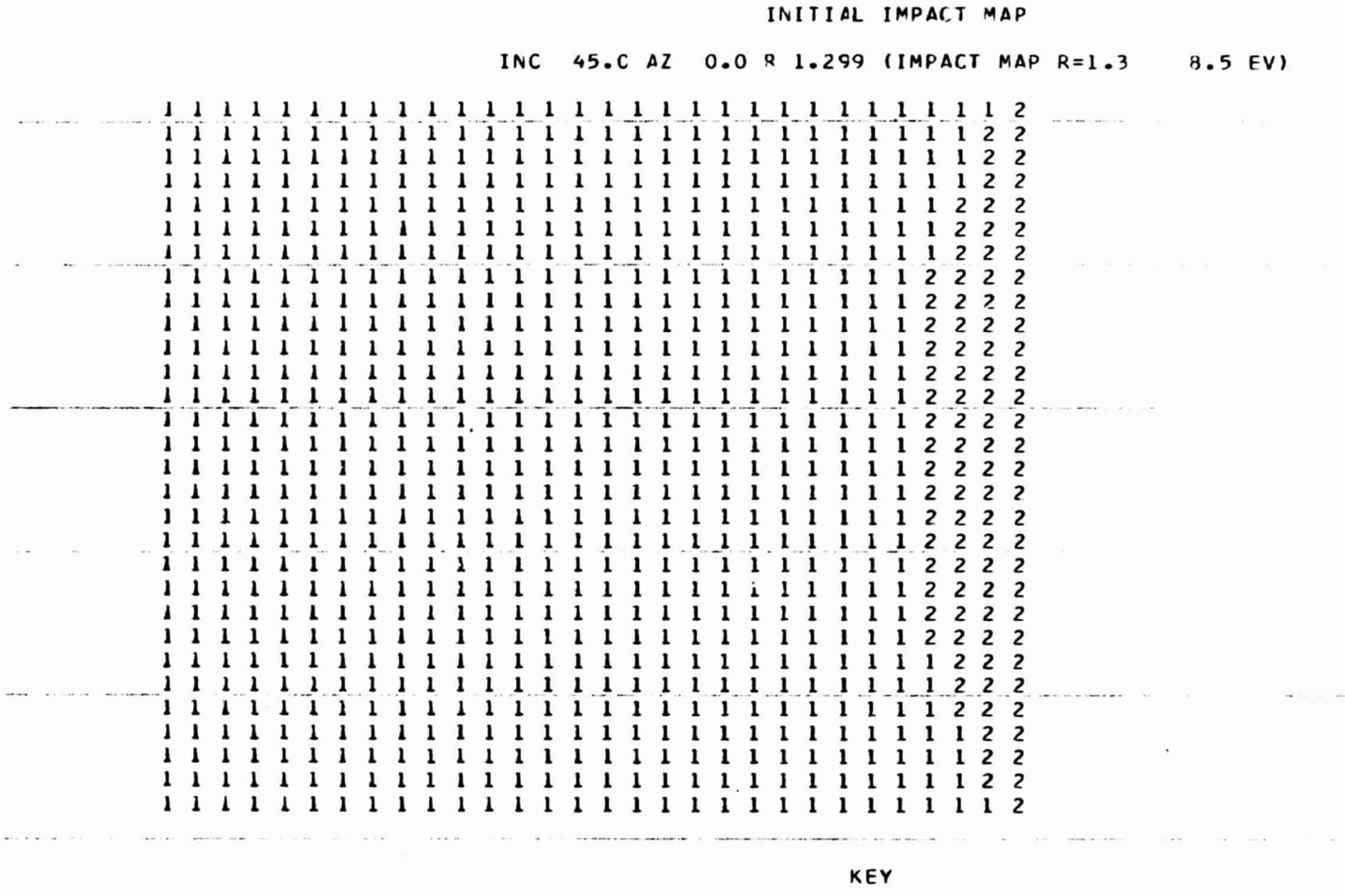

FIG. 5.2.1 INITIAL IMPACT MAP COMPUTER OUTPUT.
Ar/W mass ratio, $R^* = 1.3$, $E_o^* = 20$, $\theta_o = 45^o$, $\phi_o = 0^o$. The energy value given on the output (i.e., 8.5 ev) is not significant in the context of the present model. The key is given in terms of multiples of the lattice spacing.

FINAL DISPOSITION MAP

INC 45.0 AZ 0.0 R 1.299 (IMPACT MAP R=1.3 8.5 EV)

```
1 1 1 4 4 4 4 4 C C C C C C C C C 0 0 0 0 0 0 C 0 0 0 0 0 1
1 1 4 4 4 4 4 C C C C C 0 0 C C C 0 0 C 0 0 0 C 0 0 0 0 1 1
1 4 4 4 4 4 C 0 C C C C 0 0 C C C 0 0 C 0 0 0 C 0 0 0 0 1 1
1 4 4 4 4 C C C C C C C C 0 C C 0 0 0 0 0 0 C C C 0 0 0 0 1 1
4 4 4 4 C C C C C C C C 0 0 C 0 0 0 0 0 0 0 0 C 0 0 0 1 1 1
4 4 4 4 C C C C C C C C 0 0 C C C 0 0 C 0 0 0 C 0 0 0 1 1 4
4 4 4 C C C C C C C C C C 0 C 0 0 C 0 0 0 0 0 0 C 0 0 0 1 1 4
4 4 4 C C C C C C C C C C 0 C C 0 0 0 0 0 0 C 0 C 0 0 1 1 1 4
4 4 C C C C C C C C C C C 0 0 C C 0 0 0 0 0 0 0 C 0 0 1 1 4 4
4 4 C C C C C C C C C C C 0 0 C C 0 0 0 C 0 0 0 C 0 0 1 1 4 4
4 4 C C C C C C C C C C C 0 0 C C C 0 0 C 0 0 0 C 0 0 1 1 4 4
4 4 C 0 C C C C C C C C C 0 0 0 0 C 0 0 C 0 C C C 0 0 1 1 4 4
4 C C C C C C 0 C C C C C 0 0 0 0 C 0 0 0 0 0 0 C 0 0 1 4 4 4
4 C C C C C C C C C C C C C C 0 C C 0 0 0 0 0 0 C 0 0 1 4 4 4
4 C C C C C C C C C C C C 0 0 C 0 C 0 0 0 0 0 0 C 0 0 1 4 4 4
4 C C C C C C C C C C C C 0 0 C 0 C 0 0 0 0 0 0 C 0 0 1 4 4 4
4 C C C C C C C C C C C C 0 0 C 0 C 0 0 0 0 0 0 C 0 0 1 4 4 4
4 C C C C C C C C 0 C C C 0 0 0 0 0 0 0 0 C 0 0 0 C 0 0 1 4 4 4
4 C C 0 C C C C C C C C C 0 0 C C C 0 0 0 0 0 0 0 C 0 0 1 4 4 4
4 4 C C C C C C C C C C C C C C 0 0 C 0 0 0 0 0 0 C C 0 0 1 1 4 4
4 4 C C C C C C C C C C C 0 0 0 0 C C C C C 0 0 0 0 C 0 0 1 1 4 4
4 4 C C C C C C C C C C C 0 0 0 0 0 0 C C 0 0 0 0 0 C 0 0 1 1 4 4
4 4 C C C C C C C C C C C 0 0 C C 0 0 0 0 0 0 0 0 0 C 0 0 1 1 4 4
4 4 4 C C C C C C C C C C 0 0 C C 0 0 0 0 0 0 0 0 0 C 0 0 1 1 4 4
4 4 4 C C C C C C C C C C 0 0 C C 0 0 0 0 0 0 0 0 0 C 0 0 1 1 4 4
4 4 4 C C C C C C C C C C 0 0 C C 0 0 0 0 0 0 0 0 0 C 0 0 1 1 4 4
4 4 4 4 C C C C C C C C C 0 0 C C 0 0 0 0 0 0 0 0 0 C 0 0 1 1 4 4
4 4 4 4 C C C 0 C C C C C C 0 0 C 0 0 0 0 0 0 0 0 0 C 0 0 1 1 4
4 4 4 4 C C C C C C C C C 0 0 C C 0 0 0 0 0 0 0 0 0 C 0 0 1 1 1
1 4 4 4 4 C C C C C C C C 0 0 C C 0 0 0 0 0 0 0 0 0 C 0 0 0 1 1
1 4 4 4 4 4 C C C C C C C 0 0 C C 0 0 0 0 0 0 0 0 0 C 0 0 0 1 1
1 1 4 4 4 4 4 C C C C C 0 0 C C C 0 0 0 C 0 0 0 0 0 C 0 0 0 1 1
1 1 1 4 4 4 4 4 C C C C 0 0 C C C 0 0 0 0 0 0 0 0 0 C 0 0 0 0 1
```

KEY

C=ESCAPED+FIRST 1=ESCAPED+MULTIPLE 2=TRAPPED+FIRST 3=TRAPPED+MULTIPLE 4=SEMI+FIRST 5=SEMI+MULTIPLE

FIG. 5.2.2 FINAL DISPOSITION MAP COMPUTER OUTPUT.
Corresponds to the case of FIG. 5.2.1.

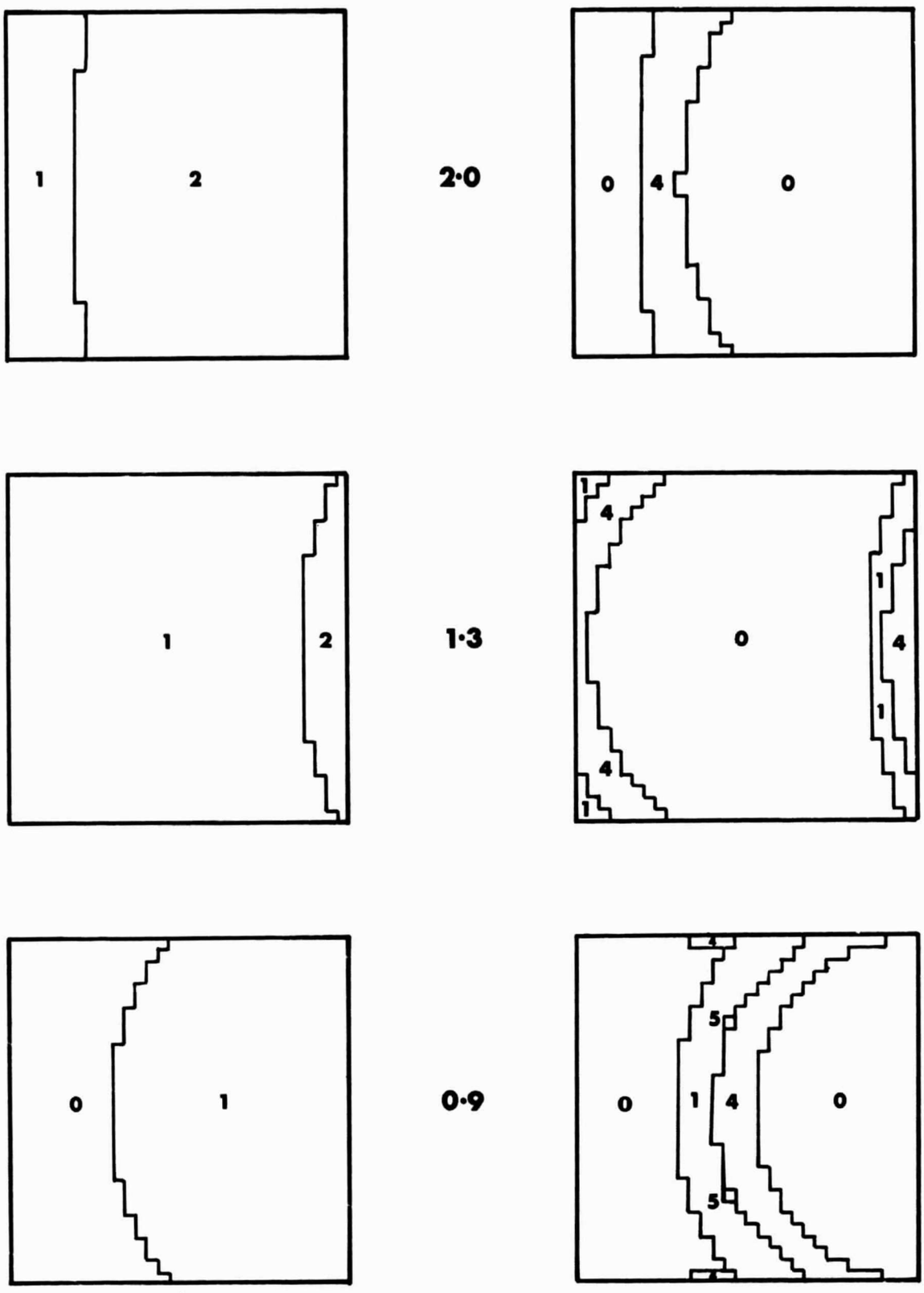

FIG. 5.2.3 INITIAL IMPACT AND FINAL DISPOSITION MAPS FOR THREE VALUES OF R*.
Ar/W mass ratio, $E_o^* = 20$, $\theta_o = 45^o$, $\phi_o = 0^o$.
Impact on the left. Final disposition on the right.

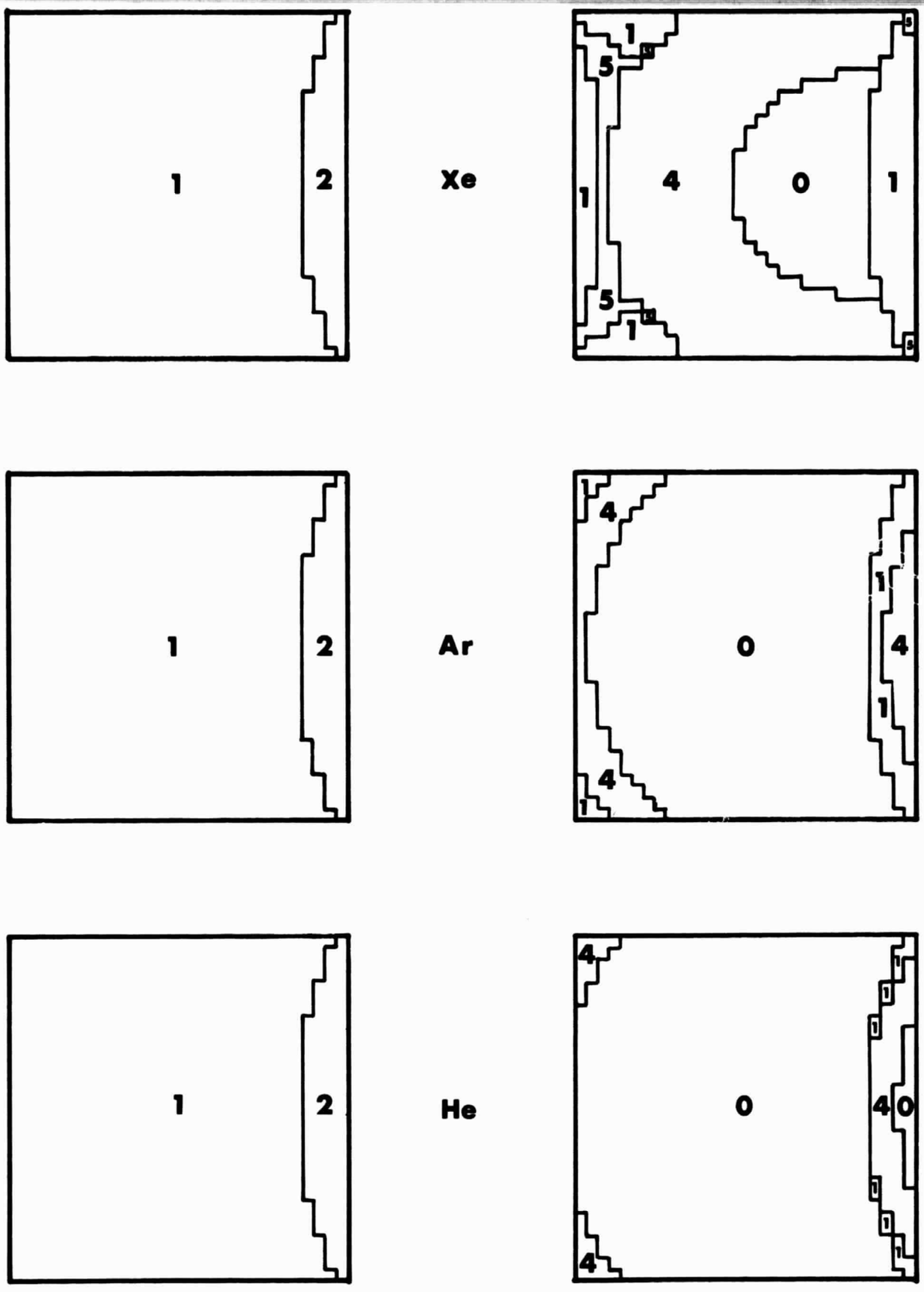

FIG. 5.2.4 INITIAL IMPACT MAP AND FINAL DISPOSITION MAPS FOR VALUES OF THE MASS RATIO CORRESPONDING TO H_e, Ar and Xe ON TUNGSTEN.
$R^* = 1.3$, $E_o^* = 20$, $\theta_o = 45^o$, $\phi_o = 0^o$. Same key as FIG. 5.2.3.
Impact on the left. Final disposition on the right.

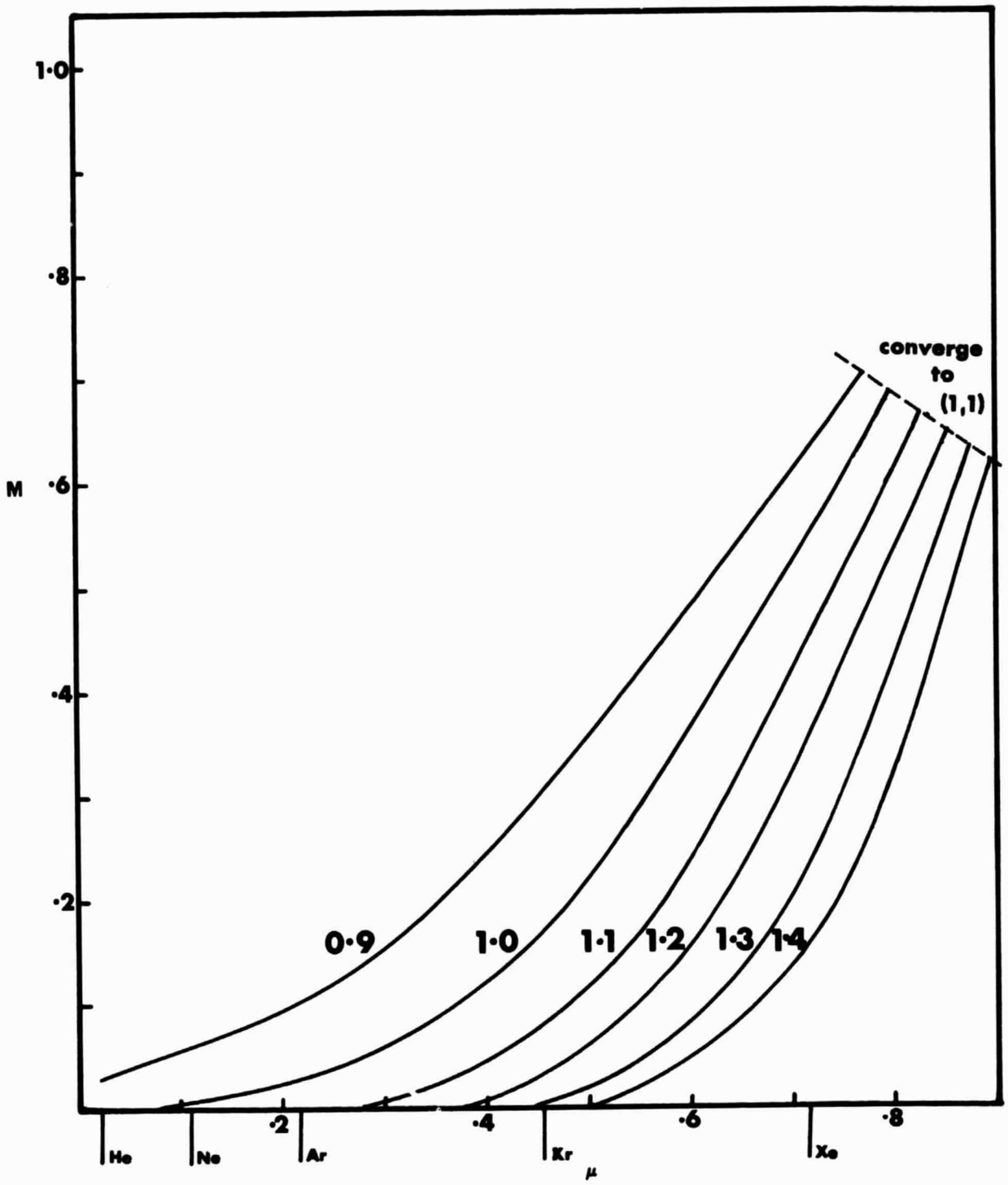

FIG. 5.3.1 FRACTION OF PARTICLES WHICH HAVE MULTIPLE COLLISIONS (M) AS A FUNCTION OF MASS RATIO (μ) FOR CURVES OF EQUAL R*.
$\theta_o = 0^o$, $\phi_o = 0^o$. The values of the rare-gas-tungsten mass ratios are plotted on the μ axis.

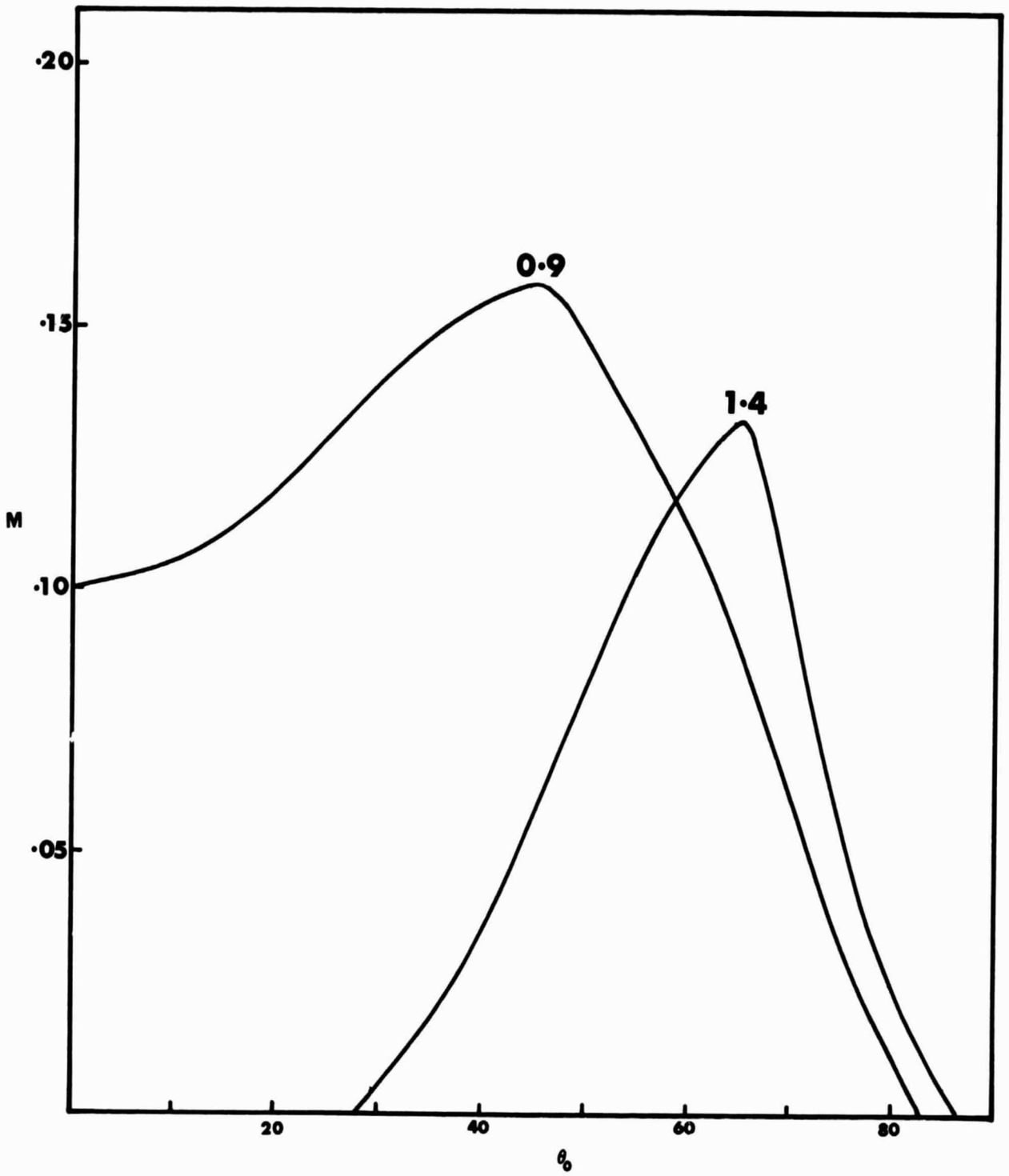

FIG. 5.3.2 FRACTION OF PARTICLES WHICH HAVE MULTIPLE COLLISIONS (M) AS A FUNCTION OF INCIDENCE ANGLE (θ_o) FOR TWO VALUES OF R*.
Ar/W mass ratio. $\phi_o = 0^o$.

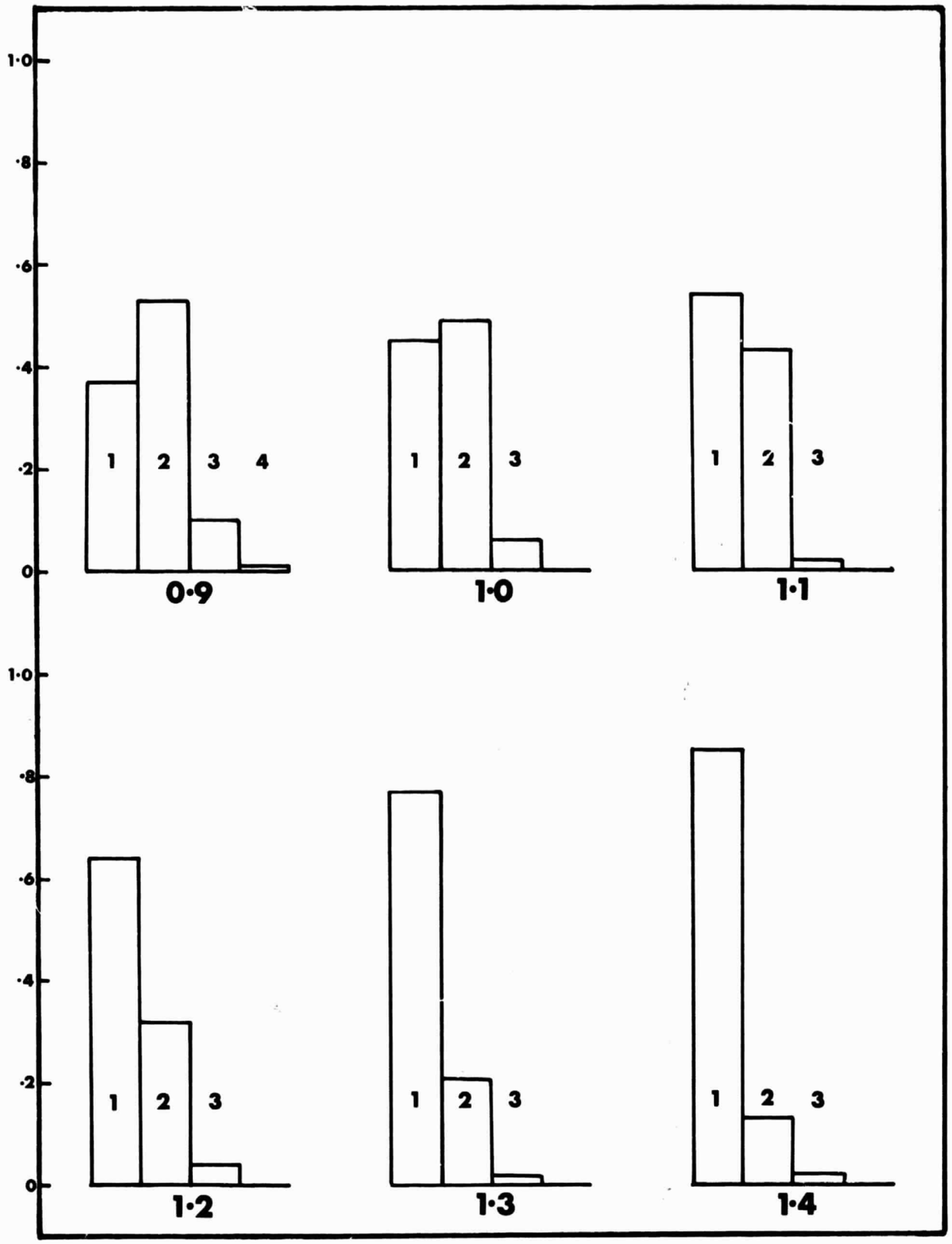

FIG. 5.3.3 COMPLEXITY OF THE COLLISION PROCESS FOR VALUES OF R*. Xe/W mass ratio, $\theta_o = 0^o$, $\phi_o = 0^o$. The bars labelled "n" give the fraction of particles which have n and only n collisions with the surface atoms.

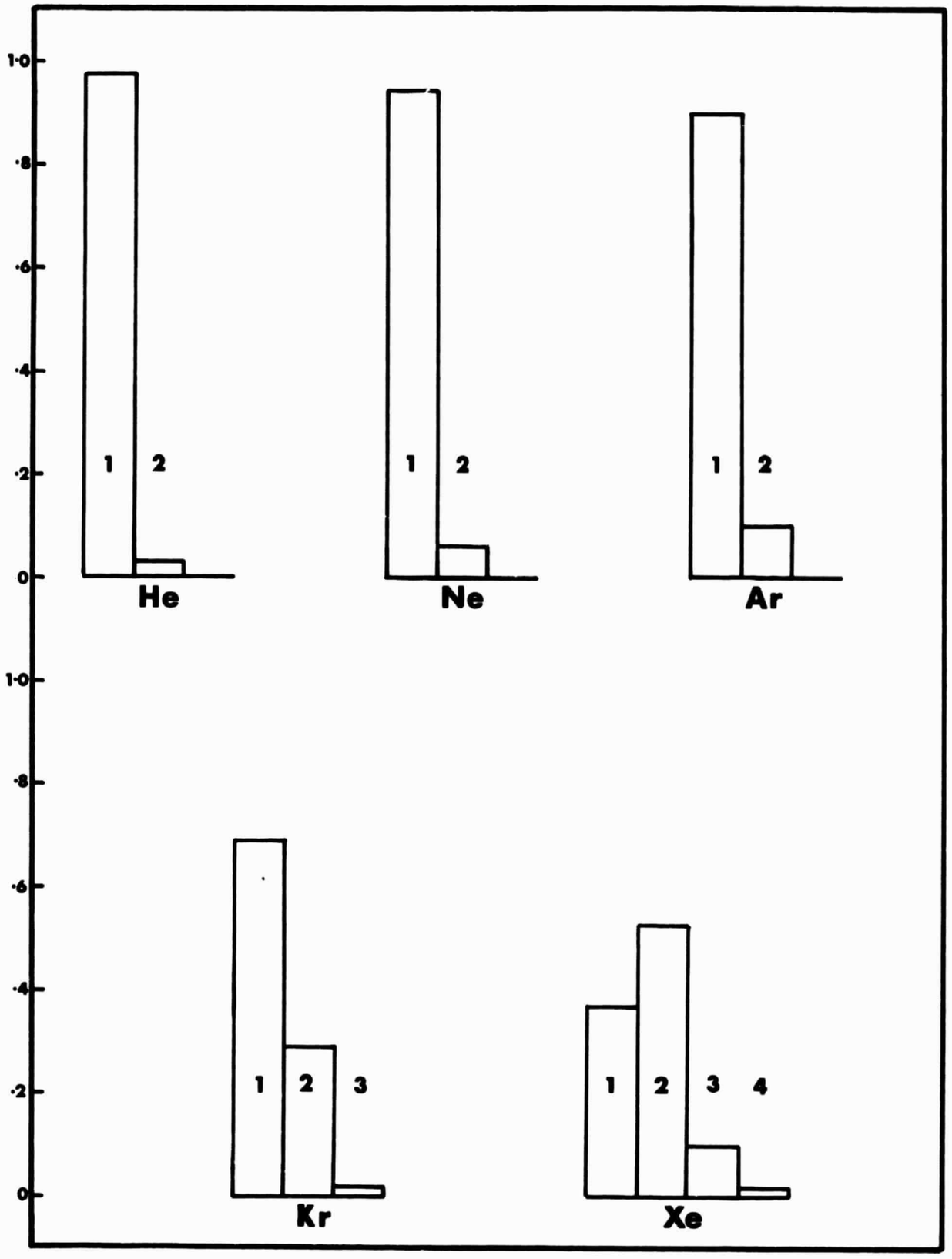

FIG. 5.3.4 COMPLEXITY OF THE COLLISION PROCESS FOR THE RARE-GAS-TUNGSTEN MASS RATIOS. $R^* = 0.9$, $\theta_o = 0^o$, $\phi_o = 0^o$.

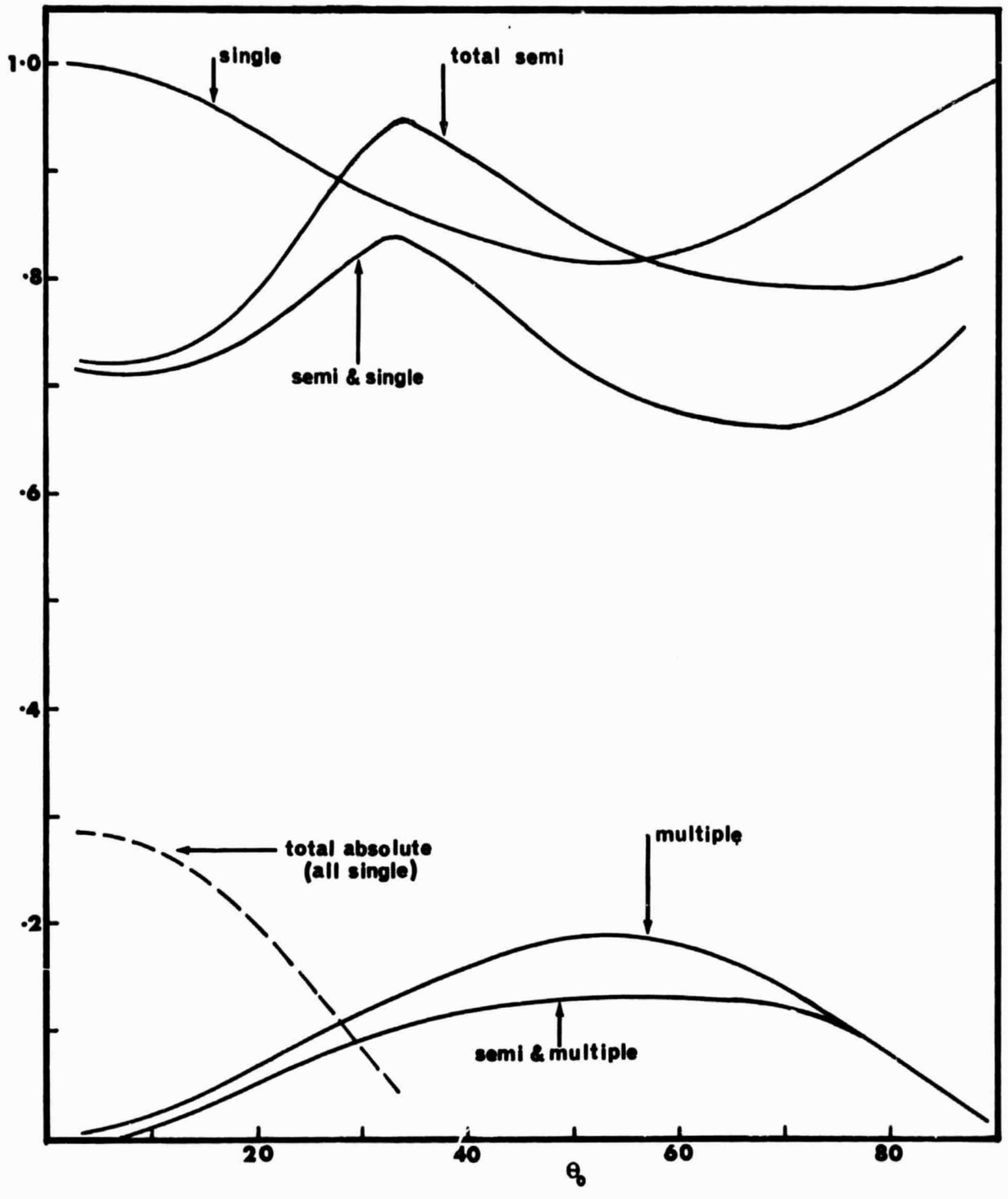

FIG. 6.1.1 COMPONENTS OF THE SEMI-TRAPPED PARTICLES AS A FUNCTION OF INCIDENCE ANGLE (θ_o). Kr/W mass ratio. $R^* = 1.3$, $E_o^* = 4.5$, $\phi_o = 0^o$.

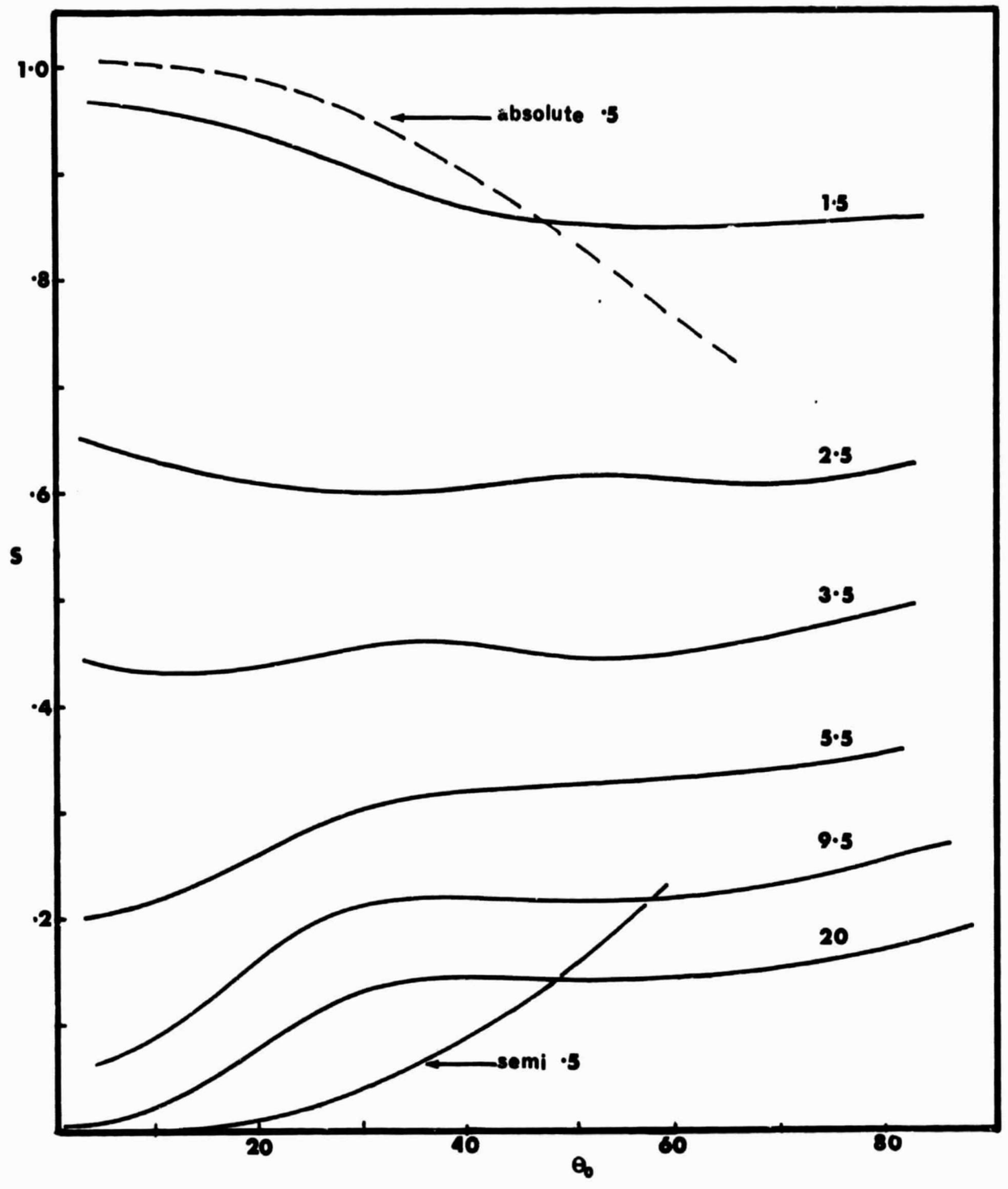

FIG. 6.1.2 FRACTION SEMI-TRAPPED (S) AS A FUNCTION OF INCIDENCE ANGLE (θ_o) FOR CURVES OF EQUAL E_o^*.
Ar/W mass ratio, $R^* = 1.3$, $\phi_o = 0^o$.

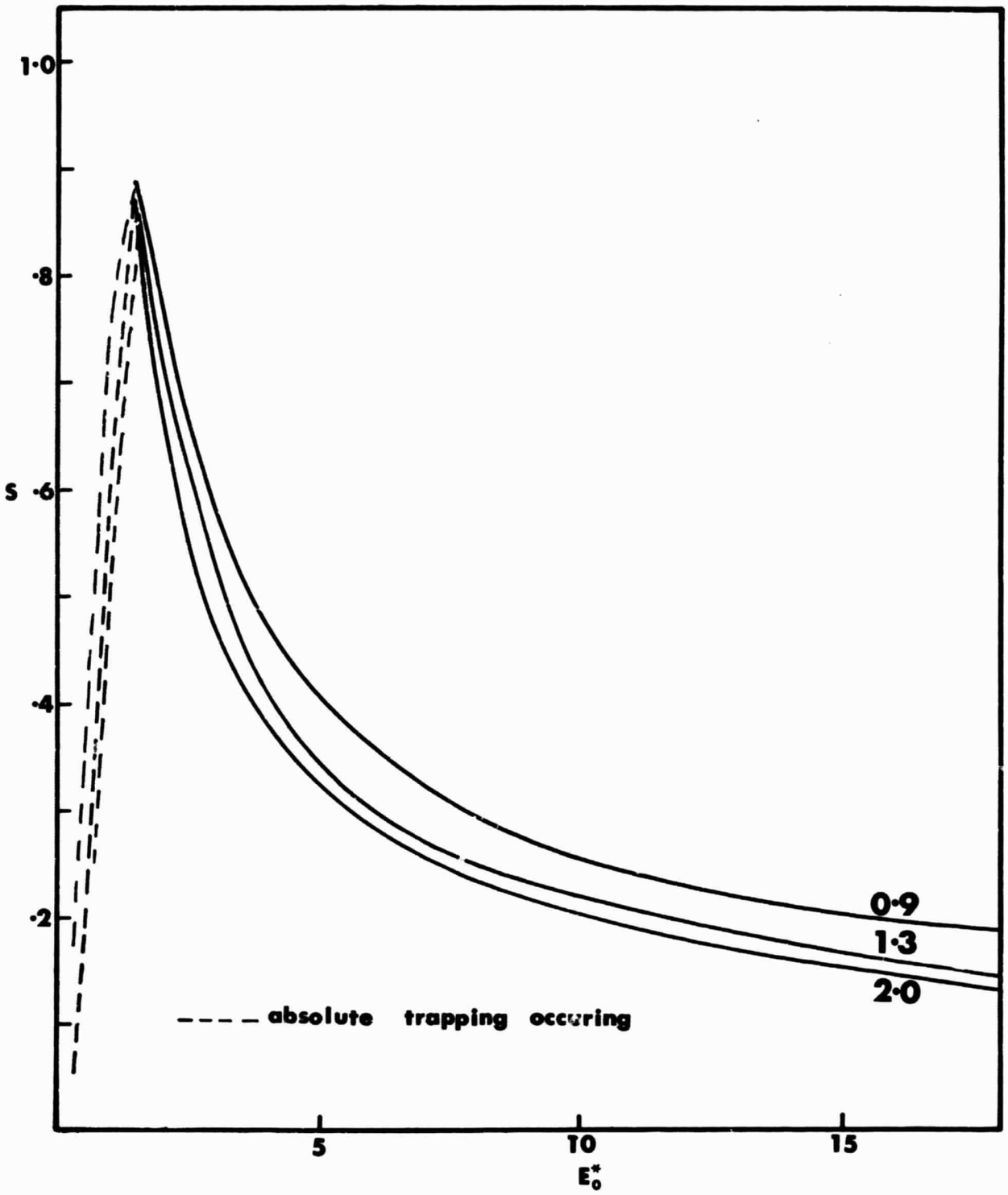

FIG. 6.1.3 FRACTION SEMI-TRAPPED (S) AS A FUNCTION OF E_o^* FOR CURVES OF EQUAL R*.
Ar/W mass ratio. $\theta_o = 45^o$, $\phi_o = 0^o$.

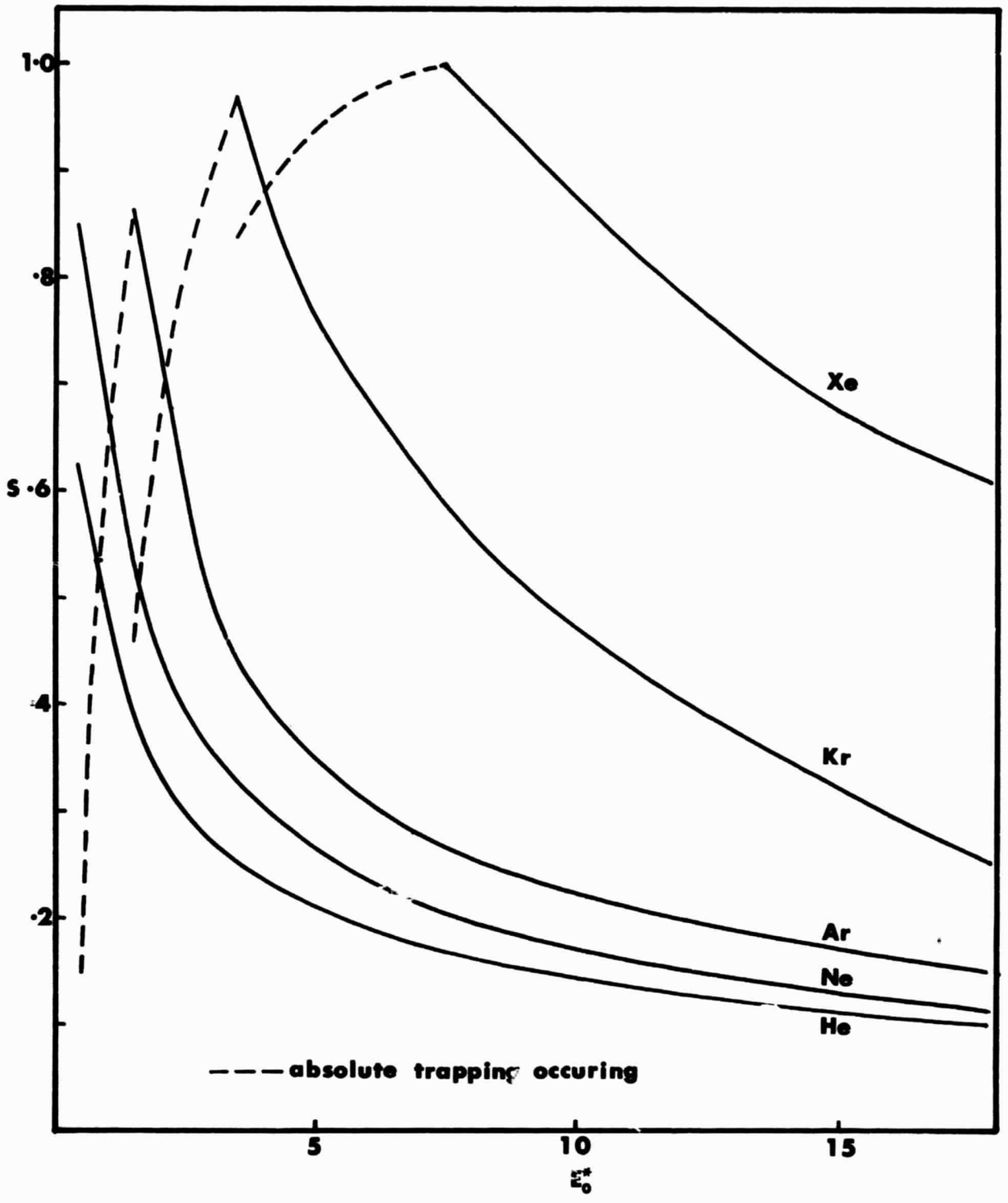

FIG. 6.1.4 FRACTION SEMI-TRAPPED (S) AS A FUNCTION OF E_o^* FOR THE RARE-GAS-TUNGSTEN MASS RATIOS. $R^* = 1.3$, $\theta_o = 45^o$, $\phi_o = 0^o$

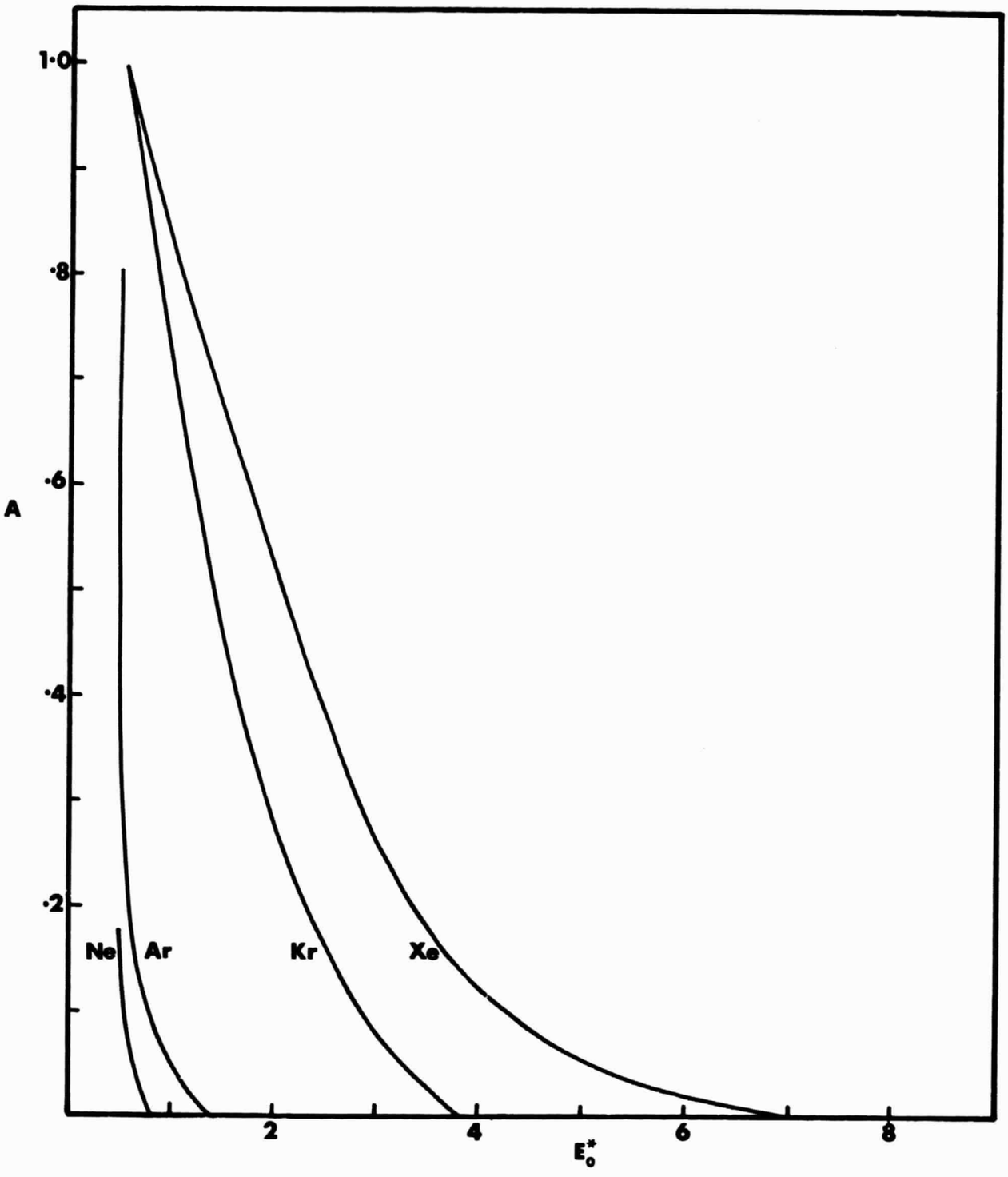

FIG. 6.1.5 FRACTION ABSOLUTELY TRAPPED (A) (ON THE INITIAL ENCOUNTER OF THE BEAM WITH THE SURFACE) AS A FUNCTION OF E_o^* FOR THE RARE-GAS-TUNGSTEN MASS RATIOS.
$R^* = 1.3$, $\theta_o = 45^o$, $\phi_o = 0^o$.

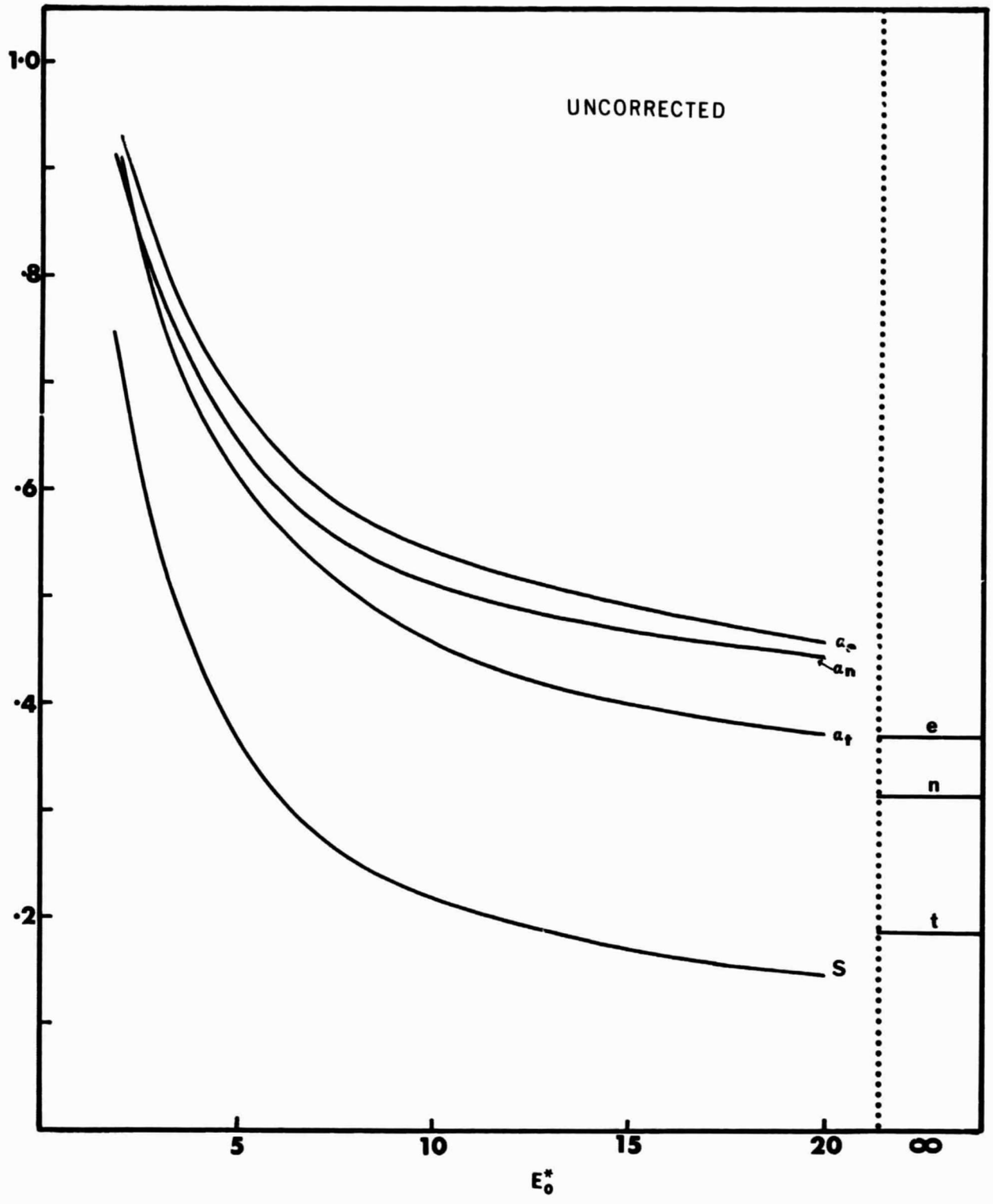

FIG. 6.1.6 UNCORRECTED ACCOMODATION COEFFICIENTS AS A FUNCTION OF E_o^*. Ar/W mass ratio. $R^* = 1.3$, $\theta_o = 45^o$, $\phi_o = 0^o$. The fraction semi-trapped (S) has been plotted for comparison. The no-field values are shown at the right for illustrative purposes.

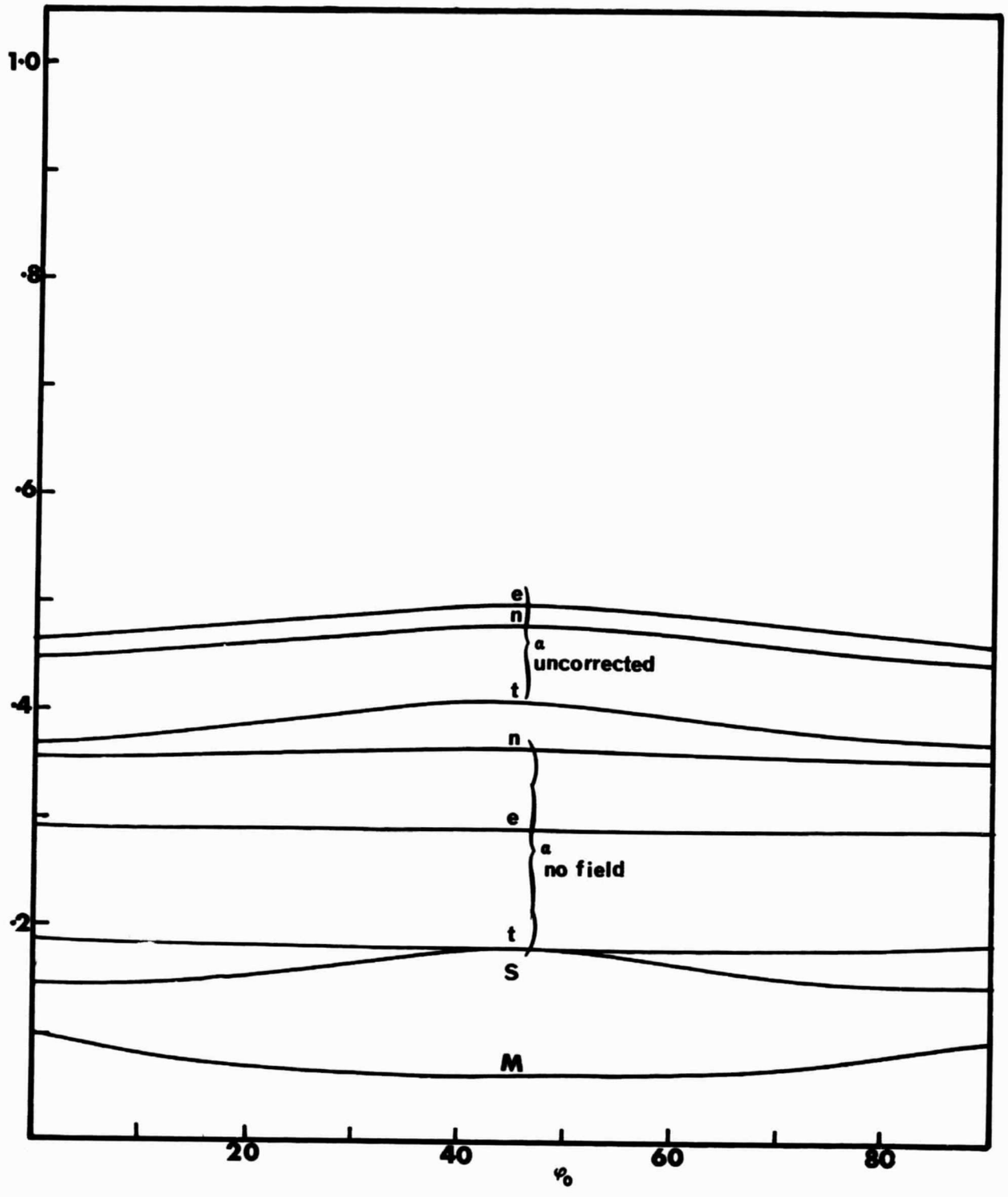

FIG. 6.1.7 EFFECT OF THE INITIAL AZIMUTH ANGLE (ϕ_o) ON SEVERAL QUANTITIES OF INTEREST.
Ar/W mass ratio $R^* = 1.3$, $E_o^* = 20$, $\theta_o = 45^o$.

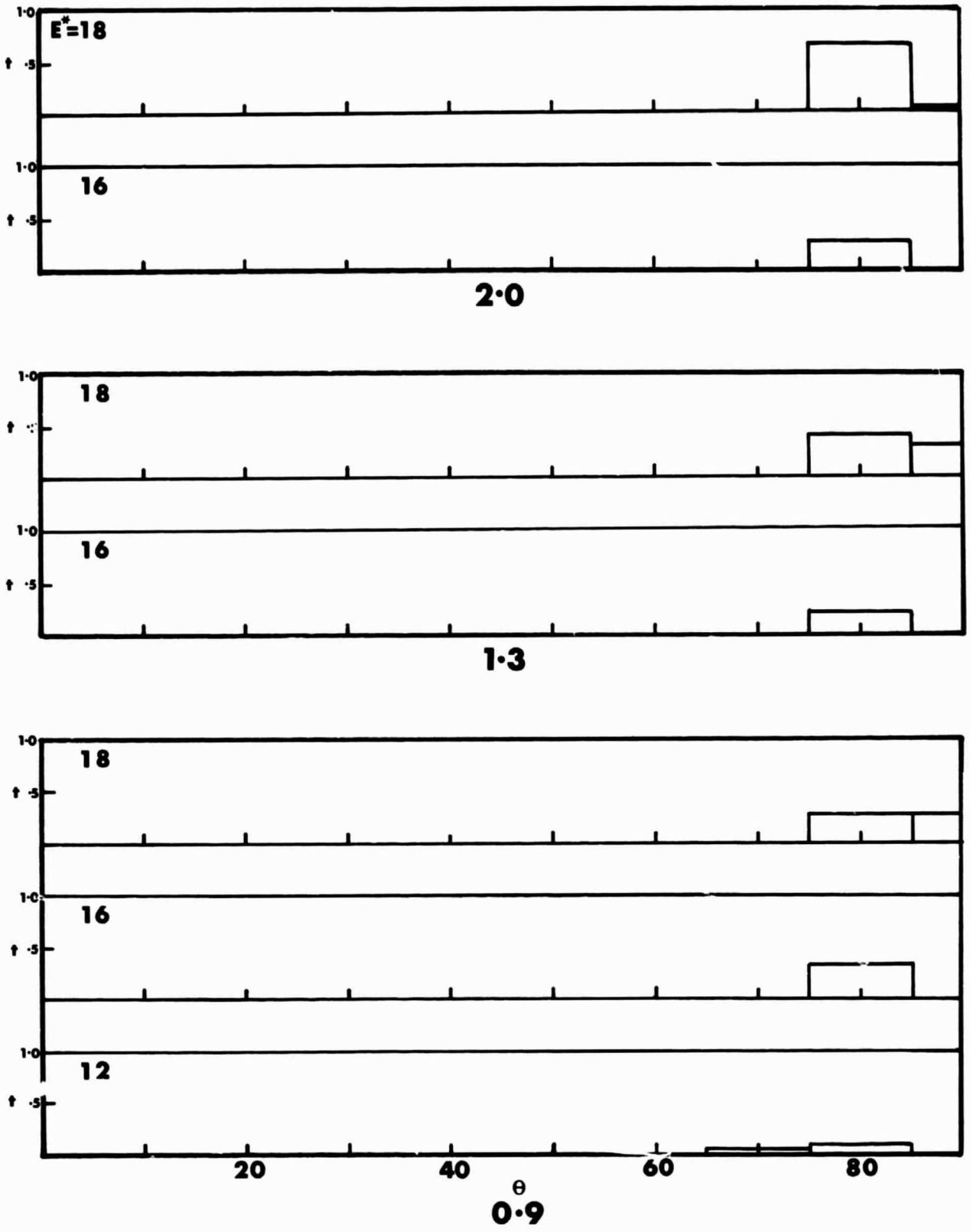

FIG. 6.2.1 THE SEMI-TRAPPED DISTRIBUTIONS FOR VALUES OF R*.
Ar/W mass ratio $E_o^* = 20$, $\theta_o = 45^o$, $\phi_o = 0^o$.
See text for a full explanation of the notation used.

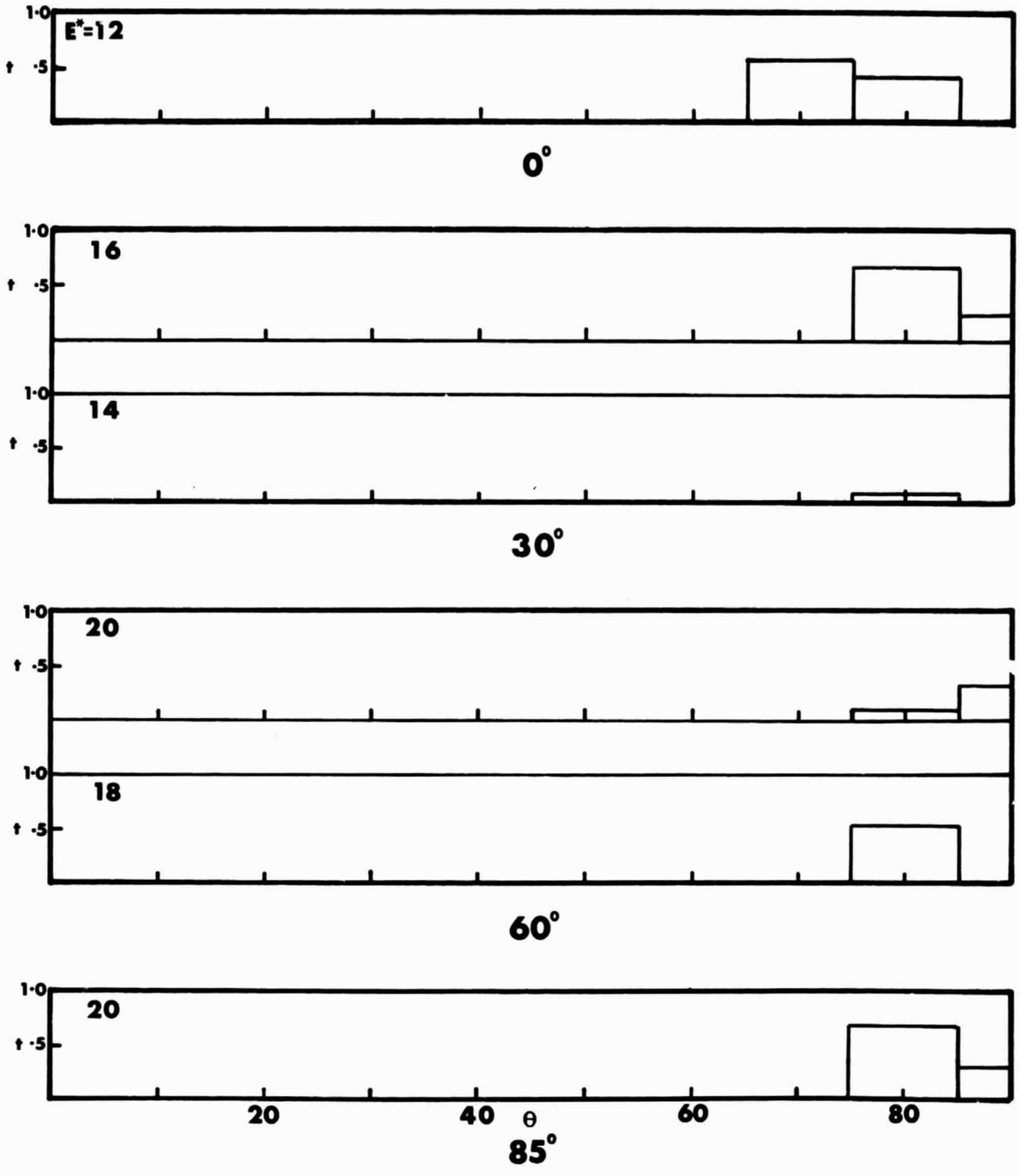

FIG. 6.2.2 THE SEMI-TRAPPED DISTRIBUTIONS FOR VALUES OF INCIDENCE ANGLE (θ_o). Ar/W mass ratio. $R^* = 1.3$, $E_o^* = 20$, $\phi_o = 0^o$.

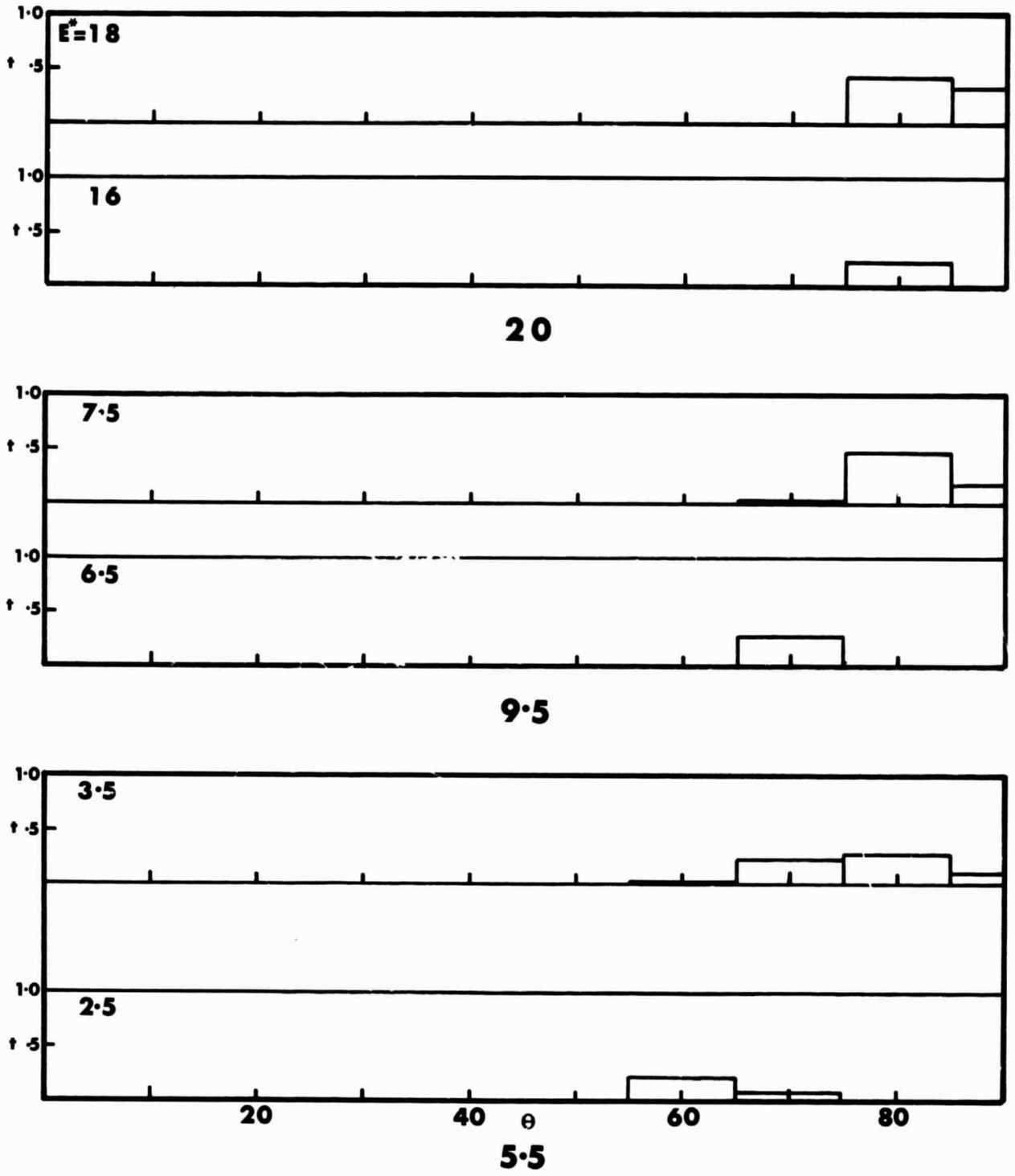

FIG. 6.2.3 THE SEMI-TRAPPED DISTRIBUTIONS FOR INITIAL VALUES OF E_o^*.
Ar/W mass ratio. $R^* = 1.3$, $\theta_o = 45^o$, $\phi_o = 0^o$.

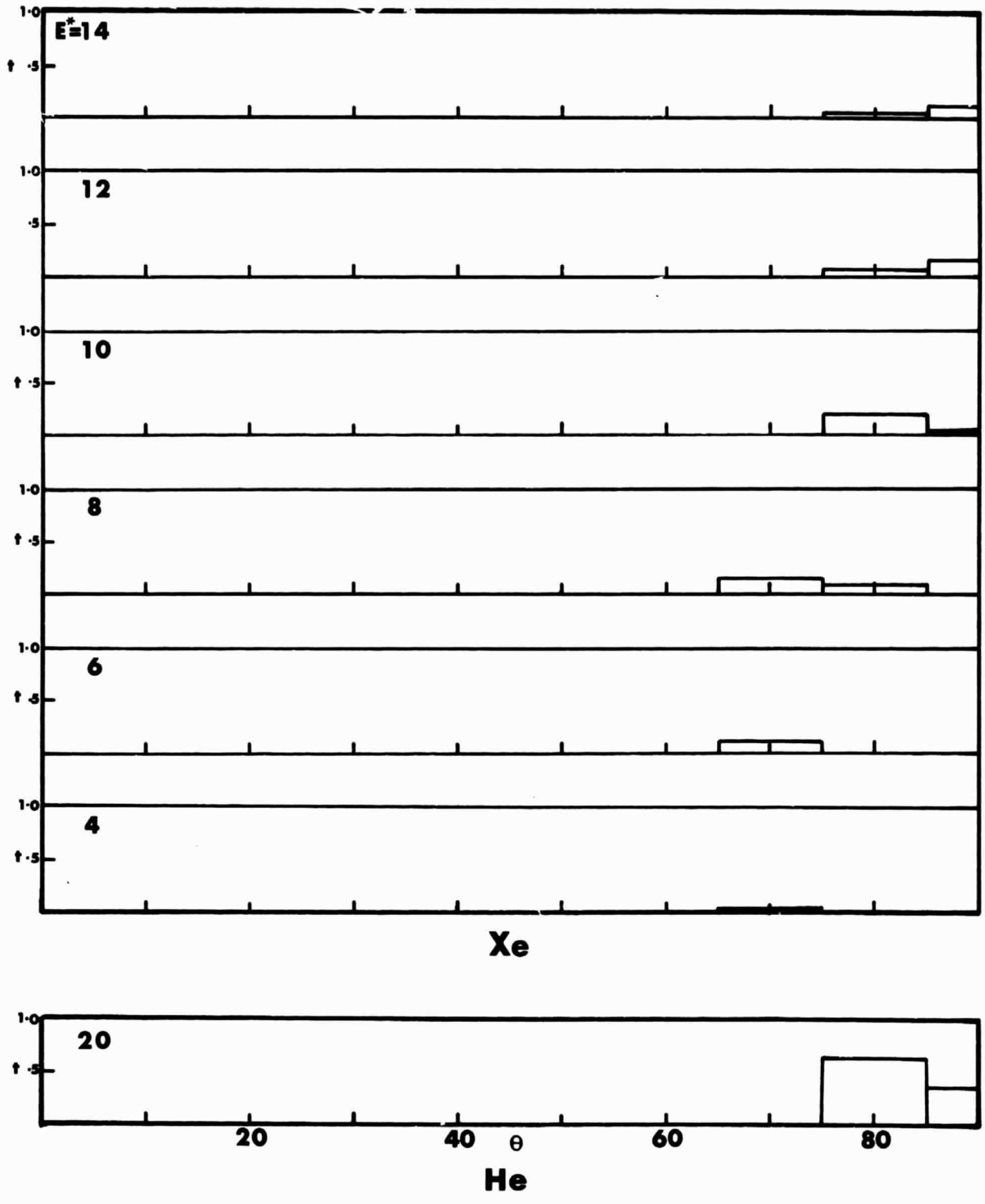

FIG. 6.2.4 THE SEMI-TRAPPED DISTRIBUTIONS FOR MASS RATIOS CORRESPONDING TO He/W AND Xe/W. $R^* = 1.3$, $E_o^* = 20$, $\theta_o = 45^o$, $\phi_o = 0^o$

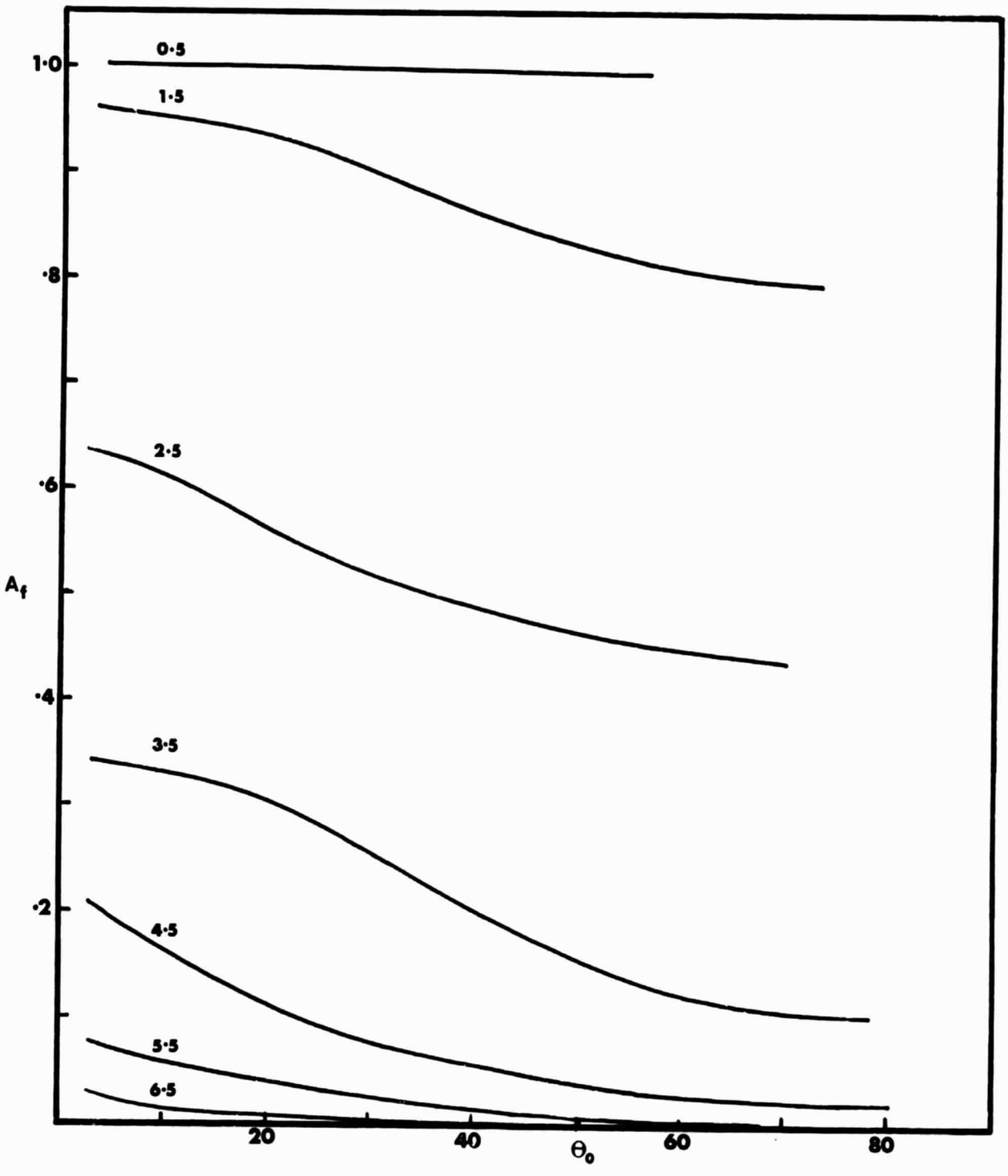

FIG. 6.3.1 FINAL TRAPPING FRACTION (AFTER ACCOUNTING FOR THE SEMI-TRAPPED PARTICLES), DENOTED A_f AS A FUNCTION OF INCIDENCE ANGLE (θ_o) FOR VALUES OF E_o^*.
Ar/W mass ratio, $R^* = 1.3$, $\phi_o = 0^o$.

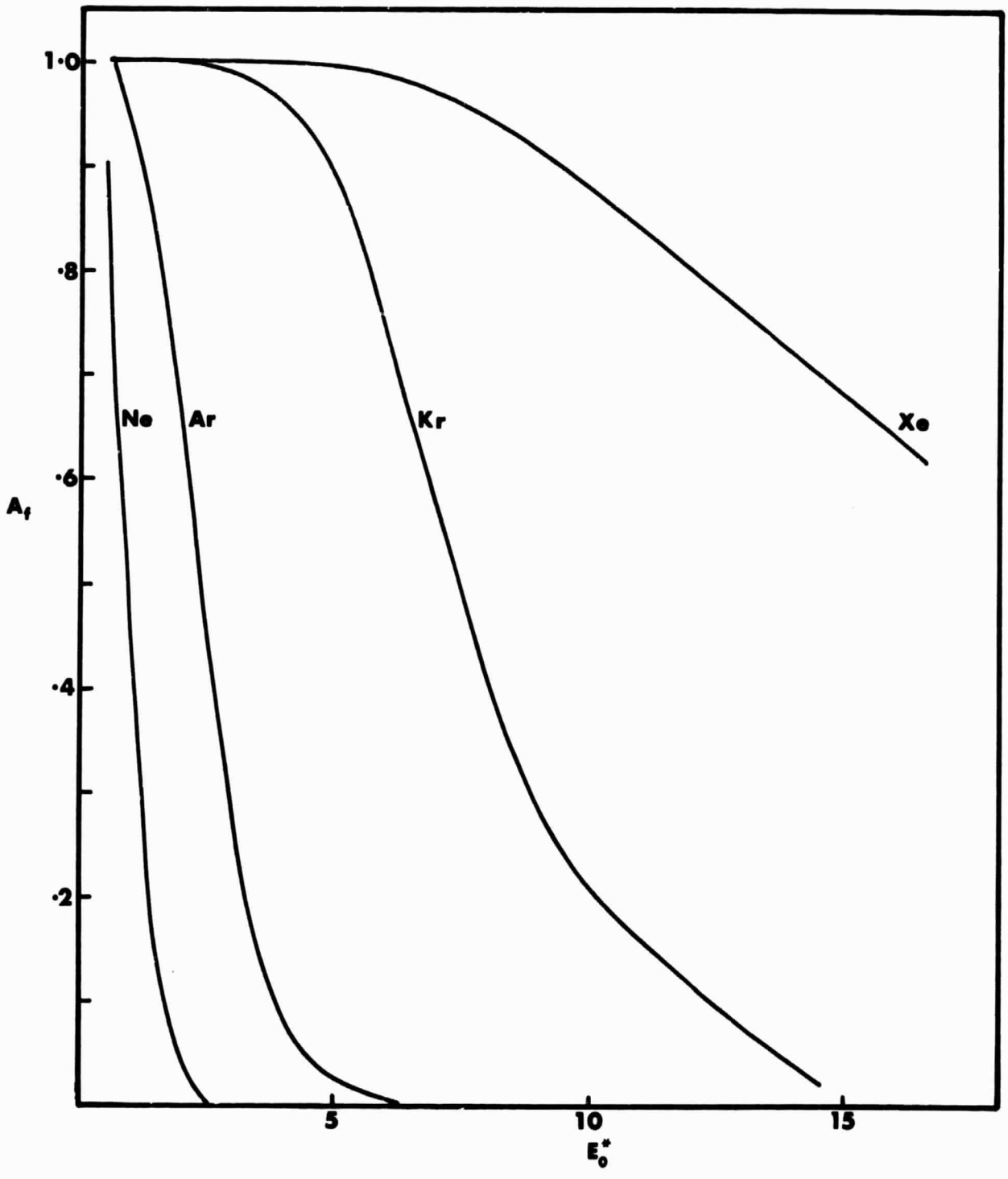

FIG. 6.3.2 FINAL TRAPPING FRACTION(A_f) AS A FUNCTION OF E_o^* FOR THE RARE-GAS-TUNGSTEN MASS RATIOS.
$R^* = 1.3$, $\theta_o = 45^o$, $\phi_o = 0^o$.

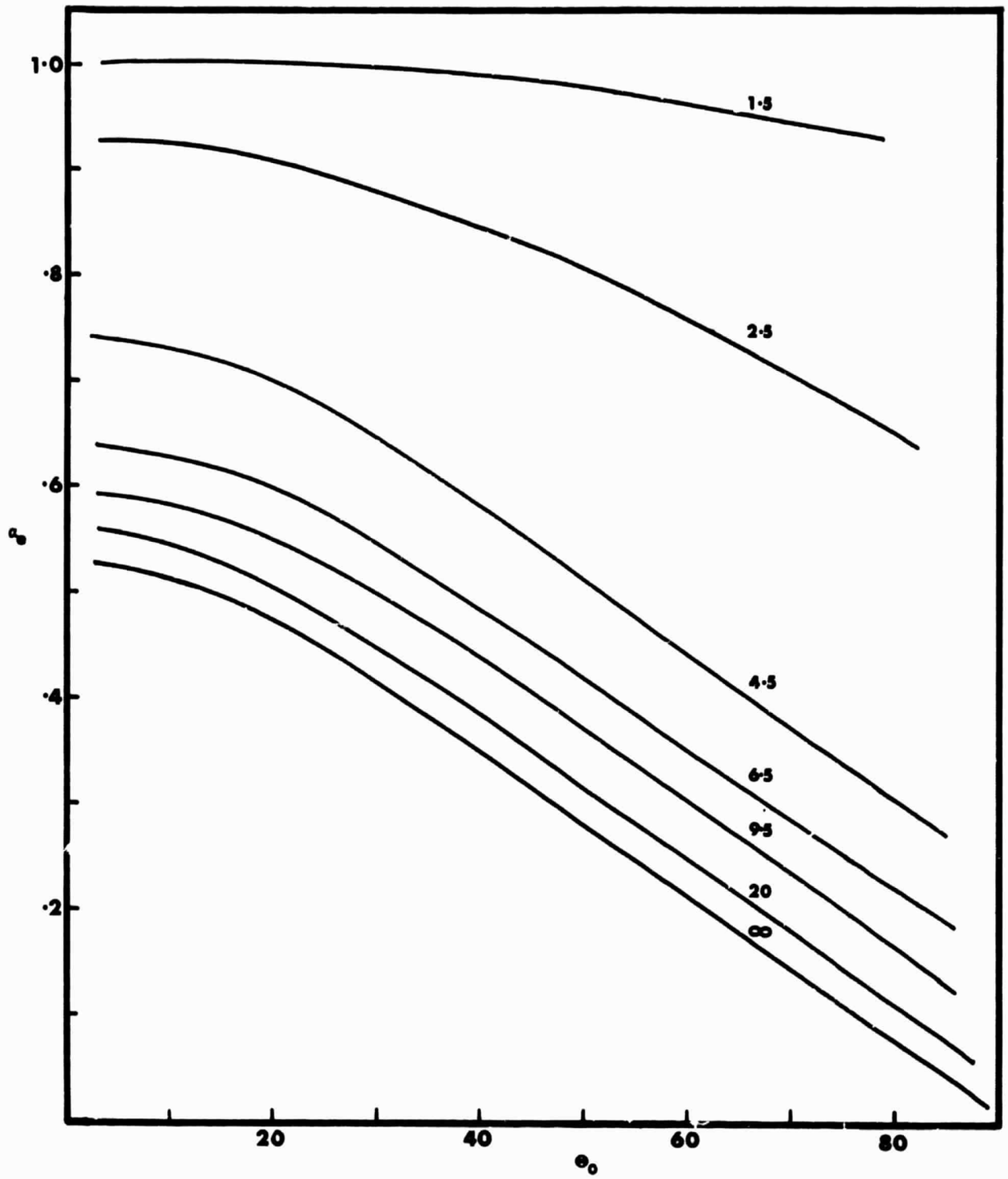

FIG. 6.4.1 CORRECTED ENERGY ACCOMMODATION COEFFICIENT AS A FUNCTION OF INCIDENCE ANGLE (θ_o) FOR VALUES OF E_o^*.
Ar/W mass ratio. $R^* = 1.3$, $\phi_o = 0°$.

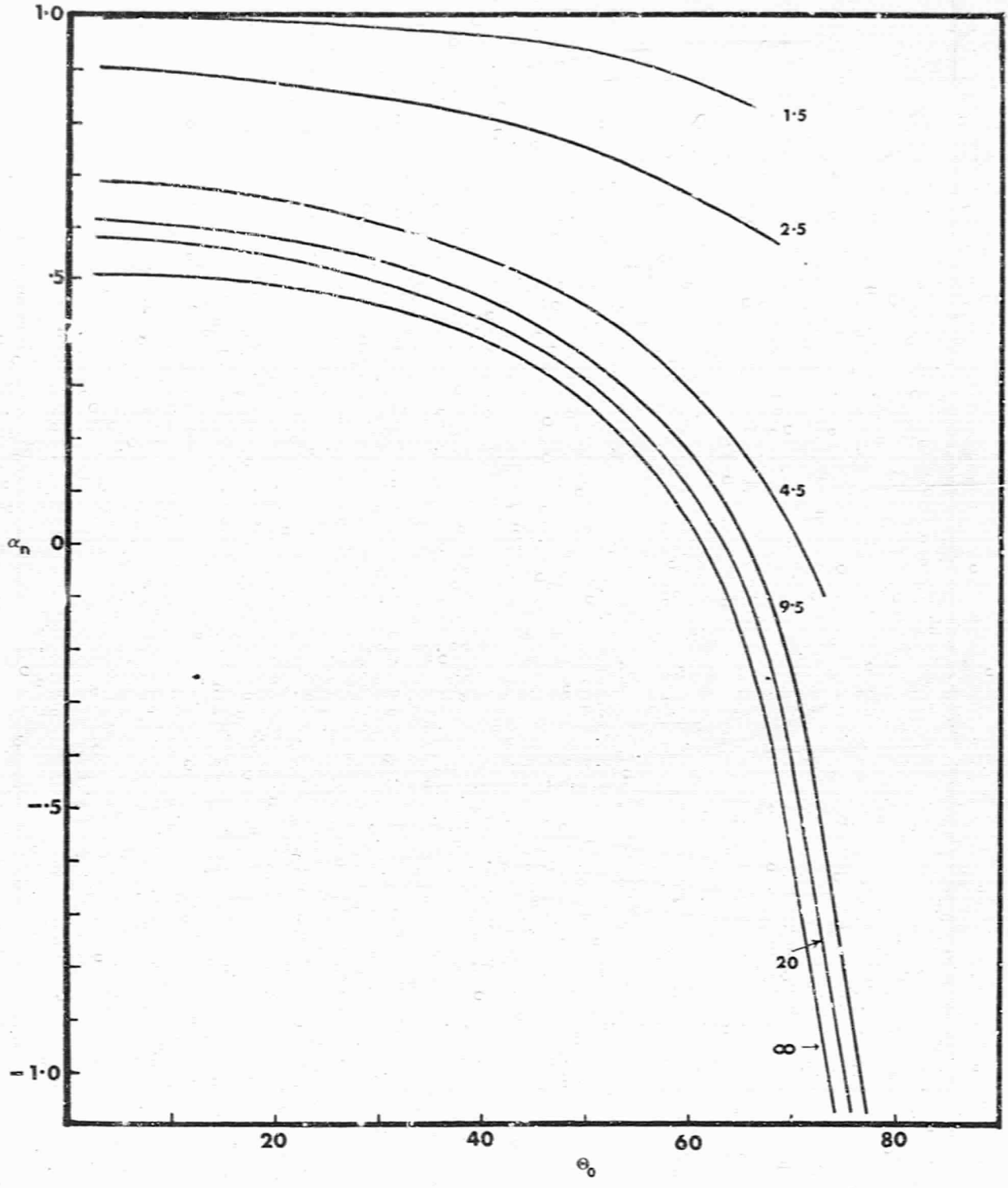

FIG. 6.4.2 CORRECTED NORMAL MOMENTUM ACCOMMODATION COEFFICIENT AS A FUNCTION OF INCIDENCE ANGLE (θ_o) FOR VALUES OF E_o*.
Ar/W mass ratio. R* = 1.3, ϕ_o = 0°.

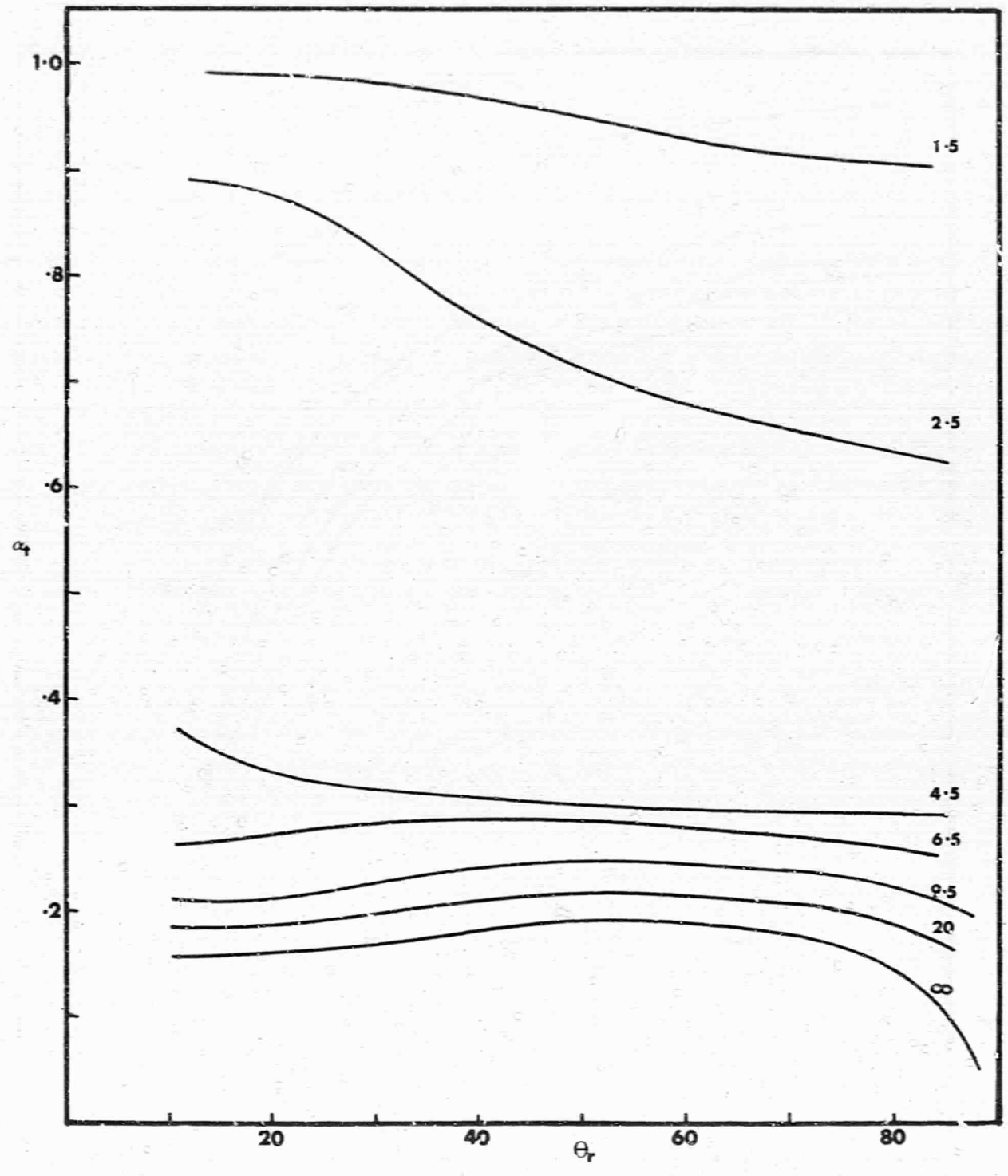

FIG. 6.4.3 CORRECTED TANGENTIAL MOMENTUM ACCOMMODATION COEFFICIENT AS A FUNCTION OF INCIDENCE ANGLE (θ_o) FOR VALUES OF E_o*.
Ar/W mass ratio. R* = 1.3, ϕ_o = 0o.

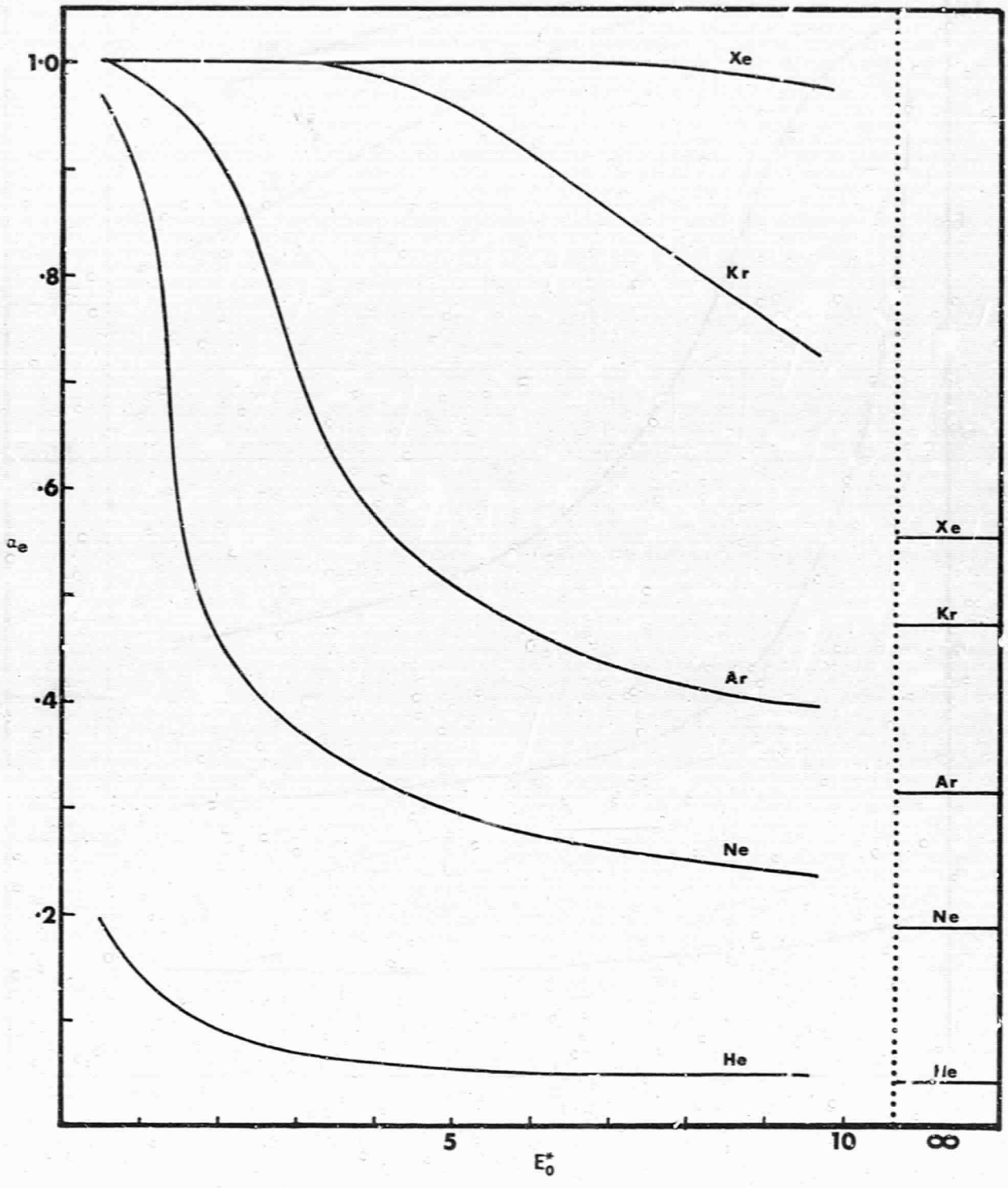

FIG. 6.4.4 CORRECTED ENERGY ACCOMMODATION COEFFICIENT AS A FUNCTION OF E_o^* FOR THE RARE-GAS-TUNGSTEN MASS RATIOS.
$R^* = 1.3$, $\theta_o = 45^o$, $\phi_o = 0^o$.

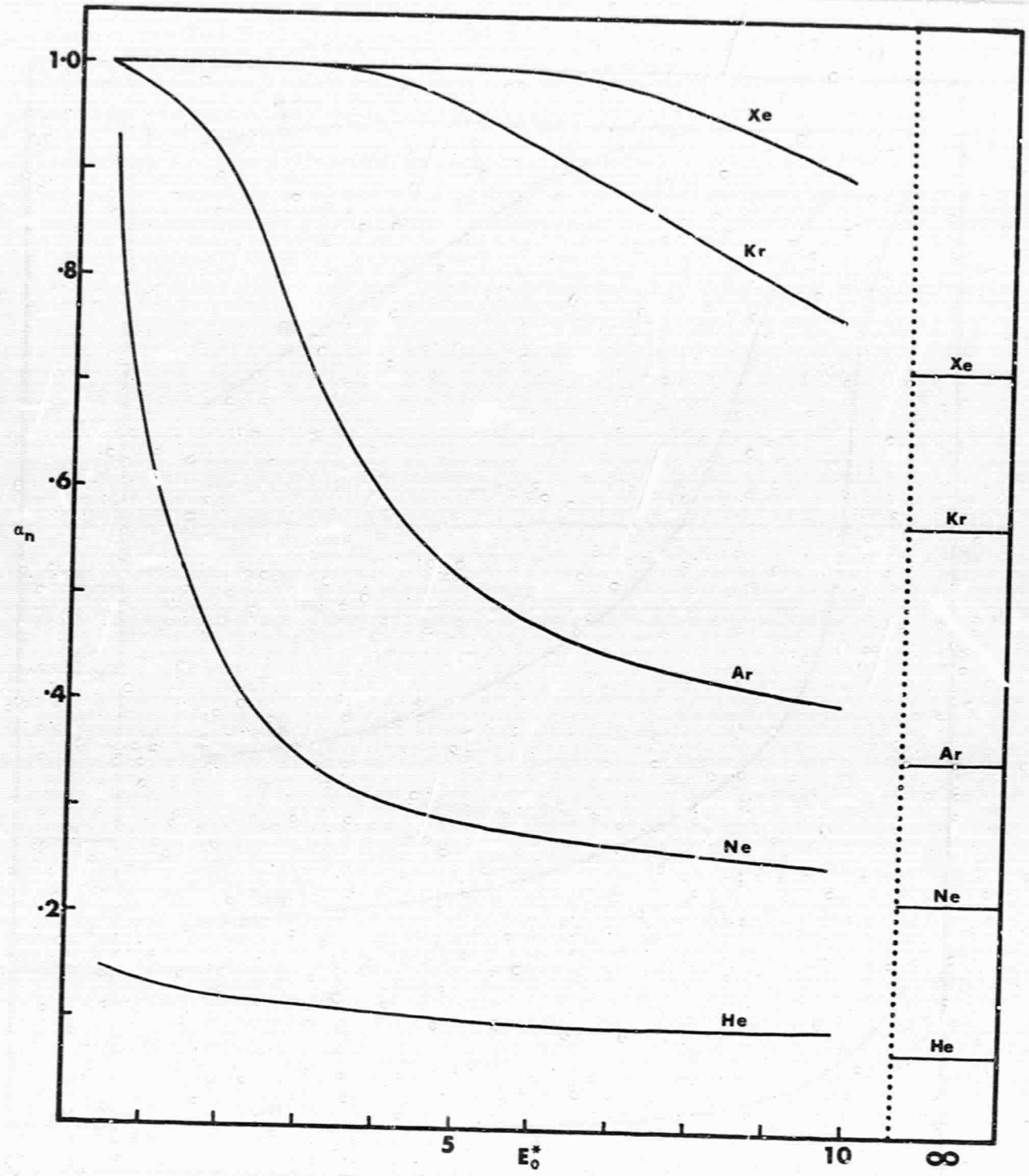

FIG. 6.4.5 CORRECTED NORMAL MOMENTUM ACCOMMODATION COEFFICIENT AS A FUNCTION OF E_o^* FOR THE RARE-GAS-TUNGSTEN MASS RATIOS.
$P^* = 1.3$, $\theta_o = 45^o$, $\phi_o = 0^o$.

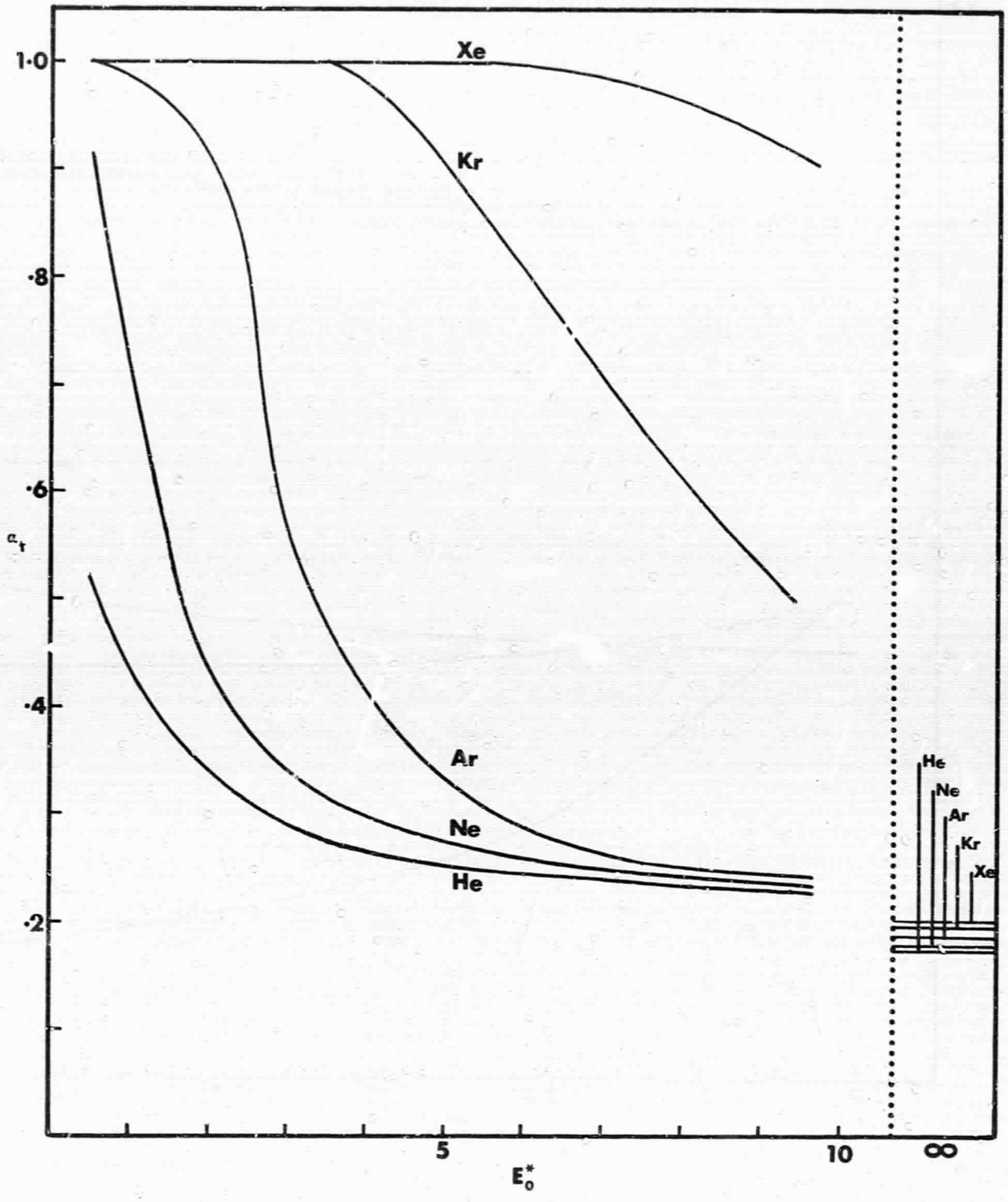

FIG. 6.4.6 CORRECTED TANGENTIAL MOMENTUM ACCOMMODATION COEFFICIENT AS A FUNCTION OF E_o^* FOR THE RARE-GAS-TUNGSTEN MASS RATIOS.
$R^* = 1.3$, $\theta_o = 45^\circ$, $\phi_o = 0^\circ$.

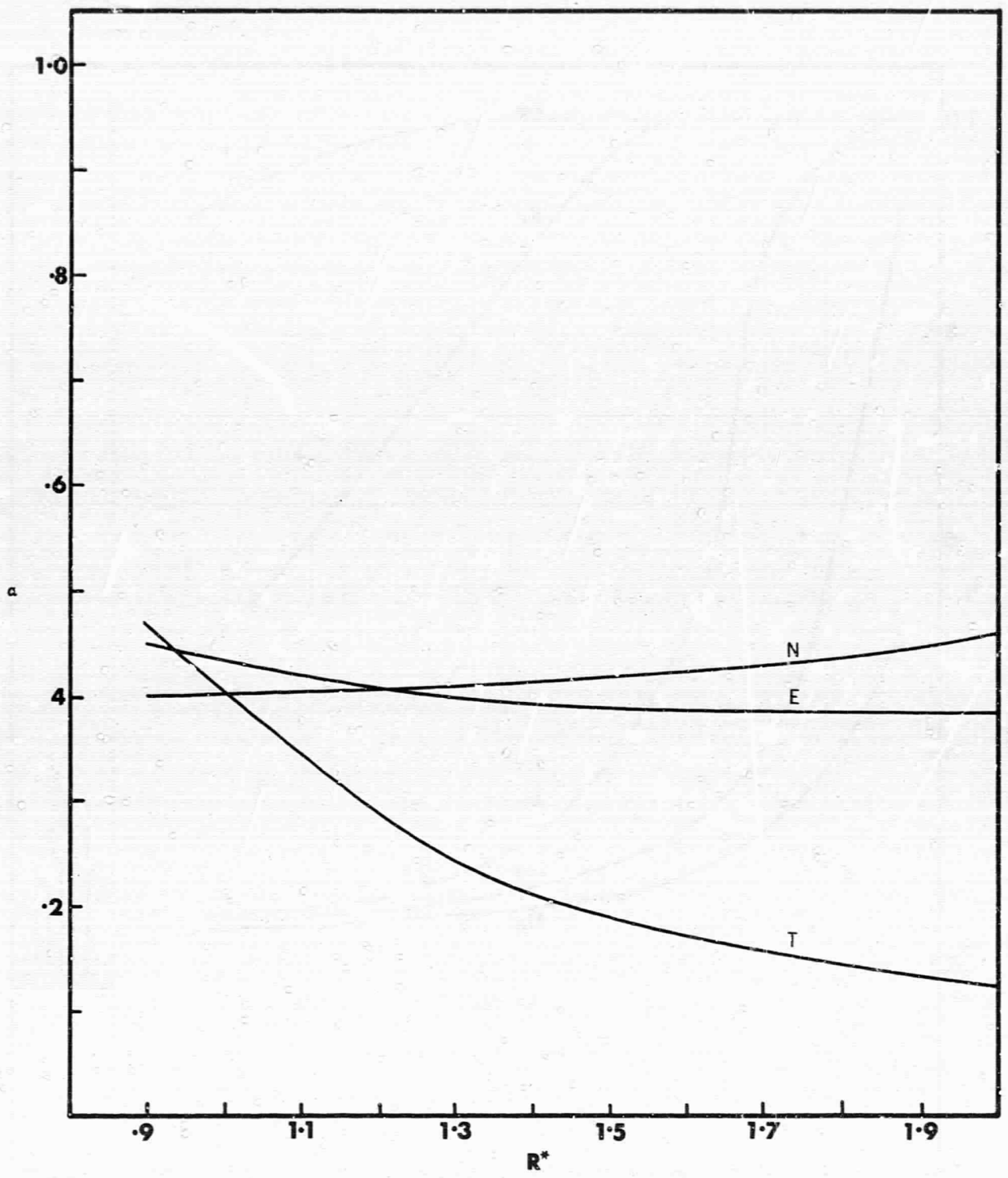

FIG. 6.4.7 CORRECTED ACCOMMODATION COEFFICIENTS AS A FUNCTION OF R*.
Ar/W mass ratio. $E_o^* = 9.5$, $\theta_o = 45^o$, $\phi_o = 0^o$.

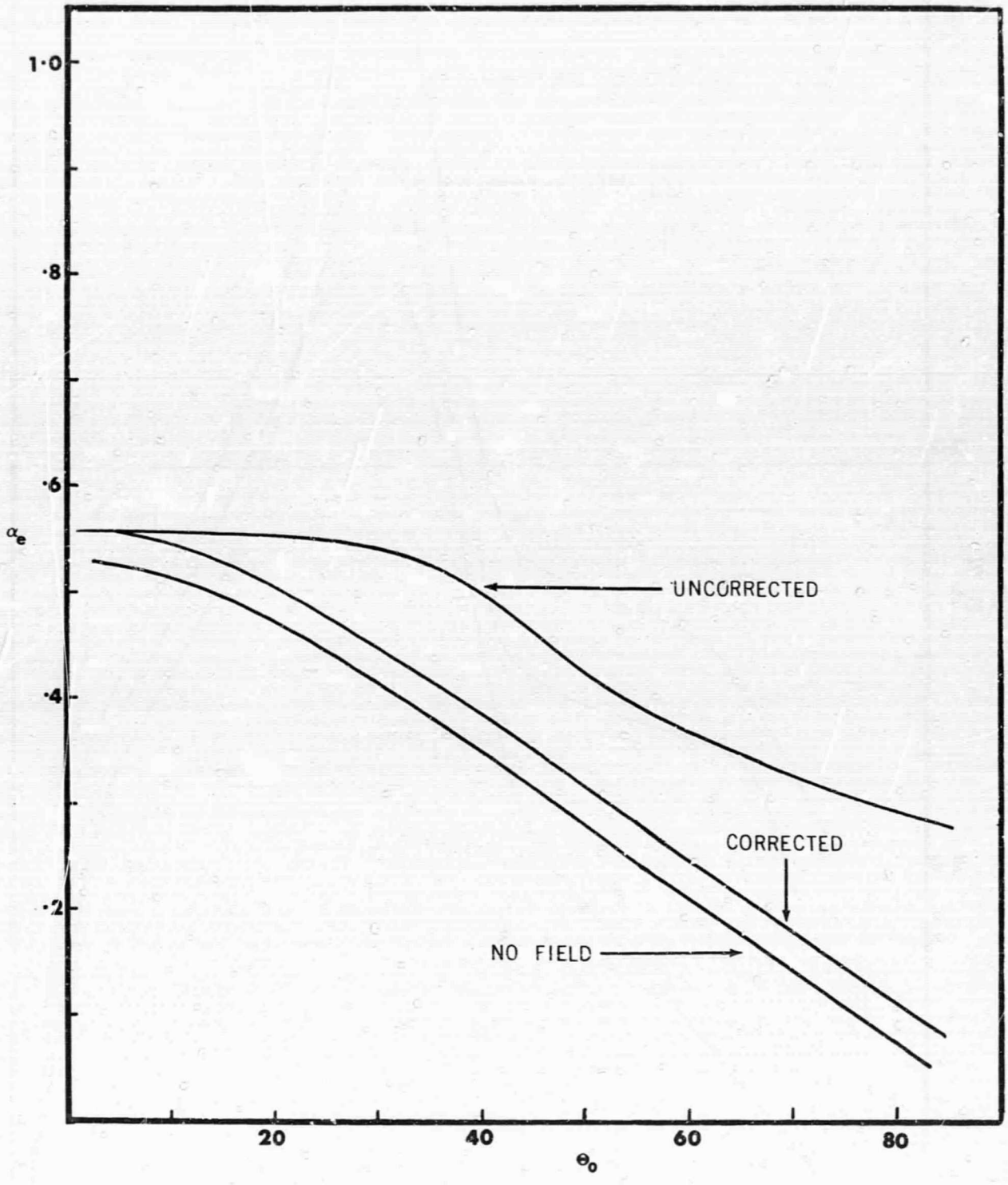

FIG. 6.4.8 COMPARISON OF THE ENERGY ACCOMMODATION COEFFICIENTS FOR THE UNCORRECTED, CORRECTED AND NO-FIELD CASES, AS A FUNCTION OF INCIDENCE ANGLE (θ_o).
Ar/W mass ratio. $R^* = 1.3$, $E_o^* = 20$, $\phi_o = 0^o$.

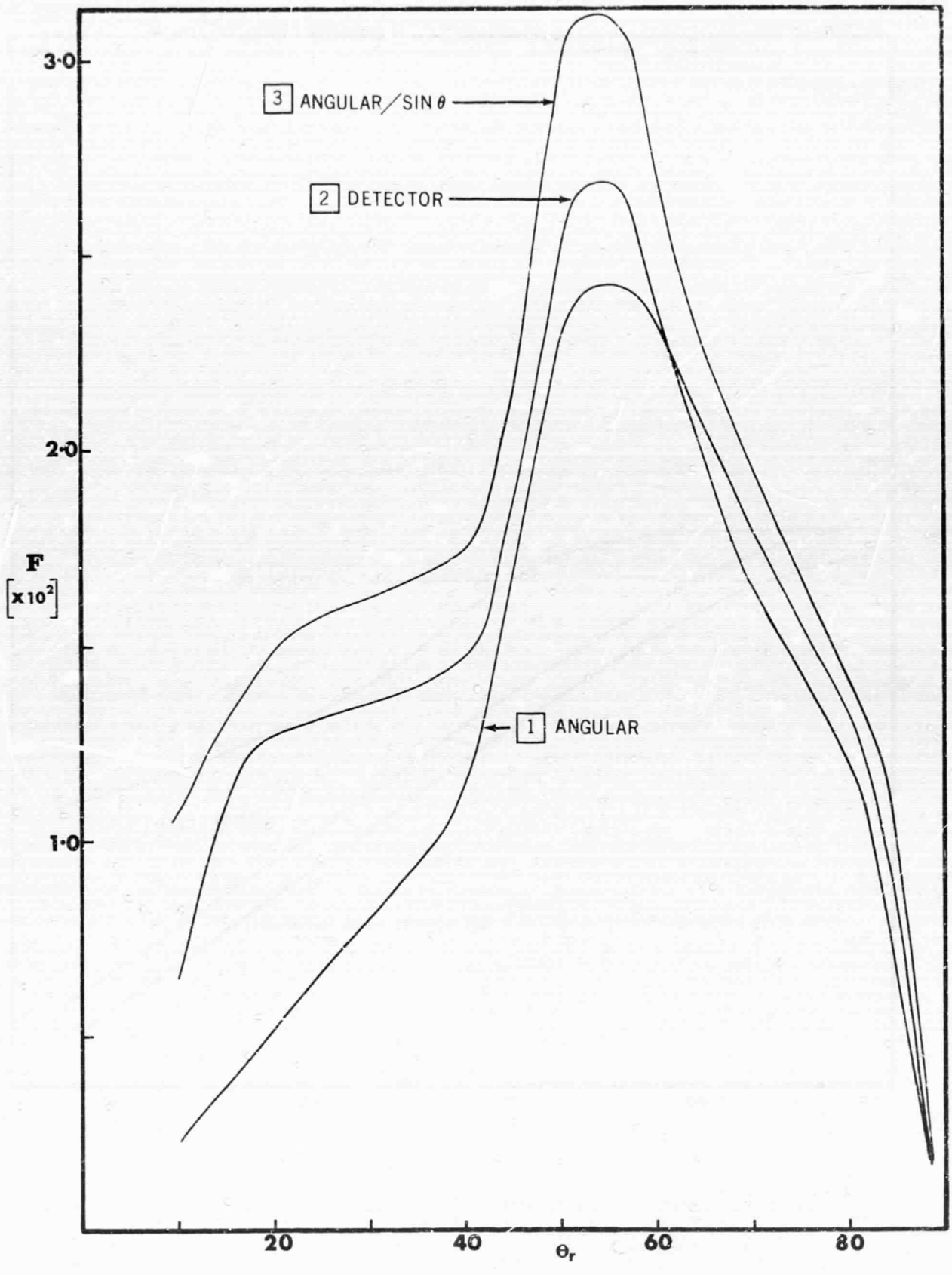

FIG. 7.1.1. COMPARISON OF THE NORMALIZED PRIMARY FLUX FOR THE ANGULAR, DETECTOR AND DETECTOR-ANGULAR APPROXIMATION.
Detector mode, all 10° resolution. Ar/W mass ratio, $R^* = 1.3$, $E_o^* = 20$, $\theta_o = 45°$, $\phi_o = 0°$.

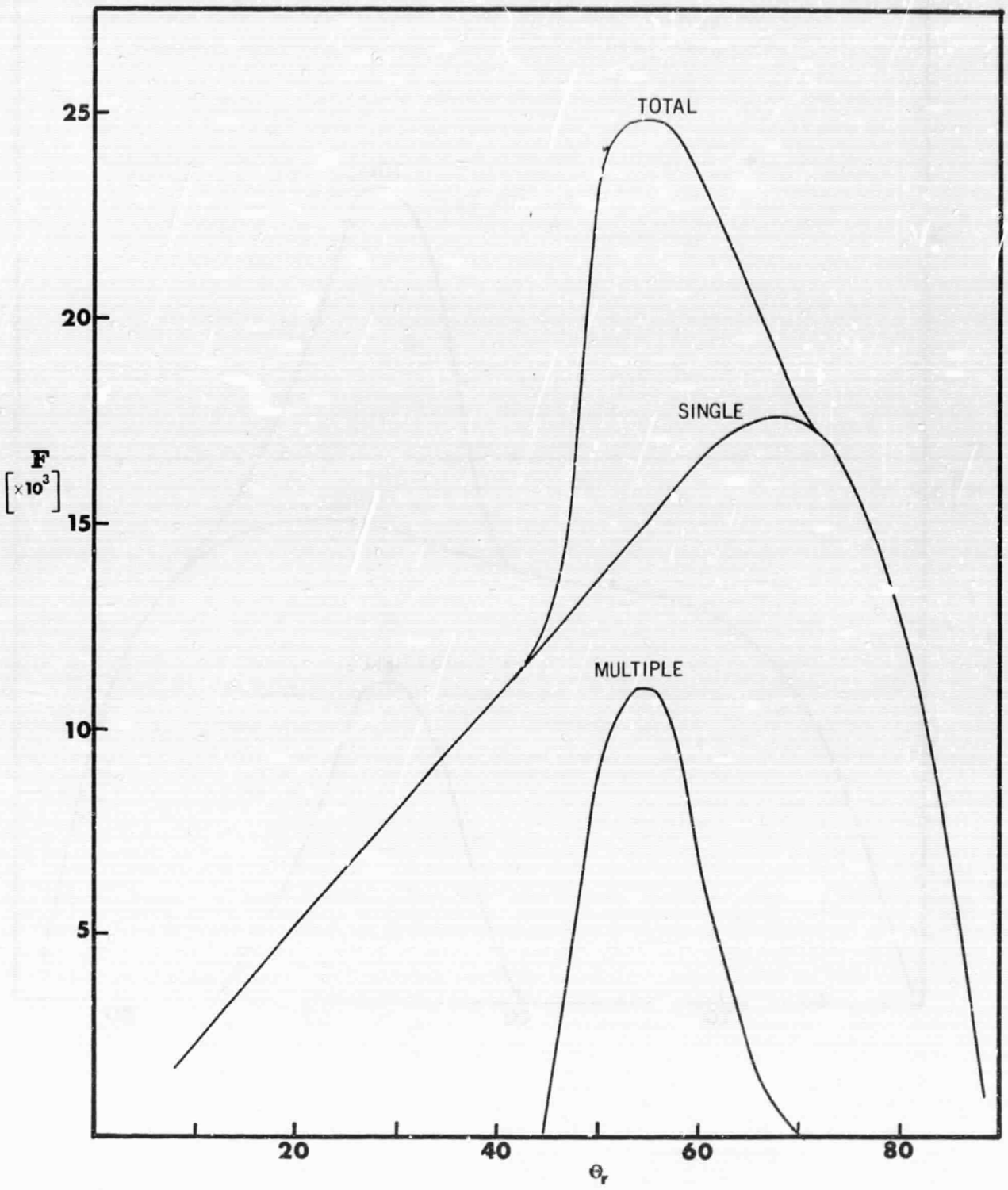

FIG. 7.1.2 STRUCTURE OF THE NORMALIZED PRIMARY FLUX IN THE ANGULAR MODE. Ar/W mass ratio. $R^* = 1.3$, $E_o^* = 20$, $\theta_o = 45^o$, $\phi_o = 0^o$

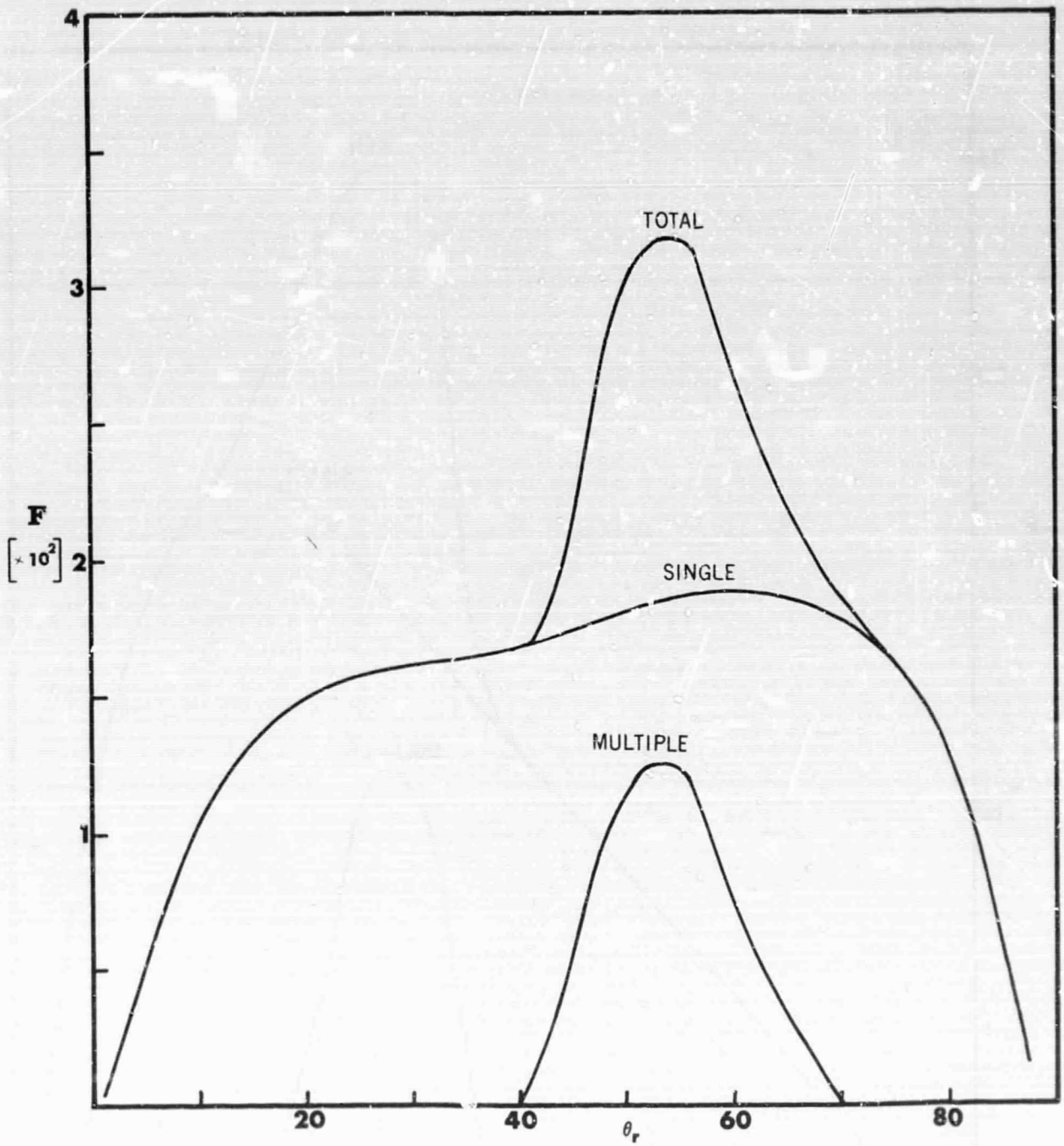

FIG. 7.1.3 STRUCTURE OF THE NORMALIZED PRIMARY FLUX IN THE ANGULAR-DETECTOR APPROXIMATION.
10° resolution, Ar/W mass ratio, $R^* = 1.3$, $E_o^* = 20$, $\theta_o = 45°$, $\phi_o = 0°$.

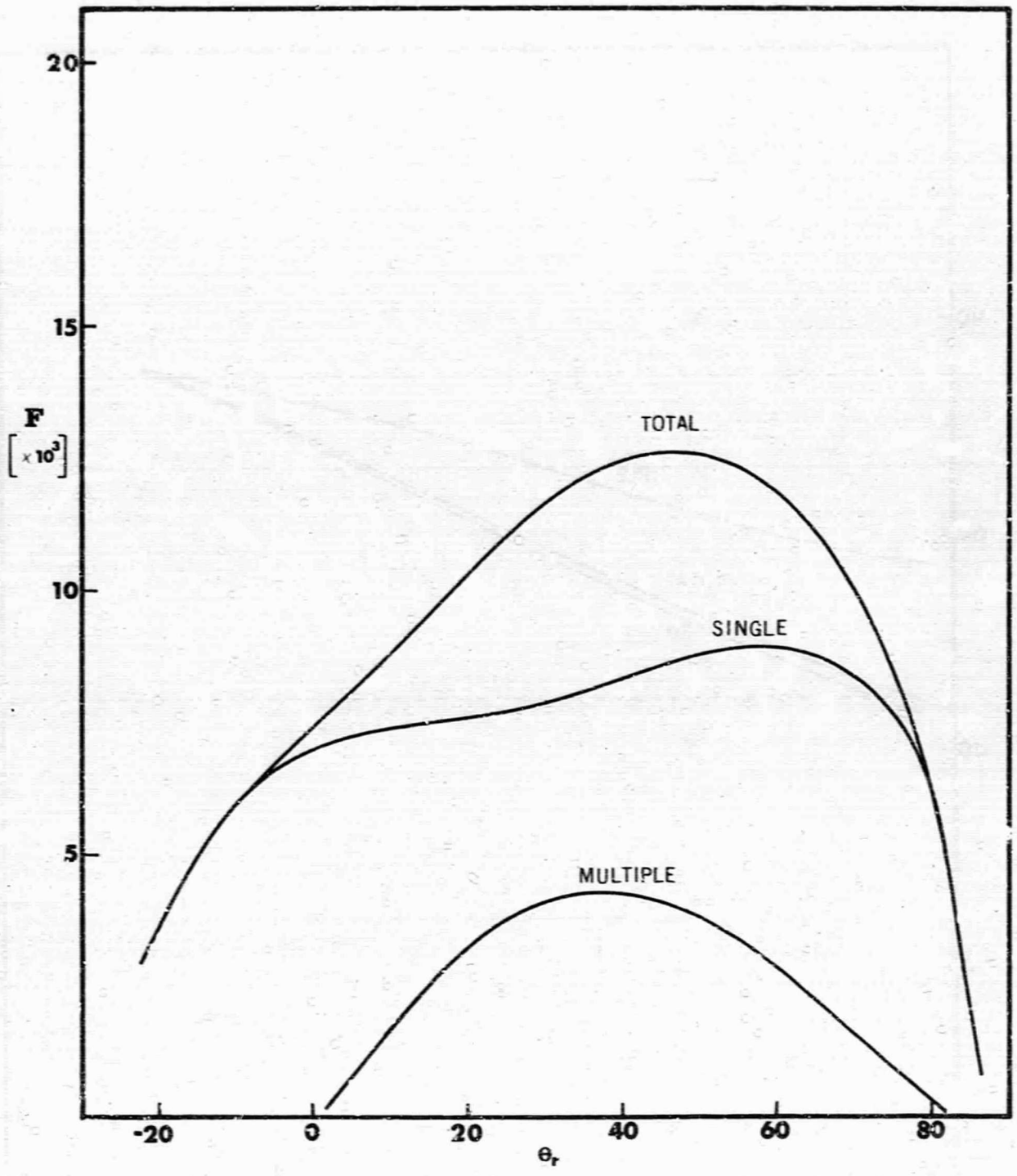

FIG. 7.1.4 STRUCTURE OF THE NORMALIZED PRIMARY FLUX IN THE ANGULAR-DETECTOR APPROXIMATION.
10^{o} resolution. Ar/W mass ratio, $R^* = 0.9$, $E_o^* = 20$, $\theta_o = 45^o$, $\phi_o = 0^o$.

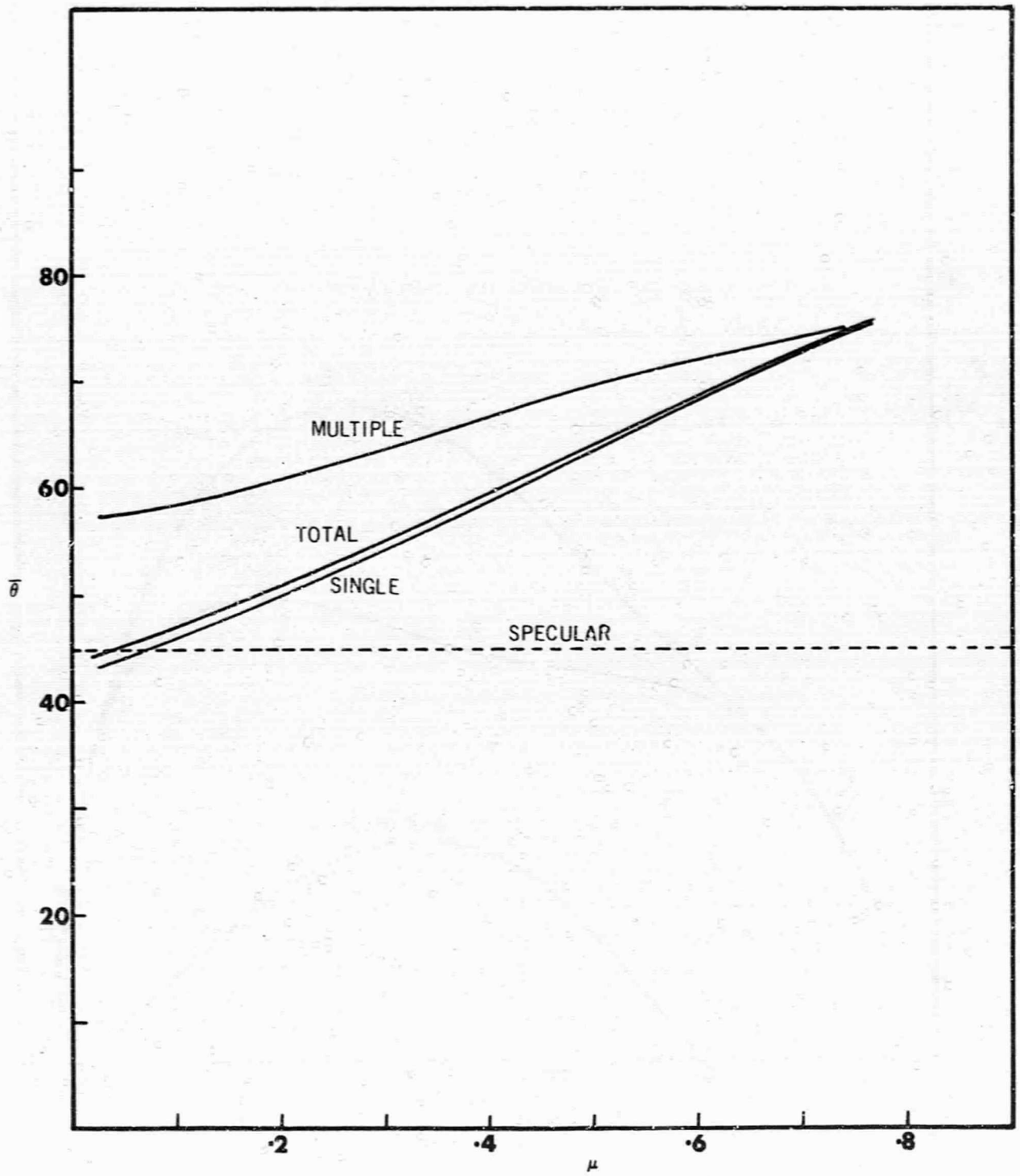

FIG. 7.1.5 THE AVERAGE REFLECTED ANGLE ($\bar{\theta}$) OF THE OUTGOING TRAJECTORIES AS A FUNCTION OF MASS RATIO (μ) FOR THE COMPONENTS OF THE REFLECTED FLUX.

$R^* = 1.3$, $E_o^* = 20$, $\theta_o = 45^o$, $\phi_o = 0^o$.

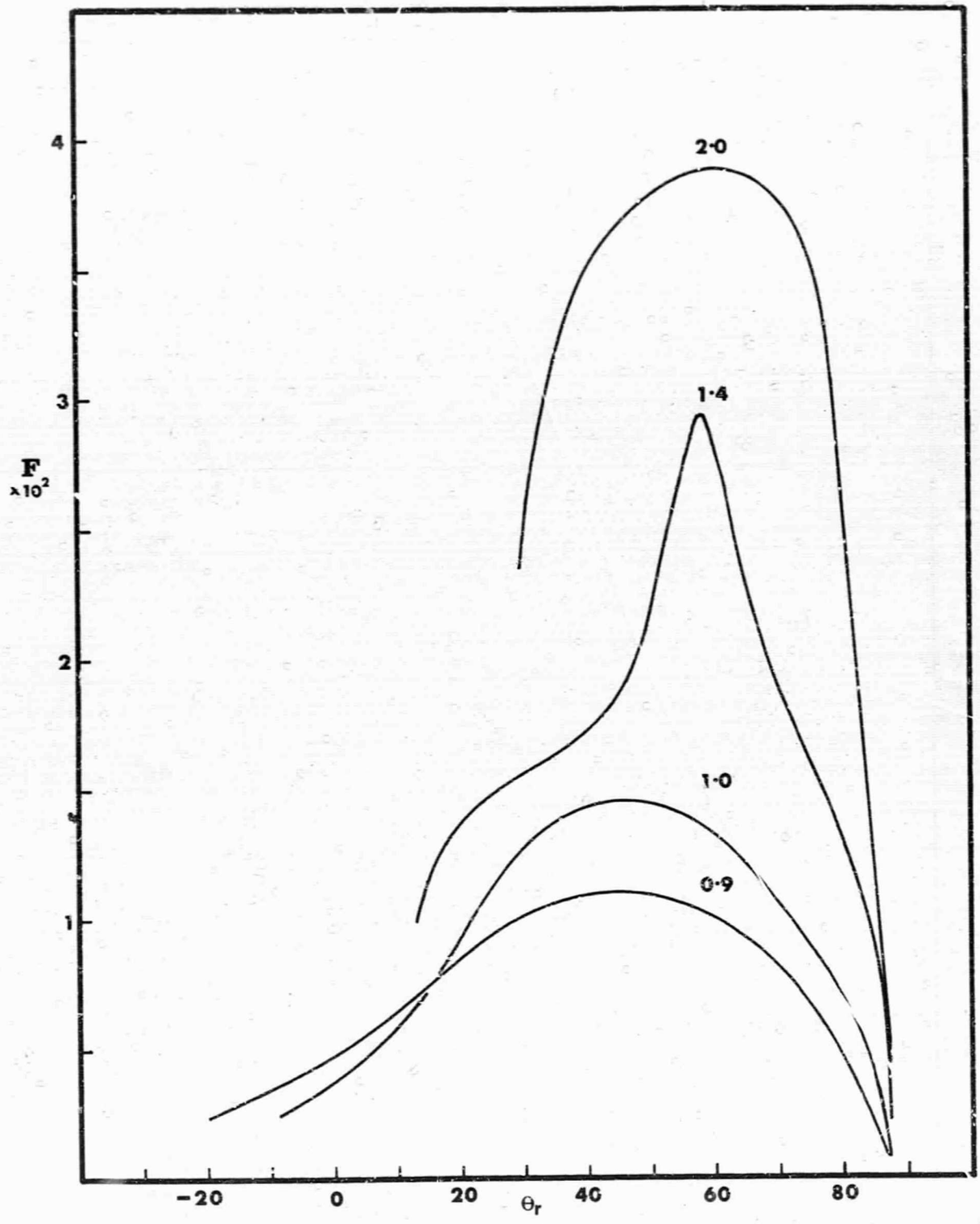

FIG. 7.2.1 THE NORMALIZED PRIMARY FLUX DISTRIBUTIONS FOR VALUES OF THE INTERACTION RADIUS R*. Detector mode 10° resolution. Ar/W mass ratio, $E_o^* = 20$, $\theta_o = 45^\circ$, $\phi_o = 0^\circ$.

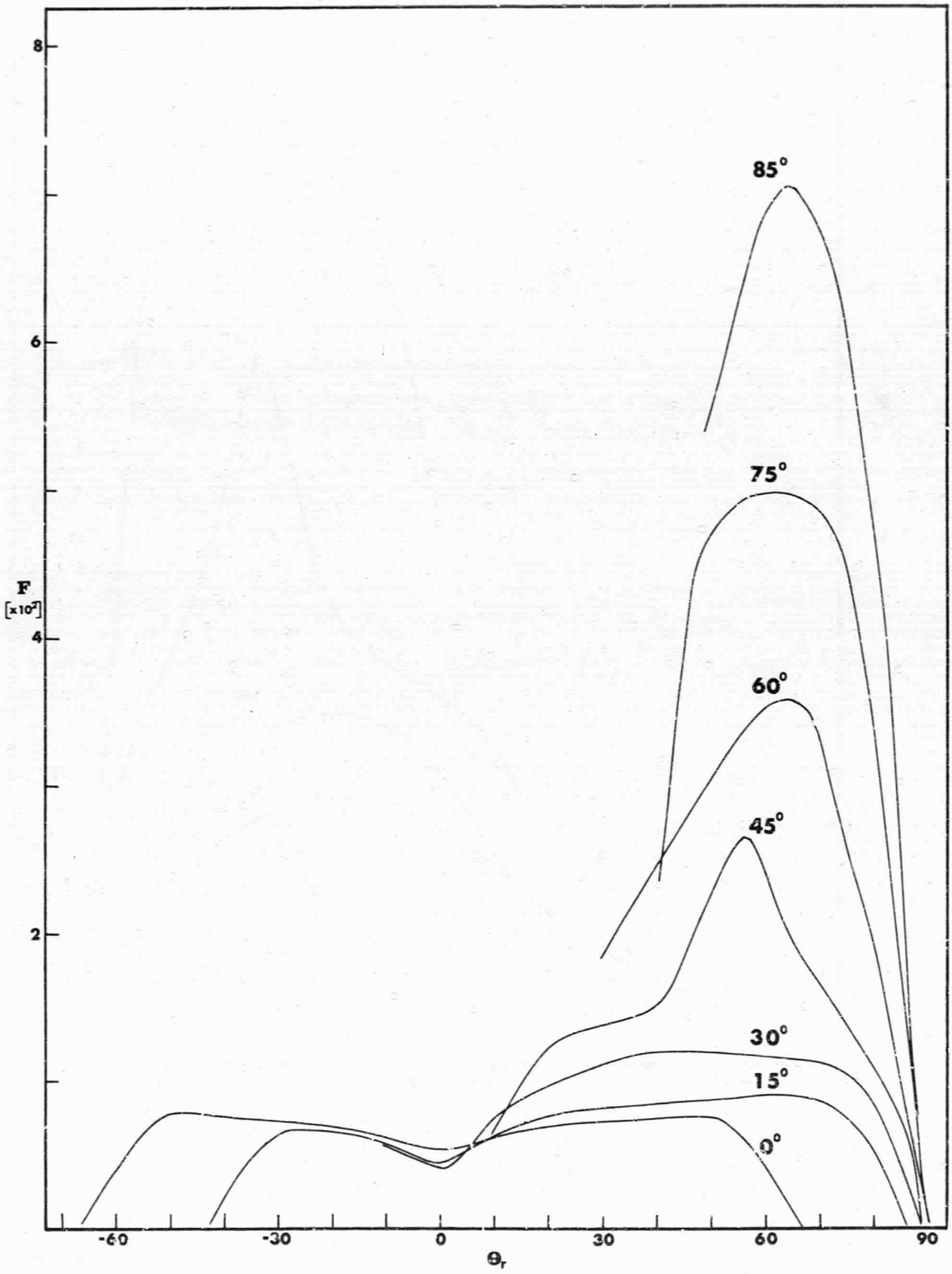

FIG. 7.2.2 THE NORMALIZED PRIMARY FLUX DISTRIBUTIONS FOR VALUES OF THE INITIAL INCIDENCE ANGLE θ_o.
Detector mode 10° resolution. Ar/W mass ratio. $R^* = 1.3$, $E_o^* = 20$, $\phi_o = 0°$

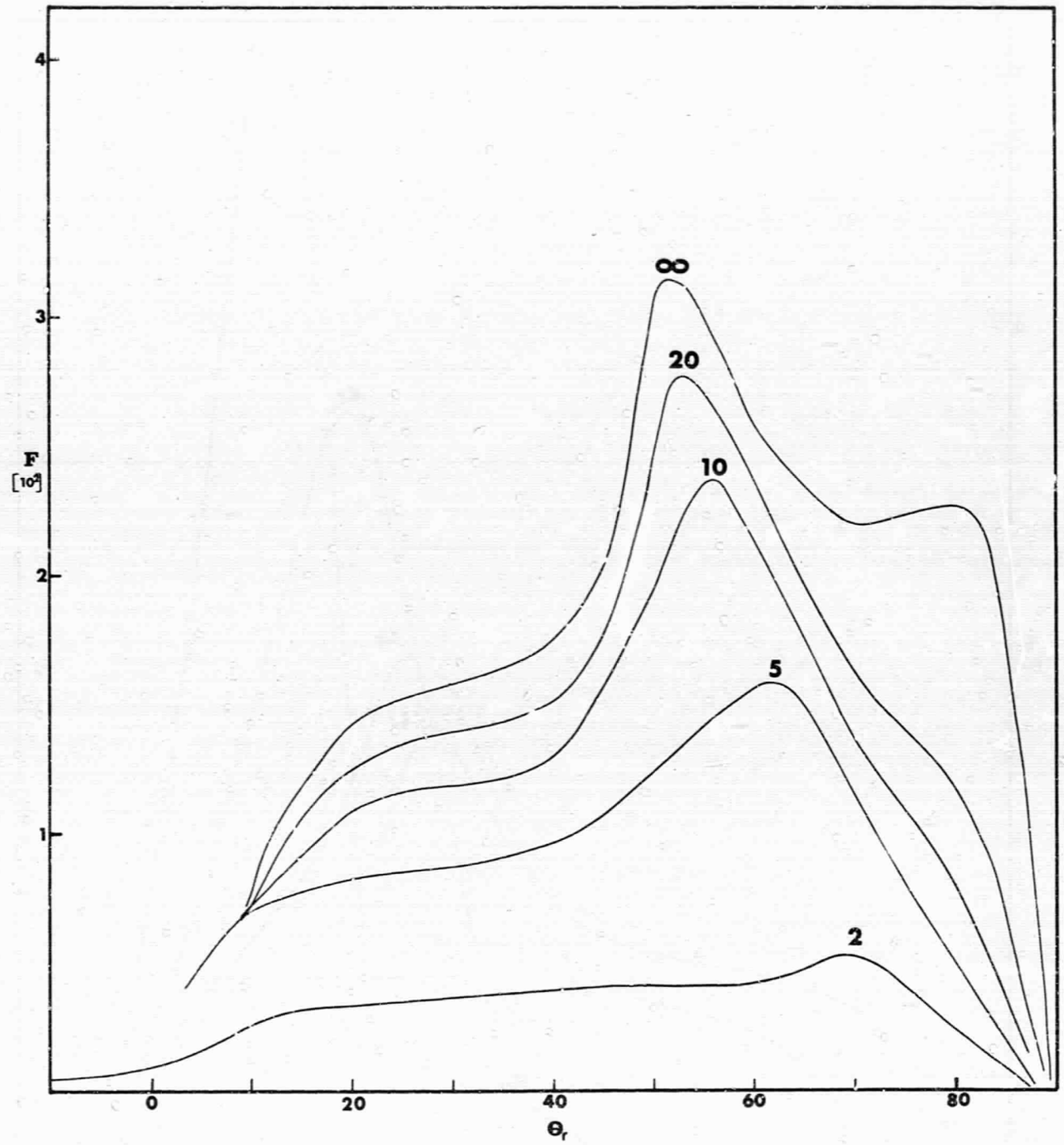

FIG 7.2.3 THE NORMALIZED PRIMARY FLUX DISTRIBUTIONS FOR VALUES OF THE INITIAL ENERGY RATIO E_o^*. Detector mode 10° resolution, Ar/W mass ratio $R^* = 1.3$. $\theta_o = 45°$, $\phi_o = 0°$.

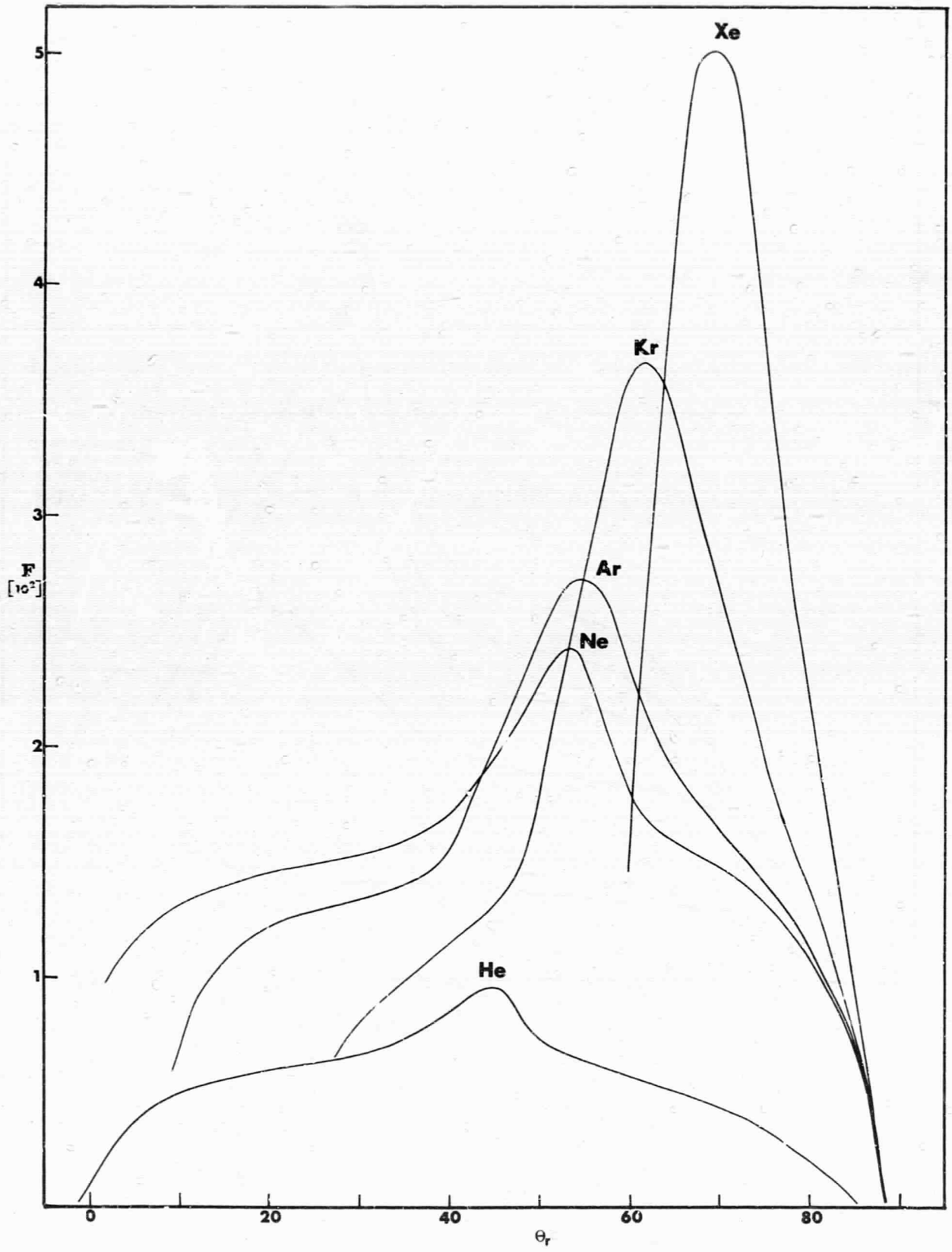

FIG. 7.2.4 THE NORMALIZED PRIMARY FLUX DISTRIBUTIONS FOR THE RARE-GAS-TUNGSTEN MASS RATIOS. Detector mode 10° resolution. $R^* = 1.3$. $E_o^* = 20$, $\theta_o = 45°$, $A_o = 0°$.

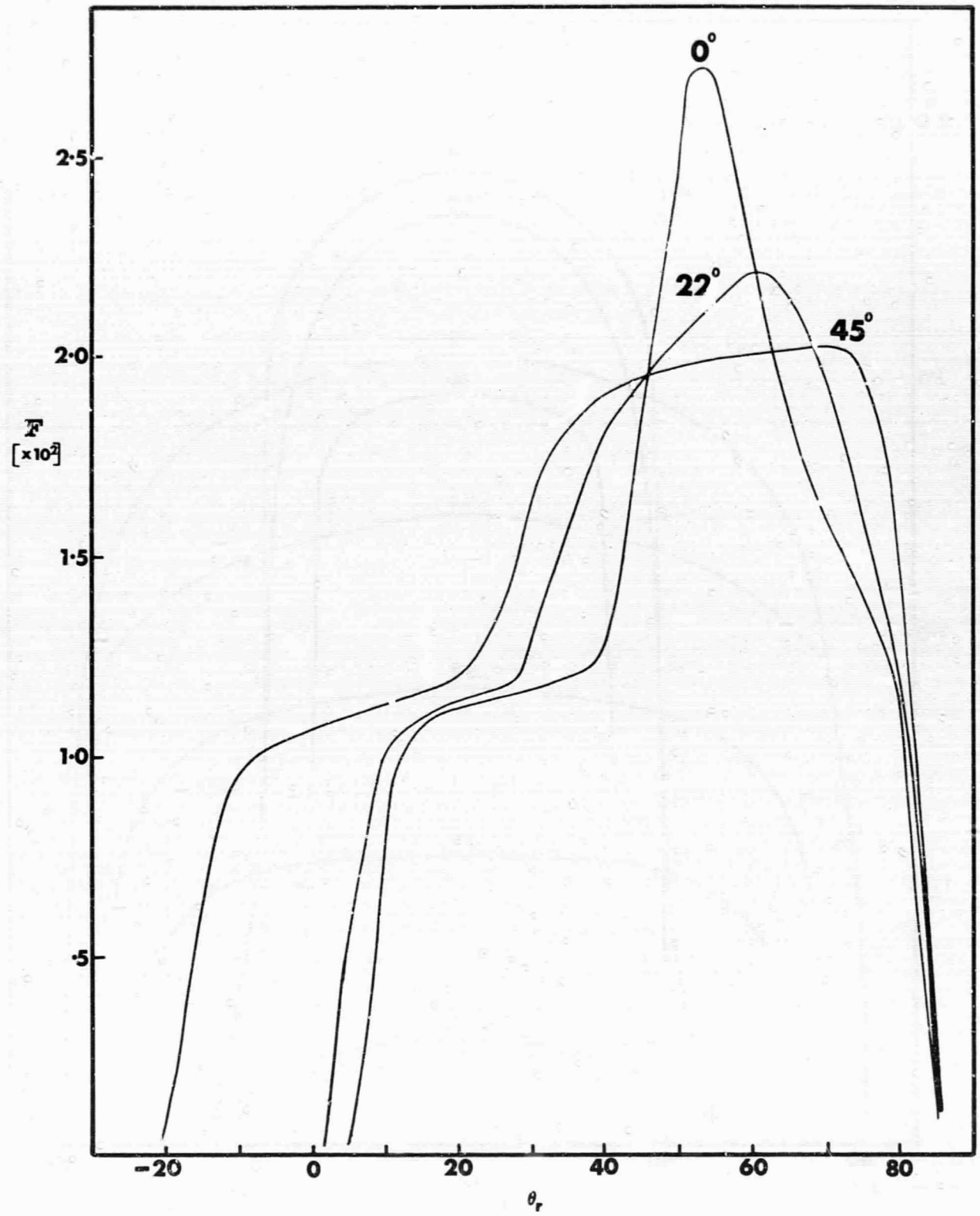

FIG. 7.2.5 THE NORMALIZED PRIMARY FLUX DISTRIBUTIONS FOR VALUES OF THE INITIAL AZIMUTH ANGLE ϕ_o.
Detector mode 10° resolution. Ar/W mass ratio. R* = 1.3,
E_o^* = 20, θ_o = 45°.

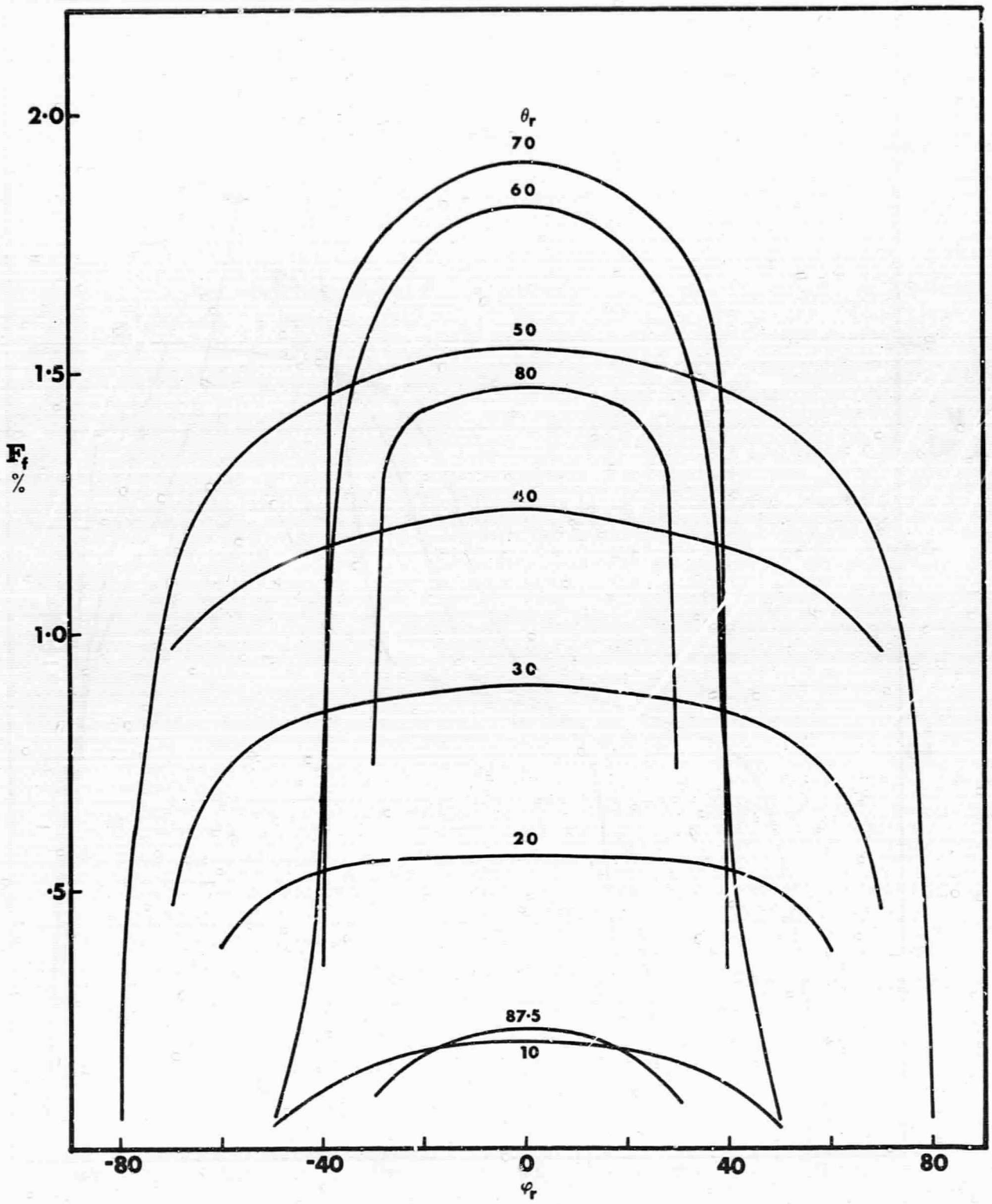

FIG. 7.3.1 THE NORMALIZED PRIMARY FLUX DISTRIBUTION IN SPACE OF THE SINGLE COLLIDERS ONLY (F_f).
Angular mode. Ar/W mass ratio, $R^* = 1.3$, $E_o^* = 20$, $\theta_o = 45^o$, $\phi_o = 0^o$.
The flux is given as a percentage of the total number of single colliders reflected. The distribution is plotted for the angles ϕ and θ over the complete reflection half-space.

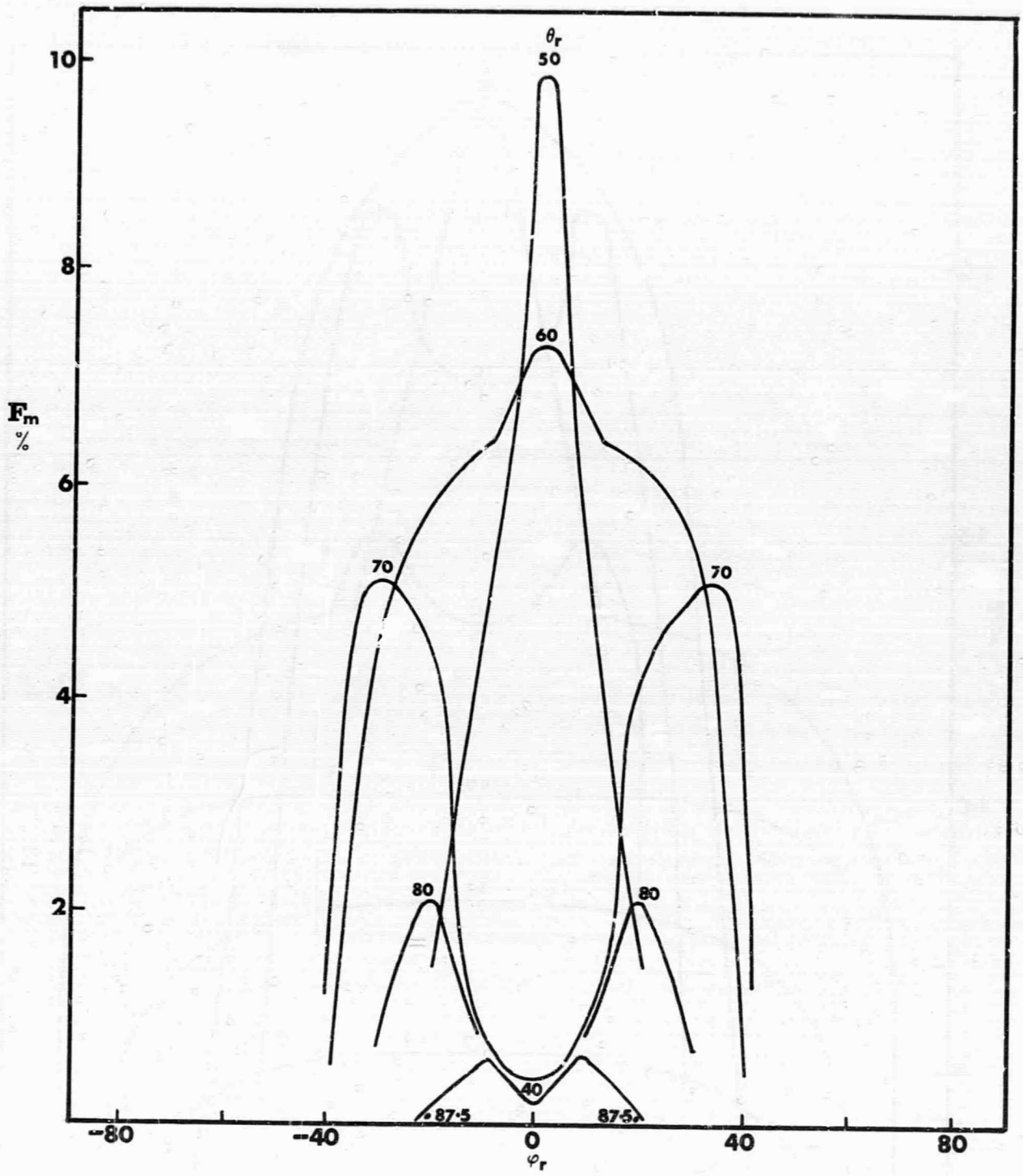

FIG. 7.3.2 THE NORMALIZED PRIMARY FLUX DISTRIBUTION IN SPACE OF THE MULTIPLE COLLIDERS ONLY (F_m).

Corresponds to the case of FIG. 7.3.1. The flux is given as a percentage of the total number of multiple colliders reflected.

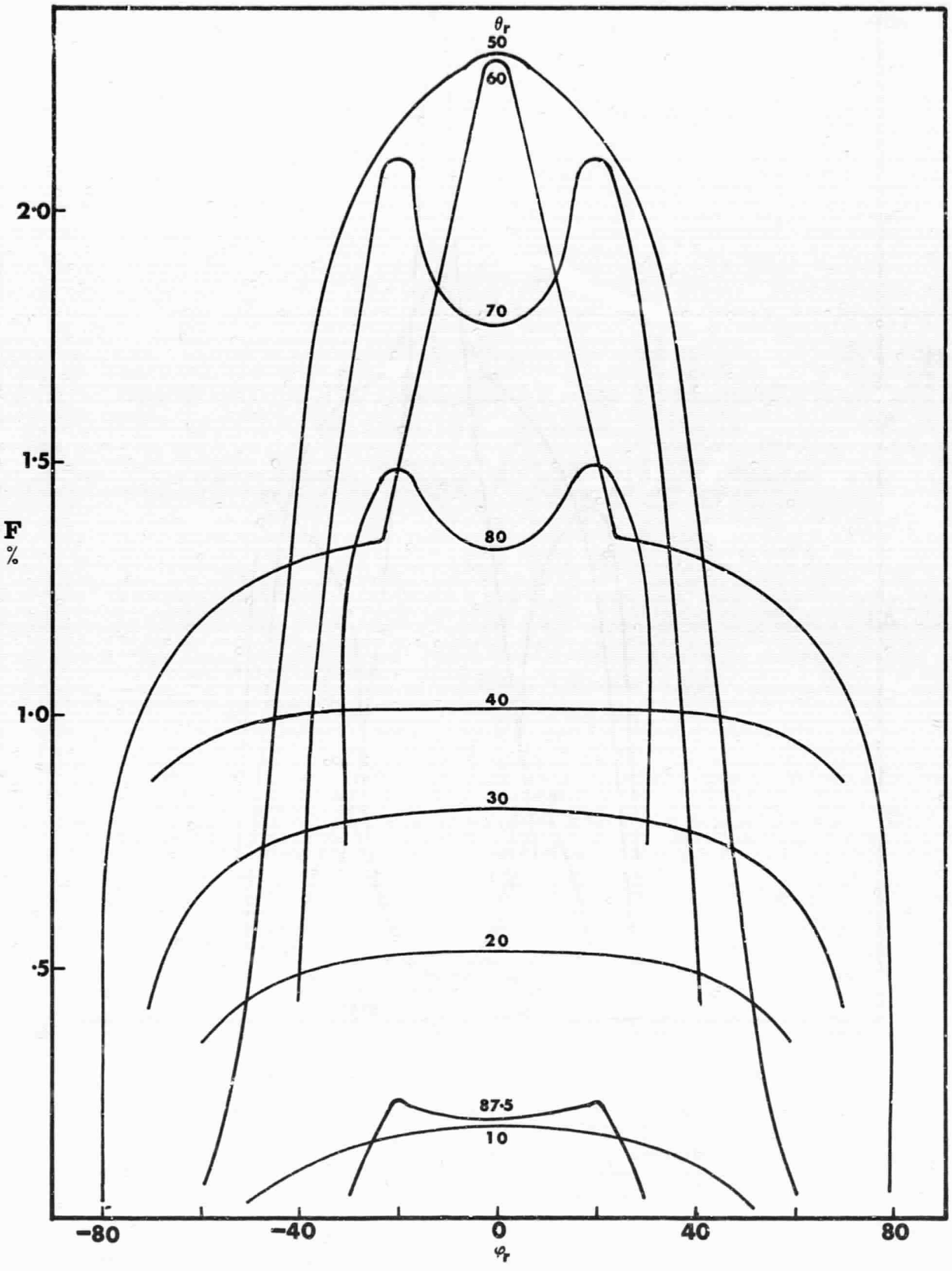

FIG. 7.3.3 THE NORMALIZED PRIMARY FLUX DISTRIBUTION IN SPACE OF THE TOTAL (SINGLE AND MULTIPLE COMBINED) PARTICLES (F).
This is the sum of the cases shown in FIGS. 7.3.1 and 7.3.2. The flux is given as a percentage of the total particles reflected.

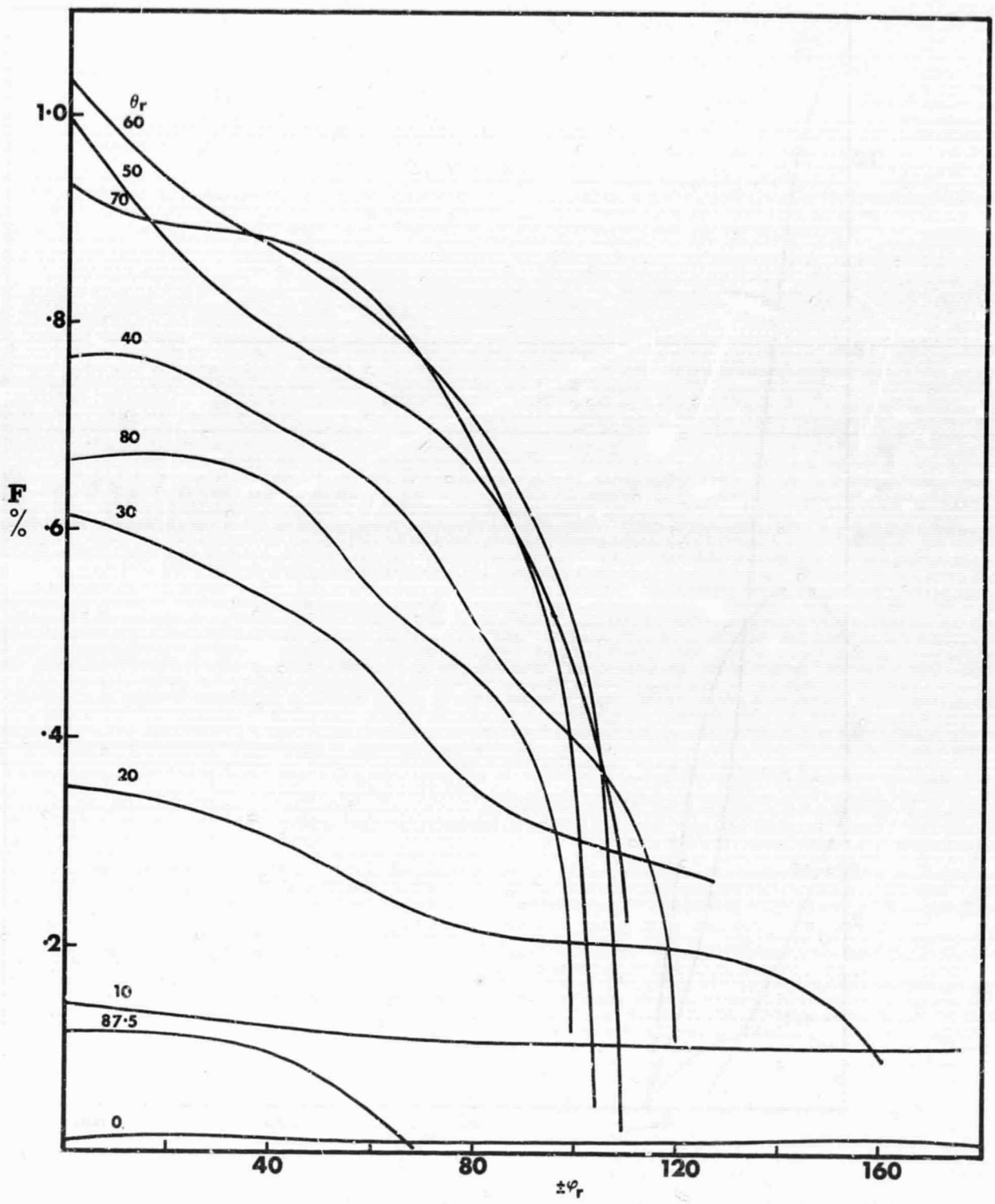

FIG. 7.3.4 THE NORMALIZED PRIMARY FLUX DISTRIBUTION IN SPACE FOR A SMALL VALUE OF R*. Angular mode. Ar/W mass ratio. $R^* = 0.9$, $E_o^* = 20$, $\theta_o = 45^o$, $\phi_o = 0^o$. The flux is given as a percentage of the total number of reflected particles.

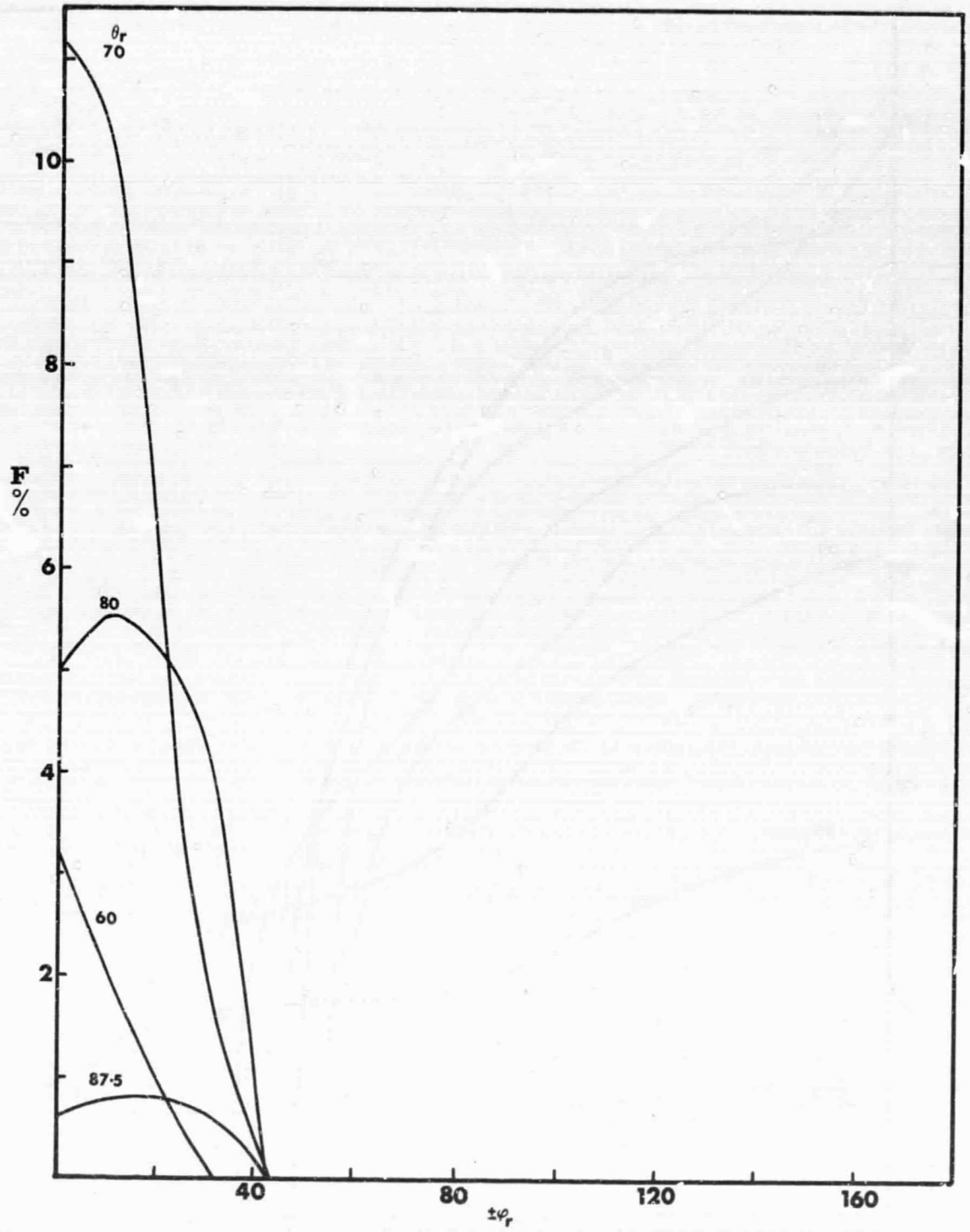

FIG. 7.3.5 THE NORMALIZED PRIMARY FLUX DISTRIBUTION IN SPACE FOR A LARGE VALUE OF THE MASS RATIO. Angular mode. Xe/W mass ratio. $R^* = 1.3$, $E_o^* = 20$. $\theta_o = 45^o$, $\phi_o = 0^o$. The flux is given as a percentage of the total number of reflected particles.

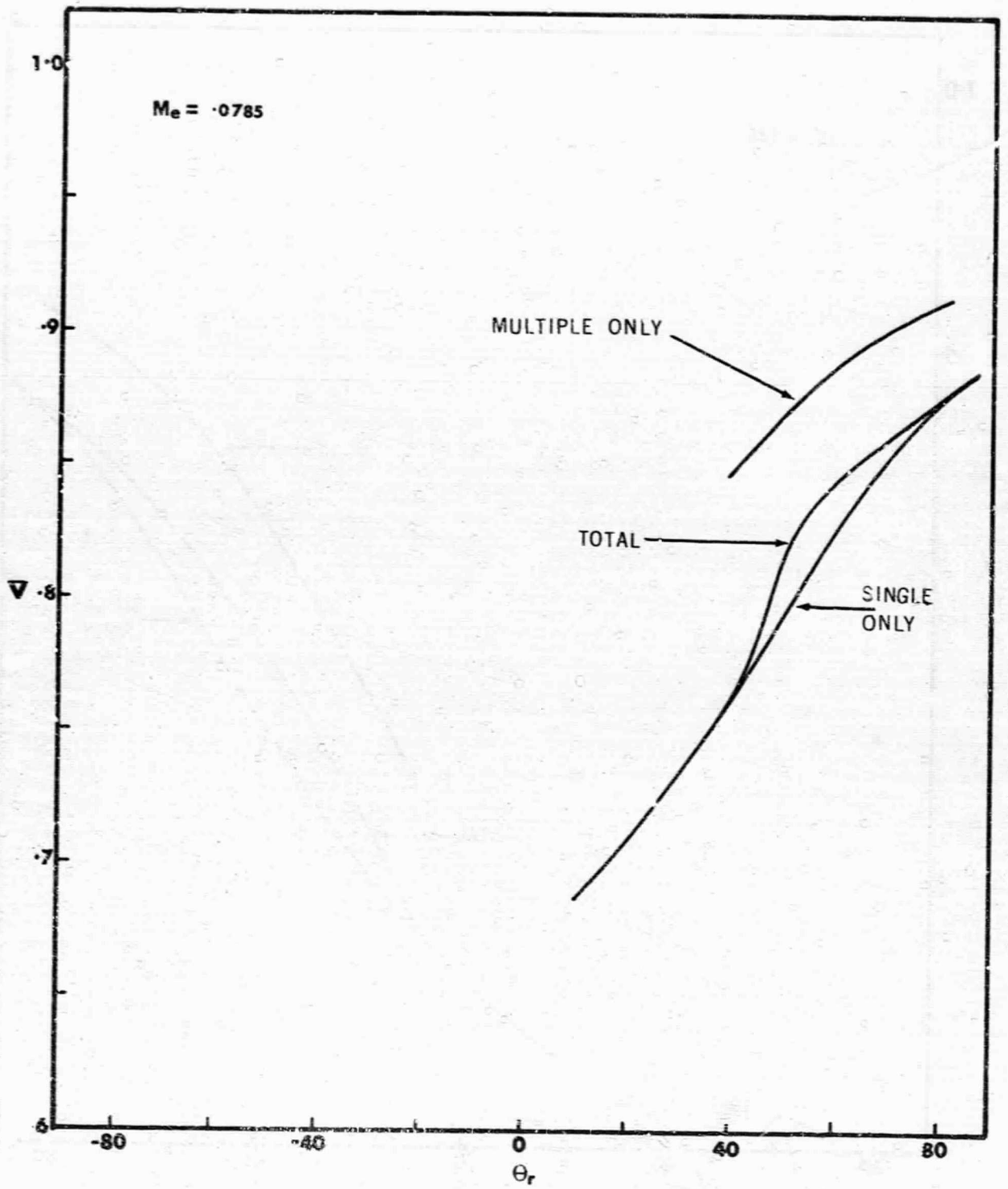

FIG. 8.1.1 STRUCTURE OF THE PRIMARY VELOCITY MEAN DISTRIBUTION IN THE ANGULAR DETECTOR APPROXIMATION R* = 1.3.
10° resolution, Ar/W mass ratio, R* = 1.3, E_o^* = 20, $\theta_o = 45^{\circ}$, $\phi_o = 0^{\circ}$.
Corresponds to FIG. 7.1.3 which gives the flux for the same case.

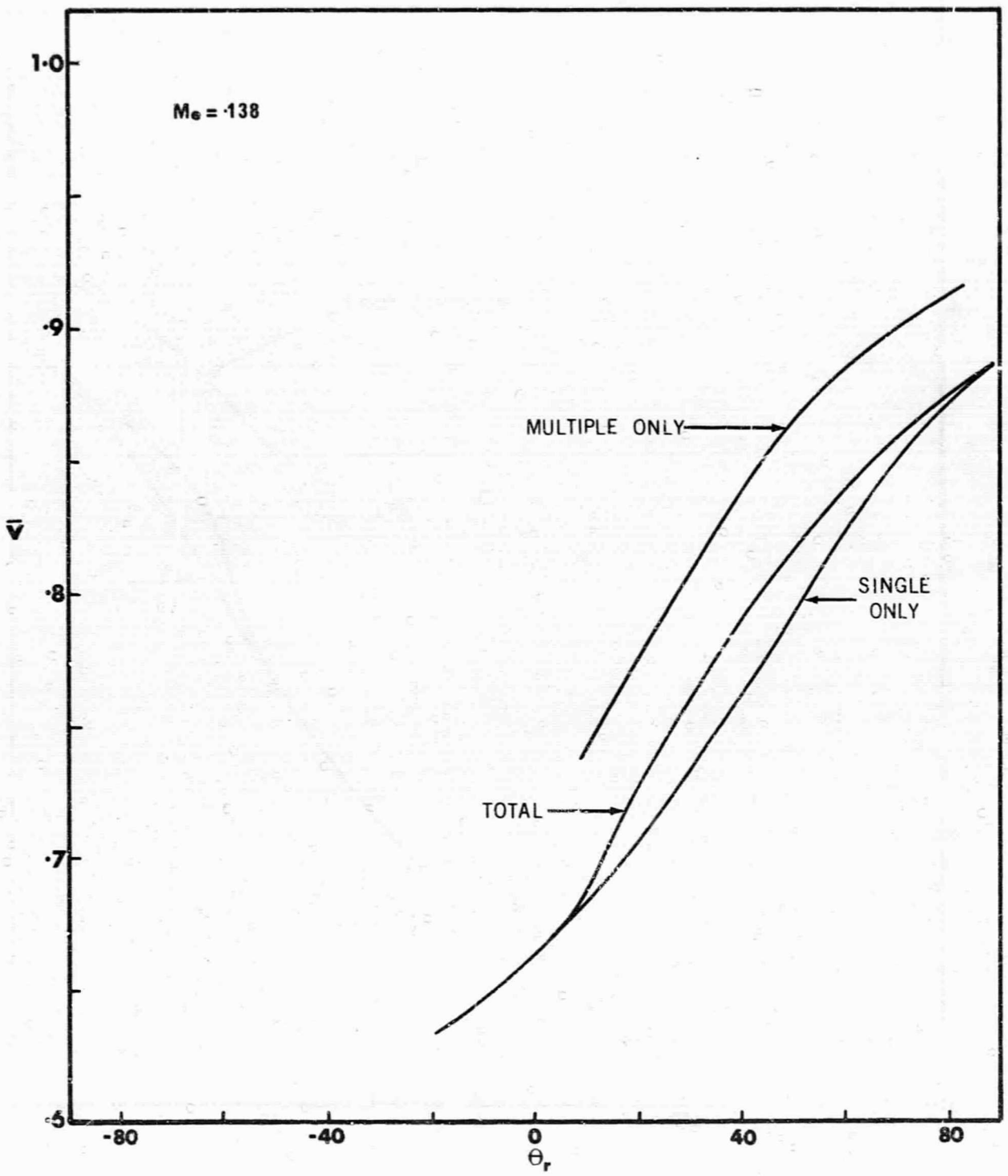

FIG. 8.1.2 STRUCTURE OF THE PRIMARY VELOCITY MEAN DISTRIBUTION IN THE ANGULAR-DETECTOR APPROXIMATION.
10^{o} resolution, Ar/W mass ratio, $R^{*} = 0.9$, $E_o^{*} = 20$, $\theta_o = 45^{o}$, $\phi_o = 0^{o}$.
Corresponds to FIG. 7.1.4 which gives the flux for the same case.

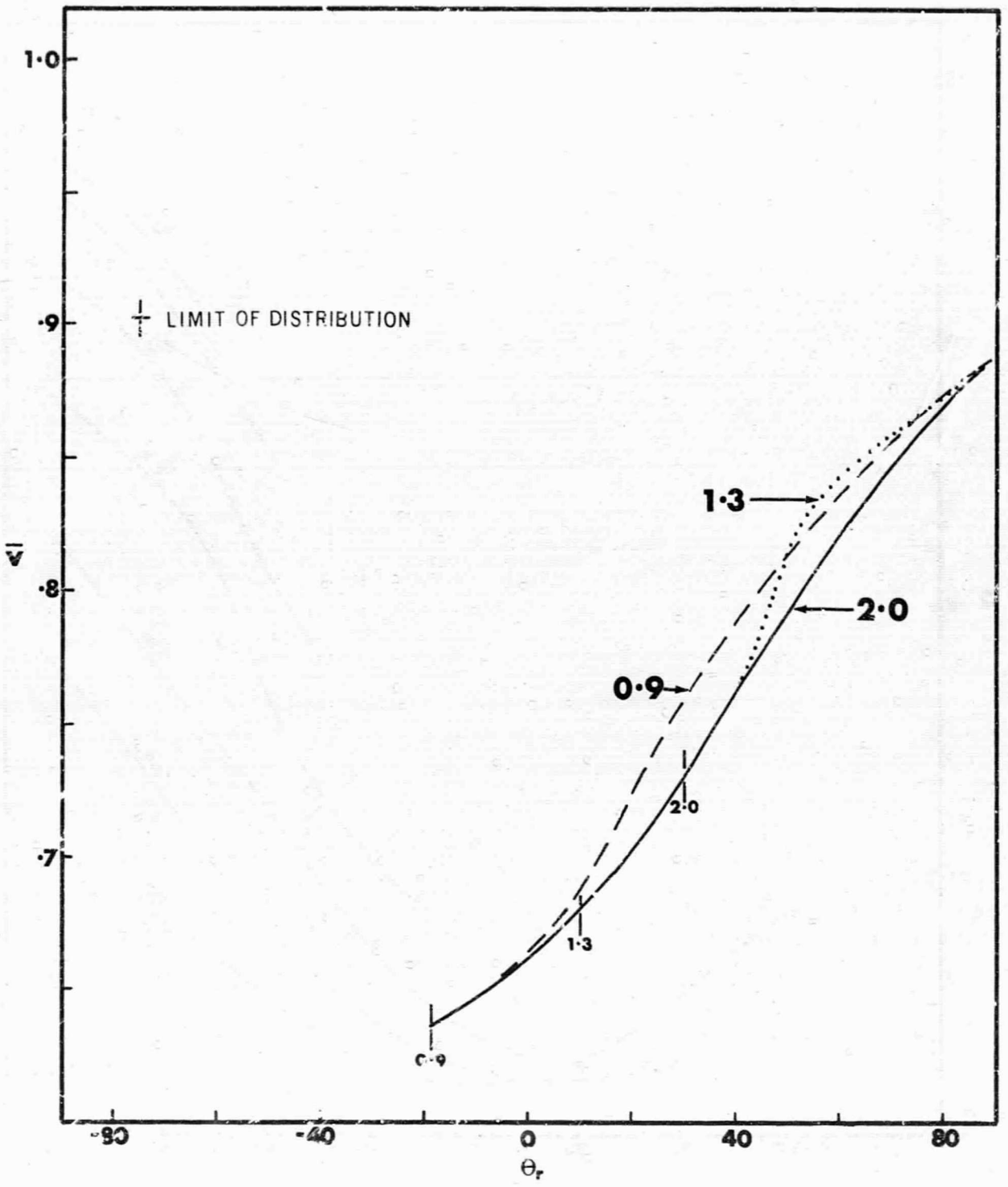

FIG. 8.2.1 THE PRIMARY VELOCITY MEAN DISTRIBUTIONS FOR VALUES OF THE INTERACTION RADIUS R*.
Detector mode 10° resolution. Ar/W mass ratio, $E_o^* = 20$, $\theta_o = 45°$, $\phi_o = 0°$.

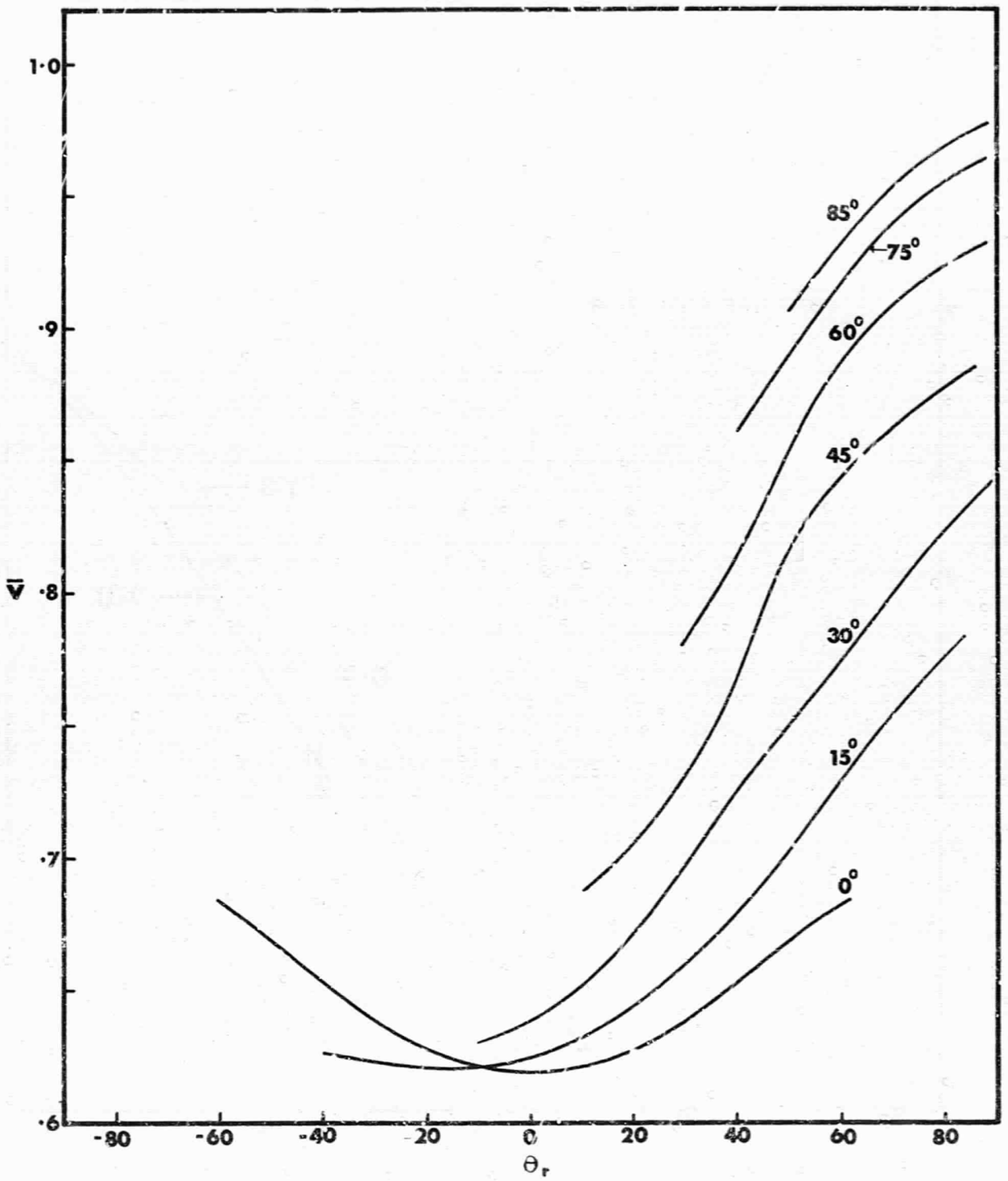

FIG. 8.2.2 THE PRIMARY VELOCITY MEAN DISTRIBUTIONS FOR VALUES OF THE INITIAL INCIDENCE ANGLE θ_o.
Detector mode 10° resolution. Ar/W mass ratio R* = 1.3,
$E_o^* = 20$, $\phi_o = 0°$.
Corresponds to FIG. 7.2.2.

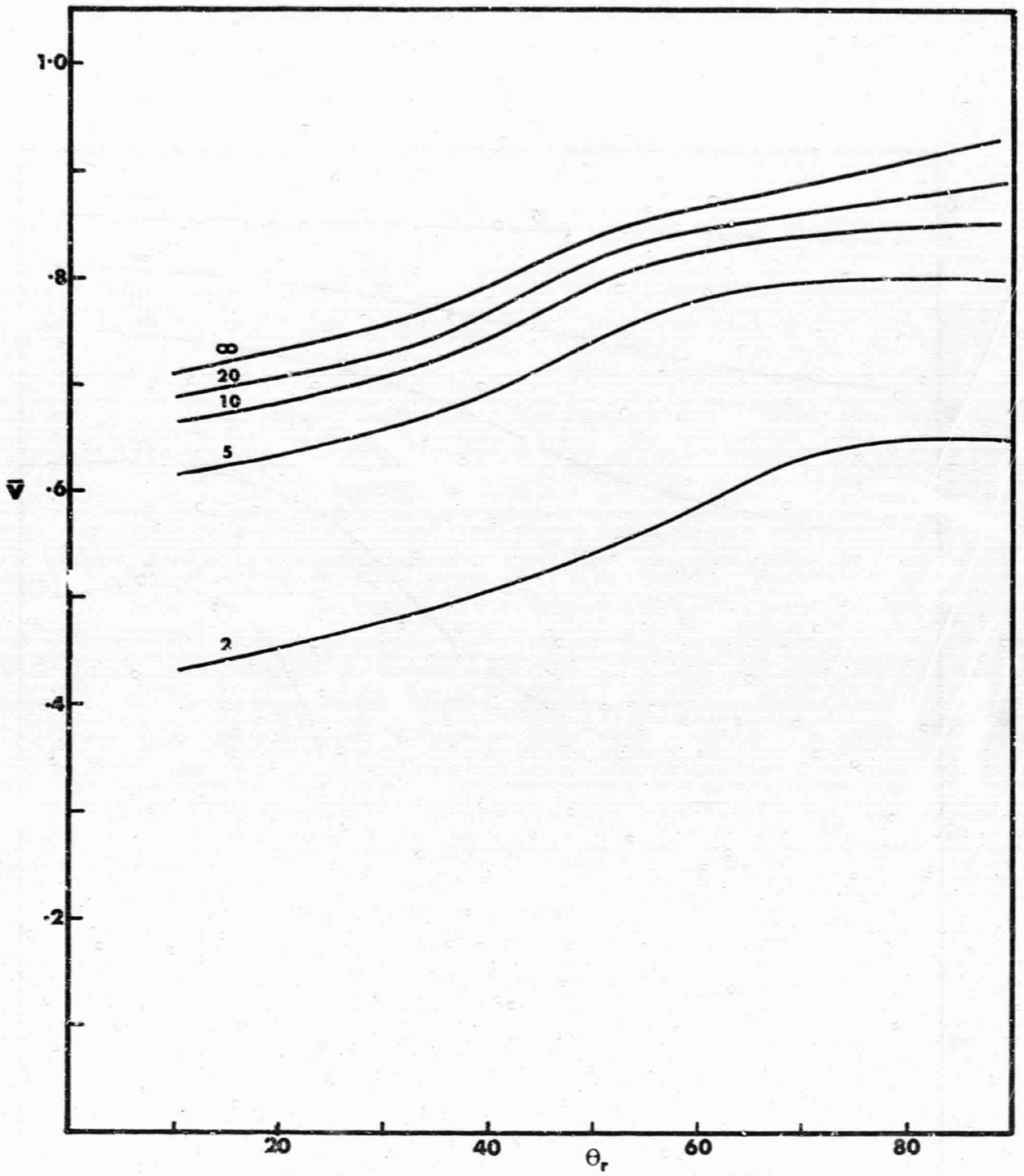

FIG. 8.2.3 THE PRIMARY VELOCITY MEAN DISTRIBUTIONS FOR VALUES OF THE INITIAL ENERGY RATIO E_o*.
Detector mode 10° resolution, Ar/W mass ratio R* = 1.3,
$\theta_o = 45°$, $\phi_o = 0°$.
Corresponds to FIG. 7.2.3.

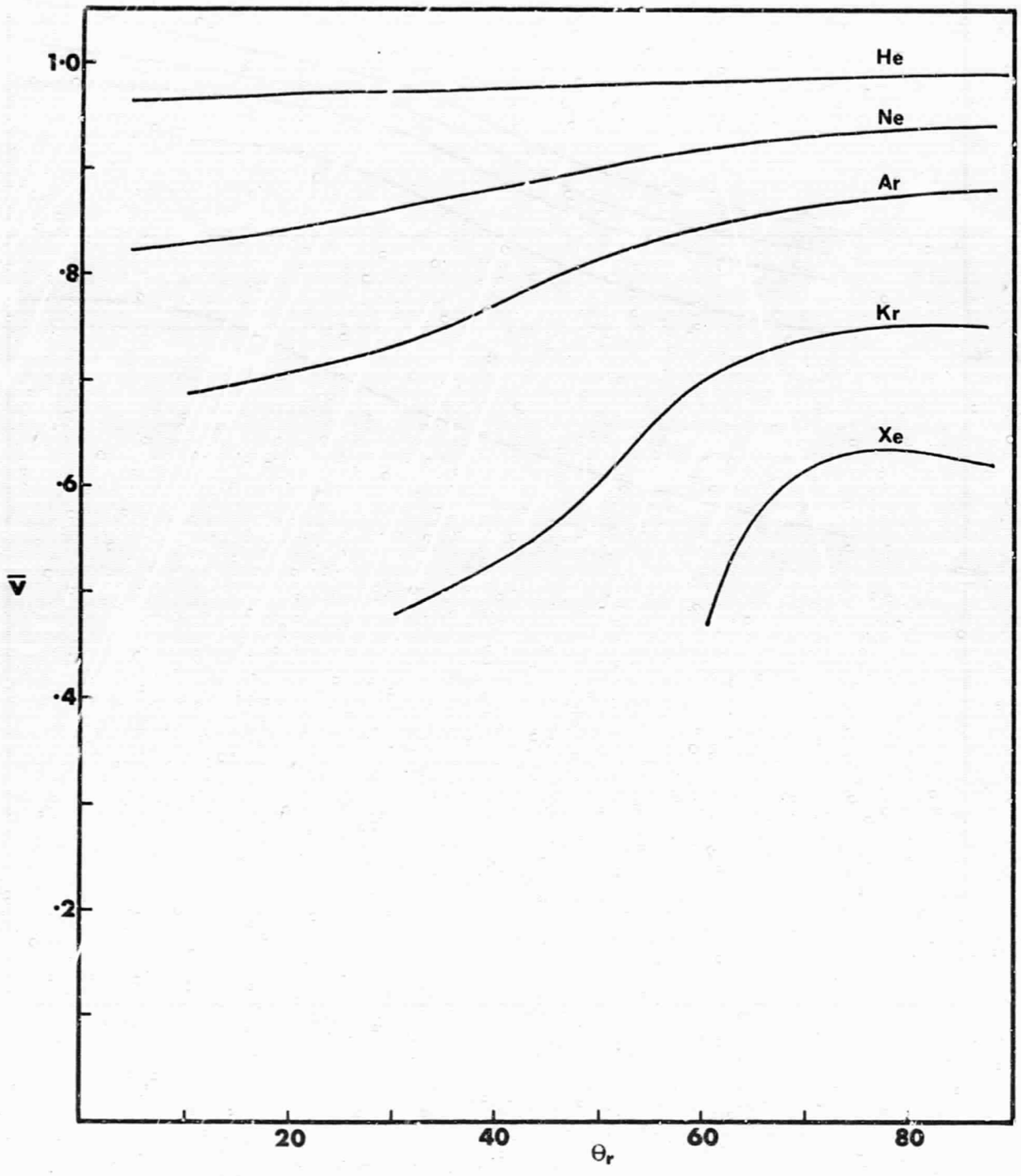

FIG. 8.2.4 THE PRIMARY VELOCITY MEAN DISTRIBUTIONS FOR THE RARE-GAS-TUNGSTEN MASS RATIOS.
Detector mode 10° resolution R* = 1.3, E_o* = 20, θ_o = 45°, φ_o = 0°.

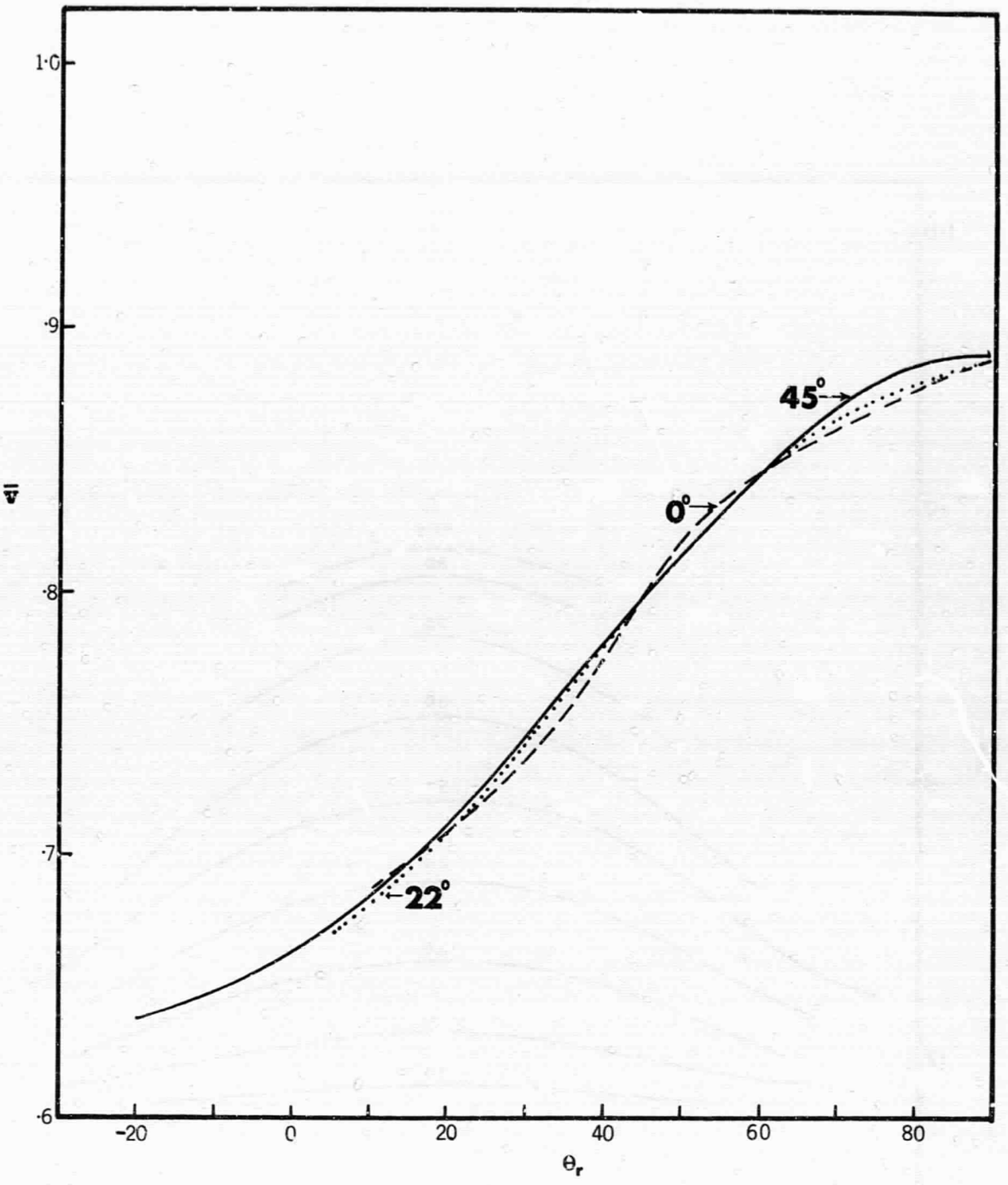

FIG. 8.2.5 THE PRIMARY VELOCITY MEAN DISTRIBUTIONS FOR VALUES OF THE INITIAL AZIMUTH ANGLE ϕ_o. Detector mode 10° resolution, Ar/W mass ratio R* = 1.3, E_o* = 20, θ_o = 45°. Corresponds to FIG. 7.2.5.

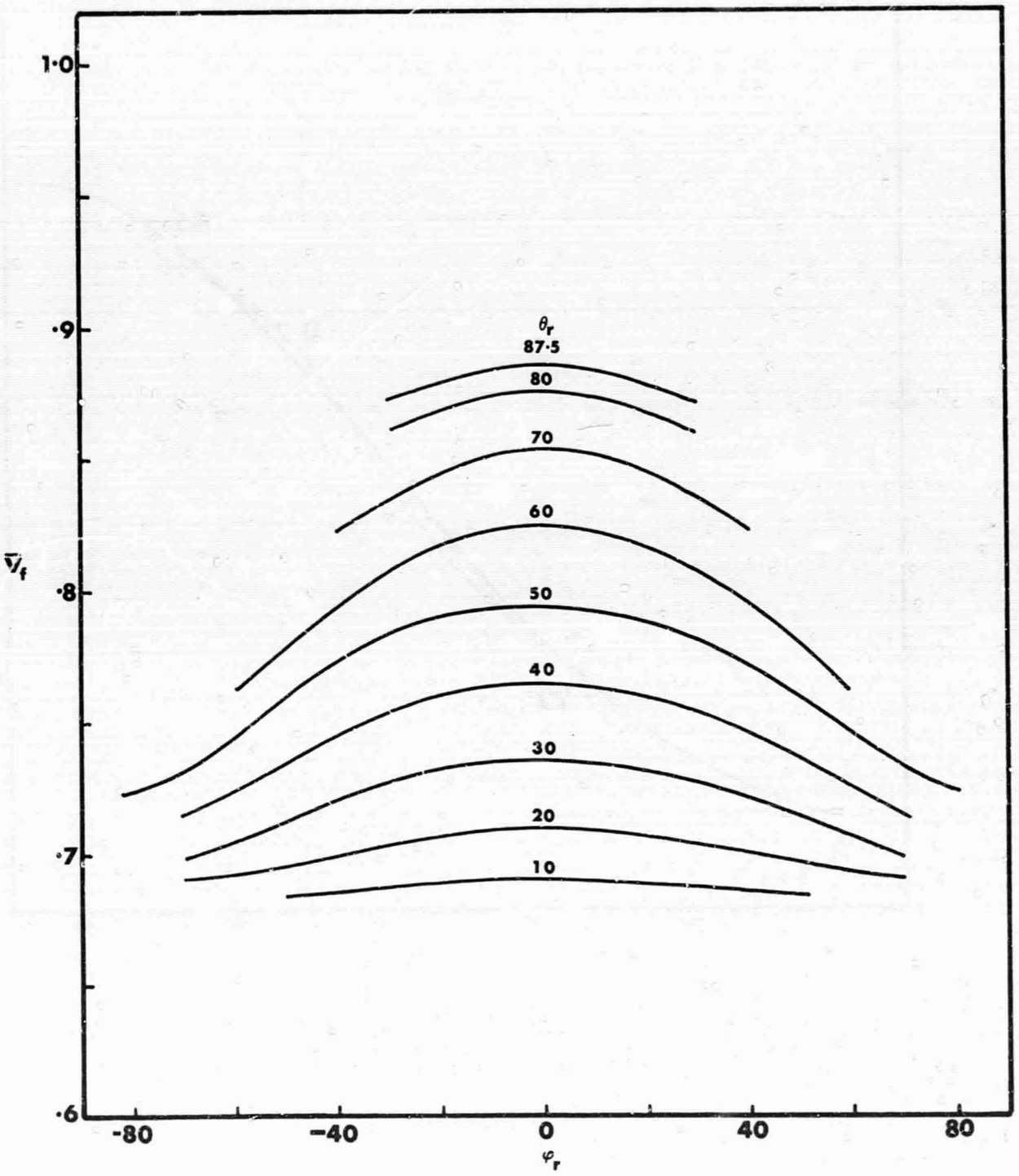

FIG. 8.3.1 THE PRIMARY VELOCITY MEAN DISTRIBUTION IN SPACE OF THE SINGLE COLLIDERS ONLY ($\bar{v}_f$).
Angular mode. Ar/W mass ratio, R* = 1.3, E_o* = 20, $\theta_o = 0^o$.
The distribution is plotted for the angles ϕ and θ over the complete reflection half space.
Corresponds to FIG. 7.3.1.

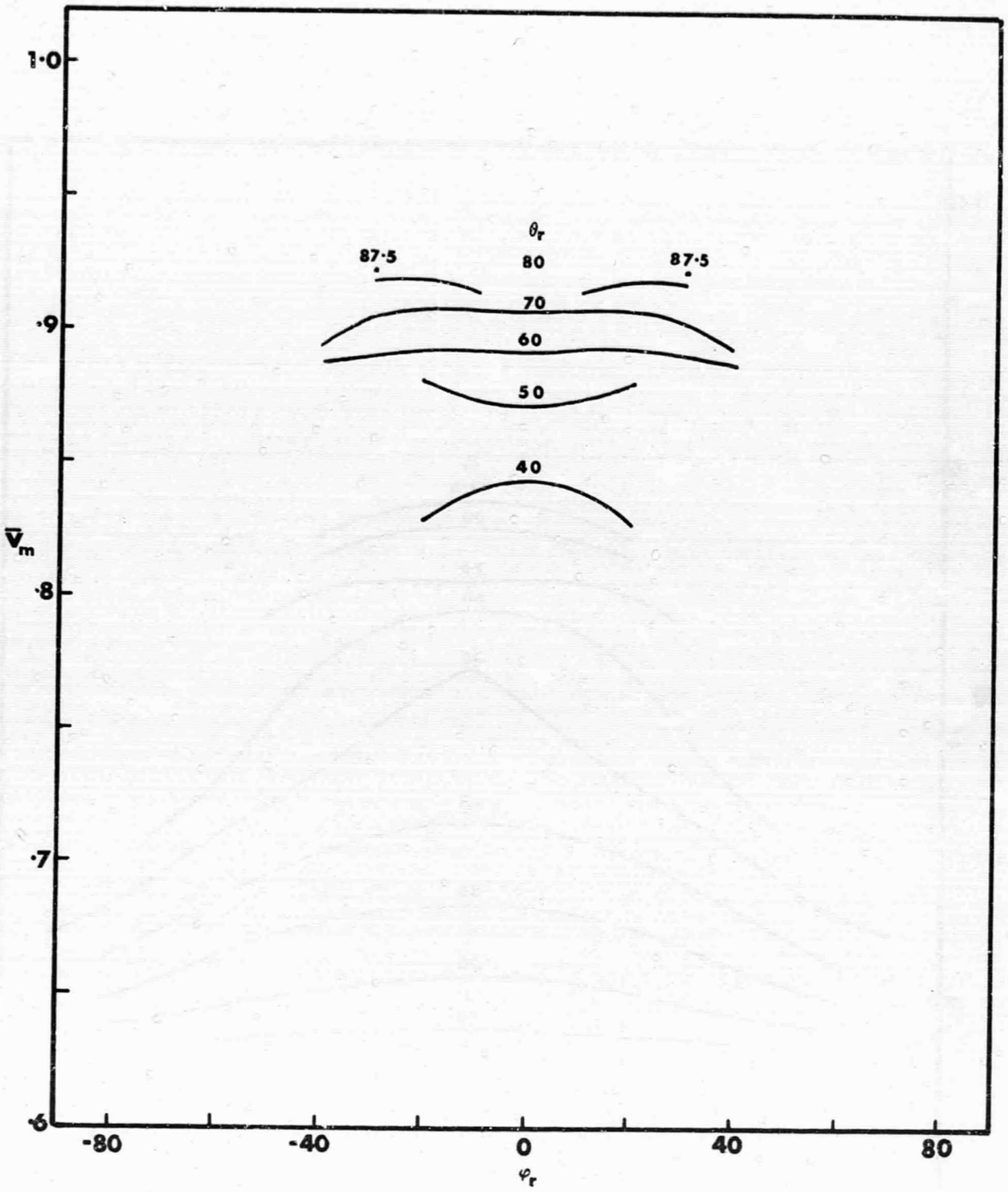

FIG. 8.3.2 THE PRIMARY VELOCITY MEAN DISTRIBUTION IN SPACE OF THE MULTIPLE COLLIDERS ONLY ($\bar{v}_m$).
Same case as FIG. 8.3.1.
Corresponds to FIG. 7.3.2.

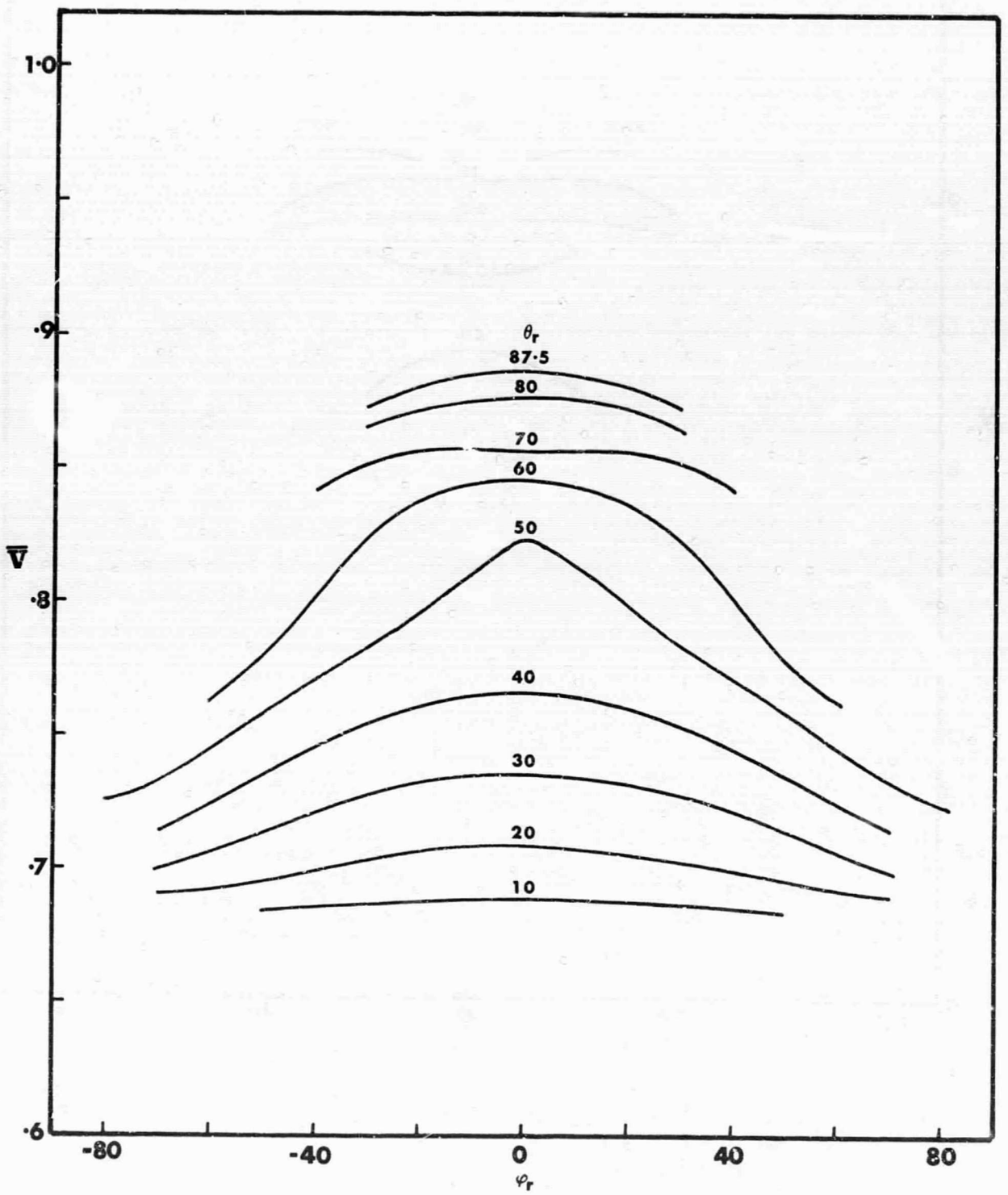

FIG. 8.3.3 THE PRIMARY VELOCITY MEAN DISTRIBUTION IN SPACE OF THE TOTAL (SINGLE AND MULTIPLE COMBINED) PARTICLES ($\bar{V}$).
Combination of FIG. 8.3.1 and FIG. 8.3.2.
Corresponds to FIG. 7.3.3.

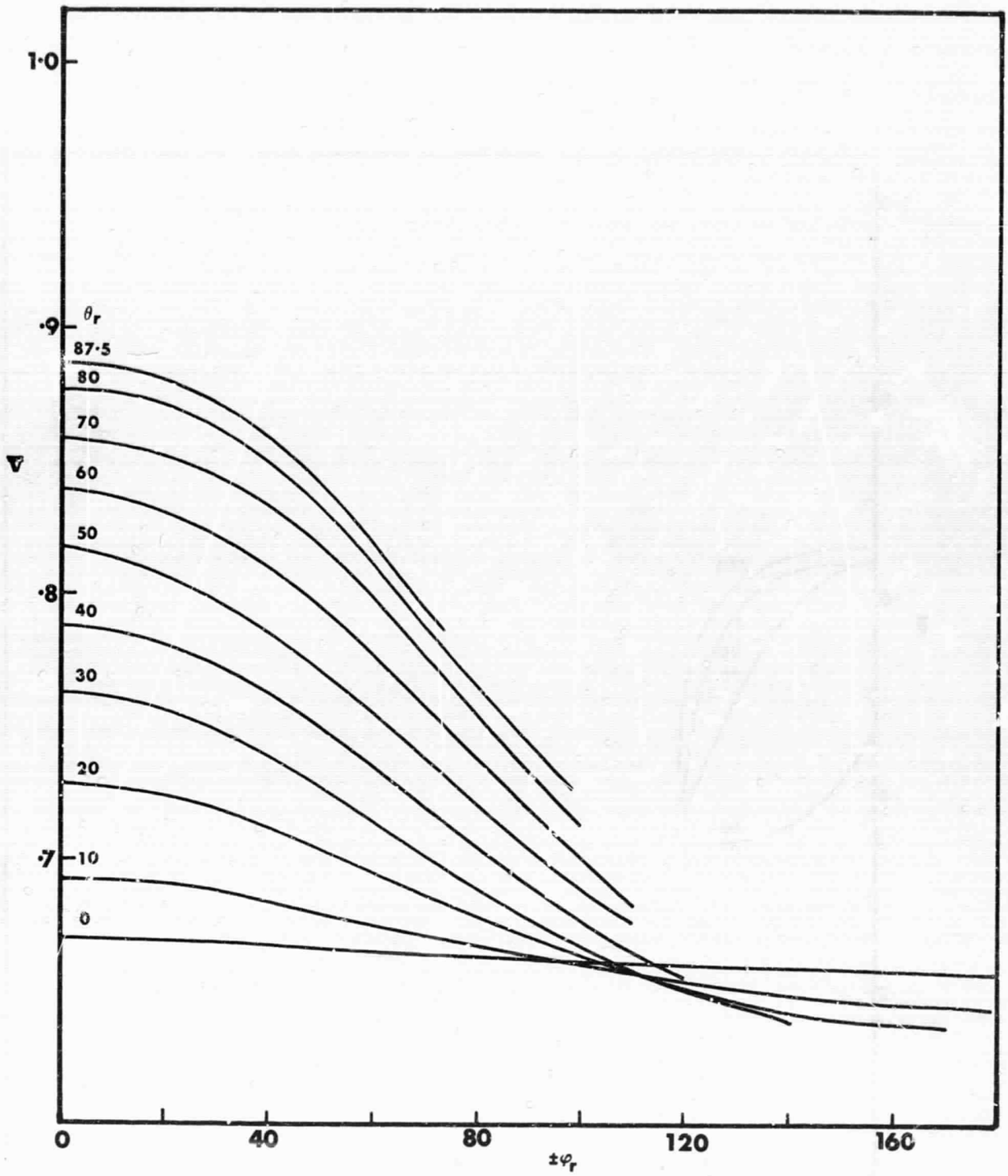

FIG. 8.3.4 THE PRIMARY VELOCITY MEAN DISTRIBUTION IN SPACE FOR A SMALL VALUE OF R*. Angular mode, Ar/W mass ratio, R* = 0.9, E_o^* = 20, θ_o = 45°, ϕ_o = 0°. Corresponds to FIG. 7.3.4.

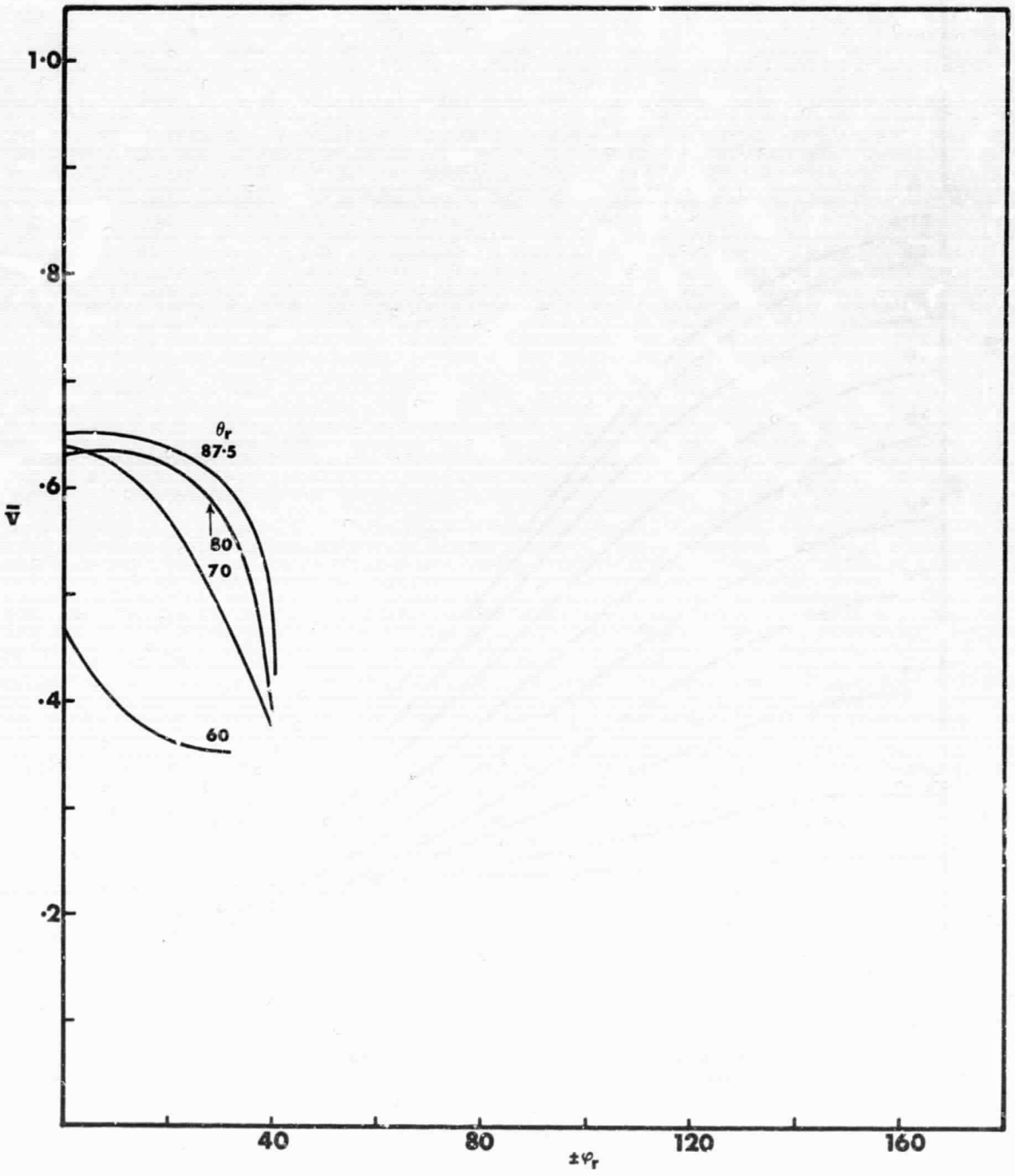

FIG. 8.3.5 THE PRIMARY VELOCITY MEAN DISTRIBUTION IN SPACE FOR A LARGE VALUE OF THE MASS RATIO. Angular mode. Xe/W mass ratio, $P^* = 1.3$, $E_o^* = 20$, $\theta_o = 45^o$, $\phi_o = 0^o$.

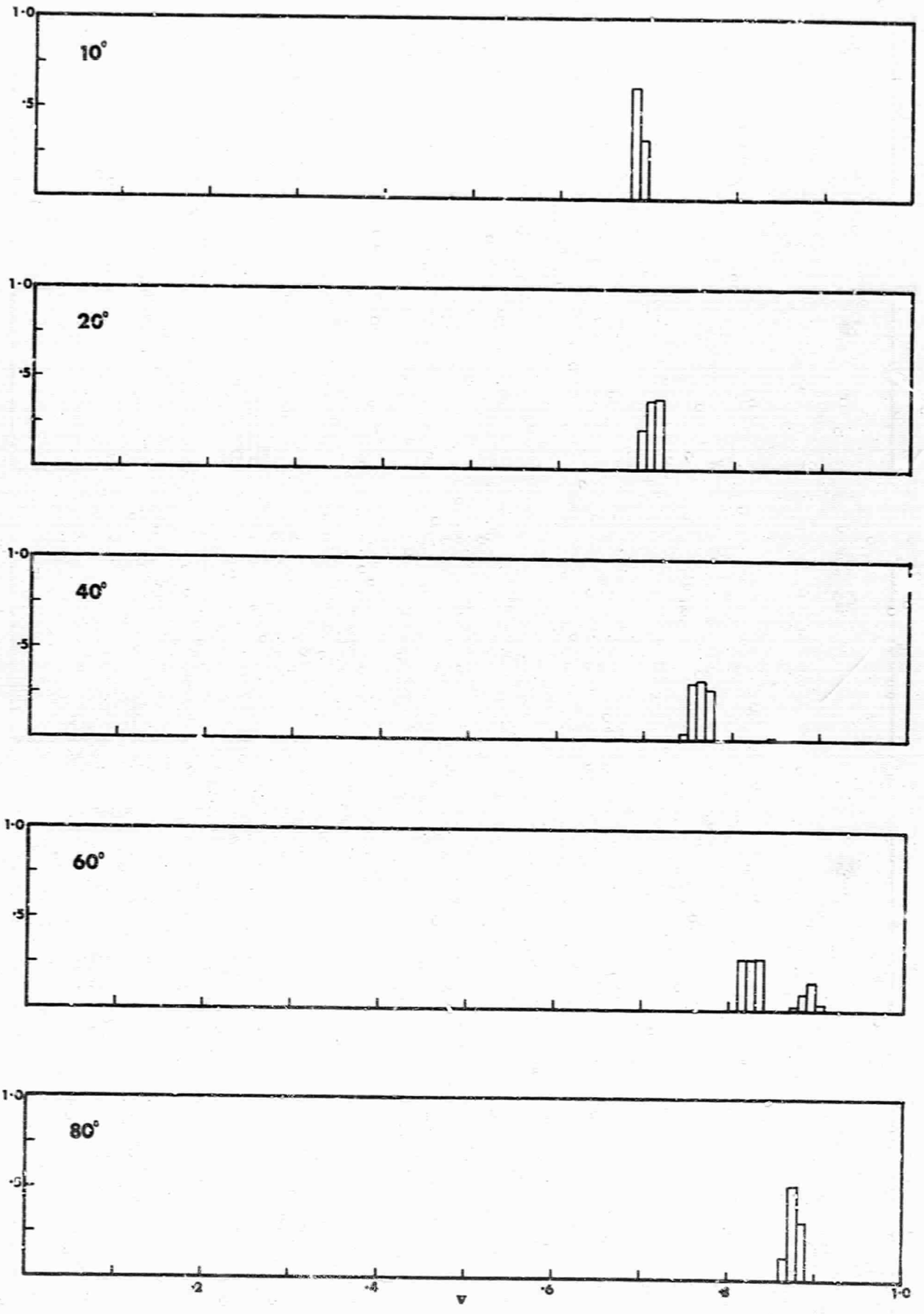

FIG. 8.4.1 THE PRIMARY VELOCITY DISTRIBUTIONS AS A FUNCTION OF THE ANGLE OF THE DETECTOR FOR FIXED INCIDENCE ANGLE.

Detector mode 10^{0} resolution. Ar/W mass ratio, $P^{*} = 1.3$, $E_{0}^{*} = 20$, $\theta_{0} = 45^{0}$, $\phi_{0} = 0^{0}$. The bars represent the fraction of the particles in the detector which have velocities in the ranges shown.

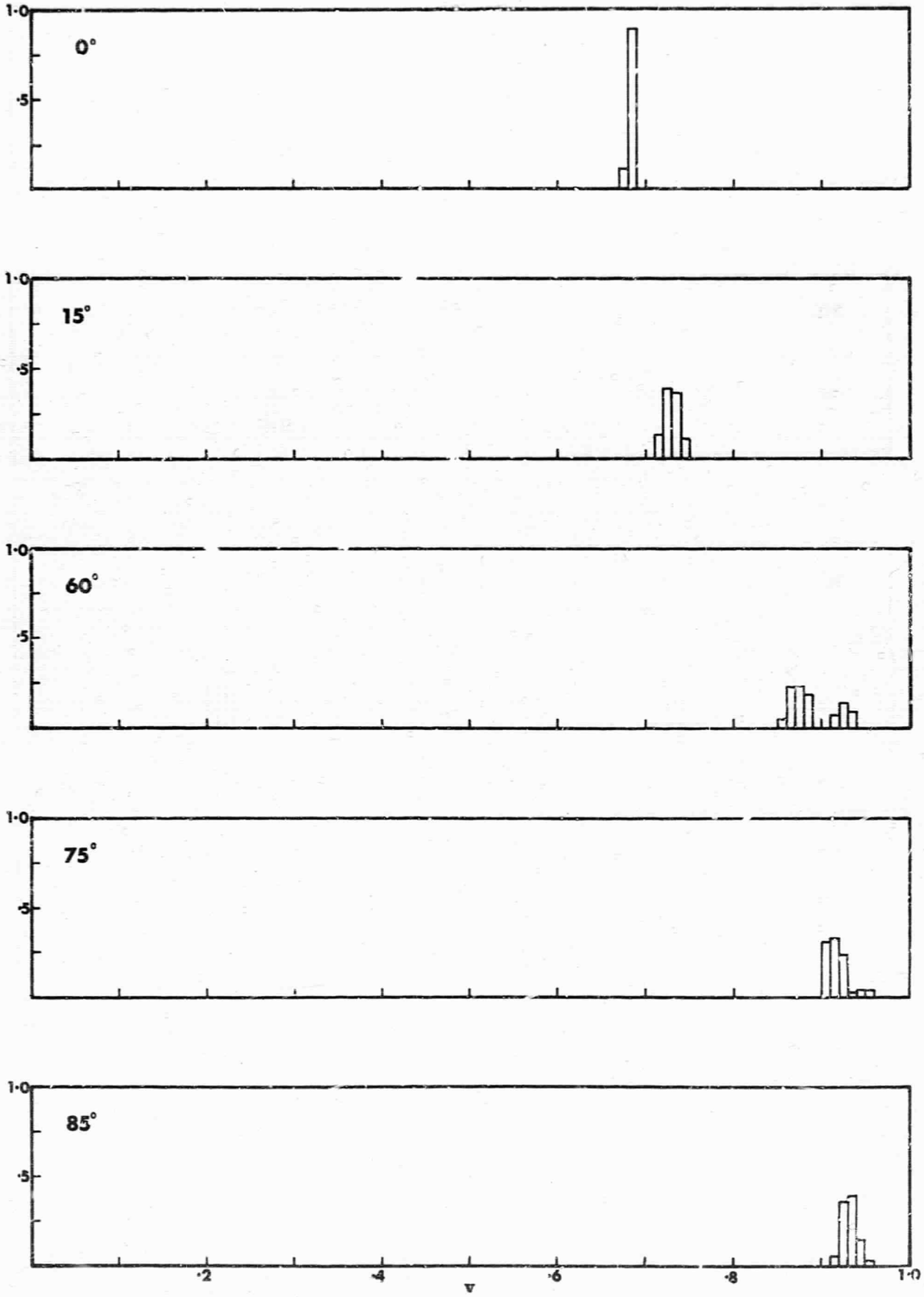

FIG. 8.4.2 THE PRIMARY VELOCITY DISTRIBUTIONS AS A FUNCTION OF INITIAL INCIDENCE ANGLE. DETECTOR FIXED AT 60_0.
Detector mode 10^0 resolution. Ar/W mass ratio. $R^* = 1.3$, $E_0^* = 20$, $\phi_0 = 0^0$.

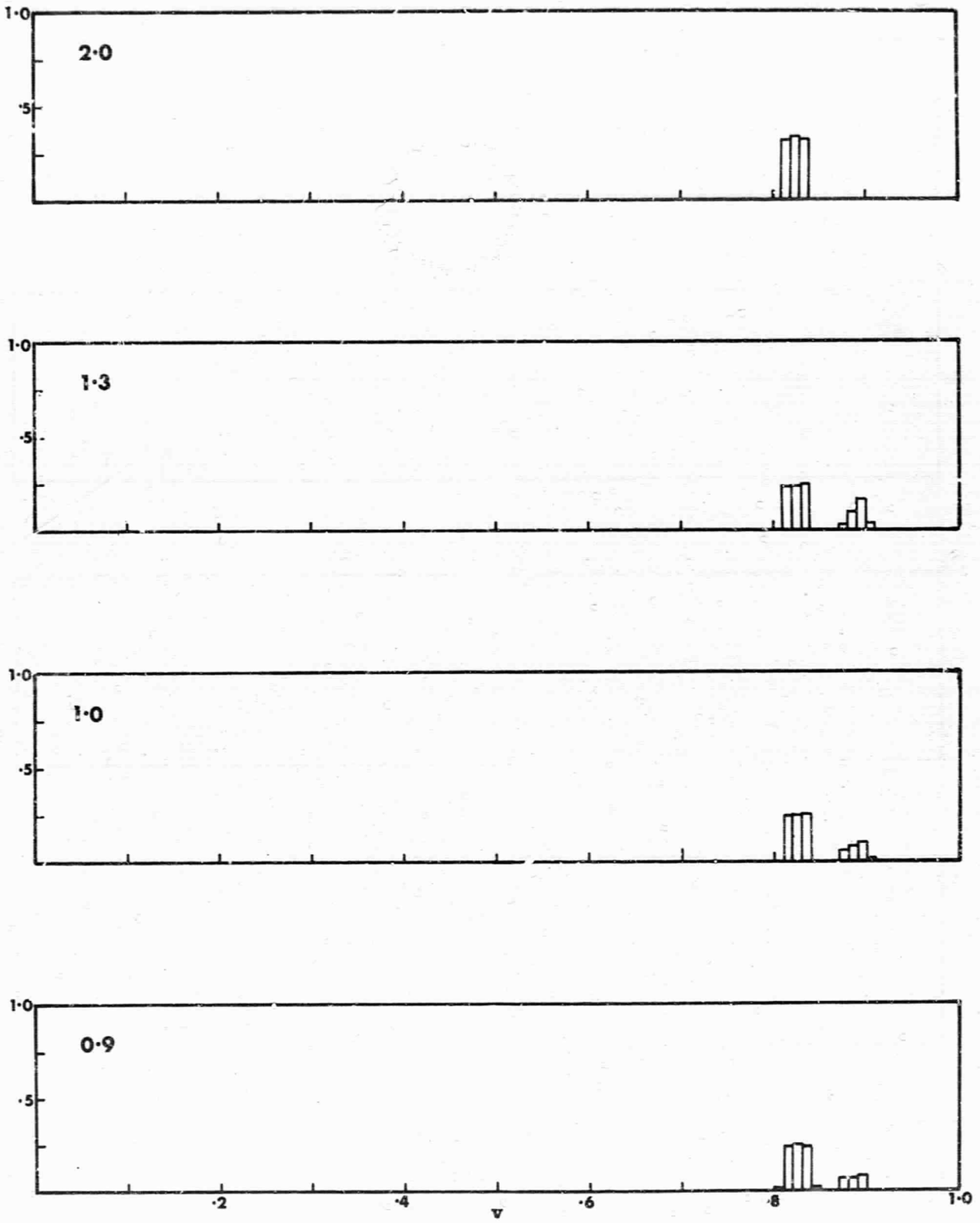

FIG. 8.4.3 THE PRIMARY VELOCITY DISTRIBUTIONS AS A FUNCTION OF INTERACTION RADIUS. DETECTOR FIXED AT 60°. Detector mode 10° resolution. Ar/W mass ratio, $E_o^* = 20$, $\theta_o = 45°$, $\phi_o = 0°$.

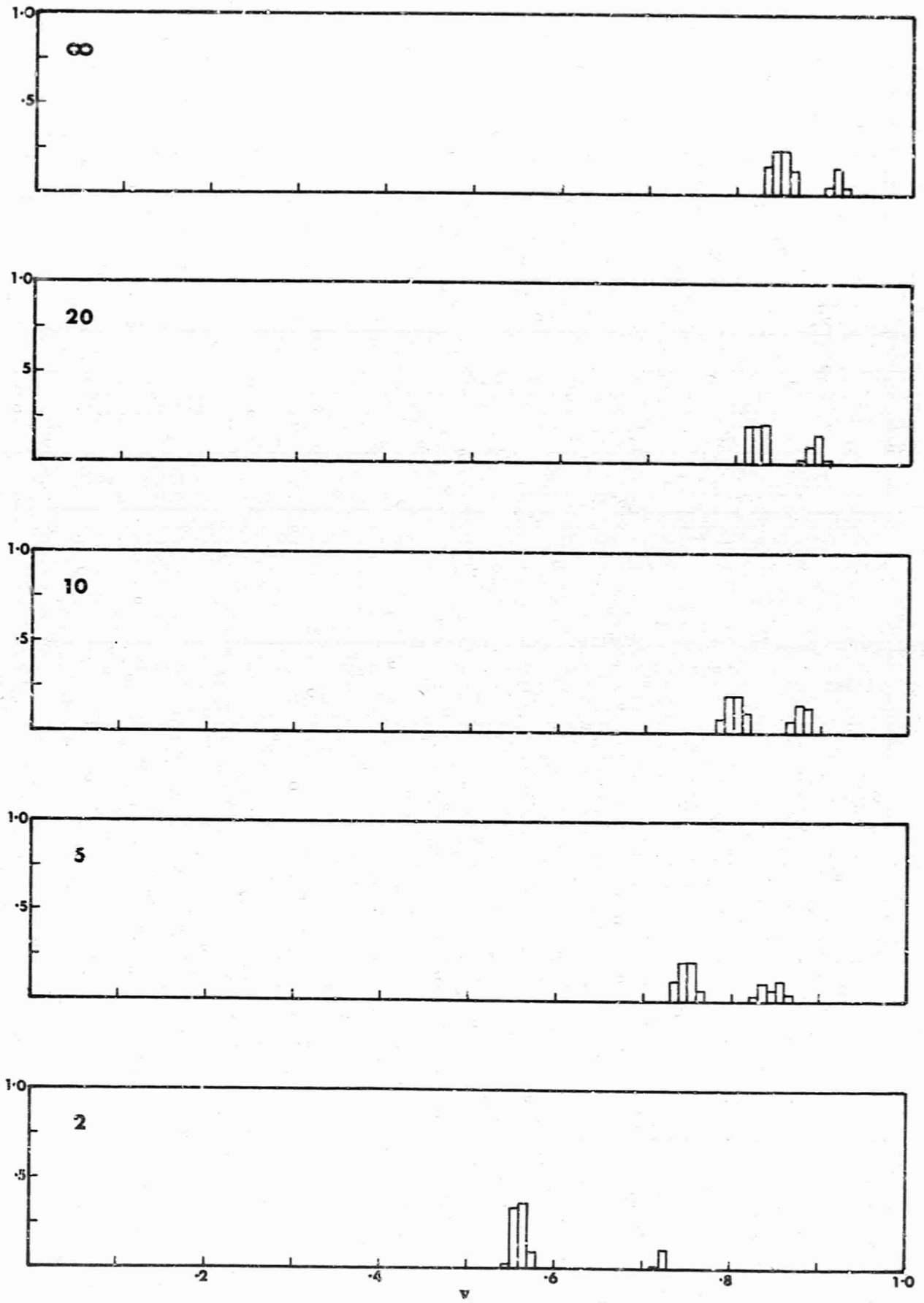

FIG. 8.4.4 THE PRIMARY VELOCITY DISTRIBUTIONS AS A FUNCTION OF INITIAL ENERGY RATIO. DETECTOR FIXED AT 60°.
Detector node 10° resolution, Ar/W mass ratio, $R^* = 1.2$, $\theta_0 = 45°$, $\phi_0 = 0°$.

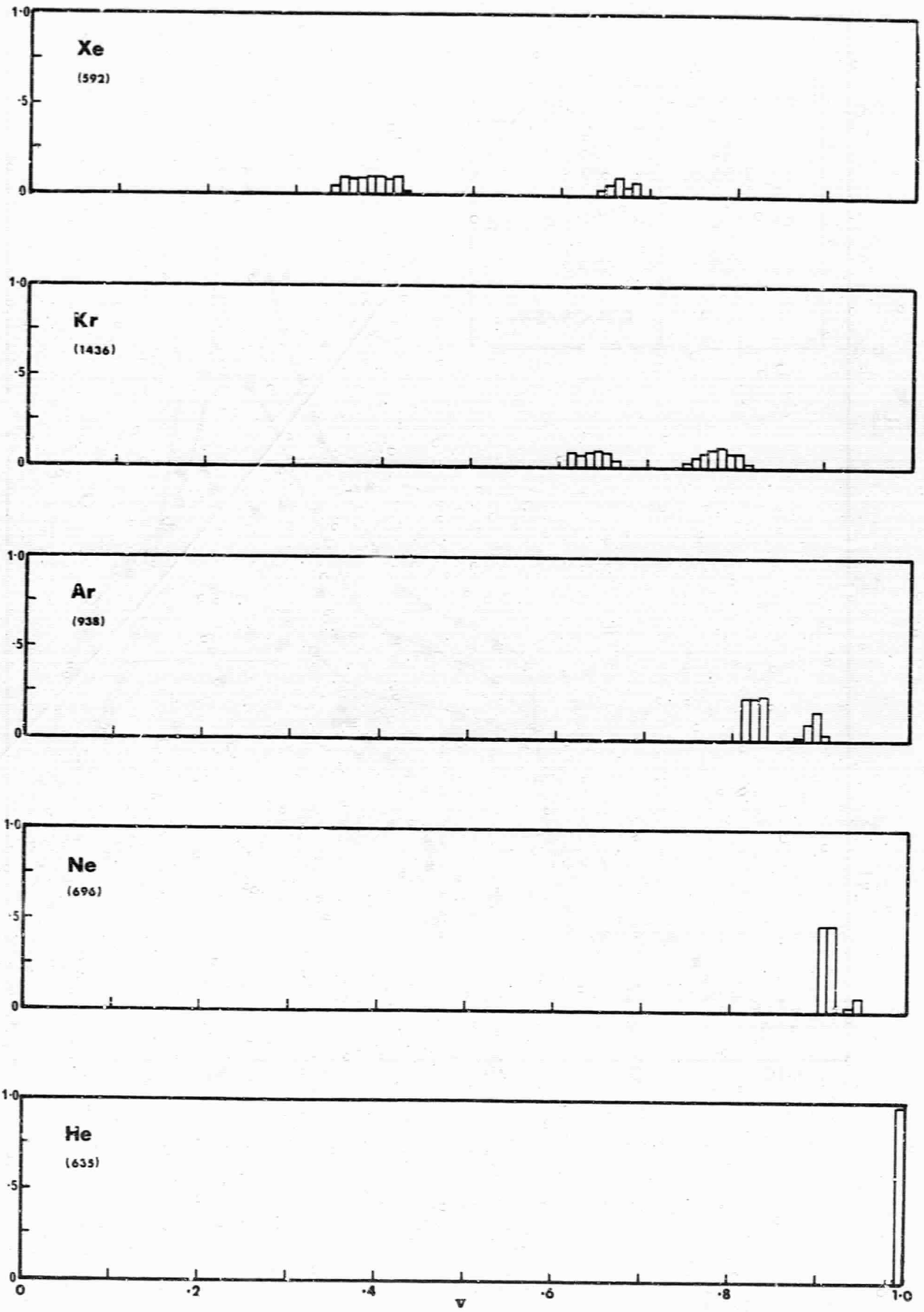

FIG. 8.4.5 THE PRIMARY VELOCITY DISTRIBUTIONS FOR VALUES OF THE RARE-GAS-TUNGSTEN MASS RATIOS. DETECTOR FIXED AT 60°. $R^* = 1.3$, $E_o^* = 20$, $\theta_o = 45°$, $\phi_o = 0°$.

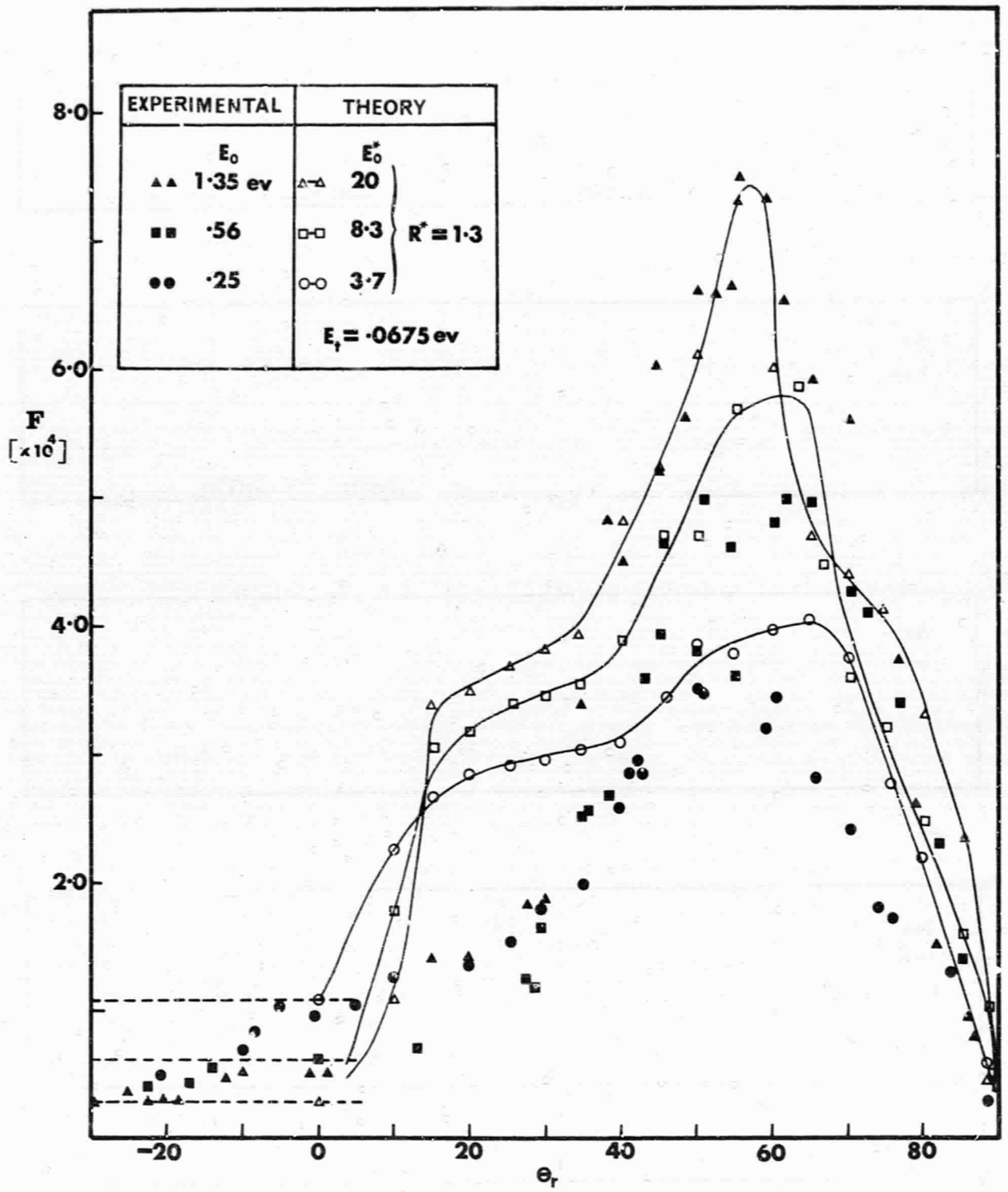

FIG. 9.1 COMPARISON OF THE THEORY AND THE EXPERIMENT OF O'KEEFE. Ar/W mass ratio. $\theta_0 = 45°$, $\phi_0 = 8°$. Other parameters as shown. Experimental points from Ref. 3. The dashed lines indicate the flux levels obtained when the semi-trapped particles are distributed equally over the whole reflection space.